
















The Kepler Giant Planet Search. I: A Decade of Kepler Planet Host Radial Velocities from W. M. Keck Observatory

LAUREN M. WEISS ¹ HOWARD ISAACSON ^{2,3} GEOFFREY W. MARCY,² ANDREW W. HOWARD ⁴
BENJAMIN J. FULTON ^{5,6} ERIK A PETIGURA ⁷ ERIC AGOL ⁸ DANIEL FABRYCKY ⁹ ERIC B. FORD ^{10,11,12,13}
DANIEL JONTOF-HUTTER ¹⁴ MIKI NAKAJIMA ¹⁵ JAMES E. OWEN ¹⁶ LESLIE A. ROGERS ¹⁷ JASON ROWE ¹⁸
JASON H. STEFFEN ^{19,20} AND HILKE E. SCHLICHTING ²¹

¹*Department of Physics and Astronomy, University of Notre Dame, Notre Dame, IN 46556, USA*

²*Department of Astronomy, University of California Berkeley, Berkeley CA 94720, USA*

³*Centre for Astrophysics, University of Southern Queensland, Toowoomba, QLD, Australia*

⁴*Department of Astronomy, California Institute of Technology, Pasadena, CA 91125, USA*

⁵*Cahill Center for Astronomy & Astrophysics, California Institute of Technology, Pasadena, CA 91125, USA*

⁶*IPAC-NASA Exoplanet Science Institute, Pasadena, CA 91125, USA*

⁷*Department of Physics & Astronomy, University of California Los Angeles, Los Angeles, CA 90095, USA*

⁸*Astronomy Department, University of Washington, Seattle, WA 98195*

⁹*Dept. of Astronomy & Astrophysics, University of Chicago, 5640 S. Ellis Ave., Chicago, IL 60637*

¹⁰*Department of Astronomy & Astrophysics, The Pennsylvania State University, 525 Davey Laboratory, University Park, PA 16802, USA*

¹¹*Center for Exoplanets & Habitable Worlds, The Pennsylvania State University, 525 Davey Laboratory, University Park, PA 16802, USA*

¹²*Center for Astrostatistics, The Pennsylvania State University, 525 Davey Laboratory, University Park, PA, 16802, USA*

¹³*Institute for Computational and Data Sciences, The Pennsylvania State University, 525 Davey Laboratory, University Park, PA, 16802, USA*

¹⁴*Dept. of Physics, University of the Pacific, Stockton, CA 95211*

¹⁵*Department of Earth and Environmental Sciences, University of Rochester, Rochester, NY 14627, USA*

¹⁶*Astrophysics Group, Department of Physics, Imperial College London, Prince Consort Rd, London SW7 2AZ, UK*

¹⁷*Department of Astronomy and Astrophysics, University of Chicago, Chicago, IL 60637, USA*

¹⁸*Department of Physics & Astronomy, Bishop's University, 2600 Rue College, Sherbrooke, QC J1M 1Z7, Canada*

¹⁹*Department of Physics and Astronomy, University of Nevada, Las Vegas, 4505 South Maryland Parkway, PO Box 454002, Las Vegas, NV 89154, USA*

²⁰*Nevada Center for Astrophysics, 4505 South Maryland Parkway, PO Box 454002, Las Vegas, NV 89154, USA*

²¹*Department of Earth, Planetary, and Space Sciences, The University of California, Los Angeles, 595 Charles E. Young Drive East, Los Angeles, CA 90095, USA*

ABSTRACT

Despite the importance of Jupiter and Saturn to Earth's formation and habitability, there has not yet been a comprehensive observational study of how giant exoplanets correlate with the architectural properties of close-in, sub-Neptune sized exoplanets. This is largely because transit surveys are particularly insensitive to planets at orbital separations $\gtrsim 1$ AU, and so their census of Jupiter-like planets is incomplete, inhibiting our study of the relationship between Jupiter-like planets and the small planets that do transit. To establish the relationship between small and giant planets, we conducted the Kepler Giant Planet Survey (KGPS). Using W. M. Keck Observatory HIRES, we spent over a decade collecting 2858 RVs (2181 of which are presented here for the first time) of 63 sun-like stars that host 157 transiting planets. We had no prior knowledge of which systems would contain giant planets beyond 1 AU, making this survey unbiased in detected Jovians. In this paper, we announce RV-detected companions to 20 stars from our sample. These include 13 Jovians ($0.3 M_J < M \sin i < 13 M_J$, $1 < a < 10$ AU), 7 non-transiting sub-Saturns, and 3 stellar-mass companions. We also present updated masses and densities of 84 transiting planets. The KGPS project leverages the longest-running and most data-rich collection of RVs of the NASA *Kepler* systems yet, and will provide a basis for addressing

whether giant planets help or hinder the growth of sub-Neptune sized and terrestrial planets. Future KGPS papers will examine the relationship between small, transiting planets and their companions.

1. INTRODUCTION

The mode of formation of the solar system, and now of exoplanet systems, is a major unsolved problem in astrophysics and planetary science. Jupiter and Saturn are thought to have influenced the architecture of the solar system by delaying and stunting the formation of terrestrial planets (Walsh et al. 2011) and shepherding water-bearing comets toward Earth (Meech & Raymond 2019). Do exoplanet systems with small inner planets also have exterior giant planets? If that is the case, how do those planets’ properties correlate with inner planetary system properties?

The NASA Kepler Mission, which has discovered thousands of planets between the sizes of Mars and Neptune within 1 AU of their host stars (Borucki et al. 2010), provides a unique opportunity to investigate whether giant planets help or hinder the growth of small worlds in other planetary systems. However, Kepler’s short (4-year) mission duration impaired its sensitivity to Jovian analogs (planets of $0.3\text{--}13 M_J$ with orbits at 1-10 AU). Furthermore, planets at the orbital distance of Jupiter (5 AU) have only a 0.1% chance of transiting their star—a prerequisite for detection of their transits with Kepler. Thus, the occurrence of Jovian siblings to the small Kepler planets cannot readily be determined from the Kepler data alone.

Dynamical measurements of the Kepler planet-hosting stars provide an excellent means for detecting Jovian companions to small planets. Radial velocity (RV) measurements have successfully identified Jovian companions in several Kepler systems and measured their orbital periods, eccentricities, and $M \sin i$ ’s (e.g. Marcy et al. 2014; Mills et al. 2019b; Weiss et al. 2020; Zhang et al. 2021). Although the ESA Gaia mission has great promise for finding Jovians around nearby stars, the majority of Kepler stars are too distant (~ 1000 pc) to produce sufficient single-measurement astrometric precision to characterize planetary orbits from Jovian-mass companions at 1-10 AU.

Because Jovian planets could have orbital periods substantially longer than the *Kepler* Mission, detecting Jovians via RVs requires long-term monitoring (Note that Jupiter, at 5 AU, has a period of 11 years.) Since 2009, we have conducted the Kepler Giant Planet Search (KGPS). In this survey, we have been measuring RVs of Kepler stars hosting small ($< 4 R_\oplus$) planets to discover and characterize giant planet companions to these sub-Neptunes. KGPS includes several major objectives, which are addressed in a series of papers. This paper (I) includes our sample selection criteria, a presentation of the RVs collected, a newly developed algorithm to find giant planets in systems with known small transiting planets, and orbital and $M \sin i$ properties of the non-transiting planets in our survey, 8 of which are new discoveries. Paper II (He et al. in prep.) is about the differences between the architectural properties of the transiting planets that have Jovian companions versus those that do not. In Paper III, we will use a sub-sample of KGPS that is carefully curated to avoid biases to measure the occurrence of Jovian planets in systems with sub-Neptunes, and compare this Jovian frequency to the frequency of Jovians in the solar neighborhood. The KGPS sample will provide future opportunities to look for correlations between the physical and dynamical properties of the small, inner planets and the giant, outer planets (Papers IV and up, see Table 1).

2. SAMPLE SELECTION

Table 1: Kepler Giant Planet Search (KGPS) Paper Series

No.	Title
KGPS I	A Decade of Kepler Planet Host Radial Velocities from M. W. Keck Observatory
KGPS II	Inner System Gap Complexity is a Strong Predictor of Outer Giant Planet Occurrence
KGPS III	The Occurrence of Jovian Companions to Small Transiting Planets
KGPS IV+	Additional Patterns in the Architectures of Systems with Small and Jovian Planets

This paper and others in the KGPS series include RV follow-up of *Kepler* planetary systems with the following properties, based on their characterization in [Petigura et al. \(2017\)](#):

1. A sun-like host star, defined as:
 - (a) a sun-like effective temperature ($4300 \text{ K} < T_{\text{eff}} < 6300 \text{ K}$),
 - (b) slowly rotating ($v \sin i < 10.1 \text{ ms}^{-1}$),
 - (c) a main-sequence or only moderately evolved star ($\log g > 4.0$),
 - (d) low magnetic activity ($\log R'_{\text{HK}} < -4.8$),
 - (e) and within a magnitude-limited sample ($V < 13.6$),¹
2. Having a sufficient RV baseline to detect Jupiter analogs, defined as:
 - (a) The earliest RV from 2018 or earlier,
 - (b) At least 10 RVs,
3. Having at least one small ($R_p < 4 R_{\oplus}$)² transiting planet with $P < 100$ days,
4. Having no known giant planets beyond 1 AU.³

Some of the stars in this paper were also selected as part of an RV follow-up survey of *Kepler* transit planet host stars with three or more transiting planets (as of early 2015) with effective temperatures ranging from 4700-6150K, low rotation speeds ($v \sin i < 10 \text{ m/s}$), with Kepler magnitudes brighter than 13.2. Those targets were KOIs 94, 282, 316, 623, 1781, 1909, 2169, 2732, and 3083.

Some of the stars in this paper were also selected as part of an RV follow-up survey of multi-planet systems with interesting dynamical architectures and/or significant transit timing variations (TTVs). Those targets are KOIs 84, 85, 103, 244, 245, 246, 260, 262, 274, 275, 277, and 1930. The systems KOIs 85, 244, and 246 were analyzed in [Mills et al. \(2019b\)](#). We present additional RVs of those systems and an updated analysis here.

Some of the stars in this paper have recently been observed with moderate cadence RVs as part of a program to measure precise planet masses in multi-planet systems. Those targets are KOIs 41, 111, and 316. Here, we report the discoveries and upper limits on the masses of non-transiting companions in those systems. Detailed studies of the physical properties of the transiting planets in those systems are in preparation. We have removed RVs that were obtained for Rossiter-McLaughlin observations, since those RVs do not represent the center-of-mass motion of the host star and are not suitable for detecting additional companions. Those stars were KOIs 94 and 244, both of which have their Rossiter-McLaughlin observations and analysis described in [Albrecht et al. \(2013\)](#).

Some of the stars in this paper are currently monitored at moderate to high cadence on HIRES based on student-led observing proposals. RVs from those student-led proposals are not included in this paper but will be reported in student-led papers soon.

In this paper, we also report the long-term HIRES RVs of several stars that fall outside of the sample criteria described. Nonetheless, we have long RV baselines that will likely be useful to the community. These systems include several systems that are famous for their high multiplicity, small planets, and habitable-zone planets, but are fainter than our magnitude cutoff. KOI-157 (Kepler-11, $V > 13.6$) was the first six-transiting planet system and one of the *Kepler* Mission's earliest discoveries ([Lissauer et al. 2011](#)). KOI-351 (Kepler-90, $V > 13.6$) is a system with eight transiting planets ([Cabrera et al. 2014](#); [Schmitt et al. 2014](#); [Shallue & Vanderburg 2018](#)), making it the highest multiplicity exoplanet system known. Its outermost transiting planet, KOI-351 h, is nearly the size of Jupiter and has an orbital period of 331 days. KOI-377 (Kepler-9, $V > 13.6$) was the first system with multiple transiting planets discovered by *Kepler*, and also the first example of transit timing variations (TTVs) discovered by *Kepler* ([Holman et al. 2010](#)). KOI-701 (Kepler-62, $V > 13.6$) is a sun-like star with five transiting planets, including one with $R_p < 1.5 R_{\oplus}$ which is arguably the most “Earth-like” exoplanet currently known based on its size, orbital distance, and host star

¹ Gaia magnitudes were not available when targets were first selected

² Based on additional information from Gaia, all of the planetary systems that were initially selected for this survey still satisfy the criterion that at least one planet has $R_p < 4 R_{\oplus}$.

³ Transits would be one way to identify candidate Jovian planets, although Jupiter-sized transiting planets can have ultra-low densities. Jovian companions can also be inferred dynamically (e.g., Kepler-56), where RVs were obtained because the planets were known to be misaligned from the star's rotation axis by a presumed Jovian perturber.

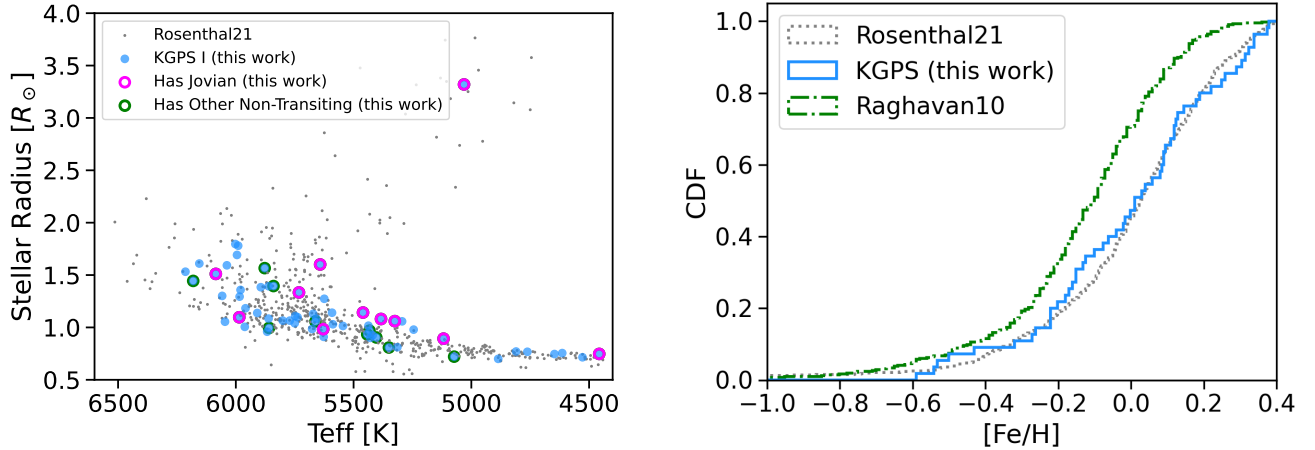


Figure 1: Left: Stellar radius vs. effective temperature for stars in the KGPS sample (blue) and other Kepler stars with RV follow-up reported here (orange) compared to the California Legacy Survey (Rosenthal et al. 2021). Stars for which we detected Jovian companions are ringed in magenta. The outlier in the giant branch is KOI-1241 (Kepler-56). Right: The continuous distribution function (CDF) of stellar metallicities from three different surveys: Raghavan et al. (2010); Rosenthal et al. (2021), and KGPS.

properties (Borucki et al. 2013). KOI-1241 (Kepler-56) is an evolved star that was originally suspected (and later confirmed) to harbor a cold giant planet that is responsible for mis-aligning its transiting planets, and so it does not meet the strictly “giant-blind” aspect of our sample selection (Huber et al. 2013; Otor et al. 2016). KOI-1781, which was originally selected as part of the KGPS survey, is moderately active (which we only determined after obtaining multiple spectra).

Our full catalog is generally RV-quiet, main sequence stars (Fig. 1, left). We did not place any cuts on the metallicity of stars in our sample. This is noteworthy because the occurrence of giant planets in RV surveys correlates significantly with host star metallicity (Fischer & Valenti 2005; Petigura et al. 2018). To assess the possible effect of the stellar metallicity of our sample on the results, we compared the distribution of iron abundances of our host stars to two samples from the literature (Fig. 1, right). Rosenthal et al. (2021) (CLS-I) is a 30-year, blind RV survey of nearby sun-like stars that were selected in a manner similar to the KGPS selection criteria (e.g., for their viability for precision RV follow-up), whereas Raghavan et al. (2010) is a volume-limited survey of stars selected to determine stellar multiplicity. The metallicity distribution of the host stars studied in KGPS is statistically indistinguishable from the CLS-I sample ($p > 0.1$ via a Kolmogorov-Smirnov test), whereas both CLS-I and KGPS contain stars that are more metal-rich on average than the typical star in the local neighborhood ($p = 0.004$). The high metallicities of the CLS-I and KGPS samples might be related to their focus on sun-like stars, which have higher metallicity than the galactic average.

We accessed the orbital ephemerides of all planetary systems from the NASA Exoplanet Archive, searching both the composite planetary systems table and the cumulative *Kepler* candidate table to ensure that no transiting planetary candidates in these systems that are not yet “confirmed” were missed (NASA Exoplanet Archive 2022a,b).⁴ We considered all confirmed planets, confirmed stellar companions, and planet candidates in our analysis (see Appendix). We did not consider objects with false positive dispositions.

3. OBSERVATIONS

The discovery of planets via dynamical data requires an orbit determination, which is only tractable with multiple epochs of data. Radial velocities (RVs) sample the line-of-sight velocity component of the primary star in a manner that has been successfully used for discovering giant planets and determining their orbits over the past three decades (Mayor & Queloz 1995; Howard et al. 2010; Rosenthal et al. 2021). When modeling RV data, at least three free parameters are required to determine a closed orbit of a single, circular planet. Additional free parameters allow for

⁴ Accessed on 2022-02-17.)

eccentric orbits and/or additional planets in the model. We obtained at least 10 RVs covering a baseline of at least 3 years for each star in our sample, which were sufficient to detect orbital motion of the star from a Jovian companion (see Paper III). For stars with RVs that clearly indicated the presence of at least one Jupiter-mass planet, we collected far more than 10 RVs in order to improve our sampling of the orbit of the planet, including probing its eccentricity and giant planet multiplicity. In total, we collected 2858 RVs of 63 targets.

RVs were obtained at the W. M. Keck Observatory using the HIRES instrument. We used the typical setup and observational strategy of the California Planet Search team. This setup has been described extensively in prior literature (e.g., [Howard et al. 2010](#)), but we will recapitulate the main points here. The CPS observing setup ensures long-term stability of the wavelength solution of HIRES by (i) positioning the emission lines from a thorium-argon calibration lamp to ensure they fall within 0.5 pixels of a nominal configuration every night, and (ii) inserting a cell of gas-phase (50° C) molecular iodine into the light path of the instrument to imprint an I2 absorption spectrum onto each stellar spectrum for which we wish to measure an RV. The I2-imprinted spectra were forward modeled with a laboratory spectrum of I2 multiplied by a deconvolved stellar spectral template of the target star, which is then convolved with the local PSF of HIRES. The deconvolved stellar spectral template was taken without iodine immediately before and after observations of rapidly rotating B-type stars through iodine, to sample the immediate, local PSF of the Keck telescope plus HIRES instrument. This strategy produces RVs with an RMS scatter of $\sim 2.5 \text{ m s}^{-1}$ over a timescale of three decades ([Howard & Fulton 2016](#); [Weiss et al. 2016](#); [Rosenthal et al. 2021](#)).

Some modifications of the CPS observing setup, which was first developed for bright stars ($V < 10.5$ [Butler et al. 1996](#)), are necessary to attain accurate RVs of the fainter Kepler stars ($V \sim 12.5$). As described in [Marcy et al. \(2014\)](#), sky subtraction becomes important at these magnitudes, particularly in conditions with a full moon and/or highly reflective cirrus. For stars of $V > 10.5$, we used the C2 decker, which subtends $14''.0 \times 0''.86$, rather than the traditionally used B5 decker ($3''.5 \times 0''.86$), to measure the contribution of sky photons at the ends of the long slit, enabling robust sky subtraction. Only a few stars in our program (KOIs 3158, 244, 245, and 246) were sufficiently bright for B5 observations.

Integration times varied among the targets based on the program goals, but were generally constrained by our need to obtain enough photons for precise RVs, balanced by a short enough integration time to avoid noise from cosmic rays, barycentric correction errors, and lost opportunities elsewhere on the sky. Using the HIRES exposure meter, we monitored the signal-to-noise (S/N) of the incoming exposure, requiring a minimum of 30k counts (arbitrary units that result in S/N per pixel > 70). The maximum exposure time was 45 minutes. Stars with $V < 9$ were observed with two consecutive exposures to average over p-mode oscillations, but the only stars for which this applied were HIP94931 (KOI-3158=Kepler-444) and KOI-69 (Kepler-93). We did not observe any targets in weather conditions that did not permit our minimum S/N in 45 minutes.

Only one star (KOI-3158) had a bright companion within $2.''0$; for this target, we used the image rotator to ensure the companion was out of the slit, minimizing contamination from the companion. Other stars that had companions within $2.''0$ were at least 5 magnitudes brighter than their companions in the V band, and so contamination from the companion was comparable to the Poisson noise for S/N=100.

Twenty-two of the Kepler planet-hosting stars in our sample were described in [Marcy et al. \(2014\)](#), which presented 677 HIRES RVs. Here, we present 2181 RVs, augmenting the total HIRES RV catalog of Kepler’s planet-hosting stars to 2858 RVs. The RVs of our 63 targets are available in machine-readable tables.⁵

4. ORBIT FITTING

Multi-planet systems pose a variety of challenges to accurate orbital fitting, especially if the orbital periods are not known *a priori*. It is useful to sample the shortest-period planets at least as often as every half-orbital period to disambiguate the true signals from the aliases ([Dawson & Fabrycky 2010](#)); meanwhile, long-term monitoring is also necessary to detect the longest-period planets ([Blunt et al. 2019](#); [Rosenthal et al. 2021](#)).

4.1. The KGPS Algorithm

When fitting systems with transiting planets, (i) the orbital period and phase of the transiting planets are known, and (ii) the assumption of long-term orbital stability implies that additional planets, particularly massive giant planets, do not have orbits so close to the transiting planets that they would destabilize the system. These key advantages of

⁵ We will make this table available upon acceptance and/or at the referee’s request.

searching for new planets in a system with known transiting planets, as compared to a blind planet search, inspired us to develop a custom algorithm for identifying non-transiting planets in the Kepler systems, which we call the “KGPS” algorithm (Figure 2). The key steps are:

1. Search for additional published RVs with RV precision of $< 5 \text{ m s}^{-1}$ (e.g. HARPS-N, [Cosentino et al. 2012](#)).
2. Model and optimize a linear combination of orbits for the N transiting planets. In all cases, we assumed that the transiting planets were in circular orbits. This assumption is motivated by previous studies showing that the stars with multiple transiting planets typically have $e < 0.1$ ([Mills et al. 2019a](#); [He et al. 2020](#); [Yee et al. 2021](#)). Further, introducing eccentricity and argument of periastron as free parameters for planets with low RV semi-amplitudes can absorb noise and/or signals from non-transiting planets. Additional free parameters were the RV zero-point γ and jitter (σ_j , which is added to the measured errors in quadrature) for the HIRES RVs, as well as γ and σ_j terms for any additional instruments. (Note that the only cases where two or more observatories were used had many more than 10 RVs.) For data sets with at least 20 degrees of freedom and for planets larger than $1.15 R_{\oplus}$, we also allowed the N RV semi-amplitudes of the planets (K_1, \dots, K_N) to vary, allowing a determination of the masses of the small planets. In cases with fewer than 20 degrees of freedom or for planets smaller than $1.15 R_{\oplus}$, we used the [Weiss & Marcy \(2014\)](#) mass-radius relation to estimate the most likely mass of each transiting planet to determine fixed values of K_1, \dots, K_N . This assumed mass-radius relationship did not produce any results that were inconsistent with our observations. We used the software package *RadVel* to develop and optimize all of our models ([Fulton et al. 2018](#)). Note that for fixed orbital periods and a circular orbit, this is a linear problem (in parameters $K \cos \omega$, $K \sin \omega$, γ , and σ_j), so there is a single global best-fit solution [Wright & Howard \(2012\)](#).
3. After subtracting the best N -planet fit, take a “fast periodogram” of the residual RVs, using the algorithm *faster* developed in [Press & Rybicki \(1989\)](#). Assess whether there is a significant peak by estimating the false alarm probability (FAP) given the peak height and the number of effectively independent frequencies considered: $\text{FAP} \approx 1 - [1 - \text{Exp}(-P_{\text{max}})]^{2N_{\nu}/f_{\text{over}}}$, where P_{max} is the maximum power and N_{ν}/f_{over} is the total number of frequencies sampled divided by the typical rate of oversampling the average Nyquist frequency ([Press & Rybicki 1989](#)). For all targets, we oversampled the Nyquist frequency by $f_{\text{over}} = 100$.
4. If there is a significant peak (false alarm probability < 0.05), assess whether the period of the peak is an appropriate guess for the orbit of an additional planet. This involves checking that the period is (1) within the window function ($< 4 \times$ the RV baseline), (2) longer than 10.0 days (signals near peaks in the window function of the RVs, such as 1 day, are often aliases of long-period structure visible by eye in the RVs), and (3) distinct from the periods of other planets in the model (with a minimum period ratio of 1.15). If any of these conditions are not met, instead propose including a linear RV trend in the model, effectively adding one free parameter (dv/dt) to represent an additional high-mass, long-period body. In cases where at least one condition (1-3) is not met and with at least 15 degrees of freedom, we also included RV curvature (d^2v/dt^2).
5. If the new proposed period passes the above criteria, fit a new model with all of the previous planets, plus a planet at the new period. We modeled each new planet orbit with 2-4 free parameters: the RV semi-amplitude K_{N+1} and the time nearest conjunction, t_c (even if the planet does not transit). Note that the orbital period was fixed during this step. We used information from the phase of the Lomb-Scargle periodogram to guess a time of conjunction. In cases with at least 15 degrees of freedom, we also included two eccentricity parameters, modeled using the basis of $\sqrt{e} \sin \omega$ and $\sqrt{e} \cos \omega$, which effectively assert a uniform prior for $e \in [0, 1)$ and $\omega \in [0, 2\pi)$.
6. Compute and compare the Bayesian Information Criterion (BIC, with difference ΔBIC) of the N -planet and $N + 1$ -planet models ([Kass & Raftery 1995](#)). While some authors consider ΔBIC of 10 to be sufficient to distinguish the models, we adopt a more conservative ΔBIC threshold of 20, with the lower-scoring model being strongly preferred. This is particularly important since we effectively tried thousands of different orbital periods before selecting the best one to model via the Lomb Scargle periodogram. The choice of 20 is arbitrary, but based on a qualitative calibration based on trial and error; a substantially lower value leads to several dubious planetary signals, whereas a substantially higher value misses signals that are apparent by eye. The choice of ΔBIC of 20 is also advantageous, since it matches that adopted by [Rosenthal et al. \(2021\)](#) for claiming a planet

detection. For trends, we only required ΔBIC of 10, since we only searched for one trend per system (as compared to thousands of orbital periods).

7. While the $N + 1$ -planet model is preferred, increment N and repeat steps 3-6.
8. When the search has converged on a preferred model, use a Markov-Chain Monte Carlo (MCMC) algorithm to explore uncertainties in the free parameters. We used **RadVel**, which employs the affine-invariant sampler of **emcee** (Foreman-Mackey et al. 2013). Our priors were: (a) the RV semi-amplitudes are positive ($K_1, \dots, K_N > 0$), (b) eccentricities are bounded between 0 and 1, and (c) the RV jitter is bounded between 0 and 20 m s^{-1} .

The KGPS algorithm includes steps to account for the number of RVs and the degrees of freedom (DOF) to reduce model complexity and speed up model selection compared to purely blind algorithms (e.g., **rvsearch**, Rosenthal et al. 2021). The output of the KGPS search algorithm for each system is shown in Table 2.

4.2. Empirical Estimates of Stellar Jitter

One nuisance parameter in our model is the stellar jitter, σ_j . This parameter is added in quadrature to the intrinsic RV errors in a manner that accounts for stellar-induced RV variability. Often, the stellar jitter is measured empirically for a given star based on the RMS of the RV residuals. However, in cases where we have only 10 RVs per star and are looking to detect non-transiting planets, a larger-than-expected RMS of the RV residuals could be due to non-transiting planets rather than stellar variability.

To disentangle whether the scatter in the RVs is likely caused by a non-transiting planet or by stellar physics, we make empirical estimates of the expected stellar jitter for each star in our sample. The empirical estimates are based on measured RV scatter for large samples of stars with many observations and known stellar properties. Our stellar jitter estimate incorporates Mt. Wilson calcium activity index (S_{HK}), measured as an excess above an empirically determined activity baseline ($\Delta S = S_{\text{HK}} - S_{\text{BL}}$) as a function of photometric color ($B - V$)

$$\begin{aligned}\sigma_{j,S} &= 2.3 + 17.4 \Delta S \text{ m s}^{-1} \quad (0.4 < B - V < 0.7) \\ \sigma_{j,S} &= 2.1 + 4.7 \Delta S \text{ m s}^{-1} \quad (0.7 < B - V < 1.0) \\ \sigma_{j,S} &= 1.6 - 0.003 \Delta S \text{ m s}^{-1} \quad (1.0 < B - V < 1.3) \\ \sigma_{j,S} &= 2.1 + 2.7 \Delta S \text{ m s}^{-1} \quad (1.3 < B - V < 1.6)\end{aligned}$$

(Isaacson & Fischer 2010), the line-of-sight projected stellar rotational velocity $v \sin i$

$$\sigma_{j,\text{rot}} = 0.876 + 0.140 \frac{v \sin i}{\text{km s}^{-1}} + 0.009 \left(\frac{v \sin i}{\text{km s}^{-1}} \right)^2 \text{ m s}^{-1} \quad (1)$$

(Chontos et al. 2022), and the stellar mass M_\star (Luhn et al. 2020)

$$\begin{aligned}\sigma_{j,M} &= 2.5 \text{ m s}^{-1} \quad (M_\star < 1.2) \\ \sigma_{j,M} &= 3.5 \text{ m s}^{-1} \quad (1.2 < M_\star < 1.3) \\ \sigma_{j,M} &= 4.0 \text{ m s}^{-1} \quad (1.3 < M_\star < 1.5) \\ \sigma_{j,M} &= 5.0 \text{ m s}^{-1} \quad (1.5 < M_\star < 1.7) \\ \sigma_{j,M} &= 5.5 \text{ m s}^{-1} \quad (M_\star > 1.7).\end{aligned}$$

We computed the expected jitter from each of these relations and chose the maximum value as the expected intrinsic stellar jitter for each star in our sample. In addition to the physical jitter, we defined “photometric” jitter by empirically fitting a lower envelope to the observed RMS of the RVs as a function of the stellar flux relative to a $V=12.0$ star (F/V_{12}) for our sample:

$$\sigma_{j,\text{phot}} = \frac{0.81}{F/V_{12}} + 2.2 \text{ m s}^{-1}. \quad (2)$$

We combined the expected intrinsic stellar jitter and the photometric jitter for a total expected value of:

$$\sigma_j = \sqrt{\text{Max}(\sigma_{j,S}, \sigma_{j,\text{rot}}, \sigma_{j,M})^2 + \sigma_{j,\text{phot}}^2}. \quad (3)$$

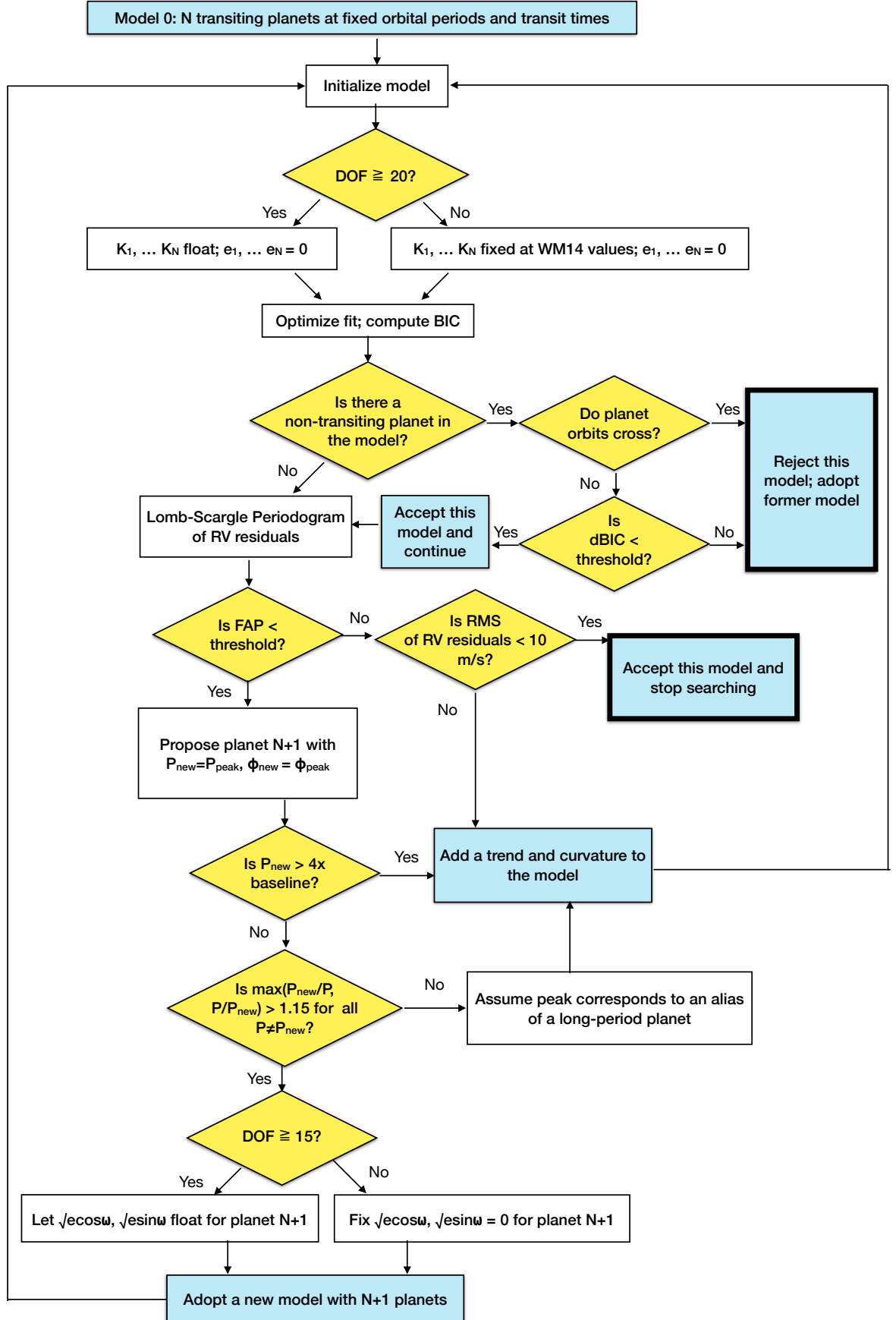


Figure 2: KGPS Algorithm. This algorithm was applied to 63 systems to search for non-transiting giant planets while accounting for the known (transiting) planets.

The expected jitter values and observed RMS of the RV residuals are given in Table 3. We plotted the observed RMS as a function of estimated jitter in Fig. 3. The RMS of the RVs for each system is shown twice: once before any planets are fit (open triangles), and once after fitting the small transiting planets and any non-transiting companions as prescribed in Fig. 2 (filled circles). Systems for which our model improved the RMS of the RVs by at least a factor of 5 are highlighted in blue. These are the systems in which we have detected giant planets.

More than half of the points in Figure 3 are below the “expected” curve. Either our method for estimating jitter by combining three methods from the literature is overly conservative, or we are over-fitting the RVs in some cases. The cases where we included a giant planet in the model substantially reduced the RMS of the RVs in a way that does not suggest pure “over-fitting.” It is likely that our estimate of the jitter is overly conservative. For instance, some of the “jitter” ($\sim 1 \text{ ms}^{-1}$) stems from noise in the Doppler algorithm itself, notably the deconvolution of the stellar spectrum and errors in the HIRES PSF determination. Evidence of this “systematic jitter,” as distinguished from stellar jitter, is visible in the constant terms of 1.6 to 2.3 in the four equations for jitter from (Isaacson & Fischer 2010), but this jitter might be double-counted when we add the “photometric” jitter in quadrature. Furthermore, any empirical estimate of a jitter term will by definition include the RMS of undetected (low-mass) planets. A careful study of RV variability across a large sample of stars that incorporates multiple jitter predictors (stellar activity, mass, rotation, and magnitude) and identifies as many low-mass planets as possible would enable a more precise estimate of the jitter of each star, but such an effort is beyond the scope of this paper.

4.3. Refined Orbital Estimates

The KGPS algorithm yielded several systems for which the best-fit model included one or more non-transiting, eccentric companions. The KGPS Algorithm has limitations in its ability to identify the most likely orbital periods of long-period companions, particularly in cases where the companion is eccentric and has a longer period than the RV baseline. For every system in which one or more non-transiting companions were detected, we examined whether a superior fit could be found by eye to the best-fit model from the KGPS Algorithm. We then used the best fit (as determined either by eye or the KGPS algorithm) to seed a new MCMC analysis in which the orbital periods and eccentricities of the non-transiting companion(s) were allowed to vary, as well as any transiting companions suspected of having significant RV amplitudes. The MCMC chains had 48 walkers each and ran until the chains were “well-mixed,” based on having a maximum Gelman-Rubin statistic of ≤ 1.03 , a minimum autocorrelation time factor of ≥ 75 , a maximum relative change in autocorrelation time $\leq .01$, and at least 1000 independent draws. In cases where the periodogram yielded peaks of similar heights but at different orbital periods, we tested models with the companion at each of the possible periods.

In most cases, the MCMC algorithm yielded nearly identical results to the KGPS algorithm. A few notable exceptions are KOIs 148, 246, and 316, in which an additional long-period planet was detected by eye. In KOIs-148 and 246, these additional companions are based on low-amplitude, moderately eccentric signals with periods comparable to the RV baseline, whereas in KOI-316, a high-amplitude signal is missed by the KGPS algorithm because the signal has very uneven time sampling, leading to a low-significance peak in the periodogram.

Other substantial updates were in KOIs 94 and 2169. In KOI-94, the RV data yield a significant improvement in the orbital period of one of the transiting planets (KOI-94 d), a warm Jupiter-sized planet with an RV semi-amplitude of $\sim 20 \text{ ms}^{-1}$. The system is known to have planet-planet interactions (based on observed transit timing variations), and the baseline from our RV survey (12 years) is substantially longer than the baseline of Kepler photometry (4 years), and so it is not surprising that we are detecting a modest deviation from the best-fit linear ephemeris for this planet. In KOI-2169, the orbit of the stellar-mass companion is very eccentric and has a much longer period than the RV baseline, which resulted in a poor fit in the KGPS algorithm. We used the publicly available algorithm `rvsearch` to explore a fine grid in the period-eccentricity solution space for this companion and identify a better fit (Rosenthal et al. 2021).

5. RESULTS

The best-fit models for individual planetary systems are summarized in Table 2 and the Appendix. Among the 63 planetary systems here, we detected 27 non-transiting planets: 8 of which are first announced here, 13 of which are Jovian ($M \sin i > 0.3 M_J$, $1 < a < 10 \text{ AU}$), and 7 of which are sub-Saturnian ($M \sin i < 0.3 M_J$). We also detected 5 significant RV trends, three of which are demonstrably from stellar (rather than planetary-mass) companions. In cases where the planet or stellar companions were already known, we provide updated orbital parameters and $M \sin i$ values.

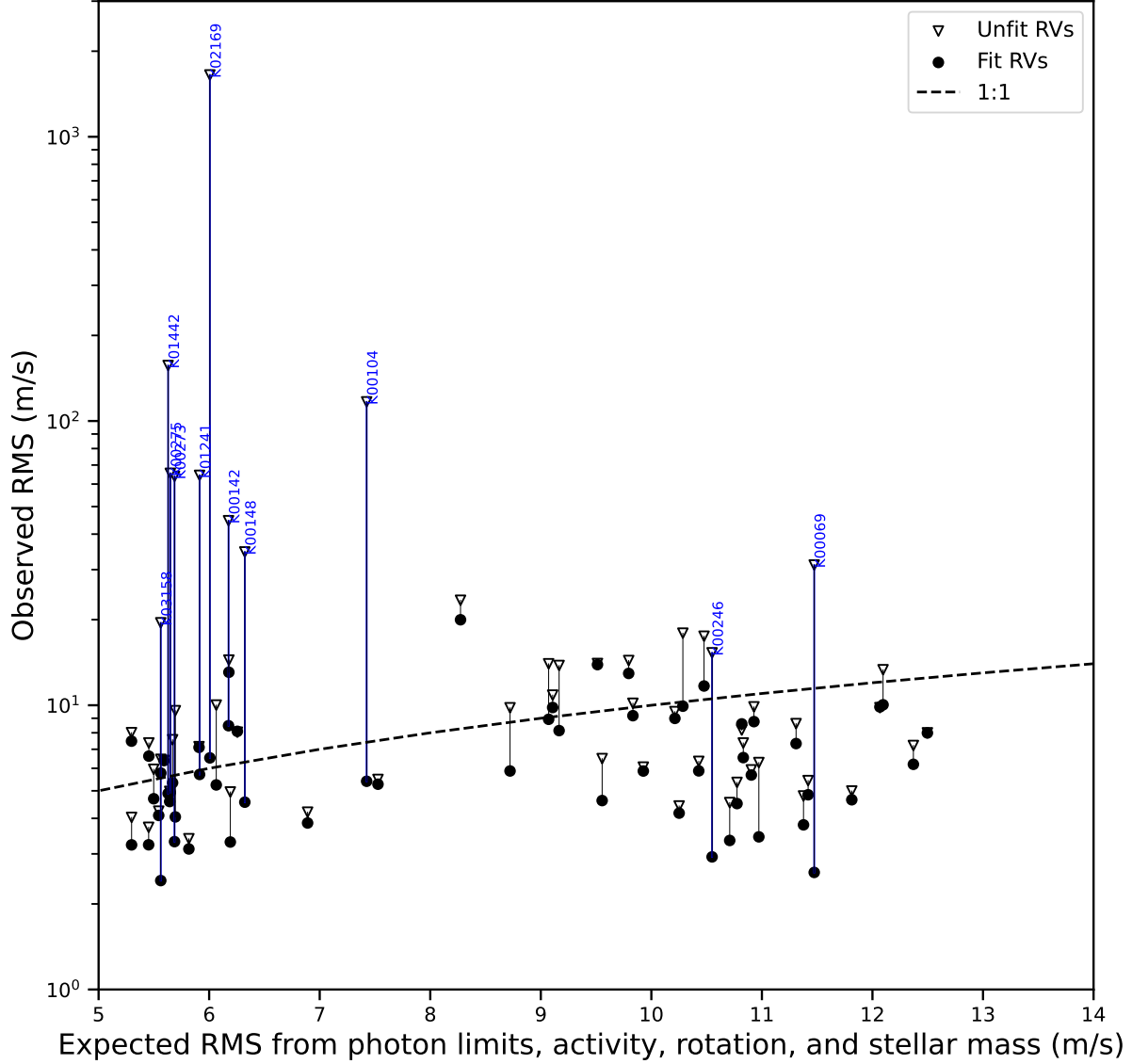


Figure 3: Observed RMS scatter of the RVs vs. expected RMS from jitter. The jitter is computed based on the Mt. Wilson S_{HK} index, the stellar mass, the stellar rotation, and photon limits. The vertical axis for triangles shows the RMS of the unfit (raw) RVs, the vertical axis for dots shows the RMS of the residuals to the best-fit model that includes transiting planets and any detected non-transiting planets and companions. The RVs for some systems had significant reductions in their RMS (factor of 5 or more) when the model included a massive companion (blue).

An overview of each star’s observing program is presented in Table 3. The resulting planetary system architectures and physical properties are presented in Table 4, and the orbital properties of the non-transiting planets are presented in Table 5.

5.1. Preliminary Architectural Patterns

Visualizations of the system architecture are presented in Figure 4. Each row corresponds to a planetary system, and the systems are ranked by the semi-major axis of the innermost known planet (typically, a transiting planet). Each body (planetary or stellar) orbiting the primary star is indicated with a circle, and the circle size is scaled to the square root of the body’s mass or $M \sin i$, if known. In cases where the RVs were insufficient to meaningfully constrain the planet mass, a mass-radius relationship was assumed (Weiss & Marcy 2014). Each circle is colored by the object’s eccentricity, if known (the transiting planets are assumed to have zero eccentricity.)

A few notable patterns emerge in Figure 4. The two most massive objects in our survey, Kepler-444 BC (represented by a single circle with the combined mass of Kepler-444 B and Kepler-444 C) and Kepler-1130 B, are also the most eccentric objects in our survey, and they accompany systems of high-multiplicity, small planets: the Kepler-444 planets are Mars-sized, and the Kepler-1130 planets are Earth-sized. In both of these systems, the periastron passage distance of the stellar-mass companion(s) with respect to the primary are on the order of a few AU, well inside the typical physical extent of a forming protoplanetary disc of ~ 100 AU (Weiss et al. 2022). It is likely that these stellar-mass companions truncated the protoplanetary disks in which the small planets formed, leaving less rocky material in the innermost ~ 1 AU of the disk from which the planets formed that is typical for stars that do not have such close-approaching companions. Discovering more systems with architectures analogous to Kepler-444 and Kepler-1130 is critical for building a sample from which to study the effect of eccentric S-type binary stars on the formation and architectures of planetary systems.

In contrast, the Jovian-mass planets we detected are not associated with particularly small or particularly close-in planets. Figure 5 shows the semi-major axes and masses of the bodies of Figure 4, including the transiting planets and their RV-detected companions. Systems that contain a Jovian-mass or larger body are shown in color, with the color corresponding to the mass of the most massive companion detected in the system. Two of these massive companions are transiting: KOI-94 d (Kepler-89 d) and KOI-351 h (Kepler-90 h), whereas the other companions were all detected via RVs (and in the case of Kepler-444, also direct imaging), and either do not transit or have not yet been detected in transits. The KGPS survey spans seven orders of magnitude in companion mass and four orders of magnitude in orbital separation.

5.2. Upper Limits on Companion Masses

It is desirable to have a constraint on the $M \sin i$ upper limit for companions in each system based on the RVs. For each system, we used the best-fit model output from KGPS but allowed dv/dt to vary to test the hypothesis that the RVs have some long-term trend consistent with the presence of a long-period companion on a circular orbit ($P \gtrsim 4 \times$ the RV baseline, typically $\gtrsim 10$ AU). The absence of a significant trend or significant peaks in the Lomb-Scargle periodogram via KGPS generally rules out the presence of any companions with $M \sin i \gtrsim 1 M_J$ within 10 AU with 3σ confidence, although the exact upper limits depend on the RV baseline, the number of RVs, and RMS. The 3σ upper limits on $M \sin i$ for all the *Kepler* systems are shown in Figure 6. All of the cases where the upper limit on $M \sin i$ is larger than $10 M_J$ at 10 AU correspond to systems with detected long-period planets. There is typically sufficient freedom in the fit to the orbital parameters of the long-period non-transiting planets, especially massive ones, that a large value of dv/dt cannot be ruled out. These same dv/dt upper limits typically correspond to $M \sin i < 1 M_J$ at 5 AU, which is interior to the nominal lowest period of $4 \times$ the RV baseline for most systems, but in combination with a non-detection in the Lomb-Scargle periodogram, the lack of a significant trend rules out the majority of possible Jovian companions interior to 5 AU. Detailed injection-recovery to determine each star’s sensitivity to planets as a function of mass and orbital period will be addressed in Paper II of this series.

6. DISCUSSION

Intriguingly, the presence of Jupiter class planets has an unknown effect on the formation of temperate terrestrial planets in the Earth and Venus regime. Giant planets form early during planet formation, while the protoplanetary disk still has substantial gases. A nascent giant planet sculpts the distribution of gases and solids in the protoplanetary disk, potentially creating gaps and/or ring structures. These radial features form sites where the agglomeration of solids—which is essential for forming a next generation of small planets—is either enhanced or suppressed. Accordingly, giant planets are predicted to either hinder or help the formation of small planets, depending on whether pairwise planetesimal collisions (e.g., Walsh et al. 2011; Levison & Agnor 2003) or pebble accretion (e.g., Chen et al. 2020; Schlecker et al. 2021) is the dominant mode of small planet formation.

The radial velocity data presented here are currently the largest collection for planet host stars detected by Kepler in terms of number of systems observed and the time baselines of the RVs. This study is an extension of the Cumming

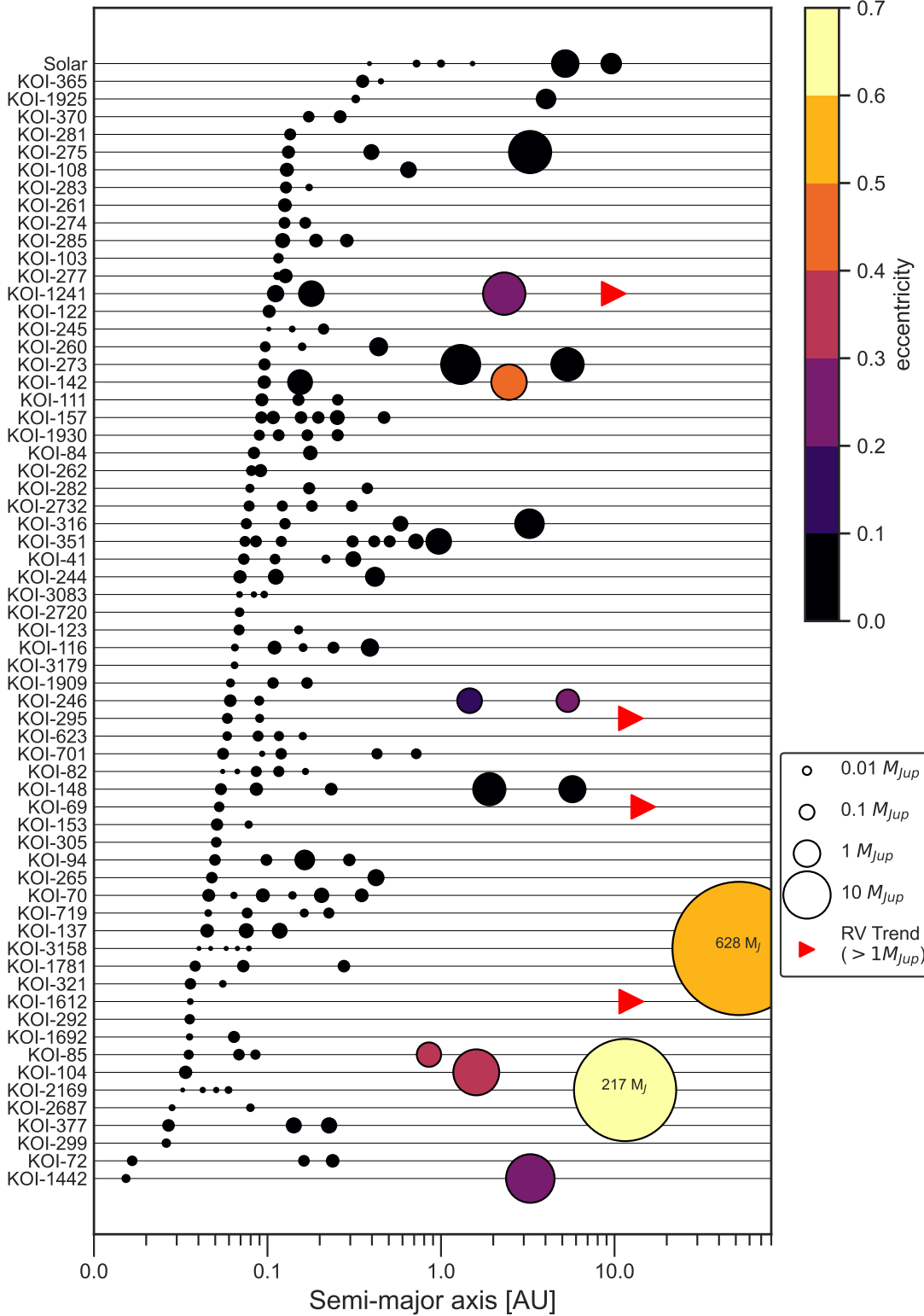


Figure 4: Architectures of the KGPS I planetary systems. Systems are ranked by the semi-major axis of the innermost known (transiting) planet. Point sizes scale with the square root of planet masses, $M \sin i$'s, or mass estimates from the [Weiss & Marcy \(2014\)](#) mass-radius relationship. Colors correspond to eccentricities (if measured); low-mass planets are assumed to have circular orbits.

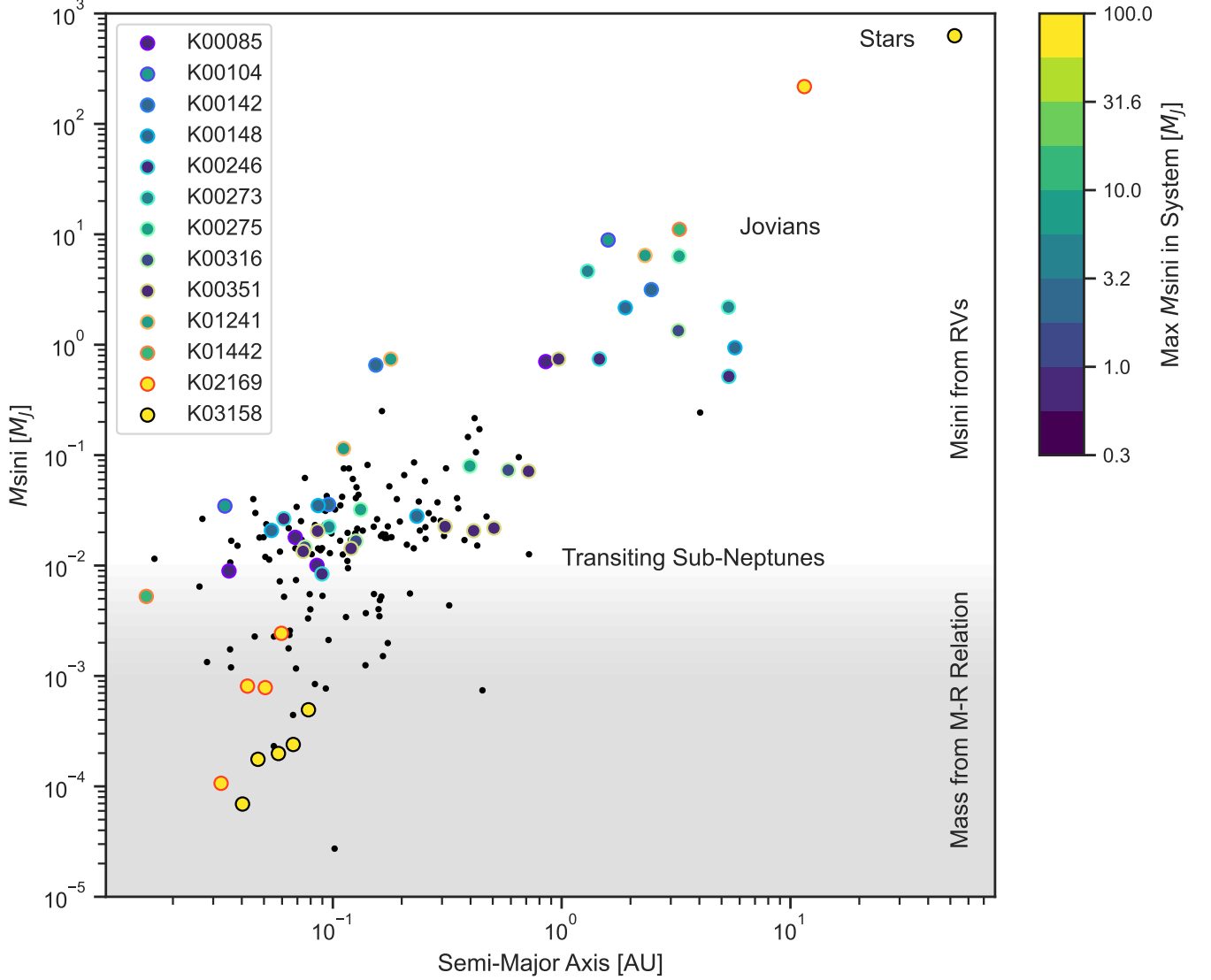


Figure 5: The Masses (or $M \sin i$ values or mass estimates) vs. semi-major axes of the KGPS-I transiting planets and companions. For systems with a giant planet ($M \sin i > 0.3 M_J$), the circle fill color corresponds to the maximum detected companion mass in the system (capped at 100 Jupiter masses), and the edge color encircling each point corresponds to the planetary system. Black dots correspond to transiting planets in our survey for which giant planets were not detected. Planet masses or $M \sin i$ values are reported where they are measured, but mass estimates are used for $m \lesssim 3 \times 10^{-2} M_J$ (see text for details). Companions that have eccentric, stellar-mass companions at large separations (KOIs 2169 and 3158, yellow) have planets that are smaller and closer to their stars than the typical transiting planets from the KGPS sample, whereas transiting planets that have giant planet companions (non-yellow colors) have comparable sizes and orbits to the transiting planets without detected giant planet companions.

et al. (2008) result that provided early insight in the frequency of massive planets around sun-like stars, based on one decade of Keck-HIRES RV data. Contemporary studies by Rosenthal et al. (2021, 2022) have extended the RV baselines from 10 to 30 years and increased the total number of stars, yielding ever more distant giant planets and an improved characterization of giant planet occurrence in field stars. While these legacy RV studies have established the occurrence of Jupiter-like planets for sun-like field stars, they are largely insensitive to the *Kepler*-like planets ($\sim 10 M_\oplus$, $P \sim 30$ days) that we know are also abundant around sun-like stars (Batalha et al. 2013; Fressin et al. 2013; Petigura et al. 2013; Bryson et al. 2021, and references therein).

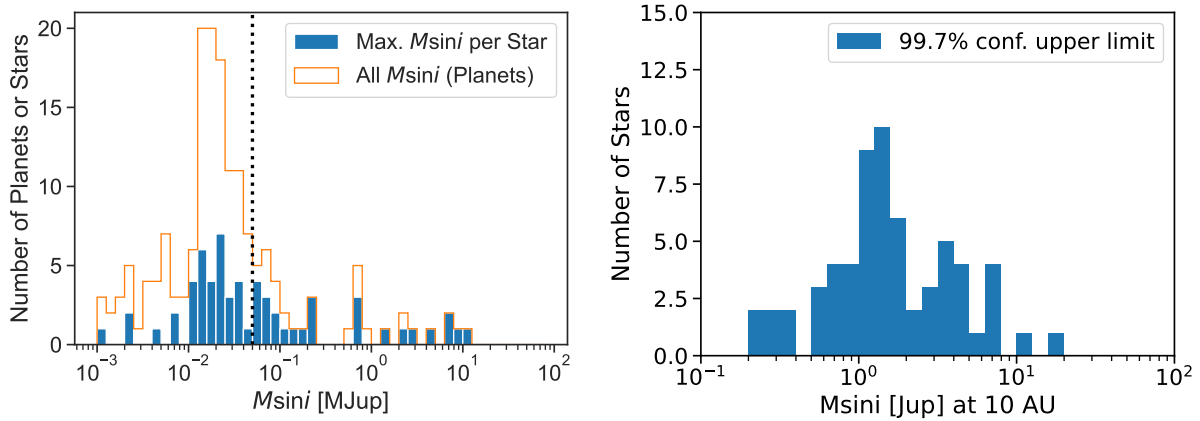


Figure 6: Left: The $M \sin i$ values (measured or estimated from the [Weiss & Marcy 2014](#) mass-radius relation) of all the transiting and non-transiting planets in KGPS I (orange histogram), and the maximum $M \sin i$ value per star (blue). Right: Upper limits on $M \sin i$ for *Kepler* stars with RVs. The upper limits are based on the best-fit model in which a linear trend (dv/dt) is adopted.

The current work presents a similar search for giant planets to the RV legacy surveys, but every star hosts a transiting planet or planets with known radii, and in some cases masses. While knowing the frequency of cool and cold giant planets is valuable in itself, the presence of those planets around systems of small transiting planets in the super-Earth and mini-Neptune regime can be used to test the predictions of various theories of planet formation. The presence or absence of Jupiter mass planets in the systems of compact multi-planet systems ([Jontof-Hutter et al. 2018](#)), especially those in and near orbital resonance, will be invaluable to the theorists exploring how these systems arose, changed, and settled into their final states. For several stars, the first ~ 3 RVs collected were insufficient for detecting a giant planet (e.g., KOI-316) or accurately characterizing orbital properties (e.g., KOI-2169). These cases provide nice examples of why stopping RV follow-up after obtaining just a few RVs can lead to a gross mischaracterization of the system architecture. Long-term RV monitoring with many visits (at least 10) seems necessary to accurately map the architectures of long-period companions.

While the RV precision needed to detect Jupiter mass planets has existed for nearly 30 years [Marcy & Butler \(1992\)](#), a significant portion of that time had to pass in order to measure their orbital periods. Designing and maintaining a long-term RV monitoring program is challenging, particularly in an era in which telescope time-allocation committees expect short-term results.⁶ This work reflects that richness of a data set that has had the proper time to age. This work presents a marked improvement upon the early glimpse of the giant planet companions to *Kepler* planets revealed in [Marcy et al. \(2014\)](#), in terms of the number of giant planets and the characterization of their orbits, as well as a more complete view of the systems of small transiting planets that do not have giant companions. Future papers in the KGPS series will explore the relationship between small and giant planets revealed through this unique data set. Patterns in the relationship between giant planets and small (including terrestrial) planets might reveal how Jupiter affected our own small planets and whether this formation channel is common or rare.

7. CONCLUSION

This is the first paper in a series called the Kepler Giant Planet Search. In this paper, we presented RVs and best-fit Keplerian orbital solutions based on a decade of observations of the NASA *Kepler* field with the W. M. Keck Observatory HIRES instrument. These constitute 2858 RVs in total, collected for 63 stars, the majority of which (56) constitute a homogeneous, magnitude-limited survey of RV-quiet, sun-like stars. Our RVs improved the mass determinations for 84 transiting planets and revealed 27 planets that are not known to transit, 8 of which are announced here for the first time. Future papers will address architectural patterns observed in these planetary systems, our detection efficiency, and the joint occurrence of giant planets and small transiting planets.

⁶ Even the so-called long-term, multi-semester programs offered at major observatories are typically capped at 2 years, or 1/5 the length of our observing effort.

Facilities: Kepler,Keck:I,TNG,OHP:1.93m

Software: astropy,radvel,rvsearch,kgps

This work would not have been possible without the generosity of various time allocations committees that provided support in the form of Keck-HIRES observing time over a decade. We acknowledge support in the form of observational resources at W. M. Keck Observatory from the following institutions: NASA, the University of Hawai‘i, the University of California, California Institute of Technology, and the University of Notre Dame. We acknowledge support from the NASA-Keck Key Strategic Mission Support program (grant no. 80NSSC19K1475), NASA Exoplanet Research Program (grant no. 80NSSC23K0269), and NASA JPL RSAs 1537000, 1607073, and 1633061. E.B.F. acknowledges the support of the Pennsylvania State University, the Penn State Eberly College of Science and Department of Astronomy & Astrophysics, the Center for Exoplanets and Habitable Worlds and the Center for Astrostatistics.

This work was supported by a NASA Keck PI Data Award, administered by the NASA Exoplanet Science Institute. Data presented herein were obtained at the W. M. Keck Observatory from telescope time allocated to the National Aeronautics and Space Administration through the agency’s scientific partnership with the California Institute of Technology and the University of California. The Observatory was made possible by the generous financial support of the W. M. Keck Foundation.

This dataset made use of the NASA Exoplanet Science Institute at IPAC, which is operated by the California Institute of Technology under contract with the National Aeronautics and Space Administration.

The authors thank Fred Adams, Konstantin Batygin, Juliette Becker, Tony Bloch, Sarah Blunt, Paul Dalba, Bekki Dawson, Matthias He, Lea Hirsch, Jack Lissauer, Jack Lubin, Sarah Millholland, Alan Reyes, Lee Rosenthal, Evan Sinukoff, Judah van Zandt, Josh Winn, and Jason Wright for helpful conversations.

The authors wish to recognize and acknowledge the very significant cultural role and reverence that the summit of Maunakea has always had within the indigenous Hawaiian community. We are most fortunate to have the opportunity to conduct observations from this mountain.

Star	BJD	RV(m s ⁻¹)	error(m s ⁻¹)	S-value	log(R'_{HK})
hip94931	6109.92011900	13.66	1.12	0.176	-5.01
hip94931	6110.83062200	16.97	1.26	0.178	-5.01
hip94931	6111.89694800	12.98	1.16	0.180	-5.00
hip94931	6112.86924400	14.24	1.19	0.177	-5.01
hip94931	6113.80918900	19.82	1.22	0.180	-5.00
hip94931	6114.83172700	19.03	1.21	0.176	-5.02
hip94931	6115.85339700	17.17	1.04	0.177	-5.01
hip94931	6133.92901300	18.14	1.22	0.175	-5.02
hip94931	6134.96738100	19.52	1.24	0.177	-5.01
hip94931	6138.03081300	14.57	1.27	0.177	-5.01

Table 2. Results of KGPS Automated Planet and Trend Search

KOI	nRVs	Baseline	Last Obs.	New Comp. Num.	Period	K	RMS	FAP	ΔBIC
		(years)			(d)	m s^{-1}	m s^{-1}		
K00041	134	13.4	2022-11-14	4.5
K00041	134	13.4	2022-11-14	1	60.9	3.8	3.8	0.00002	-45.9
K00069	184	13.1	2022-09-06	29.8
K00069	184	13.1	2022-09-06	trend	2.7	0.0	-837.2
K00070	143	9.1	2018-09-30	6.2
K00070	143	9.1	2018-09-30	1	35.0	4.3	5.4	0.00493	-29.5
K00072	226	10.0	2019-08-20	4.0
K00072	226	10.0	2019-08-20	1	25.5	1.7	3.8	0.03815	-18.9
K00082	73	9.3	2019-08-29	3.9
K00084	124	7.9	2017-07-29	5.6
K00084	124	7.9	2017-07-29	1	28.5	3.8	4.9	0.02454	-24.0
K00085	79	11.1	2022-06-15	13.7
K00085	79	11.1	2022-06-15	1	257.9	20.7	7.4	0.0	-80.2
K00094	72	7.3	2017-04-10	9.0
K00103	21	12.2	2021-10-29	8.0
K00104	39	12.0	2022-06-14	111.4
K00104	39	12.0	2022-06-14	1	811.7	231.4	8.4	0.00079	-1205.7
K00108	28	12.2	2021-10-29	6.6
K00111	44	11.3	2021-10-26	4.5
K00116	48	9.8	2019-08-18	6.0
K00116	48	9.8	2019-08-18	1	90.6	7.0	3.5	0.00174	-44.6
K00122	36	7.9	2017-07-29	4.9
K00123	38	10.9	2020-08-10	6.3
K00137	25	8.8	2018-06-29	5.2
K00142	58	9.0	2022-06-19	44.1
K00142	58	9.0	2022-06-19	1	22.2	56.2	27.8	0.00043	-144.8
K00142	58	9.0	2022-06-19	2	1370.3	54.9	10.2	0.00175	-114.7
K00148	59	12.8	2022-06-14	32.6
K00148	59	12.8	2022-06-14	1	998.1	45.5	9.1	0.0	-173.2
K00153	42	12.1	2022-06-07	8.1
K00157	31	11.6	2022-04-20	7.8
K00244	69	11.2	2021-09-27	8.6
K00244	69	11.2	2021-09-27	1	91.5	9.0	5.9	0.00009	-45.0
K00245	218	12.4	2022-09-06	3.6
K00245	218	12.4	2022-09-06	1	458.0	2.0	3.2	0.00001	-20.0
K00245	218	12.4	2022-09-06	2	15.0	1.7	2.9	0.00197	-22.2
K00246	96	12.2	2022-07-15	14.8
K00246	96	12.2	2022-07-15	1	635.7	18.2	3.8	0.0	-244.3
K00246	96	12.2	2022-07-15	2	362.3	5.1	2.9	0.00003	-55.9
K00260	35	5.3	2019-11-11	10.1
K00260	35	5.3	2019-11-11	trend	9.8	0.98921	5.2
K00261	55	10.9	2021-06-19	6.7
K00262	39	9.8	2022-04-02	trend	13.9	0.99485	6.7

Table 2 continued on next page

Table 2 (*continued*)

KOI	nRVs	Baseline	Last Obs.	New Comp. Num.	Period	K	RMS	FAP	ΔBIC
		(years)			(d)	m s^{-1}	m s^{-1}		
K00262	39	9.8	2022-04-02	14.0
K00265	49	10.8	2022-06-11	4.6
K00265	49	10.8	2022-06-11	1	93.9	4.5	3.3	0.03644	-27.6
K00273	116	12.1	2022-09-12	63.8
K00273	116	12.1	2022-09-12	1	525.4	113.5	12.4	0.0	-1318.0
K00273	116	12.1	2022-09-12	2	4447.5	24.3	5.1	0.0	-76.9
K00274	17	7.9	2018-06-25	8.1
K00275	35	7.8	2022-06-15	65.4
K00275	35	7.8	2022-06-15	1	1901.3	89.3	4.5	0.00017	-424.7
K00277	25	9.2	2021-10-11	7.5
K00281	11	10.1	2021-09-15	4.1
K00282	10	6.9	2021-07-27	5.9
K00283	46	6.9	2017-08-05	4.8
K00285	23	9.9	2021-06-24	5.8
K00292	31	8.0	2018-07-09	5.8
K00295	14	10.7	2022-05-16	17.6
K00295	14	10.7	2022-05-16	trend	11.7	0.99948	-12.6
K00299	42	7.9	2018-06-23	7.1
K00305	45	7.0	2017-08-06	5.3
K00316	38	11.8	2022-06-10	9.3
K00321	58	11.9	2022-05-13	4.6
K00351	34	11.2	2022-06-14	9.2
K00365	28	7.0	2017-07-09	3.1
K00370	11	6.8	2021-07-09	13.9
K00370	11	6.8	2021-07-09	trend	12.9	1.0	0.8
K00377	49	11.7	2022-02-22	11.4
K00377	49	11.7	2022-02-22	trend	10.0	0.98636	-7.0
K00623	11	7.0	2021-09-12	9.0
K00701	17	4.8	2017-05-13	5.3
K00719	10	9.8	2021-07-09	5.4
K01241	47	10.1	2022-06-18	49.6
K01241	47	10.1	2022-06-18	1	971.5	97.6	7.9	0.00019	-295.6
K01241	47	10.1	2022-06-18	trend	48.0	0.00019	-10.4
K01442	98	11.0	2022-05-10	1	2068.6	172.4	5.6	0.0	-3854.9
K01442	98	11.0	2022-05-10	123.6
K01612	56	11.1	2022-06-21	6.5
K01612	56	11.1	2022-06-21	trend	4.6	0.01541	-30.0
K01692	14	10.8	2022-06-11	trend	13.1	1.0	1.8
K01692	14	10.8	2022-06-11	13.5
K01781	14	9.7	2022-02-21	22.6
K01781	14	9.7	2022-02-21	trend	20.0	1.0	-1.2
K01909	11	6.1	2021-09-19	8.8
K01925	97	10.7	2022-11-14	4.1
K01925	97	10.7	2022-11-14	1	344.9	4.1	3.2	0.00037	-36.3
K01930	11	7.0	2021-09-21	8.8

Table 2 *continued on next page*

Table 2 (*continued*)

KOI	nRVs	Baseline	Last Obs.	New Comp. Num.	Period	K	RMS	FAP	ΔBIC
		(years)			(d)	m s^{-1}	m s^{-1}		
K02169	34	10.2	2022-09-13	1649.3
K02169	34	10.2	2022-09-13	1	6226.4	2244.6	56.7	0.00133	-227801.5
K02687	26	9.3	2021-06-23	7.3
K02720	22	6.3	2018-08-06	4.4
K02732	11	6.0	2021-08-15	9.2
K03083	11	6.2	2021-10-29	6.4
K03158	207	9.8	2022-04-11	19.5
K03158	207	9.8	2022-04-11	1	72.4	1.5	2.4	0.00169	-27.1
K03158	207	9.8	2022-04-11	trend	2.6	0.0	-820.5
K03179	11	7.9	2021-07-09	9.9

Table 3. Stellar Properties and RV Data Summary

KOI	g mag	M_{\star} (M_{\odot})	[Fe/H]	NTP	NSS	NGP	NSC	NRV	ΔT (years)	RV RMS (m s^{-1})	σ_{jit} (m s^{-1})	dv/dt (S/N)	$< M \sin i$ at 10 AU (M_{J} , 99.7% conf.)
41	11.1	1.12	0.12	3	1	0	0	134	13.4	3.3	10.3	2.7	0.22
69	9.9	0.89	-0.20	1	0	0	0	184	13.1	2.6	11.2	112.3	7.41
70	12.5	0.93	0.04	5	1	0	0	143	9.1	5.3	4.6	2.0	1.43
72	10.9	0.90	-0.17	2	1	0	0	226	10.0	3.8	11.0	0.1	0.29
82	11.5	0.80	0.10	5	0	0	0	73	9.3	3.9	6.3	1.6	0.75
84	11.9	0.88	-0.12	1	1	0	0	124	7.9	4.7	4.6	3.2	1.39
85	11.0	1.24	0.09	3	0	1	0	79	11.1	8.1	8.7	1.5	1.51
94	12.2	1.20	0.04	4	0	0	0	72	7.3	8.9	8.5	1.8	1.44
103	12.6	0.93	-0.07	1	0	0	0	21	12.2	8.0	12.1	0.3	1.23
104	12.9	0.82	0.22	1	0	1	0	39	12.0	5.4	6.6	5.4	2.89
108	12.2	1.15	0.14	2	0	0	0	28	12.2	6.5	10.4	0.4	0.93
111	12.6	0.84	-0.53	3	0	0	0	44	11.3	4.5	10.3	0.1	0.33
116	12.8	0.97	-0.10	4	1	0	0	48	9.8	3.4	10.4	1.2	0.69
122	12.3	1.12	0.33	1	0	0	0	36	7.9	4.8	11.0	1.1	1.07
123	12.3	1.03	-0.06	2	0	0	0	38	10.9	5.9	9.9	2.3	0.67
137	13.5	0.97	0.32	3	0	0	0	25	8.8	5.2	4.7	0.2	1.02
142	13.1	0.98	0.29	1	0	2 ^A	0	58	9.0	8.5	4.8	2.0	1.96
148	13.1	0.91	0.26	3	0	2	0	59	12.8	4.6	5.2	6.3	1.97
153	13.5	0.77	0.12	2	0	0	0	42	12.1	8.0	2.5	0.8	1.23
157	13.7	1.00	0.05	6	0	0	0	31	11.6	7.3	10.6	1.2	1.58
244	10.6	1.14	-0.15	2	1	0	0	69	11.2	5.9	8.3	0.1	0.55
245	9.5	0.80	-0.43	3	0	0	0	218	12.4	3.2	4.8	1.4	0.26
246	9.9	1.06	0.11	2	0	2	0	96	12.2	2.9	10.2	0.3	0.21
260	10.5	1.08	-0.32	3	0	0	0	35	5.3	9.8	8.7	1.0	12.03
261	10.3	1.01	0.01	1	0	0	0	55	10.9	6.2	12.1	3.0	1.08
262	10.4	1.10	-0.16	2	0	0	0	39	9.8	13.9	9.1	0.8	7.43
265	11.9	1.17	0.12	1	1	0	0	49	10.8	3.3	5.4	0.1	0.51
273	11.4	1.08	0.34	1	0	2	0	116	12.1	3.3	4.9	8.7	2.51
274	11.3	1.12	-0.13	2	0	0	0	17	7.9	8.1	5.6	0.3	1.50
275	11.6	1.24	0.25	2	0	1	0	35	7.8	4.9	4.8	2.1	4.09
277	12.1	0.97	-0.22	2	0	0	0	25	9.2	7.5	4.4	0.1	0.99
281	11.9	0.86	-0.50	1	0	0	0	11	10.1	4.1	4.6	0.4	0.66
282	11.8	0.90	-0.26	3	0	0	0	10	6.9	5.9	9.5	0.1	1.91
283	11.5	1.06	0.18	2	0	0	0	46	6.9	4.7	11.5	1.8	1.23
285	11.7	1.25	0.19	3	0	0	0	23	9.9	5.8	4.8	0.1	0.94
292	12.8	0.91	-0.22	1	0	0	0	31	8.0	5.7	10.3	1.3	1.24
295	12.2	0.97	-0.22	2	0	0	0	14	10.7	11.7	10.0	4.7	4.11
299	12.9	0.98	0.09	1	0	0	0	42	7.9	7.1	4.8	0.5	1.19

Table 3 continued on next page

Table 3 (*continued*)

KOI	g mag	M_{\star} (M_{\odot})	[Fe/H]	NTP	NSS	NGP	NSC	NRV	ΔT (years)	RV RMS (m s^{-1})	σ_{jit} (m s^{-1})	dv/dt (S/N)	$< M \sin i$ at 10 AU (M_{J} , 99.7% conf.)
305	13.0	0.81	0.13	1	0	0	0	45	7.0	5.3	6.7	0.5	1.18
316	12.7	1.08	0.38	3	0	1	0	38	11.8	4.0	4.6	0.4	1.34
321	12.5	1.06	0.30	2	0	0	0	58	11.9	4.6	4.6	0.3	0.54
351	13.7	1.11	0.14	8	0	1 ^B	0	34	11.2	9.9	9.4	0.5	1.80
365	11.2	0.87	-0.18	2	0	0	0	28	7.0	3.1	5.1	0.3	0.83
370	11.9	1.20	0.01	2	0	0	0	11	6.8	12.9	9.3	1.2	6.33
377	13.8	1.03	0.00	3	0	0	0	49	11.7	10.0	11.4	0.4	1.89
623	11.8	0.85	-0.59	4	0	0	0	11	7.0	9.0	9.8	0.1	3.05
701	13.7	0.68	-0.37	5	0	0	0	17	4.8	5.2	2.5	0.6	2.56
719	12.9	0.73	0.08	4	0	0	0	10	9.8	5.4	2.5	0.1	1.36
1241	12.4	1.46	0.42	2	0	2 ^A	0	47	10.1	5.7	5.0	2.0	6.98
1442	12.5	1.08	0.38	1	0	1	0	98	11.0	4.9	4.6	8.4	4.27
1612	8.7	1.02	-0.27	1	0	0	0	56	11.1	4.6	9.2	1.3	1.42
1692	12.5	1.00	0.34	2	0	0	0	14	10.8	13.1	5.2	0.8	3.18
1781	12.2	0.83	0.18	3	0	0	0	14	9.7	20.0	7.7	2.2	4.32
1909	12.7	1.01	0.03	3	0	0	0	11	6.1	8.6	10.3	0.7	3.27
1925	9.4	0.93	0.09	1	1	0	0	97	10.7	3.2	4.7	0.6	0.39
1930	12.1	1.06	-0.02	4	0	0	0	11	7.0	8.8	10.5	0.4	3.37
2169	12.4	0.94	0.06	4	0	0	1	34	10.2	6.5	5.1	0.5	19.14
2687	10.1	1.01	-0.01	2	0	0	0	26	9.3	6.6	4.8	2.1	1.90
2720	10.3	1.00	-0.15	1	0	0	0	22	6.3	4.2	9.9	1.3	1.43
2732	12.8	1.21	0.00	4	0	0	0	11	6.0	9.2	9.2	0.3	3.74
3083	12.8	1.16	0.29	3	0	0	0	11	6.2	6.4	4.4	0.2	2.23
3158	8.6	0.73	-0.54	5	0	0	1	207	9.8	2.4	5.0	35.7	5.67
3179	12.1	0.99	-0.04	1	0	0	0	11	7.9	9.9	11.6	0.1	3.17

NOTE—A – KOI-142 and KOI-1241 each have one non-transiting giant interior to 1 AU that count toward the total number of giant planets in this table. B – KOI-351 has a transiting giant planet at 331 days (just interior to 1 AU) that counts toward the total number of giant planets in this table. Additional columns associated with this table are available in the machine-readable version.

Table 4. KGPS Planet Physical Properties

Name [†]	KOI	Per.	a	R_{pl}	K^*	$M \sin i^*$	ρ_p^*
		(d)	(AU)	(R_{\oplus})	(m s^{-1})	(M_{\oplus})	(g cm^{-3})
Kepler-100 b	41.02	6.89	0.073	1.34±0.13	1.7±0.4	5.4±1.3	12±4
Kepler-100 c	41.01	12.8	0.11	2.34±0.08	1.0±0.4	4.0±1.7	1.7±0.7
Kepler-100 d	41.03	35.3	0.22	1.54±0.23	0.32±0.35	1.8±1.9	2.7±3.0
Kepler-100 e	41.10	60.89±0.04	0.31	...	3.7±0.5	24.1±3.3	...
Kepler-93 b	69.01	4.73	0.053	1.63±0.06	1.50±0.24	3.6±0.6	4.6±0.8
Kepler-93 B	K00069 B	> 19141	> 15	...	> 89
Kepler-20 b	70.02	3.7	0.046	2.01±0.18	4.1±0.6	9.5±1.5	6.5±1.4
Kepler-20 e	70.04	6.1	0.064	0.78±0.10	...	0.56	6.5
Kepler-20 c	70.01	10.9	0.094	2.88±0.13	4.1±0.7	13.6±2.3	3.1±0.6
Kepler-20 f	70.05	19.6	0.14	0.94±0.04	...	1.2	7.8
Kepler-20 g	70.10	34.95±0.04	0.21	...	4.3±0.7	21.0±3.4	...
Kepler-20 d	70.03	77.6	0.35	2.49±0.07	2.0±0.7	13±4	4.6±1.5
Kepler-10 b	72.01	0.837	0.017	1.49±0.04	2.72±0.32	3.7±0.4	6.1±0.8
Kepler-10 c	72.02	45.3	0.24	2.34±0.06	2.4±0.5	12.1±2.6	5.2±1.1
Kepler-102 b	82.05	5.29	0.055	0.471±0.024	...	0.074	3.9
Kepler-102 c	82.04	7.07	0.067	0.554±0.026	...	0.14	4.6
Kepler-102 d	82.02	10.3	0.086	1.34±0.09	1.5±0.7	4.5±1.9	10±5
Kepler-102 e	82.01	16.1	0.12	2.41±0.14	1.4±0.6	4.7±2.1	1.9±0.8
Kepler-102 f	82.03	27.5	0.17	0.753±0.033	...	0.48	6.2
Kepler-19 b	84.01	9.29	0.084	2.30±0.06	2.4±0.7	7.4±2.1	3.3±1.0
Kepler-19 c	84.10	28.52±0.08	0.18	...	3.7±0.8	16.6±3.5	...
Kepler-65 b	85.02	2.15	0.035	1.52±0.09	1.2±1.1	2.8±2.6	4±4
Kepler-65 c	85.01	5.86	0.069	2.58±0.06	1.7±1.2	6±4	1.8±1.3
Kepler-65 d	85.03	8.13	0.085	1.78±0.11	0.9±1.0	3.2±3.5	3.1±3.4
Kepler-65 e	85.10	257.2±0.8	0.85	...	20.4±2.0	223±22	...
KOI-94 b	94.04	3.74	0.05	1.64±0.12	2.1±1.4	6±4	7±5
KOI-94 c	94.02	10.4	0.099	3.86±0.10	1.6±1.5	6±6	0.6±0.5
KOI-94 d	94.01	22.3	0.16	10.31±0.24	16.2±1.8	80±9	0.40±0.05
KOI-94 e	94.03	54.3	0.3	6.12±0.14	1.2±1.2	8±8	0.19±0.20
K00103.01	103.01	14.9	0.12	2.59±0.07	1.0±1.6	3±6	1.1±1.8
Kepler-94 b	104.01	2.51	0.034	3.04±0.12	5.9±1.4	11.0±2.6	2.1±0.5
Kepler-94 c	104.10	816.4±0.7	1.6	...	236.0±3.1	(2.82±0.04)×10 ³	...
Kepler-103 b	108.01	16.0	0.13	3.26±0.08	3.2±1.6	14±7	2.2±1.1
Kepler-103 c	108.02	180.0	0.65	5.61±0.20	3.2±1.9	30±19	0.9±0.6
Kepler-104 b	111.01	11.4	0.093	2.38±0.06	3.2±0.9	9.9±2.8	4.1±1.2
Kepler-104 c	111.02	23.7	0.15	2.36±0.08	1.8±1.0	7±4	3.0±1.6
Kepler-104 d	111.03	51.8	0.25	2.63±0.14	1.1±0.9	6±5	1.7±1.4
Kepler-106 b	116.03	6.16	0.065	0.86±0.04	...	0.82	7.1

Table 4 *continued on next page*

Table 4 (continued)

Name [†]	KOI	Per.	a	R_{pl}	K^*	$M \sin i^*$	ρ_p^*
		(d)	(AU)	(R_{\oplus})	(m s^{-1})	(M_{\oplus})	(g cm^{-3})
Kepler-106 c	116.01	13.6	0.11	2.39±0.07	3.7±0.7	13.3±2.4	5.4±1.0
Kepler-106 d	116.04	24.0	0.16	1.01±0.06	...	1.5	8.3
Kepler-106 e	116.02	43.8	0.24	2.62±0.17	0.1±0.5	6.6±2.4	2.0±0.8
Kepler-106 f	116.10	90.64±0.24	0.39	...	6.8±0.8	46±6	...
Kepler-95 b	122.01	11.5	0.1	3.12±0.09	2.8±0.9	10.2±3.4	1.9±0.6
Kepler-109 b	123.01	6.48	0.069	2.33±0.07	1.5±1.3	5±4	2.0±1.7
Kepler-109 c	123.02	21.2	0.15	2.54±0.07	0.4±1.3	2±6	0.6±2.0
Kepler-18 b	137.03	3.5	0.045	1.81±0.21	5.4±1.7	13±4	12±4
Kepler-18 c	137.01	7.64	0.075	4.27±0.11	6.5±1.6	20±5	1.40±0.35
Kepler-18 d	137.02	14.9	0.12	5.11±0.13	6.3±1.7	24±6	0.99±0.27
KOI-142 b	142.01	10.9	0.096	3.80±0.20	3.3±1.5	11±5	1.1±0.5
KOI-142 c	142.10	22.2672±0.0006	0.15	...	47.7±1.7	208±7	...
KOI-142 d	142.11	1425±14	2.5	...	63.8±3.3	(1.00±0.05)×10 ³	...
Kepler-48 b	148.01	4.78	0.054	1.85±0.09	2.7±1.1	6.6±2.8	5.7±2.5
Kepler-48 c	148.02	9.67	0.086	2.56±0.07	3.5±1.0	11.1±3.3	3.6±1.1
Kepler-48 d	148.03	42.9	0.23	1.98±0.07	1.7±1.1	9±6	6±4
Kepler-48 e	148.10	998±4	1.9	...	46.6±1.3	687±20	...
Kepler-48 f	148.11	(5.2±0.4)×10 ³	5.7	...	12±4	(3.0±0.9)×10 ²	...
Kepler-113 b	153.02	4.75	0.051	2.00±0.07	3.3±1.5	7.5±3.4	5.2±2.3
Kepler-113 c	153.01	8.93	0.078	2.66±0.17	0.4±1.2	1.1±3.3	0.3±1.0
Kepler-11 b	157.06	10.3	0.092	1.92±0.06	2.2±2.2	7±7	6±6
Kepler-11 c	157.01	13.0	0.11	3.05±0.08	3.1±2.1	11±8	2.2±1.5
Kepler-11 d	157.02	22.7	0.16	3.38±0.10	0.0±1.4	8±6	1.2±0.9
Kepler-11 e	157.03	32.0	0.2	4.04±0.11	1.6±2.0	8±10	0.7±0.8
Kepler-11 f	157.04	46.7	0.25	2.85±0.21	3.3±2.2	18±12	4.4±3.0
Kepler-11 g	157.05	118.0	0.47	3.59±0.10	0.0±1.2	9±9	1.1±1.1
Kepler-25 b	244.02	6.24	0.069	2.70±0.06	3.4±1.0	10.8±3.1	3.0±0.9
Kepler-25 c	244.01	12.7	0.11	4.63±0.10	6.0±1.0	24±4	1.34±0.23
Kepler-25 d	244.10	91.61±0.24	0.42	...	8.9±1.1	69±9	...
Kepler-37 b	245.03	13.4	0.1	0.276±0.028	...	0.0087	2.3
Kepler-37 c	245.02	21.3	0.14	0.718±0.024	...	0.4	5.9
Kepler-37 d	245.01	39.8	0.21	1.91±0.05	...	4.9	3.9
Kepler-68 b	246.01	5.4	0.061	2.31±0.05	3.0±0.5	8.4±1.5	3.8±0.7
Kepler-68 c	246.02	9.61	0.09	0.927±0.034	0.8±0.6	2.7±1.9	18±13
Kepler-68 d	246.10	632.3±2.3	1.5	...	17.4±0.7	236±10	...
Kepler-68 e	246.11	(4.46±0.10)×10 ³	5.4	...	6.5±1.8	(1.6±0.5)×10 ²	...
Kepler-126 b	260.01	10.5	0.097	1.58±0.06	0.1±1.9	4±7	6±10
Kepler-126 c	260.03	21.9	0.16	1.61±0.11	0.3±1.5	1±7	2±9
Kepler-126 d	260.02	100.0	0.44	2.54±0.06	7.0±3.0	55±23	18±8
Kepler-96 b	261.01	16.2	0.13	2.37±0.06	3.2±1.2	13±5	5.3±1.9

Table 4 continued on next page

Table 4 (*continued*)

Name [†]	KOI	Per.	a	R_{pl}	K^*	$M \sin i^*$	ρ_p^*
		(d)	(AU)	(R_{\oplus})	(m s^{-1})	(M_{\oplus})	(g cm^{-3})
Kepler-50 b	262.01	7.81	0.081	1.54±0.05	0.0±2.6	4±9	6±13
Kepler-50 c	262.02	9.38	0.091	1.82±0.18	2.8±2.8	10±10	9±9
Kepler-507 b	265.01	3.57	0.048	1.28±0.04	2.2±0.6	5.7±1.5	15±4
Kepler-507 c	265.10	93.7±0.4	0.42	...	4.3±0.7	34±5	...
Kepler-454 b	273.01	10.6	0.096	1.84±0.06	2.0±0.5	7.1±1.7	6.3±1.5
Kepler-454 c	273.10	525.0±0.6	1.3	...	112.4±0.7	1474±10	...
Kepler-454 d	273.11	(4.40±0.17)×10 ³	5.4	...	26.1±2.0	(7.0±0.5)×10 ²	...
Kepler-128 b	274.01	15.1	0.13	1.43±0.06	...	6.2	12.0
Kepler-128 c	274.02	22.8	0.17	1.42±0.17	...	6.1	12.0
Kepler-129 b	275.01	15.8	0.13	2.29±0.07	2.3±1.4	10±6	4.7±2.9
Kepler-129 c	275.02	82.2	0.4	2.40±0.08	3.2±1.2	25±9	10±4
Kepler-129 d	275.10	1936±25	3.3	...	90.0±1.9	(2.01±0.04)×10 ³	...
Kepler-36 b	277.02	13.8	0.11	1.49±0.06	0.3±1.0	1±4	2±6
Kepler-36 c	277.01	16.2	0.13	3.96±0.14	4.0±2.2	16±9	1.4±0.8
Kepler-510 b	281.01	19.6	0.14	2.62±0.17	...	6.6	2.0
Kepler-130 b	282.02	8.46	0.079	1.04±0.04	...	1.7	8.6
Kepler-130 c	282.01	27.5	0.17	2.88±0.07	...	7.2	1.7
Kepler-130 d	282.03	87.5	0.38	1.38±0.08	...	5.4	11.0
Kepler-131 b	283.01	16.1	0.13	2.06±0.05	1.7±0.9	7±4	4.3±2.3
Kepler-131 c	283.02	25.5	0.17	0.806±0.035	...	0.63	6.6
Kepler-92 b	285.01	13.7	0.12	3.70±0.12	4.4±1.9	19±8	2.1±0.9
Kepler-92 c	285.02	26.7	0.19	2.45±0.07	2.3±1.9	13±10	5±4
Kepler-92 d	285.03	49.4	0.29	2.06±0.07	1.7±1.7	12±11	7±7
Kepler-97 b	292.01	2.59	0.036	1.62±0.09	1.7±1.3	3.4±2.5	4.4±3.3
Kepler-134 b	295.01	5.32	0.059	1.63±0.04	...	4.2	5.4
Kepler-134 c	295.02	10.1	0.09	1.03±0.04	...	1.7	8.5
K00295 B	K00295 B	> 15619	> 12	...	> 31
Kepler-98 b	299.01	1.54	0.026	1.87±0.13	1.1±1.2	2.1±2.1	1.7±1.8
Kepler-99 b	305.01	4.6	0.051	1.81±0.14	1.7±0.9	3.8±2.1	3.5±2.0
Kepler-139 d	316.03	7.31	0.076	1.70±0.06	1.5±0.6	4.7±2.0	5.3±2.3
Kepler-139 b	316.01	15.8	0.13	2.38±0.07	1.3±0.5	5.3±2.1	2.2±0.9
Kepler-139 c	316.02	157.0	0.58	2.45±0.08	2.6±0.5	23±5	8.7±1.8
Kepler-139 e	316.10	(2.05±0.07)×10 ³	3.2	...	20.4±2.0	(4.3±0.4)×10 ²	...
Kepler-406 b	321.01	2.43	0.036	1.45±0.04	2.4±0.8	5.3±1.8	9.6±3.2
Kepler-406 c	321.02	4.62	0.055	0.83±0.04	...	0.72	6.9
KOI-351 b	351.06	7.01	0.074	1.30±0.07	...	4.3	11.0
KOI-351 c	351.05	8.72	0.086	1.45±0.07	...	6.5	12.0
Kepler-90 i	...	14.4	0.12	1.32±0.21	...	4.5	11.0
KOI-351 d	351.03	59.7	0.31	2.87±0.09	...	7.2	1.7
KOI-351 e	351.04	91.9	0.41	2.61±0.09	...	6.6	2.0

Table 4 *continued on next page*

Table 4 (*continued*)

Name [†]	KOI	Per.	a	R_{pl}	K^*	$M \sin i^*$	ρ_p^*
		(d)	(AU)	(R_{\oplus})	(m s^{-1})	(M_{\oplus})	(g cm^{-3})
KOI-351 f	351.07	125.0	0.51	2.77 \pm 0.12	...	6.9	1.8
KOI-351 g	351.02	211.0	0.72	7.72 \pm 0.21	2.3 \pm 2.5	23 \pm 25	0.27 \pm 0.29
KOI-351 h	351.01	332.0	0.97	11.25 \pm 0.31	20.3 \pm 2.9	236 \pm 33	0.91 \pm 0.14
Kepler-538 b	365.01	81.7	0.35	2.16 \pm 0.05	1.7 \pm 0.8	10 \pm 5	5.7 \pm 2.7
Kepler-538 c	365.02	118.0	0.45	0.63 \pm 0.06	...	0.24	5.2
Kepler-145 b	370.02	23.0	0.17	2.22 \pm 0.08	...	5.7	2.8
Kepler-145 c	370.01	42.9	0.26	3.88 \pm 0.22	...	9.5	0.9
Kepler-9 d	377.03	1.59	0.027	1.51 \pm 0.05	4.5 \pm 2.3	8 \pm 4	14 \pm 7
Kepler-9 b	377.01	19.3	0.14	8.09 \pm 0.21	6.1 \pm 2.3	26 \pm 10	0.27 \pm 0.10
Kepler-9 c	377.02	38.9	0.23	8.11 \pm 0.22	5.1 \pm 2.7	27 \pm 14	0.28 \pm 0.15
Kepler-197 b	623.03	5.6	0.059	1.112 \pm 0.035	...	2.3	9.2
Kepler-197 c	623.01	10.3	0.088	1.31 \pm 0.04	...	4.4	11.0
Kepler-197 d	623.02	15.7	0.12	1.19 \pm 0.04	...	3.0	9.8
Kepler-197 e	623.04	25.2	0.16	0.93 \pm 0.11	...	1.1	7.6
Kepler-62 b	701.02	5.71	0.055	1.44 \pm 0.05	...	6.4	12.0
Kepler-62 c	701.05	12.4	0.093	0.64 \pm 0.04	...	0.24	5.2
Kepler-62 d	701.01	18.2	0.12	2.12 \pm 0.07	...	5.4	3.1
Kepler-62 e	701.03	122.0	0.43	1.87 \pm 0.07	...	4.8	4.0
Kepler-62 f	701.04	267.0	0.72	1.54 \pm 0.08	...	4.0	6.1
Kepler-220 b	719.04	4.16	0.046	0.834 \pm 0.035	...	0.72	6.9
Kepler-220 c	719.01	9.03	0.076	1.63 \pm 0.08	...	4.2	5.4
Kepler-220 d	719.02	28.1	0.16	1.03 \pm 0.11	...	1.7	8.5
Kepler-220 e	719.03	45.9	0.23	1.32 \pm 0.05	...	4.6	11.0
Kepler-56 b	1241.02	10.5	0.11	4.77 \pm 0.21	7.5 \pm 1.5	36 \pm 7	1.9 \pm 0.4
Kepler-56 c	1241.01	21.4	0.18	10.9 \pm 0.6	38.5 \pm 1.4	236 \pm 9	1.01 \pm 0.11
Kepler-56 d	1241.10	994 \pm 5	2.3	...	95.0 \pm 2.2	(2.04 \pm 0.05) \times 10 ³	...
Kepler-56 e	K01241 B	> 14686	> 10	...	> 120
Kepler-407 b	1442.01	0.669	0.015	1.16 \pm 0.04	1.2 \pm 0.6	1.7 \pm 0.8	5.9 \pm 2.9
Kepler-407 c	1442.10	2092 \pm 5	3.3	...	173.1 \pm 0.8	3524 \pm 16	...
Kepler-408 b	1612.01	2.47	0.036	0.710 \pm 0.028	...	0.38	5.9
K01612 B	K01612 B	> 16214	> 12	...	> 15
Kepler-314 b	1692.02	2.46	0.036	0.78 \pm 0.04	...	0.55	6.4
Kepler-314 c	1692.01	5.96	0.064	2.77 \pm 0.15	...	6.9	1.8
Kepler-411 b	1781.02	3.01	0.038	1.87 \pm 0.06	...	4.8	4.1
Kepler-411 c	1781.01	7.83	0.073	3.24 \pm 0.11	...	8.0	1.3
Kepler-411 d	1781.03	58.0	0.28	3.38 \pm 0.12	...	8.3	1.2
Kepler-334 b	1909.02	5.47	0.061	1.03 \pm 0.04	...	1.7	8.5
Kepler-334 c	1909.01	12.8	0.11	1.37 \pm 0.04	...	5.3	11.0
Kepler-334 d	1909.03	25.1	0.17	1.39 \pm 0.05	...	5.6	11.0
Kepler-409 b	1925.01	69.0	0.32	0.98 \pm 0.04	0.06 \pm 0.18	1.4 \pm 1.1	8 \pm 6

Table 4 *continued on next page*

Table 4 (*continued*)

Name [†]	KOI	Per.	a	R_{pl}	K^*	$M \sin i^*$	ρ_p^*
		(d)	(AU)	(R_{\oplus})	(m s^{-1})	(M_{\oplus})	(g cm^{-3})
Kepler-409 c	1925.10	$(3.0 \pm 0.9) \times 10^3$	4.0	...	3.5 ± 1.3	77 ± 28	...
Kepler-338 e	1930.04	9.34	0.09	1.77 ± 0.27	...	4.6	4.6
Kepler-338 b	1930.01	13.7	0.12	2.49 ± 0.08	...	6.3	2.2
Kepler-338 c	1930.02	24.3	0.17	2.39 ± 0.08	...	6.1	2.4
Kepler-338 d	1930.03	44.4	0.25	2.83 ± 0.31	...	7.1	1.7
Kepler-1130 e	2169.04	2.19	0.032	0.388 ± 0.029	...	0.034	3.2
Kepler-1130 c	2169.02	3.27	0.042	0.644 ± 0.030	...	0.26	5.3
Kepler-1130 d	2169.03	4.27	0.051	0.639 ± 0.029	...	0.25	5.3
Kepler-1130 b	2169.01	5.45	0.06	0.85 ± 0.10	...	0.77	7.0
Kepler-1130 B	2169.10	$(1.46 \pm 0.19) \times 10^4$	12.0	...	2181 ± 26	$(6.92 \pm 0.07) \times 10^4$...
K02687.01	2687.01	1.72	0.028	0.730 ± 0.022	...	0.42	6.0
K02687.02	2687.02	8.17	0.08	0.961 ± 0.028	...	1.3	7.9
K02720.01	2720.01	6.57	0.069	1.17 ± 0.04	0.8 ± 1.2	2.3 ± 3.5	8 ± 12
Kepler-403 b	2732.01	7.03	0.078	1.77 ± 0.19	...	4.6	4.5
Kepler-403 d	2732.02	13.6	0.12	1.76 ± 0.07	...	4.6	4.6
K02732.04	2732.04	24.6	0.18	1.40 ± 0.07	...	5.7	12.0
Kepler-403 c	2732.03	54.3	0.31	2.32 ± 0.32	...	5.9	2.6
K03083.02	3083.02	6.23	0.069	0.71 ± 0.05	...	0.37	5.8
K03083.03	3083.03	8.29	0.084	0.65 ± 0.05	...	0.27	5.4
K03083.01	3083.01	10.2	0.096	0.82 ± 0.05	...	0.67	6.7
Kepler-444 b	3158.01	3.6	0.04	0.348 ± 0.030	...	0.022	2.9
Kepler-444 c	3158.02	4.55	0.047	0.44 ± 0.04	...	0.056	3.6
Kepler-444 d	3158.03	6.19	0.058	0.45 ± 0.04	...	0.063	3.7
Kepler-444 e	3158.04	7.74	0.067	0.48 ± 0.04	...	0.076	3.9
Kepler-444 f	3158.05	9.74	0.078	0.57 ± 0.05	...	0.16	4.7
Kepler-444 BC	3158.10	327 ± 28	52.2 ± 3.0
K03179.01	3179.01	5.99	0.065	0.84 ± 0.08	...	0.75	6.9

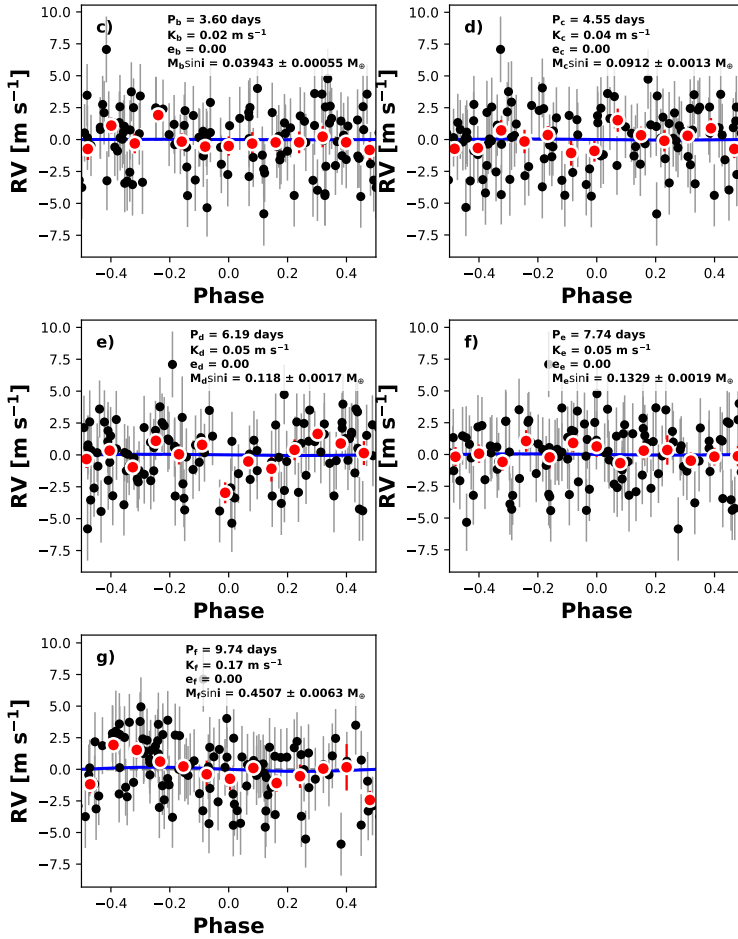
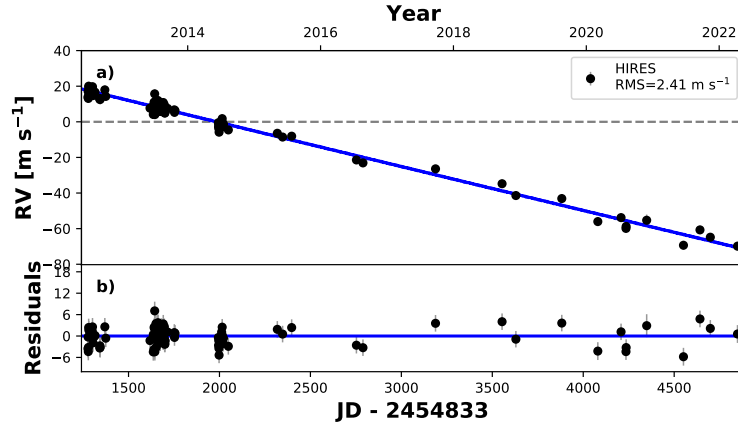
NOTE—* Values for K , $M \sin i$, and e are fixed for planets with no reported errors on these values. Planet masses are based on a mass-radius relation (Weiss & Marcy 2014) and eccentricities are circular.

[†]Non-transiting companions are given KOI indices beginning with KNNNN.10 for consistency with Marcy et al. (2014). For names, companions with planetary masses are given lowercase letters, companions with stellar masses are given uppercase letters, and companions with ambiguous masses are left nameless. Additional columns associated with this table are available in the machine-readable version.

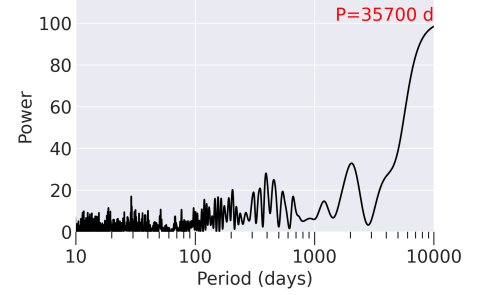
Table 5. KGPS Non-Transiting Companion Orbital Properties

Name [†]	KOI	Per. (d)	a (AU)	K (m s ⁻¹)	$M \sin i$ (M_J)	e	FAP	ΔBIC	Notes
Kepler-100 e	41.10	60.89±0.04	0.31	3.7±0.5	0.076±0.010	< 0.4	0.00002	-45.9	
Kepler-93 B	K00069 B	> 19100	> 15	> 89	> 15.5	...	0.00000	-837.2	A
Kepler-20 g	70.10	34.96±0.04	0.21	4.7±0.7	0.072±0.011	0.0	0.00493	-29.5	
Kepler-19 c	84.10	28.55±0.06	0.18	3.5±0.7	0.049±0.009	0.0	0.02454	-24.0	
Kepler-65 e	85.10	257.8±0.9	0.85	16.9±1.6	0.62±0.06	0.0	0.00000	-80.2	
Kepler-94 c	104.10	816.4±0.7	1.6	236.7±3.3	8.91±0.12	0.34707±0.00024	0.00079	-1205.7	
Kepler-106 f	116.10	90.76±0.23	0.39	6.8±0.8	0.146±0.017	0.0	0.00174	-44.6	
KOI-142 c	142.10	22.2672±0.0006	0.15	47.7±1.7	0.654±0.024	0.0	0.00043	-144.8	B
KOI-142 d	142.11	1425±14	2.5	63.8±3.3	3.15±0.17	0.430±0.029	0.00175	-114.7	
Kepler-48 e	148.10	998±4	1.9	46.6±1.3	2.16±0.06	< 0.1	0.00000	-173.2	
Kepler-48 f	148.11	(5.2±0.4)×10 ³	5.7	12±4	0.94±0.29	0.02±0.14	C
Kepler-25 d	244.10	91.58±0.22	0.42	8.9±1.1	0.216±0.027	0.0	0.00009	-45.0	D
Kepler-68 d	246.10	632.3±2.3	1.5	17.4±0.7	0.742±0.031	0.190±0.018	0.00000	-244.3	
Kepler-68 e	246.11	(4.46±0.10)×10 ³	5.4	6.5±1.8	0.52±0.14	0.29±0.13	0.00003	-55.9	E
Kepler-507 c	265.10	93.85±0.28	0.42	4.4±0.7	0.108±0.016	0.0	0.03644	-27.6	
Kepler-454 c	273.10	524.72±0.30	1.3	111.9±0.6	4.617±0.025	0.0	0.00000	-1318.0	
Kepler-454 d	273.11	(4.28±0.14)×10 ³	5.3	27.5±1.1	2.28±0.09	0.0	0.00000	-76.9	
Kepler-129 d	275.10	1875±24	3.2	88.9±2.0	6.21±0.14	0.0	0.00017	-424.7	
K00295.10	K00295.10	> 15600	> 12	> 31	> 3.9	...	0.99948	-12.6	A
Kepler-139 e	316.10	(2.05±0.07)×10 ³	3.2	20.4±2.0	1.34±0.13	< 0.15	C
Kepler-56 d	1241.10	994±5	2.3	95.0±2.2	6.43±0.15	0.2048±0.0028	0.00019	-295.6	
Kepler-56 e	K01241 B	> 14700	> 10	> 120	> 1.5	...	0.00019	-10.4	A
Kepler-407 c	1442.10	2164±12	3.3	168.9±2.5	11.23±0.16	0.0	0.00000	-3854.9	
K01612.10	K01612.10	> 16200	> 12	> 15	> 4.9	...	0.01541	-30.0	A
Kepler-409 c	1925.10	(3.0±0.9)×10 ³	4.0	3.5±1.3	0.24±0.09	< 1	0.00037	-36.3	
Kepler-1130 B	2169.10	(1.46±0.19)×10 ⁴	12.0	2181±26	217.7±2.3	0.6586±0.0004	0.00133	-227801.5	F
Kepler-444 BC	K03158 B	(8.67±0.33)×10 ⁴	52.2±3.0	>45	629±21	0.55±0.05	0.00000	-820.5	G

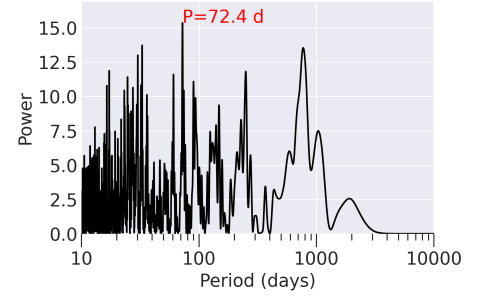
NOTE—A – Trend. B – TTV detection preceded RV discovery. C – Automated routine fails to find planet (long-period structure is evident but no peak is strongly preferred). D – Period ambiguous because of aliasing (91 or 122 days). E – Peak power at $P \approx 360$ days; 2000 day orbit preferred. F – Automated routine places companion at $P=6000$ days because of window function; a much longer period is preferred. G – Known stellar companion (Zhang et al. 2023).



(a) Kepler-444 RVs



(b) Periodogram of RVs



(c) Periodogram of Residuals

Figure 7: HIP 94931; KOI-3158 (Kepler-444). Left: RVs from Keck-HIRES. Panels include (top to bottom) the full RV time series, RV residuals, and the RVs phase-folded to the orbits of the individual planets (after subtracting the contributions from the other known planets). The phase-folded plots include weighted mean RVs binned by orbital phase (red circles). Right: Periodograms of the HIRES RVs, before (top) and after (bottom) subtracting the best-fit model that includes the transiting planets and one non-transiting stellar companions modeled as an RV trend.

APPENDIX: KGPS I STARS, PLANETS, AND RVs.

7.1. HIP 94931 (Kepler-444)

Kepler-444 (KOI-3158, HIP 94931) is a bright ($V=8.9$), nearby ($d=35.7$ pc) K dwarf (component A) hosting 5 Mars-sized transiting planets within 0.1 AU. The planetary system, including asteroseismology of the host star, was first characterized in detail by [Campante et al. \(2015\)](#). The system has a wide-separation M-dwarf binary companion (components B and C) characterized by [Dupuy et al. \(2016\)](#), which has a nearly edge-on orbit and high eccentricity with periastron passage of just a few AU. [Mills & Fabrycky \(2017\)](#) conducted a detailed analysis of the transit timing variations of the planets and measured mass upper limits for two of the planets comparable to that of Mars.

The RVs of Kepler-444 (Figure 7) exhibit a linear trend that is broadly consistent with the orbit described in [Dupuy et al. \(2016\)](#). An updated study that uses Gaia data and dynamical analysis confirms the eccentricity of the BC pair with respect to the primary found by previously (0.8, [Stalport et al. 2022](#)). However, a separate analysis by [Zhang et al. \(2023\)](#) that includes direct AO of the BC pair, Gaia data, and new HIRES RVs of the systemic BC component finds an eccentricity of BC orbit of 0.55 which changes the periastron passage of the BC component from 5 au to 8 au. The slight increase in periastron passage suggests a less severely truncated, more massive disk in which the planets formed than what was originally proposed in [Dupuy et al. \(2016\)](#), resolving the apparent conflict between the estimated primordial solid mass in the disk and the total planet mass.

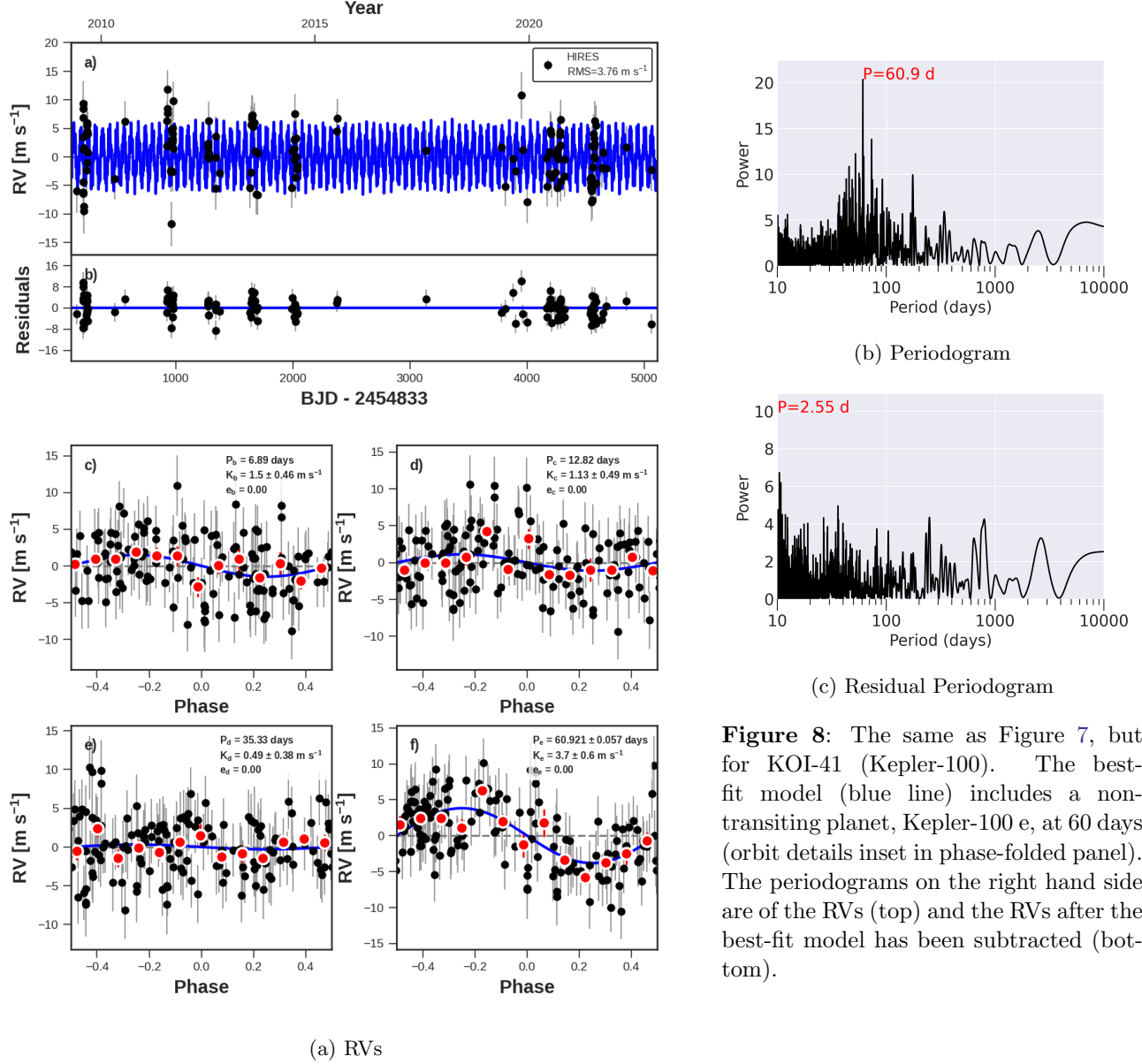


Figure 8: The same as Figure 7, but for KOI-41 (Kepler-100). The best-fit model (blue line) includes a non-transiting planet, Kepler-100 e, at 60 days (orbit details inset in phase-folded panel). The periodograms on the right hand side are of the RVs (top) and the RVs after the best-fit model has been subtracted (bottom).

KOI-41 (KEPLER-100)

Kepler-100 (KOI-41) is a $V=11.2$ sun-like star at $d=307 \text{ pc}$. Transiting planets Kepler-100 b, c, and d, which have orbital periods of 6.89, 12.82, and 35.33 days, and radii of 1.3, 2.2, and 1.6 Earth radii, were confirmed with radial velocities in [Marcy et al. \(2014\)](#). The mass measurements at the time were of order 2σ significance and/or mass upper-limits. A detailed photodynamical analysis, which reproduced the transit depth variations of the planets as well as their TTVs, resulted in more precise masses: $M_b = 5.1 \pm 1.7 M_{\oplus}$, $M_c = 14.6 \pm 2.8 M_{\oplus}$, and $M_d = 1.1 \pm 0.5 M_{\oplus}$ ([Judkovsky et al. 2022](#)). The architecture of this system cannot be explained by photo-evaporation alone because a low-mass, gas-enveloped planet exists interior to a highly irradiated rocky planet, and so other physical mechanism (including atmospheric mass-loss) was essential for sculpting the planet compositions ([Owen & Campos Estrada 2020](#)).

This star was observed for multiple programs at Keck Observatory. It was originally selected as a bright *Kepler* planet-hosting star for follow-up in [Marcy et al. \(2014\)](#). After several years of low-cadence observations, this target was selected for moderate cadence analysis to improve the mass measurements of the transiting planets. Our analysis of the full RV time series spanning 2009-2021 (Figure 8) yields $M_b = 5.5 \pm 1.3 M_{\oplus}$, $M_c = 3.8 \pm 1.7 M_{\oplus}$, and $M_d =$

$1.2 \pm 1.4 M_{\oplus}$, in agreement with the TTV solution. In addition, we discover a non-transiting planet, Kepler-100 e, at $P_e = 60.88 \pm 0.04$ d and with minimum mass $M_e \sin i_e = 24.8 \pm 3.5 M_{\oplus}$. Fixing the eccentricity of Kepler-100 e at zero results in $M_b = 4.8 \pm 1.3 M_{\oplus}$, $M_c = 4.3 \pm 1.7 M_{\oplus}$, $M_d = 2.4 \pm 1.8 M_{\oplus}$ and $M_e = 25 \pm 3 M_{\oplus}$, yielding an overall upper limit on the mass of planet d: $M_d < 7.8 M_{\oplus}$ (3σ conf.). A joint analysis of the TTV and RVs would yield even better masses and orbital constraints of the four known planets. In our 12 year RV baseline, we find no significant trend in the RV residuals (RMS=3.3 m s⁻¹), consistent with $M \sin i < 0.06 M_J$ at 5 AU or $M \sin i < 0.23 M_J$ at 10 AU (3σ conf.), after assuming a four-planet model (including non-transiting planet e).

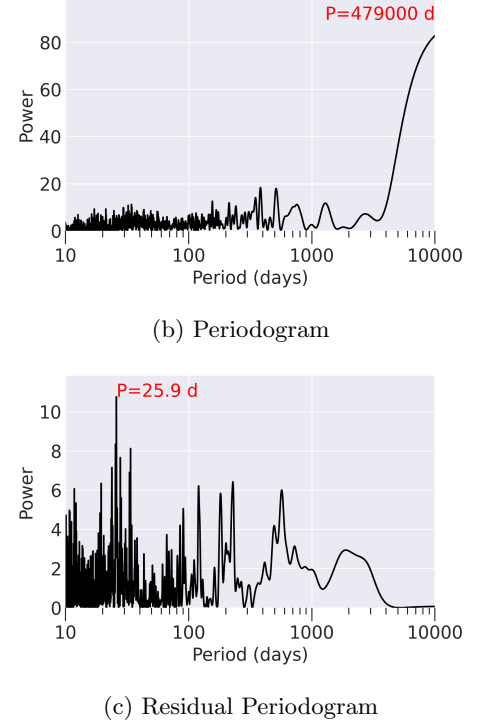
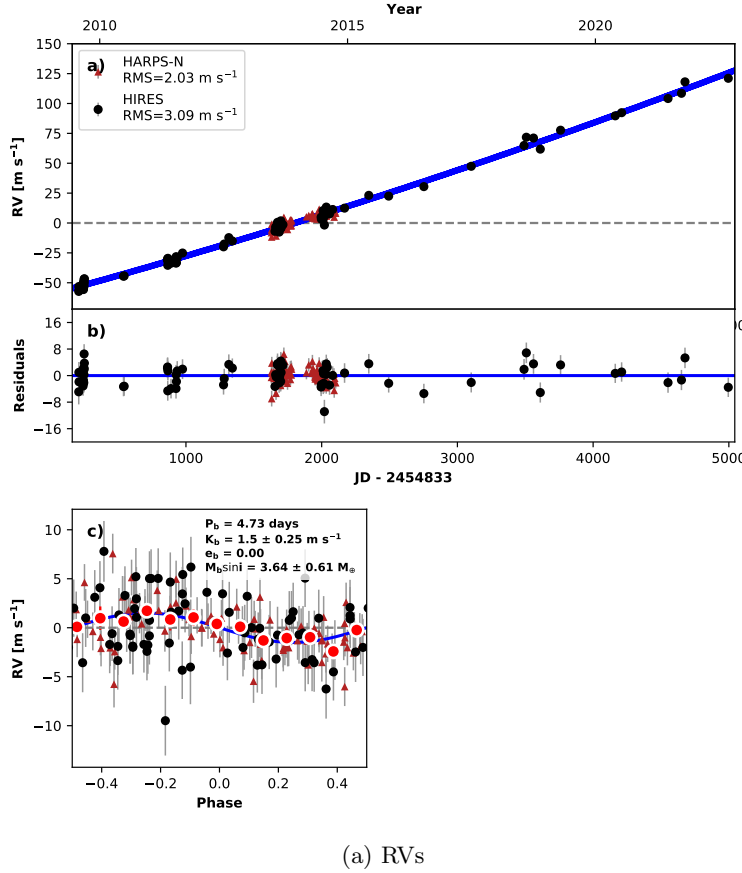
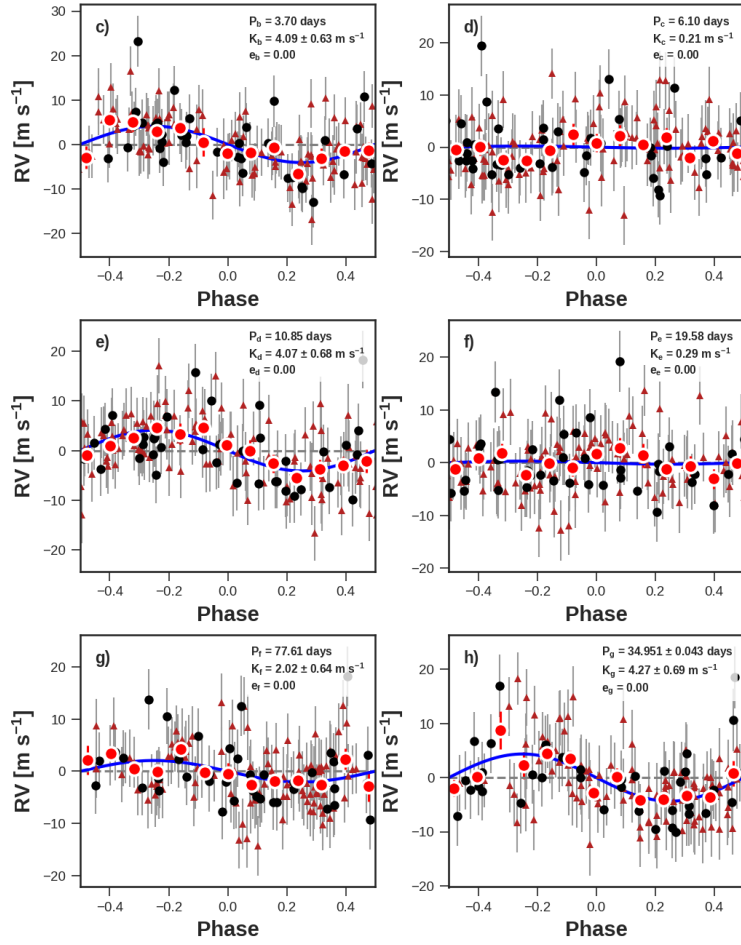
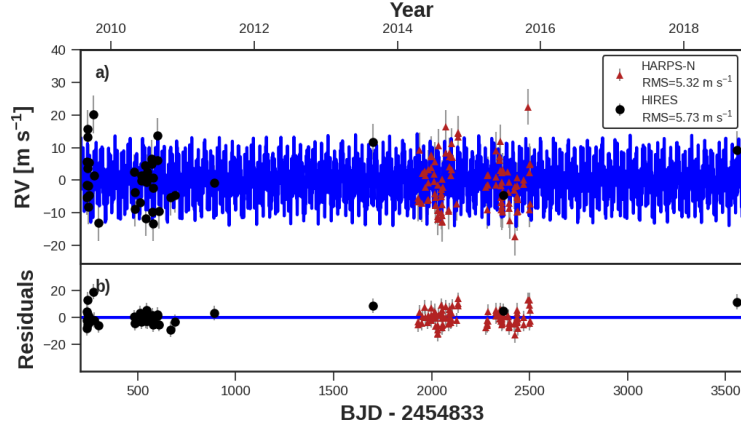


Figure 9: The same as Figure 7, but for KOI-69 (Kepler-93). Left: The RVs were taken at Keck-HIRES (black circles) and TNG-HARPS-N (maroon triangles). The best-fit model includes a stellar companion modeled as an RV trend.

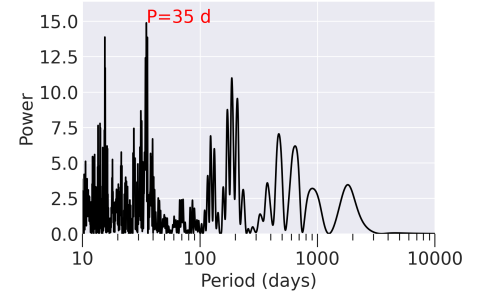
KOI-69 (KEPLER-93)

Kepler-93 (KOI-69) has one transiting planet that is notable for having one of the most precise radius measurement of a super-Earth yet reported: $R_b = 1.48 \pm 0.02 R_\oplus$, which has a radius uncertainty of 120 km (Ballard et al. 2014). The precision of the planet radius measurement is based on asteroseismology of the host star (for a precise stellar radius) and transits observed by the NASA Spitzer space telescope (for a precise transit depth). RVs from Keck/HIRES yielded a planetary mass of $M_b = 3.8 \pm 1.5 M_\oplus$ and also a long-term trend (Marcy et al. 2014). Additional RVs from TNG/HARPS-N improved the mass characterization of the planet, $M_b = 4.0 \pm 0.7 M_\oplus$, a value consistent with an Earth-like rocky composition for the planet (Dressing et al. 2015).

With 64 RVs from Keck/HIRES collected since Marcy et al. (2014), we have extended the RV baseline of Kepler-93 to twelve years (Figure 9). The RV trend is $dv/dt = 0.0373 \pm 0.0003 \text{ m s}^{-1} \text{ day}^{-1}$. For a companion at 15 AU (which corresponds to four times the RV baseline), this trend yields a minimum mass of $M \sin i > 15 M_J$, meaning that the companion is stellar or a brown dwarf, rather than planetary. The additional RVs also improve the mass precision for the transiting planet to a 6σ detection: $M_b = 3.6 \pm 0.6 M_\oplus$.



(a) RVs



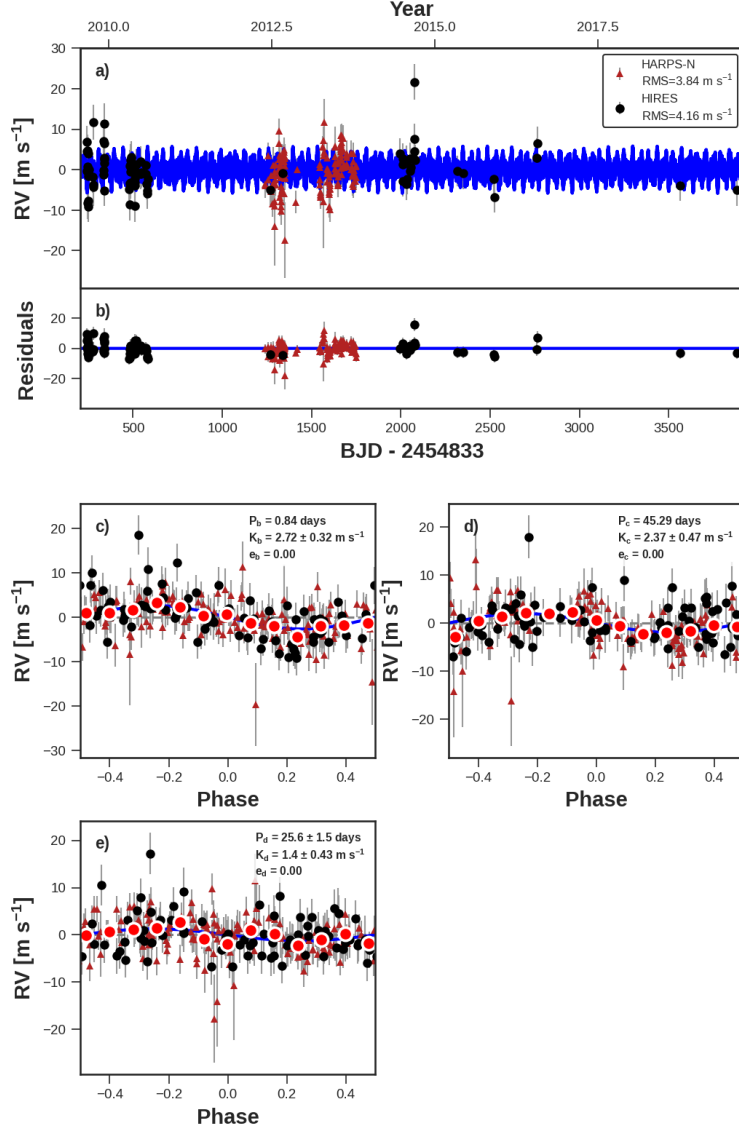
(b) Periodogram

Figure 10: The same as Figure 7, but for KOI-70 (Kepler-20). Left: The RVs were taken at Keck-HIRES (black circles) and TNG-HARPS-N (maroon triangles). The best-fit model includes a non-transiting planet, Kepler-20 g, at 35 days (orbital parameters inset in phase-folded panel).

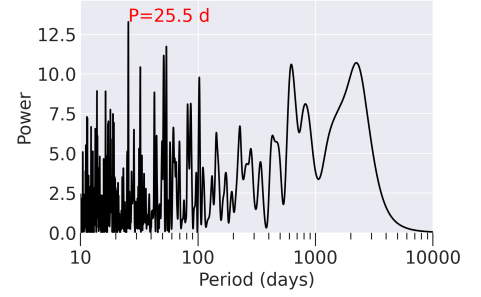
KOI-70 (KEPLER-20)

Kepler-20 (KOI-70) has five transiting planets that are notable for their unusual size ordering, with alternating super-Earth sized and Mars-sized planets. [Buchhave et al. \(2016\)](#) characterized this system using RVs from HARPS-N

and HIRES, finding a non-transiting planet with a period of 34.9d in between the 19.6d and 77.6d transiting planets. We have collected one new HIRES RVs since 2016 that is consistent with the solution from [Buchhave et al. \(2016\)](#). While the single new RV data point does not substantially improve the mass measurement of the transiting planets, it does further constrain the non-detection of an RV trend, yielding an upper limit of $M \sin i < 0.35 M_J$ at 5 AU or $M \sin i < 1.4 M_J$ at 10 AU (3σ conf., Figure 10).



(a) RVs



(b) Periodogram

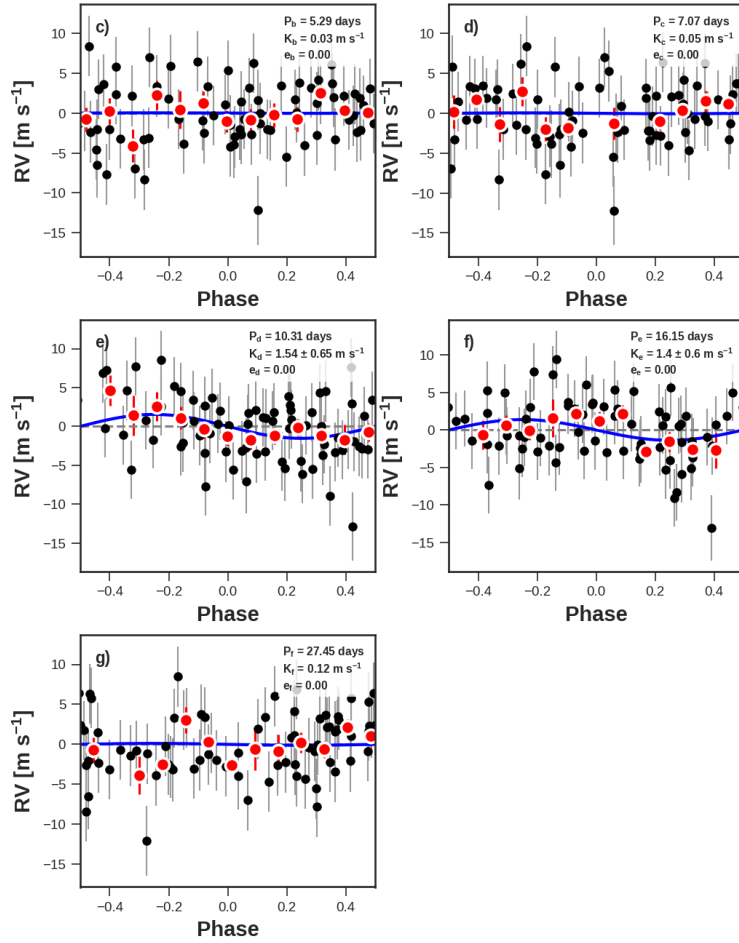
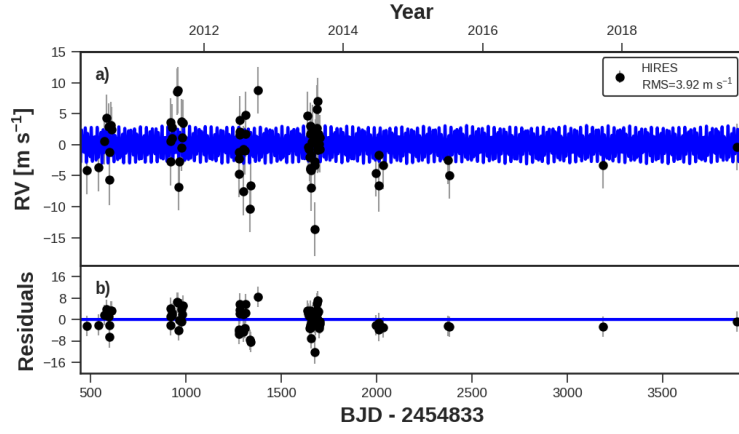
Figure 11: The same as Figure 7, but for KOI-72 (Kepler-10). Left: The RVs were taken at Keck-HIRES (black circles) and TNG-HARPS-N (maroon triangles). A planet candidate is marginally detected at 25 days ($\Delta\text{BIC}=-18$).

KOI-72 (KEPLER-10)

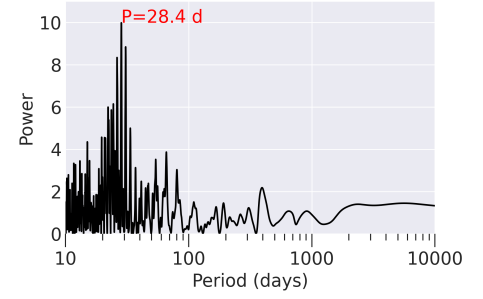
Kepler-10 (KOI-72) contains the first rocky planet discovered by the Kepler Mission with $P_b < 1$ day and a sub-Neptune sized planet at $P_c = 45.45$ days (Batalha et al. 2011). RVs were collected on both Keck-HIRES and TNG-HARPS-N, and while both sets of data are consistent with a rocky composition for planet b, the data were discrepant regarding the mass and composition of planet c, with HIRES data favoring a low mass $M_c = 7 M_\oplus$ and HARPS-N data favoring a high mass $M_c = 17 M_\oplus$ (Dumusque et al. 2014; Weiss et al. 2016). The discrepancy might be caused by additional non-transiting planets in the system sampled at different phases by the two instruments, an idea which is supported by the detection of TTVs of planet c (Weiss et al. 2016). Modeling the RVs with Gaussian processes appears to somewhat resolve the discrepancy, although the host star is an old thick-disk star that is not expected to be magnetically active (Rajpaul et al. 2017).

We have collected 14 new HIRES RVs of Kepler-10 since Weiss et al. (2016), producing an RV baseline of 12 years (Figure 11). The residuals to the best two-planet fit have $\text{RMS}=4.6 \text{ m s}^{-1}$ (HIRES) and 3.9 m s^{-1} (HARPS-N) and exhibit no RV trend, yielding an upper limit of $M \sin i < 0.11 M_J$ at 5 AU or $M \sin i < 0.46 M_J$ at 10 AU (3σ conf.) for

additional companions. Note that there is a third low-mass planet candidate ($m_p \sim 1 M_\oplus$) in the system, as indicated in [Weiss et al. \(2016\)](#), but the period is ambiguous. Because the third planet candidate is low-mass and has $P < 200$ days, our choice to exclude it from our model here does not substantially affect the upper limits on Jovian planets at long periods. However, we do detect significant structure in the periodogram of the RV residuals, with a prominent peak at $P = 25$ days (FAP=0.04, $\Delta\text{BIC}=-18.9$). This period was previously modeled as the stellar rotation period in a fit that used a Gaussian process method to remove stellar noise ([Rajpaul et al. 2017](#)), although a rotation period of 25 days is uncharacteristically fast for a 10 Gyr old thick-disk star. We consider this signal as a third planet candidate in the system, to be confirmed with more RVs. A careful analysis that jointly fits the HIRES and HARPS-N RVs as well as the TTVs might yield an improved characterization and/or confirmation of the planet candidate at 25 days.



(a) RVs



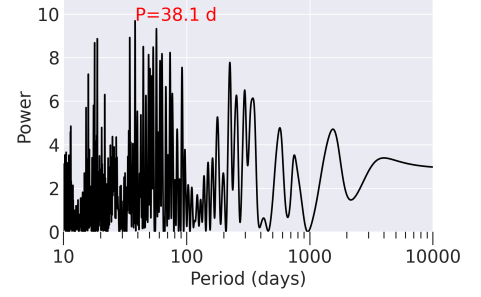
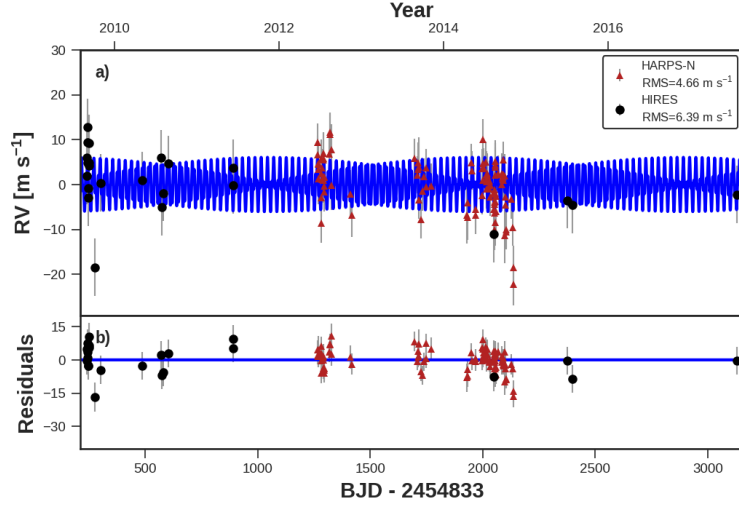
(b) Periodogram

Figure 12: The same as Figure 7, but for KOI-82 (Kepler-102). Left: The RVs were taken at Keck-HIRES (black circles) and TNG-HARPS-N (maroon triangles). No non-transiting companions are detected.

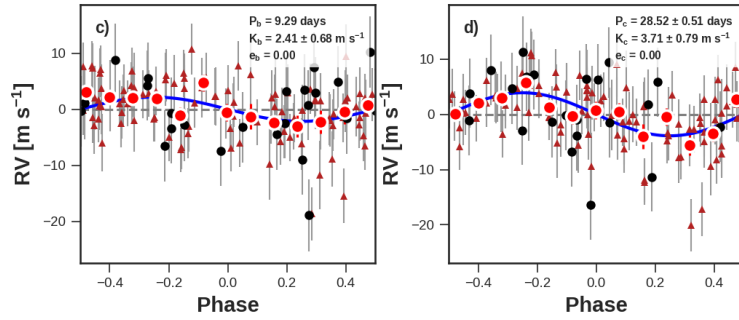
KOI-82 (KEPLER-102)

KOI-82 (Kepler-102) is a system with five transiting planets, three of which are smaller than Earth. The system was confirmed in [Marcy et al. \(2014\)](#) with HIRES RVs establishing mass upper limits for the planets. The star is active

(with a visible stellar rotation signal in the Kepler photometry, and Mt. Wilson $S_{\text{HK}} = 4.48$), which contributes to substantial RV scatter. A joint analysis of HIRES and HARPS-N RVs that included a Gaussian process trained on the rotational modulation in the Kepler lightcurve found $M_d = 2.51.4 M_{\oplus}$, $M_e = 4.71.7 M_{\oplus}$ (Brinkman et al. 2022). Here, we employ a simple circular fit to planets d and e based on the HIRES data alone, with masses for the other (smaller) planets based on an empirical mass-radius relationship (Weiss & Marcy 2014). The HIRES RVs extend from April 2010 to June 2021, comprising a baseline of 11 years. The residuals to our best fit have $\text{RMS} = 3.9 \text{ m s}^{-1}$ and no RV trend, yielding a 3σ upper limit of $M \sin i < 0.2 M_J$ at 5 AU or $M \sin i < 0.8 M_J$ at 10 AU for additional companions (Figure 12). Note that the Lomb-Scargle periodogram of the RVs has a marginal peak at 28 days, which is consistent with the stellar rotation identified in the *Kepler* light curve (Brinkman et al. 2022).



(b) Periodogram



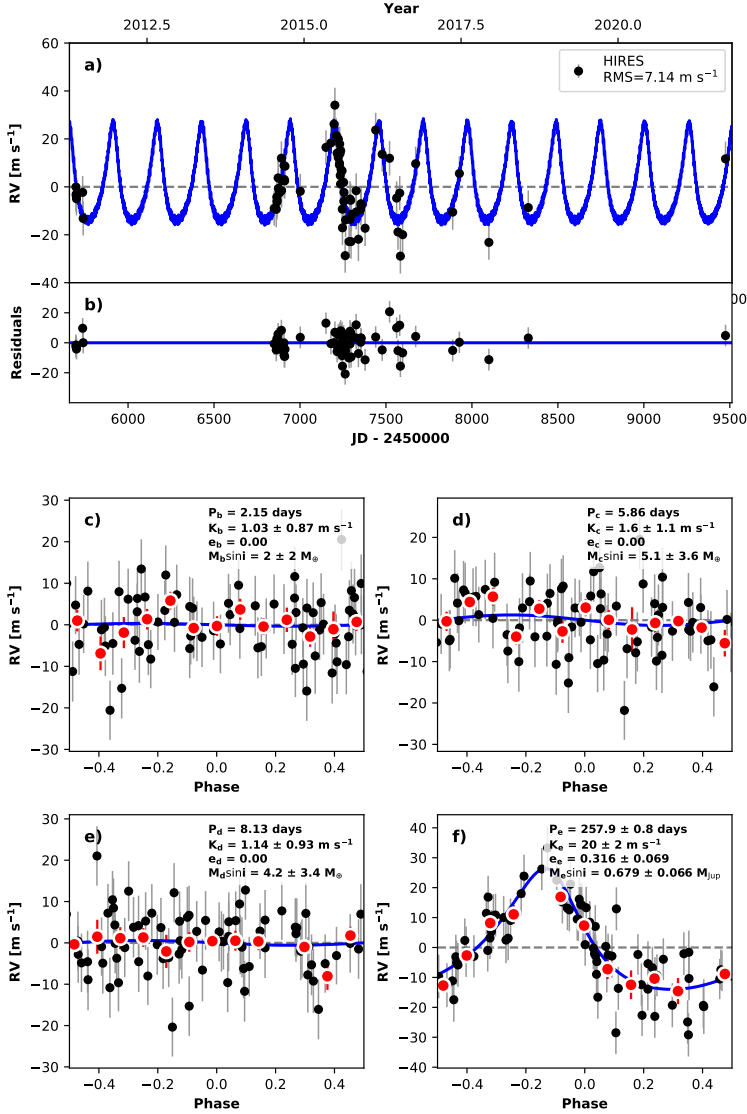
(a) RVs

Figure 13: The same as Figure 7, but for KOI-84 (Kepler-19). Left: The RVs were taken at Keck-HIRES (black circles) and TNG-HARPS-N (maroon triangles). The best-fit model includes a non-transiting planet, Kepler-19 c, at 28.54 days (orbital parameters inset in phase-folded panel).

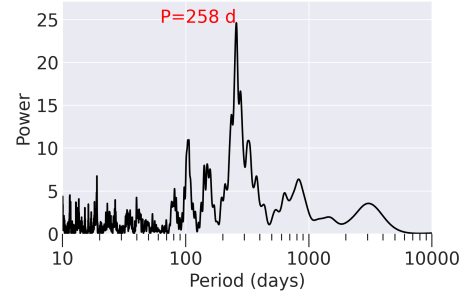
KOI-84 (KEPLER-19)

Kepler-19 (KOI-84) was first confirmed and characterized in [Ballard et al. \(2011\)](#). The system has one transiting planet (b) with $P_b = 9.3$ days and $R_b = 2.2 R_{\oplus}$. Significant transit timing variations (TTVs) of Kepler-19 b indicated the presence of a non-transiting perturber ([Ballard et al. 2011](#)). Precise RVs were collected with HARPS-N (101) in order to conduct a joint TTV-RV analysis ([Malavolta et al. 2017](#)), which resulted in a mass measurement of $M_b = 8.4 \pm 1.6 M_{\oplus}$ and the detection of two non-transiting planets: Kepler-19 c ($P_c = 28.7$ days, $M_c = 13.1 \pm 2.7 M_{\oplus}$) and Kepler-19 d ($P_d = 63$ days, $M_d = 20.3 \pm 3.4 M_{\oplus}$). The mass and radius of Kepler-19 b are consistent with a rocky interior overlaid with a substantial volatile envelope, and the masses of the non-transiting planets are also consistent with volatile-enveloped planets ([Weiss & Marcy 2014](#); [Rogers 2015](#)).

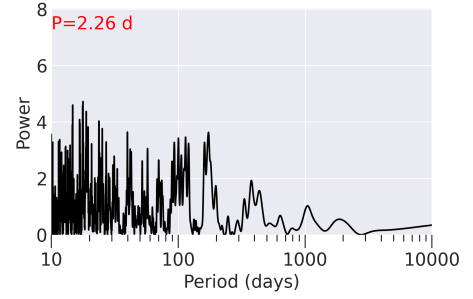
We collected 24 HIRES RVs between 2009 to 2017, resulting in a baseline of 8 years (Figure 13). We jointly analyze the HIRES and HARPS-N RVs. We recover the planet at 28.54 days (Kepler-19 c), although we do not detect the planet at 63 days (Kepler-19 d). In the periodogram of the residuals, the highest peak is near 38 days and has FAP . We obtain masses of $M_b = 7.51.9 M_{\oplus}$ and $M_c = 17.33.0 M_{\oplus}$. A joint analysis of all the RVs and TTVs is needed to re-confirm the planet at 63 days. The residual RMS of the RVs is 4.7 m s^{-1} with no significant trend, yielding an upper limit of $M \sin i < 0.3 M_J$ at 5 AU or $M \sin i < 1.8 M_J$ at 10 AU (3σ conf.).



(a) KOI-85 RVs



(b) Periodogram of RVs



(c) Periodogram of Residual RVs

Figure 14: Same as Figure 7, but for KOI-85 (Kepler-65). Left: The best-fit model (blue line) includes a non-transiting planet, Kepler-65 e (orbit details inset in phase-folded panel). The periodograms on the right hand side are of the RVs (top) and the RVs after the best-fit model has been subtracted (bottom).

KOI-85 (KEPLER-65)

KOI-85 (Kepler-65) has three transiting planets originally validated in Chaplin et al. (2013), all with $P < 10$ days and $R_p < 4 R_{\oplus}$. A non-transiting planet was identified in seven years of Keck-HIRES RVs (Mills et al. 2019b). The compact configuration of the three inner planets generates TTVs, and a photodynamical analysis of the Kepler photometry and HIRES RVs yielded precise masses for the four known planets: $M_b = 2.4^{+2.4}_{-1.6} M_{\oplus}$, $M_c = 5.4 \pm 1.7 M_{\oplus}$, $M_d = 4.14 \pm 0.80$, and $M_e = 260^{+200}_{-50} M_{\oplus}$ (planet e is non-transiting and decoupled from the inner planets, and so its inclination is not well constrained). We have collected 76 HIRES RVs between May 2011 and June 2022 (including 2 new RVs since Mills et al. 2019b) providing a baseline of 11 years (Figure 14). After fitting a four-planet model (including planet e), the residual RVs have an $\text{RMS}=7.0 \text{ m s}^{-1}$ and no apparent trend, yielding a 3σ upper limit of $M \sin i < 0.30 M_J$ at 5 AU or $M \sin i < 1.2 M_J$ at 10 AU.

KOI-94 (KEPLER-89)

KOI-94 (Kepler-89) is a V=12.2 late F-type star ($T_{\text{eff}} = 6000 \text{ K}$) with $R_{\star} = 1.20 M_{\odot}$. It has four transiting planets, including a warm Jupiter (KOI-94 d, $P_d = 22.34$ days, $R_d = 11.3 \pm 1.1 R_{\oplus}$) surrounded by three sub-Neptunes

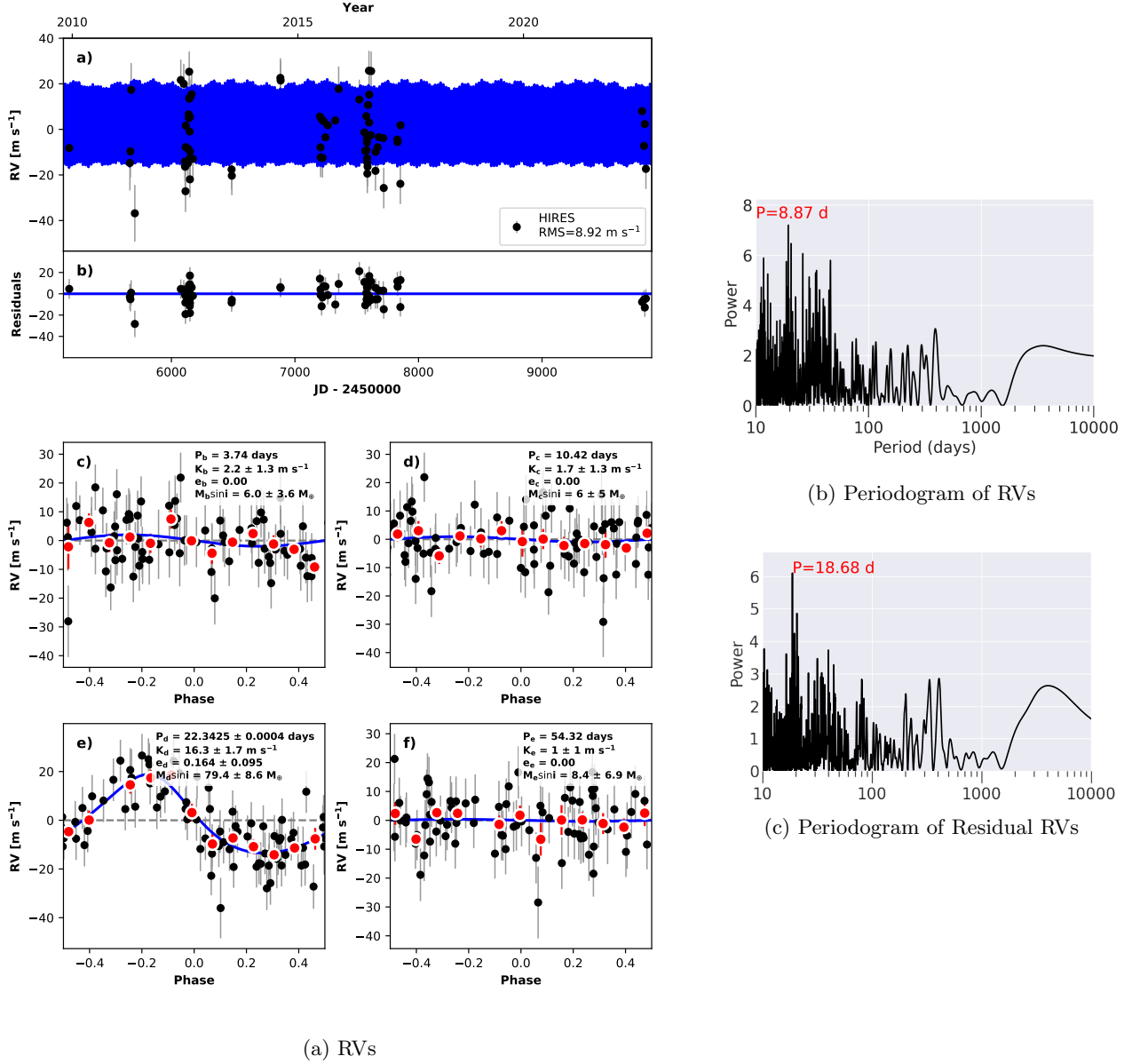


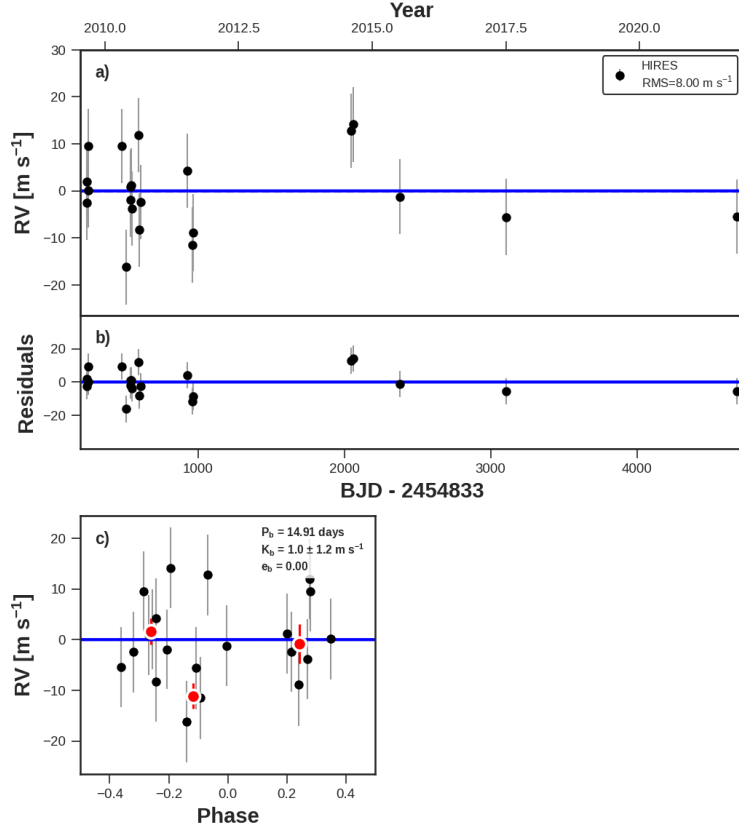
Figure 15: Same as Figure 7, but for KOI-94 (Kepler-89). For the best-fit model, we allowed the period, eccentricity, and periastron passage of the transiting planet d, which is strongly detected in the periodogram (right), to float, but with a prior informed from the TTV analysis of Jontof-Hutter et al. (2022a). No non-transiting companions are detected.

($P_b = 3.73$ days, $P_c = 10.4$ days, $P_d = 54.3$ days). Hirano et al. (2012) characterized the photometry of the system and detected a planet-planet occultation, thereby inferring that the line-of-sight projected mutual inclination between KOI-94.01 and KOI-94.03 is -1.15 ± 0.55 degrees. The system was confirmed with RVs in Weiss et al. (2013), in which the mass of KOI-94 d was measured ($M_d = 106 \pm 11 M_J$) and upper limits were set for the smaller transiting planets. A contemporaneous analysis of TTVs in this system yielded a substantially different mass for the warm Jupiter (Masuda et al. 2013), although an erroneously low stellar mass was used in the TTV analysis (1.0 vs. $1.27 M_\odot$), contributing to the discrepancy.

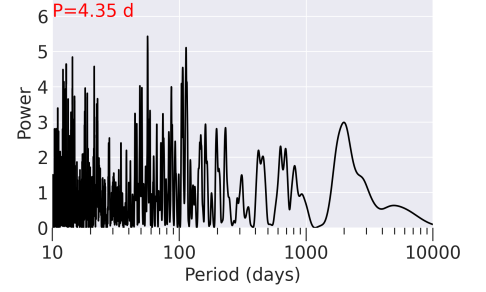
Several transits of the Kepler-89 planets (two of planet d, four of planet c, one of planet e, and none of planet b) were identified in TESS photometry, yielding an updated solution to the best fit to the TTVs (Jontof-Hutter et al. 2022a).

A four-planet model fit the observed TTVs poorly (reduced $\chi^2 = 2.48$), and Jontof-Hutter et al. (2022a) proposed two possible five-planet models that better reproduced the TTVs, although still with reduced $\chi^2 > 1.8$. In model A, the fifth planet candidate was at 118.0 days and had $7.0 M_{\oplus}$, whereas in model B, the fifth planet was at 39.99 days and had $0.71 M_{\oplus}$.

KOI-94 was selected for follow-up as part of a program to survey stars with at least 3 transiting planets from 2015 onward. We have continued monitoring KOI-94 with HIRES, and have collected 43 new RVs since 2013 and 96 RVs total on 72 unique nights (Figure 15). Note that RVs from August 10, 2022, which were part of a Rossiter-McLaughlin observation (Albrecht et al. 2013), have been removed from our analysis. Because the planets have significant TTVs, we allowed the period of the warm Jupiter (which is strongly detected in the RVs) to vary, but with a prior informed from the TTV analysis of Jontof-Hutter et al. (2022a): $P_d = 22.3425 \pm 0.0004$. The new best-fit values mass from the RVs is $M_d = 71.9 \pm 9.3 M_{\oplus}$, which significantly reduces the tension between the RV solution and the TTV solution. We also detected a moderate eccentricity of the warm Jupiter of $e_d = 0.2 \pm 0.1$, although the introduction of a fifth planet to the model might reduce the eccentricity. The residual RVs have $\text{RMS} = 8.9 \text{ m s}^{-1}$, no significant peak in the Lomb-Scargle periodogram (right panel of Fig. 15), and no apparent trend, yielding an upper limit of $M \sin i < 0.90 M_J$ at 5 AU ($M \sin i < 3.6 M_J$ at 10 AU) for additional companions. These upper limits do not exclude the putative TTV planet candidates identified in Jontof-Hutter et al. (2022a). The star’s moderate rotation ($v \sin i = 7.5 \text{ km/s}$) produces a relatively large RV errors, which will make an RV detection of the putative fifth planet challenging.



(a) RVs



(b) Periodogram

Figure 16: The same as Figure 7, but for KOI-103 (Kepler-1710). No non-transiting companions are detected.

KOI-103 (KEPLER-1710)

Kepler-1710 (KOI-103) is a $V=12.6$ sun-like star. It has one transiting planet with $P_b = 14.91$ days and $R_b = 3.20 R_\oplus$ which was recently re-confirmed with ExoMiner, a machine learning validation tool (Valizadegan et al. 2022). We have collected 21 HIRES RVs with over a decade of baseline (2009-2021, Figure 16). After fitting for the transiting planet, the residual RVs have an RMS of 8.3 m s^{-1} and no trend, yielding a 3σ upper limit of $M \sin i < 0.3 M_J$ at 5 AU ($M \sin i < 1.1 M_J$ at 10 AU) for any additional companions. The RV scatter in this system is unexplained in terms of the expected amplitude of the transiting planet and the stellar activity ($\log(R'_{\text{HK}}) = -4.77$). There are no stellar companions within $2''$ of the primary identified with either imaging nor spectroscopy that could be causing increased RV scatter. Perhaps there are unidentified non-transiting planets that are confounding a mass measurement of the transiting planet.

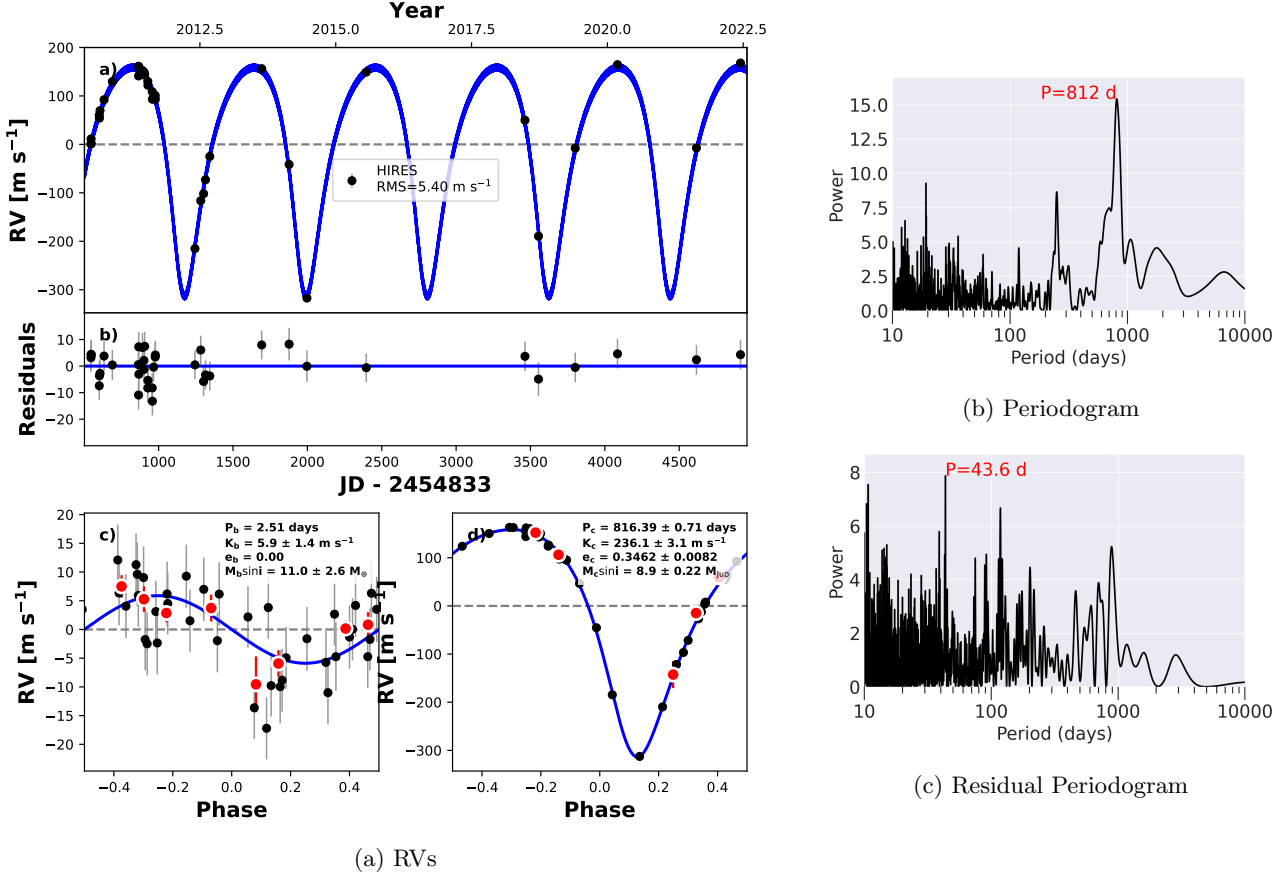


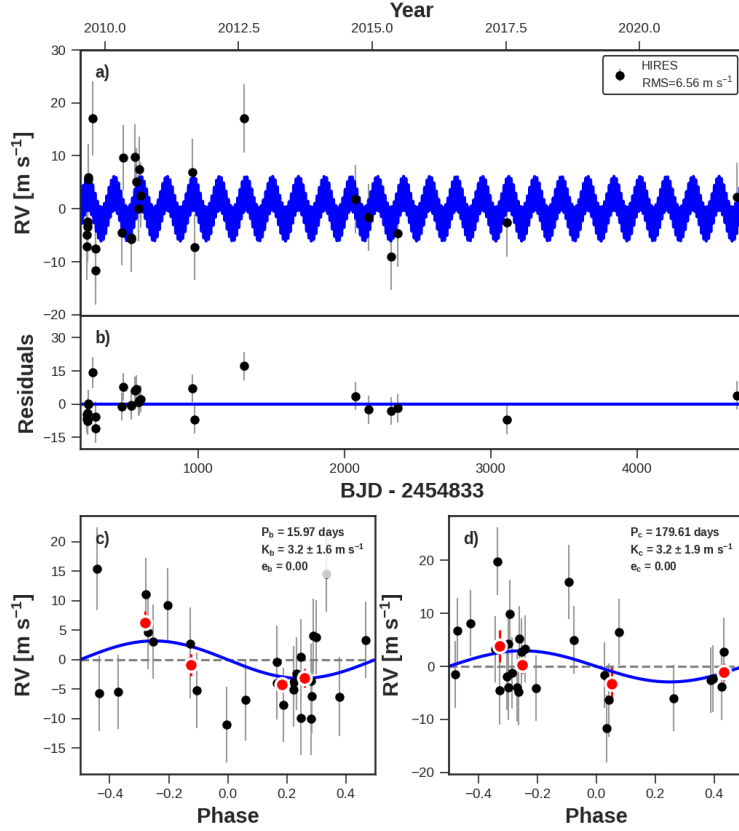
Figure 17: The same as Figure 7, but for KOI-104 (Kepler-94). Left: The best-fit model includes a non-transiting planet, Kepler-94 c (orbital parameters inset in phase-folded panel). Right: The periodogram of the RVs after removing the signals from the transiting planet (top) and both planets (bottom).

KOI-104 (KEPLER-94)

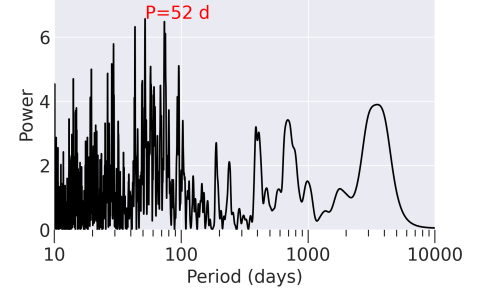
Kepler-94 (KOI-104) is a $V=12.9$ late K or early M type star with discrepant various temperatures reported in the literature ($T_{\text{eff}} = 4200 \text{ K} - 4750 \text{ K}$, Muirhead et al. 2012; Yee et al. 2017; Fulton & Petigura 2018a; Brewer & Fischer 2018; Berger et al. 2018). The system has one short-period transiting sub-Neptune ($P_b = 2.51$ days, $R_b = 3.5 R_{\oplus}$). The transiting planet was confirmed with Keck-HIRES RVs in Marcy et al. (2014) ($M_b = 10.8 \pm 1.4 M_{\oplus}$), which also revealed a long-period companion with $P_c = 820 \pm 3$ days and $M \sin i_c = 9.7 \pm 0.6 M_J$. We have collected 10 new RVs since Marcy et al. (2014), which yield refined properties for the long-period object: $P_c = 816.3 \pm 0.7$ days, $M \sin i_c = 8.9 \pm 0.2 M_J$, and $e_c = 0.35 \pm 0.0086$ (Figure 17). Because $M \sin i$ corresponds to a minimum mass, it is still unclear whether the non-transiting object is below or above the deuterium-burning limit of $13 M_J$. The HIRES RVs extend from 2010 to 2022, comprising a twelve year baseline. The residuals to our best two-planet fit (including the non-transiting companion) have $\text{RMS} = 5.4 \text{ m s}^{-1}$ and no apparent RV trend, consistent with a 3σ upper limit of $M \sin i < 0.30 M_J$ at 5 AU ($M \sin i < 1.2 M_J$ at 10 AU) on any additional companions.

Brewer & Fischer (2018) reported unusual abundances for this star. The star is apparently rich in nitrogen ($[\text{N}/\text{H}] = 0.46$, $[\text{C}/\text{H}] = 0.19$, $[\text{O}/\text{H}] = 0.10$) and very rich in sodium ($[\text{Na}/\text{H}] = 0.70$). The star is also rich in iron and nickel ($[\text{Fe}/\text{H}] = 0.38$, $[\text{Ni}/\text{H}] = 0.41$) and also in magnesium, and aluminum ($[\text{Mg}/\text{H}] = 0.30$, $[\text{Al}/\text{H}] = 0.51$). The uncertainties are reported as less than 0.1 dex for all abundances, although the star is a late K/early M type for which determining abundances can be challenging. It is noteworthy that this star has apparently high metallicities for metals and also has a super-Jovian companion (which is rare for late K and early M type stars). Perhaps the high metal abundances permitted the formation of the planet through core accretion, as suggested based on the correlation between giant planet occurrence and host star metallicity (Fischer & Valenti 2005). A more detailed examination of the host star

properties and abundances and their possible relationship to the planet properties is warranted but is beyond the scope of this paper.



(a) RVs

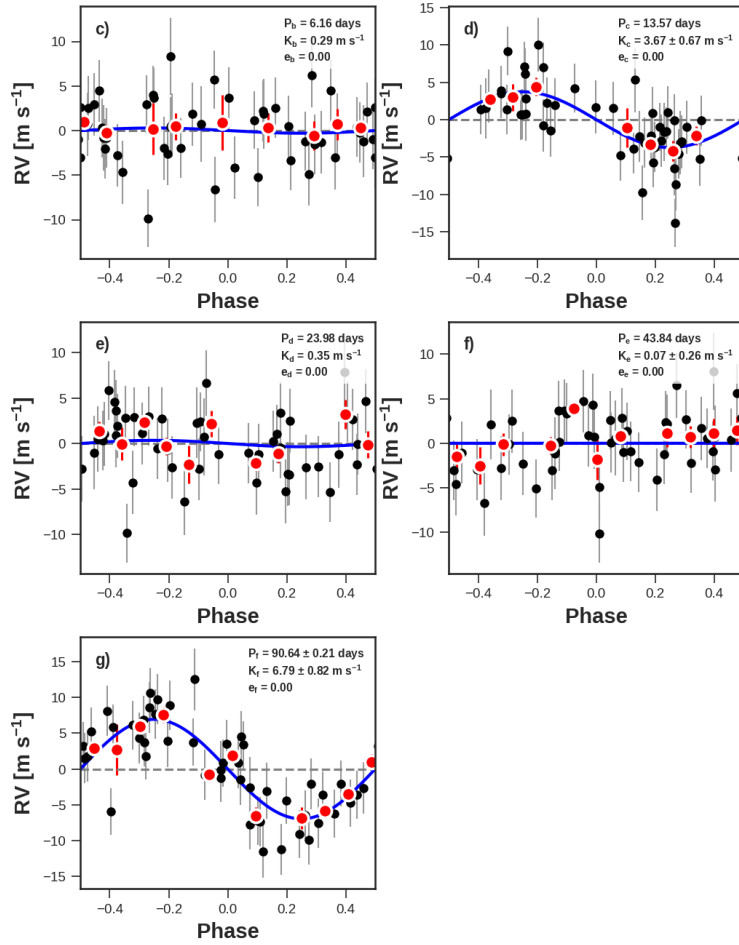
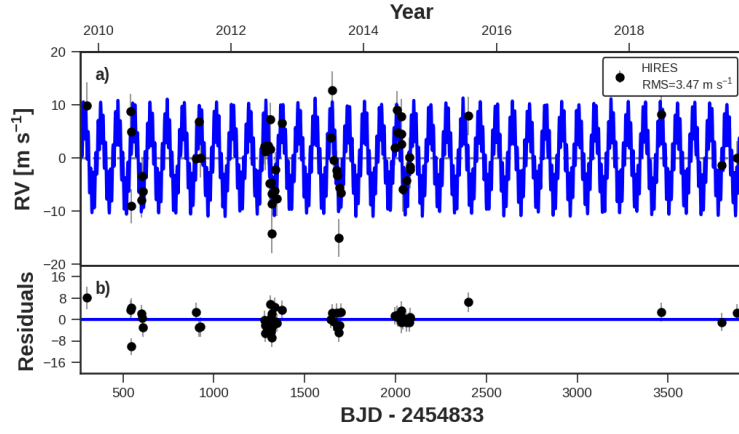


(b) Periodogram

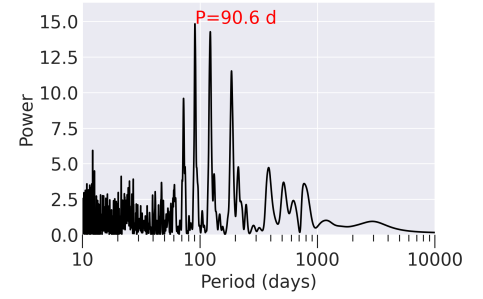
Figure 18: The same as Figure 7, but for KOI-108 (Kepler-103). No non-transiting companions are detected.

KOI-108 (KEPLER-103)

Kepler-103 (KOI-108) has two transiting planets: a sub-Neptune ($R_b = 3.37 R_\oplus$) with $P_b = 16.0$ days, and a sub-Saturn ($R_c = 5.14 R_\oplus$) with $P_c = 180$ days. The planets were confirmed with RVs from Keck-HIRES, with reported best-fit masses of 9.7 ± 8.6 and 36 ± 25 for planets b and c, respectively (Marcy et al. 2014). Although the planet masses were not detected with high confidence, these values correspond to upper limits on the planet masses that demonstrates they are planetary (rather than stellar). We have collected 6 HIRES RVs since 2013, which have not substantially improved the planet mass estimates (Figure 18). The RMS of the RV residuals is 6.8 m s^{-1} . The twelve-year RV baseline, which extends from 2009 to 2022, has no trend, placing a 3σ upper limit of $M \sin i < 0.24 M_J$ at 5 AU ($M \sin i < 1.0 M_J$ at 10 AU). TTVs have been identified by Gajdoš et al. (2019) but the planet masses were not measured based on the TTVs.



(a) RVs



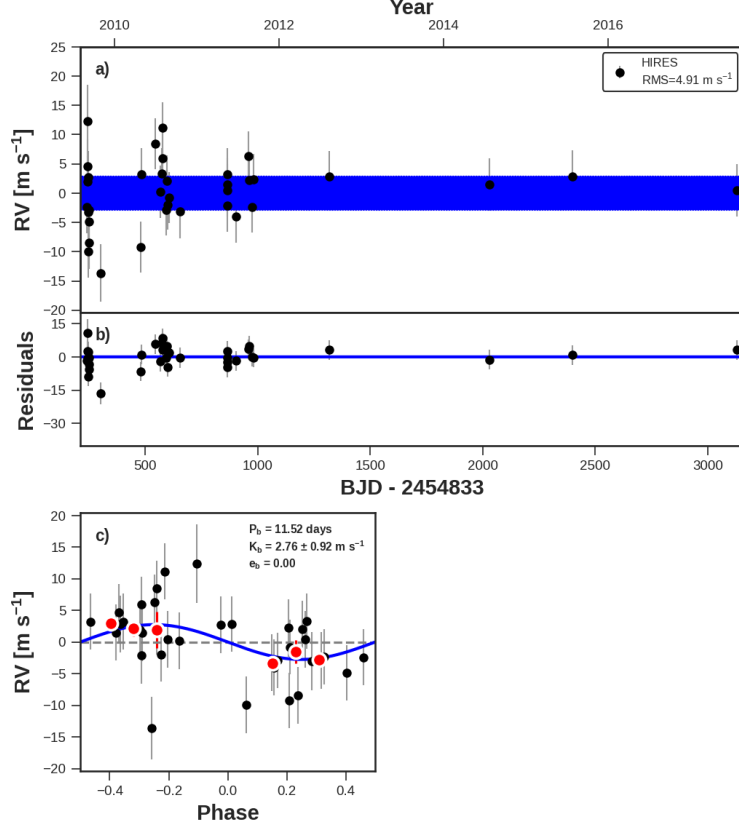
(b) Periodogram

Figure 19: The same as Figure 7, but for KOI-116 (Kepler-106). The best-fit model includes a non-transiting planet, although the period of that planet is uncertain due to aliasing (right).

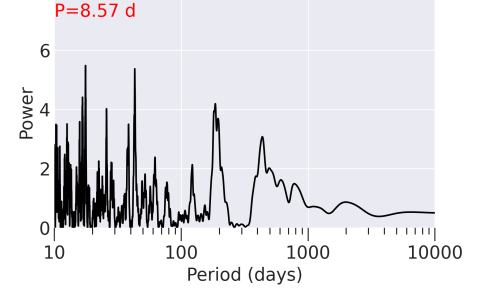
KOI-116 (KEPLER-106)

Kepler-106 (KOI-116) has four small transiting planets, with masses and/or mass upper limits published in [Marcy et al. \(2014\)](#). A periodogram of the RV residuals ($\text{RMS} = 6.0 \text{ m s}^{-1}$) reveals peaks near $P=90$, 180, and 365 days

(Fig. 19). These peaks could be driven by the seasonal window function, combined with the seasonal downward trend of the RVs in 2012, 2013, and 2014. The star is not particularly active and does not have S-value variations that correspond to these seasonal RV slopes. The RV slopes are likely caused by some combination of a (real) giant planet with an undetermined period and seasonal aliasing. Another possibility is that planets at 90, 180, and/or 365 days would continue the near-resonant chain of the inner four transiting planets. If the planet candidate at 90 days is real (FAP=0.003, $\Delta\text{BIC} = -43$), it produces an RV semi-amplitude of 7.5 m s^{-1} and has $M \sin i = 50 M_{\oplus}$. Continued monitoring at a variety of cadences, including RVs early and late in the Kepler season, will help resolve what additional planet(s) exist(s). TTVs have been identified by [Gajdoš et al. \(2019\)](#) but the planet masses were not measured. Although the mass, period, and veracity of planets with $P < 1$ year are uncertain, the RVs have no significant long-term trend, yielding a 3σ upper limit of $M \sin i < 0.25 M_J$ at 5 AU ($M \sin i < 1.0 M_J$ at 10 AU). This mass upper limit does not change with the addition of a fifth planet at 90 days.



(a) RVs

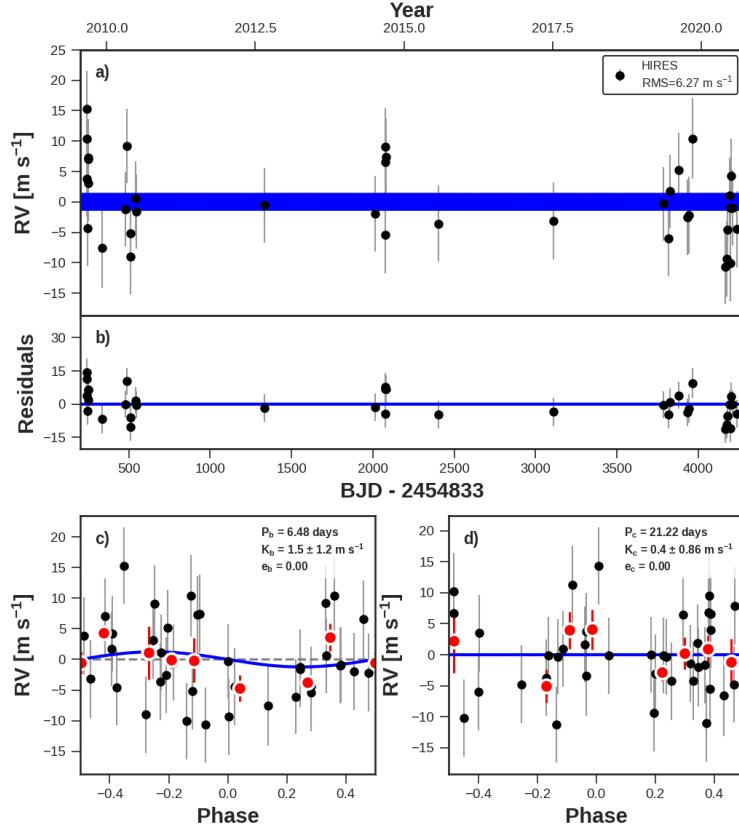


(b) Periodogram

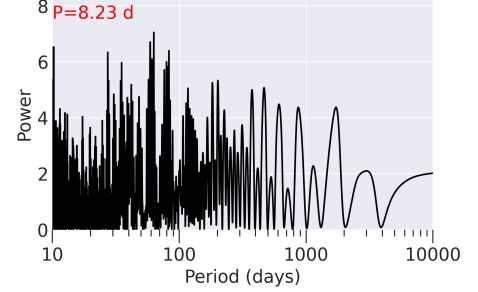
Figure 20: The same as Figure 7, but for KOI-122 (Kepler-95). No non-transiting companions are detected.

KOI-122 (KEPLER-95)

Kepler-95 (KOI-122) has one transiting planet at $P_b = 11.5$ days and $R_b = 3.4 R_\oplus$. The planet was confirmed with Keck HIRES RVs in [Marcy et al. \(2014\)](#), which yielded a mass of $M_b = 13.0 \pm 2.9 M_\oplus$. We have collected 3 new RVs since 2013, which have not substantially improved the mass of the transiting planet (Figure 20). The RV baseline extends from 2009 to 2017 with no trend, yielding a 3σ upper limit of $M \sin i < 0.30 M_J$ at 5 AU ($M \sin i < 1.2 M_J$ at 10 AU) for additional planets in the system.



(a) RVs

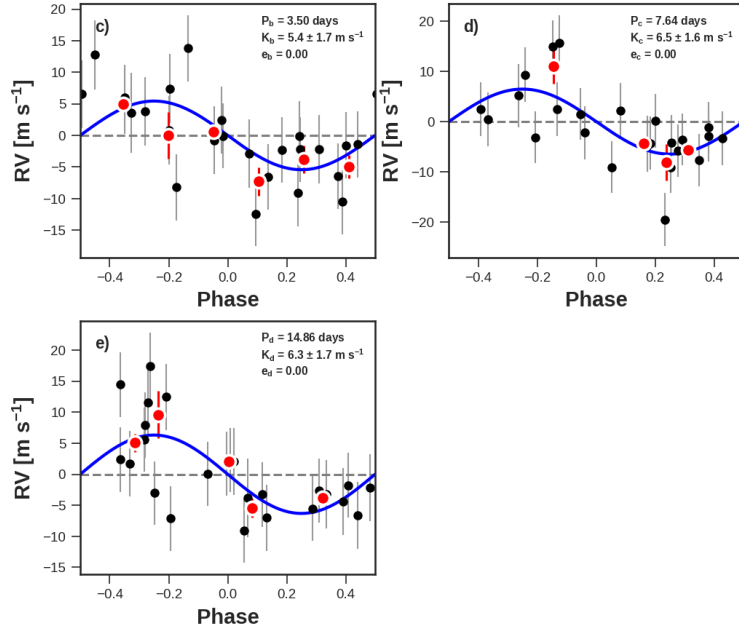
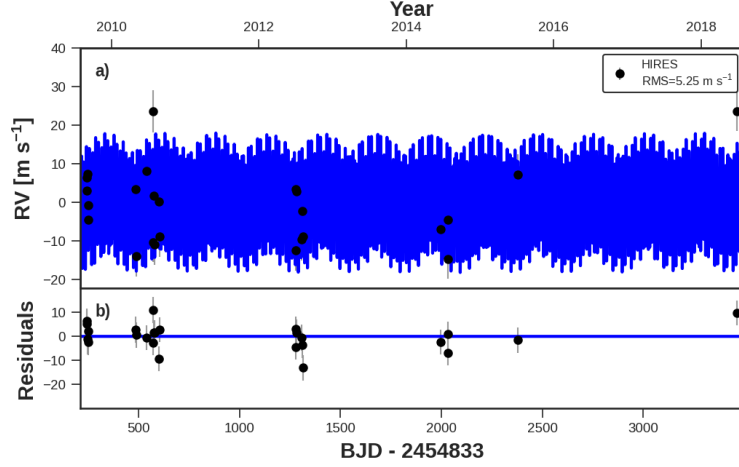


(b) Periodogram

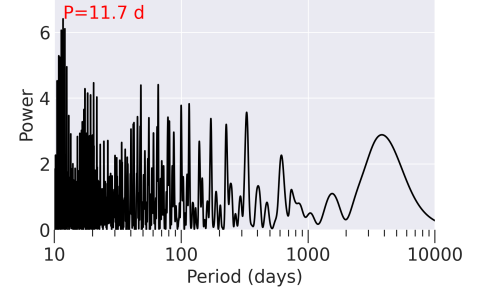
Figure 21: The same as Figure 7, but for KOI-123 (Kepler-109). No non-transiting companions are detected.

KOI-123 (KEPLER-109)

Kepler-109 (KOI-123) has two transiting planets at $P_b = 6.48$ and $P_c = 21.2$ days, both of which are smaller than Neptune ($R_b = 2.37 R_\oplus$, $R_c = 2.52 R_\oplus$). The planets were confirmed with Keck HIRES RVs in [Marcy et al. \(2014\)](#), which established mass upper limits for the planets. Since 2013, we have collected 24 new RVs, resulting in 38 total RVs collected between 2009 and 2021 (an eleven year baseline). Our best two-planet fit yields mass upper limits of $M_b = 5.0 \pm 4.4 M_\oplus$ and $M_c = 5.5 \pm 3.6 M_\oplus$, consistent with both planets being low-density sub-Neptunes with extended gas envelopes (Figure 21). The RV residuals have $\text{RMS} = 6.4 \text{ m s}^{-1}$ and no apparent trend, yielding a 3σ upper limit of $M \sin i < 0.16 M_J$ at 5 AU ($M \sin i < 0.65 M_J$ at 10 AU) for additional planets in the system.



(a) RVs



(b) Periodogram

Figure 22: The same as Figure 7, but for KOI-137 (Kepler-18). No non-transiting companions are detected.

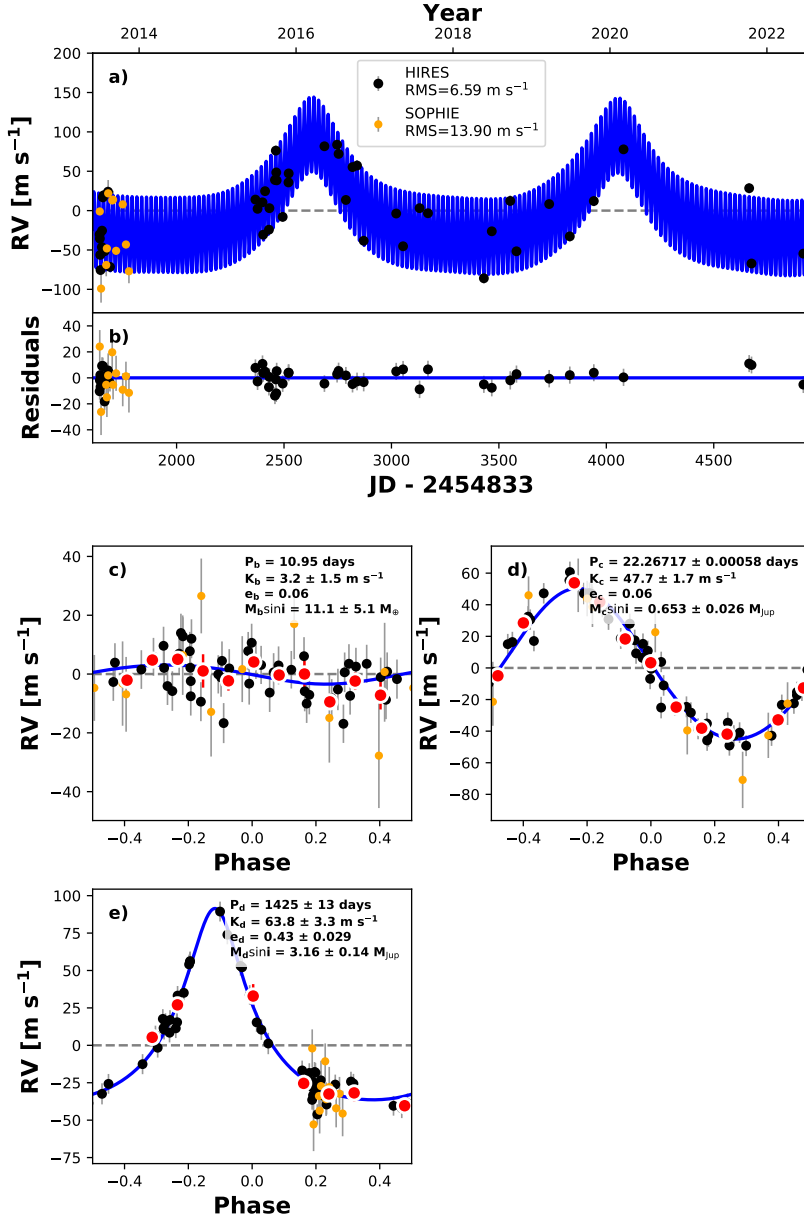
KOI-137 (KEPLER-18)

Kepler-18 (KOI-137) has three transiting planets interior to 15 days ($P_b = 3.50$ days, $P_c = 7.64$ days, $P_d = 14.86$ days) that were first announced and confirmed in [Cochran et al. \(2011\)](#). The innermost planet, Kepler-18 b, is notably smaller than the other two planets ($R_b = 2.0 R_\oplus$, $R_c = 5.49 R_\oplus$, $R_d = 6.98 R_\oplus$). The planets are near (but not in) a 4:2:1 Laplace resonant chain, and planets c and d have significant TTVs as the result of their dynamical interactions. [Cochran et al. \(2011\)](#) also collected RVs with Keck-HIRES to determine a Doppler mass for the planets, in comparison to (and in combination with) the TTV-determined masses. Their best-fit masses using TTVs and RVs were $M_b = 6.9 \pm 3.4 M_\oplus$, $M_c = 17.3 \pm 1.9 M_\oplus$, and $M_d = 16.4 \pm 1.4 M_\oplus$.

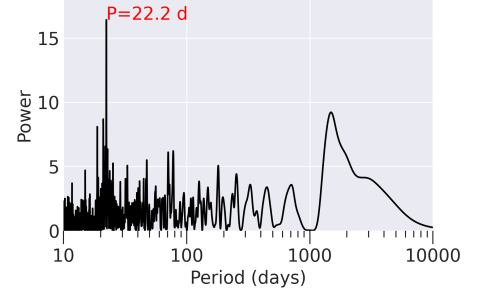
The solutions in [Cochran et al. \(2011\)](#) were based on Kepler photometry from quarters 0-6, whereas a more recent analysis by [Hadden & Lithwick \(2017\)](#) was based on the full Kepler time series (quarters 0-17). One challenge of TTVs for near-resonant systems is that the determination of mass and eccentricity can be degenerate ([Lithwick et al. 2012](#)). In Kepler-18, the mass of planet c is sensitive to whether a high-mass (and low-eccentricity) prior was adopted, with the solution for the default prior yielding a $M_c = 12.9 \pm 6.0 M_\oplus$ and the high-mas prior yielding $M_c = 21.6 \pm 3.6 M_\oplus$,

whereas the mass of planet d did not sensitively depend on the prior ($M_d = 16.2 \pm 1.4 M_\oplus$) (Hadden & Lithwick 2017). Planet b has flat TTVs, and the re-analysis in Hadden & Lithwick (2017) did not update the mass of this planet.

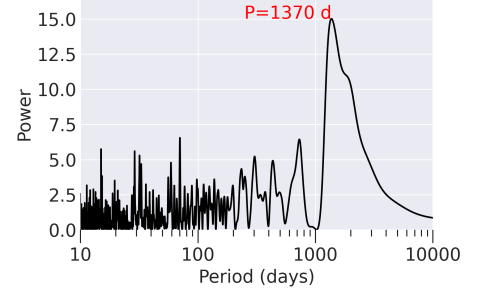
Since 2011, we have collected 11 new RVs of Kepler-18. Our analysis of the RVs alone (without incorporating TTVs) yields $M_b = 12.9 \pm 4.1 M_\oplus$, $M_c = 19.5 \pm 5.1 M_\oplus$, and $M_d = 24.0 \pm 6.5 M_\oplus$, consistent with gas-enveloped compositions for all three planets (Figure 22). There is no apparent RV trend over the nine year baseline (2009-2018), yielding a 3σ upper limit of $M \sin i < 0.40 M_J$ at 5 AU ($M \sin i < 1.6$ at 10 AU). This system would benefit from a joint analysis of the new RVs and TTVs to improve the masses and eccentricities of the planets.



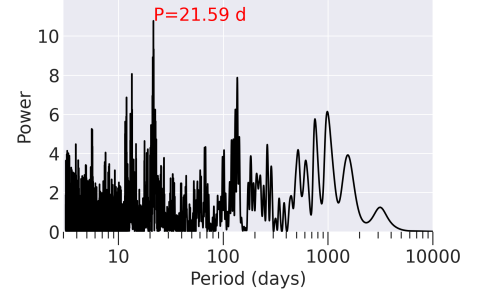
(a) RVs



(b) Periodogram (transiting planet removed)



(c) Periodogram (transiting and one giant planet removed)



(d) Residual periodogram

Figure 23: Same as Figure 7, but for KOI-142. Left: RVs are from HIRES (black circles) and SOPHIE (yellow triangles). The best-fit model has two non-transiting giant planets (details inset in RV panels, left).

KOI-142 (KEPLER-88)

KOI-142 (Kepler-88) is a system with one transiting planet ($P_b = 10.95$ days, $R_b = 3.43 R_\oplus$) that has TTVs with semi-amplitude of half a day (0.05 of the orbital period). The system was first noted in Steffen et al. (2013) and was colloquially dubbed the “King of TTVs” on account of the large TTVs of planet b. Nesvorný et al. (2013) conducted an in-depth dynamical analysis of the system, finding a unique solution for the mass and period of a giant planet perturbing the transiting planet from just outside the 2:1 mean motion resonance. The giant planet was confirmed with RVs collected at SOPHIE (Barros et al. 2014). This system is unique in that it is the only *Kepler* system we followed up for which TTVs clearly indicated an outer perturber. However, the period of the perturber was well-known (22 days). The TTVs gave no prior knowledge about whether this system would harbor a giant planet beyond 1 AU.

Eight years of Keck-HIRES RVs were also collected and analyzed in a joint RV and photodynamical model in [Weiss et al. \(2020\)](#), which confirmed and refined the mass of the giant planet in resonance and also revealed a distant Jovian-mass companion at 2.6 AU. We have collected 2 additional Keck-HIRES RVs since 2020, which are consistent with the solution in [Weiss et al. \(2020\)](#) (Figure 23). Because our baseline is comparable to the longest detected orbit in the system, any putative trend to the residuals to our best 3-planet fit is not well-constrained, and so our upper limit on additional companions is only $M \sin i < 0.067 M_J$ at 5 AU ($M \sin i < 2.7 M_J$ at 10 AU). Continued low-cadence monitoring will improve the ephemeris determination of the distant Jovian planet and might yield additional long-period planets.

KOI-148 (KEPLER-48)

KOI-148 (Kepler-48) has three transiting planets with dynamical interactions that produce TTVs, which confirmed their planetary nature (Steffen et al. 2012). Marcy et al. (2014) presented 28 RVs of the system collected with HIRES, yielding masses for the transiting planets and revealing the existence of one non-transiting giant planet (Marcy et al. 2014). There are four stellar companions within $6''$ of the primary summarized in Marcy et al. (2014). For the RV measurements, care was taken to align the field to avoid secondary light into the slit.

We have obtained 28 new RVs with HIRES since Marcy et al. (2014), resulting in 56 RVs total, which we used to improve the characterization of the masses and orbits of the planets (Figure 24). We detected a new non-transiting planet, Kepler-48 f, based on our long-term monitoring, with high confidence (FAP=2e-8, $\Delta\text{BIC} = -530$). This planet's orbital period ($P_f = 5400$ days) is distinct from the peak periodicity of the Mt. Wilson S-values (~ 2500 days). In order of increasing orbital distance, the planets have periods $P_b = 4.78$ days, $P_c = 9.67$ days, $P_d = 42.9$ days, $P_e = 1001$ days, and $P_f = 5205$ days, and minimum masses of $6.1 M_\oplus$, $11.6 M_\oplus$, $8 M_\oplus$, $2.1 M_J$, and $1.3 M_J$. We assume the three transiting planets are circular, and we find upper limits on the eccentricities of the non-transiting planets of $e_e < 0.09$ and $e_f < 0.36$ (3σ confidence).

Because our baseline is comparable to the longest detected orbit in the system, any putative trend to the residuals to our best 5-planet fit is not well-constrained, and so our upper limit on additional companions is only $M \sin i < 0.50 M_J$ at 5 AU ($M \sin i < 2.0 M_J$ at 10 AU). Future RVs will improve the characterization of the period, eccentricity, and minimum-mass of the long-period companion and will also place better constraints on the presence of additional companions.

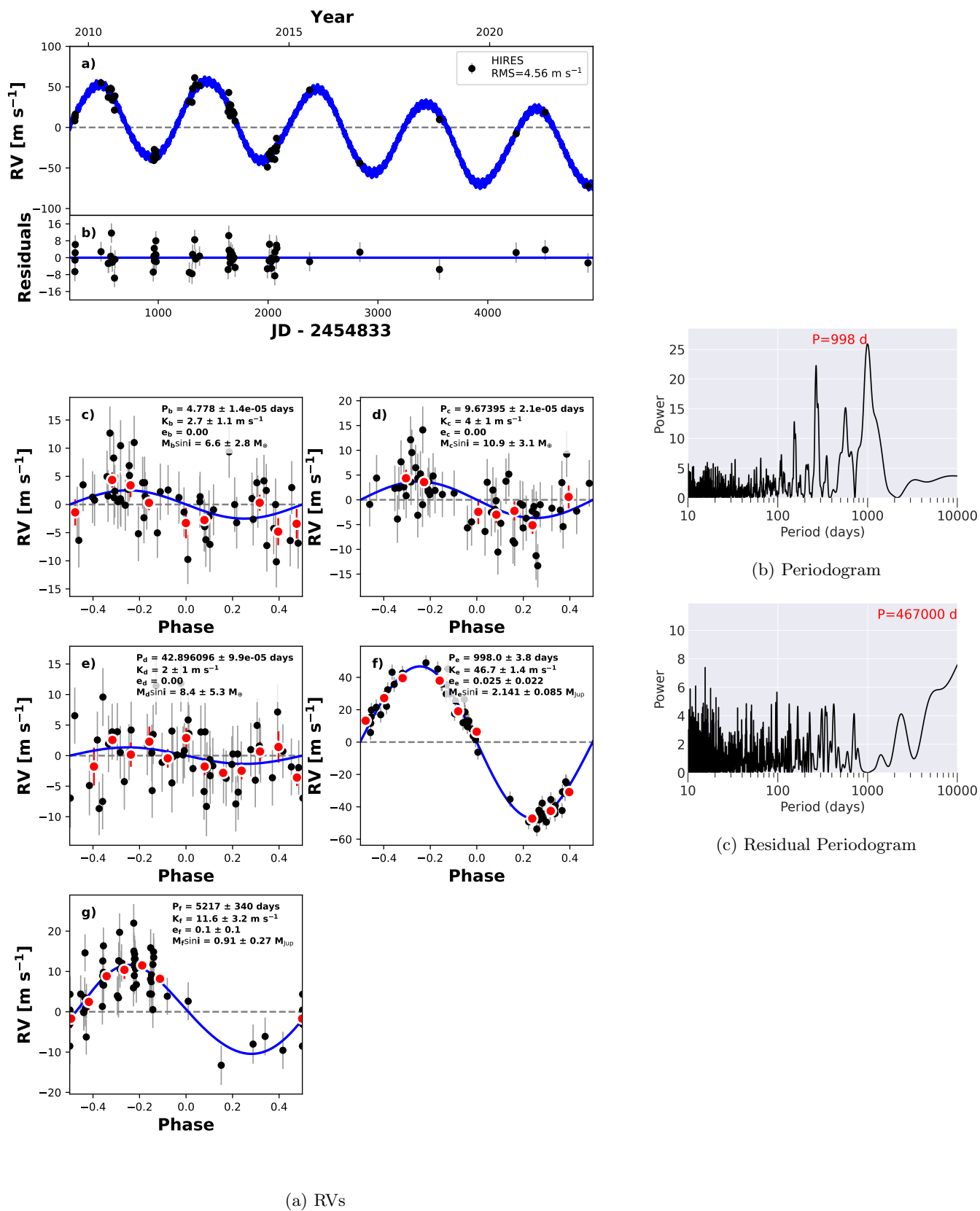
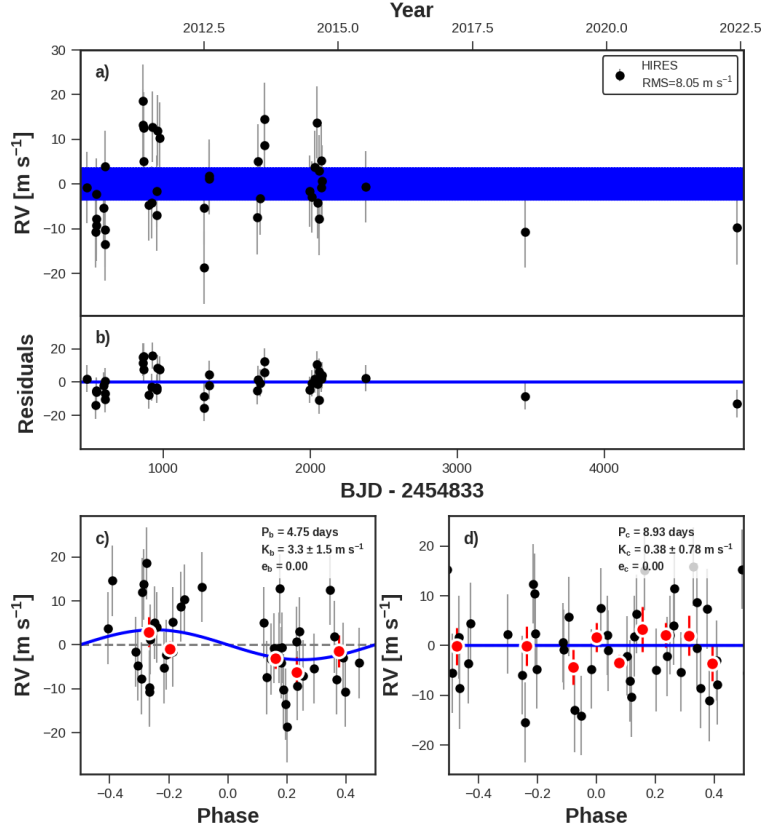
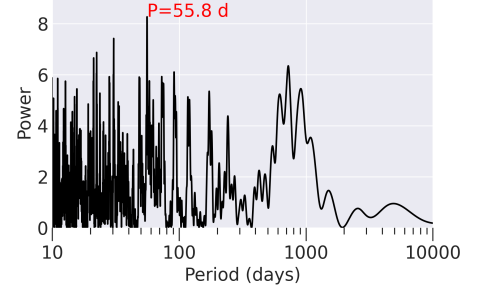


Figure 24: Same as Figure 7, but for KOI-148 (Kepler-48). The longest-period companion presented here was not detected by the KGPS algorithm, but was identified in the residuals by eye.



(a) RVs

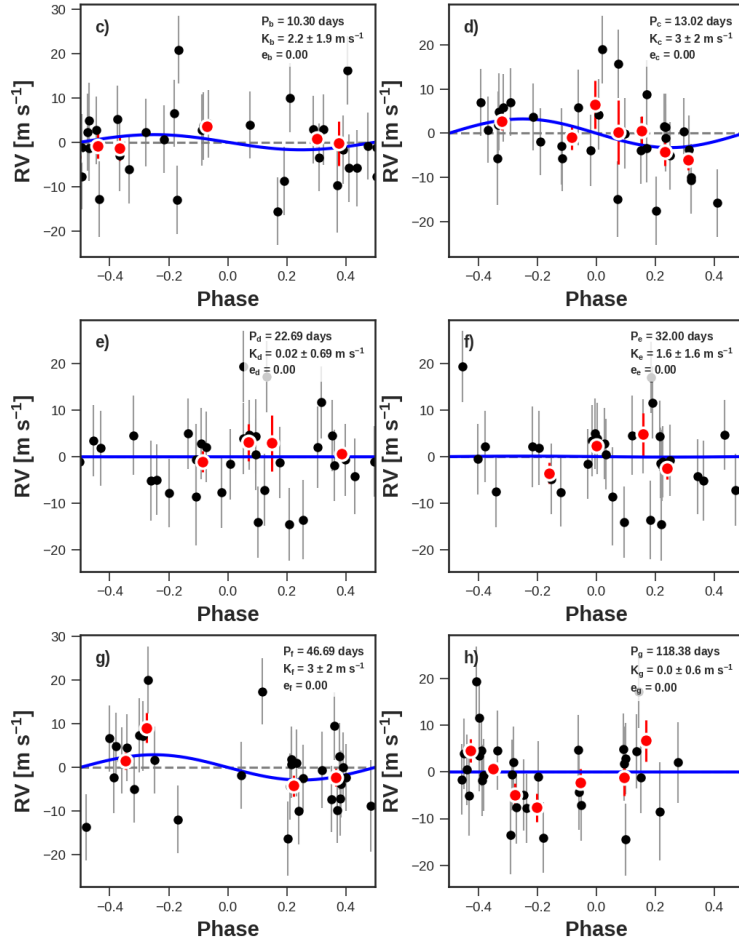
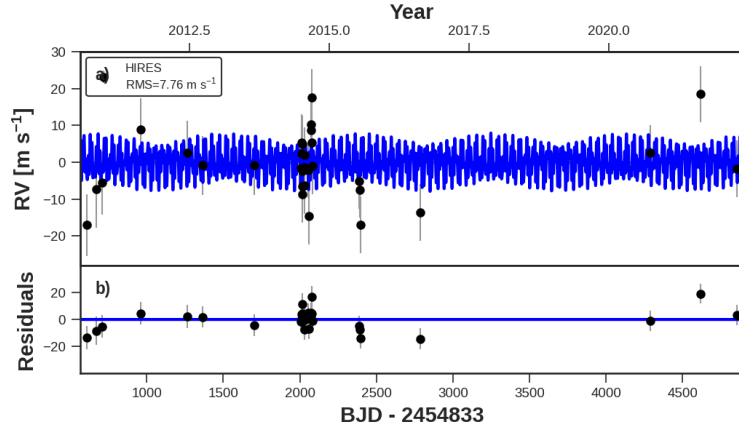


(b) Periodogram

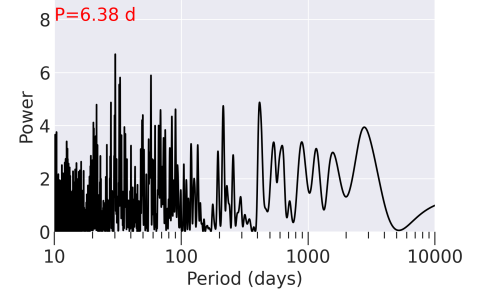
Figure 25: The same as Figure 7, but for KOI-153 (Kepler-113). No non-transiting companions are detected.

KOI-153 (KEPLER-113)

Kepler-113 (KOI-153) is a $V = 13.7$ K-type star ($T_{\text{eff}} = 4791 \text{ K}$) (Fulton & Petigura 2018b). The system has two transiting sub-Neptunes ($R_b = 1.82 \pm 0.6 R_{\oplus}$, $R_c = 2.18 \pm 0.06 R_{\oplus}$) with periods of $P_b = 4.75$ days and $P_c = 8.93$ days. The planets were confirmed with Keck-HIRES RVs in Marcy et al. (2014), which yielded a mass upper limit for the outer planet a 2.7 sigma measurement for the inner planet of $11.7 \pm 4.2 M_{\oplus}$. With 18 new HIRES RVs since 2013 (42 RVs total) we have refined the planet masses, finding $M_b = 7.0 \pm 3.3 M_{\oplus}$ and $M_c = 2.5 \pm 2.5 M_{\oplus}$ (Fig. 25). Planet b, which is near the distinction between planets with rocky surfaces and planets with volatile envelopes (Weiss & Marcy 2014; Rogers 2015; Fulton et al. 2017) is consistent with having a predominantly rock (by volume) composition, with a possible thin gas envelope, whereas planet c is consistent with having a larger gas envelope more typical of sub-Neptunes. The residual RVs (RMS= 8.2 m s^{-1}) have structure at 55 days and > 500 days, although the false positive probability (0.16) is too high to consider these signals as planet candidates. The possibility of an additional planet in the system was also noted in Marcy et al. (2014), but at periods of 1.065, 16, 0.984, and 0.515 days, none of which have become stronger signals with more data. Additional RVs will help determine whether one or both of the new candidate periods are associated with bona-fide planets. There are no strong peaks in the periodogram of the RV residuals nor any apparent trends in the RV residuals time series, to our two-planet fit, yielding a 3σ upper limit of $M \sin i < 0.31 M_J$ at 5 AU ($M \sin i < 1.3 M_J$ at 10 AU).



(a) RVs



(b) Periodogram

Figure 26: The same as Figure 7, but for KOI-157 (Kepler-11). No non-transiting companions are detected.

KOI-157 (KEPLER-11)

Kepler-11 (KOI-157) is a system with six transiting planets that has been extensively studied as an exemplary multi-planet system with significant TTVs (Lissauer et al. 2011). The planets range in size from 1.8 to 4.2 R_{\oplus} and

have ultra-low densities, based on their TTVs (Lissauer et al. 2013). A subset of the RVs presented here were used in a joint RV and TTV analysis, the results of which were that (i) the RVs alone ruled out rocky compositions for the planets, (ii) the combined RV-TTV analysis was consistent with low densities for the planets, and (iii) the RVs reduced the mass upper limit of planet g, which is dynamically decoupled from the inner 5 planets and is therefore not well-characterized by their TTVs (Weiss 2016). Between 2010 and 2022, we collected 31 RVs. The RVs provide mass upper limits for the transiting planets, as described in Weiss (2016). The residual RVs to our best six-planet fit have $\text{RMS}=7.3 \text{ m s}^{-1}$ and no apparent trend, yielding an upper limit of $M \sin i < 0.6 M_J$ at 5 AU ($M \sin i < 1.6 M_J$ at 10 AU, 3σ conf.)

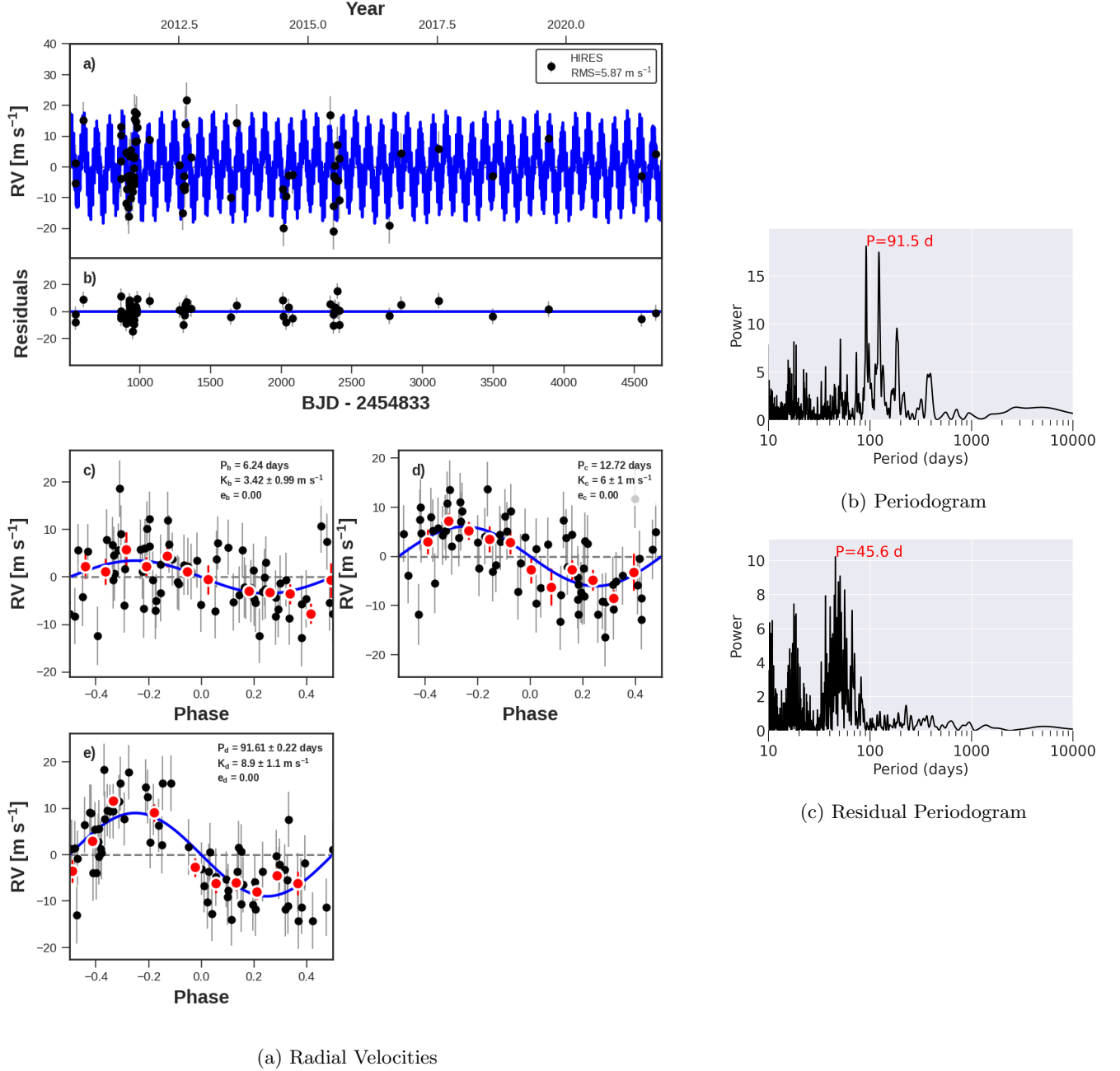


Figure 27: The same as Figure 7, but for KOI-244 (Kepler-25). The best-fit model includes a non-transiting planet, Kepler-25 d (orbital parameters inset in phase-folded panel).

KOI-244 (KEPLER-25)

Kepler-25 (KOI-244) is a system with two transiting planets near the 2:1 mean motion resonance. Dynamical interactions between the transiting planets produce TTVs, which confirm the planetary nature of the system (Steffen et al. 2012). Marcy et al. (2014) collected 62 RVs of this system with Keck-HIRES. The RVs also revealed a non-transiting planet at $P_d = 91$ or 122 days. Hadden & Lithwick (2014) performed N-body forward modeling to fit the TTVs of the transiting planets and found upper limits on the planet masses. A photodynamical analysis that jointly fit the Kepler photometry and the HIRES RVs (including 5 new RVs) revealed a reduction in the planet mass-eccentricity degeneracy when using photometry alone (Mills et al. 2019b). The results are consistent with a low-

eccentricity resonant state but do not indicate that the planets are definitively librating within the resonance. Two complete transits were observed with Keck-HIRES Doppler spectroscopy to measure the Rossiter-McLaughlin (RM) effect, finding the orbital plane of the planets and the axis of stellar rotation to be well-aligned [Albrecht et al. \(2013\)](#). The detection of the planets transiting in NASA TESS photometry was leveraged to update their orbital ephemerides, improving the precision of the linear ephemerides by an order of magnitude ([Battley et al. 2021](#)). [Jontof-Hutter et al. \(2022b\)](#) combine legacy Kepler photometry with new TESS photometry to determine that the TTV solution does not change with the inclusion of TESS data for this system.

We have collected 2 new RVs since 2019, bringing the total number of non-RM RVs to 69 (Figure 27). The new RVs and updated ephemerides have not substantially changed the characterization of any of the known planets. However, the non-detection of an RV trend in the residuals to a three-planet model (including planet d at either 91 or 122 days) over the baseline of 2011 to 2022 yields a 3σ upper limit on additional long-period companions of $M \sin i < 0.70 M_J$ at 10 AU.

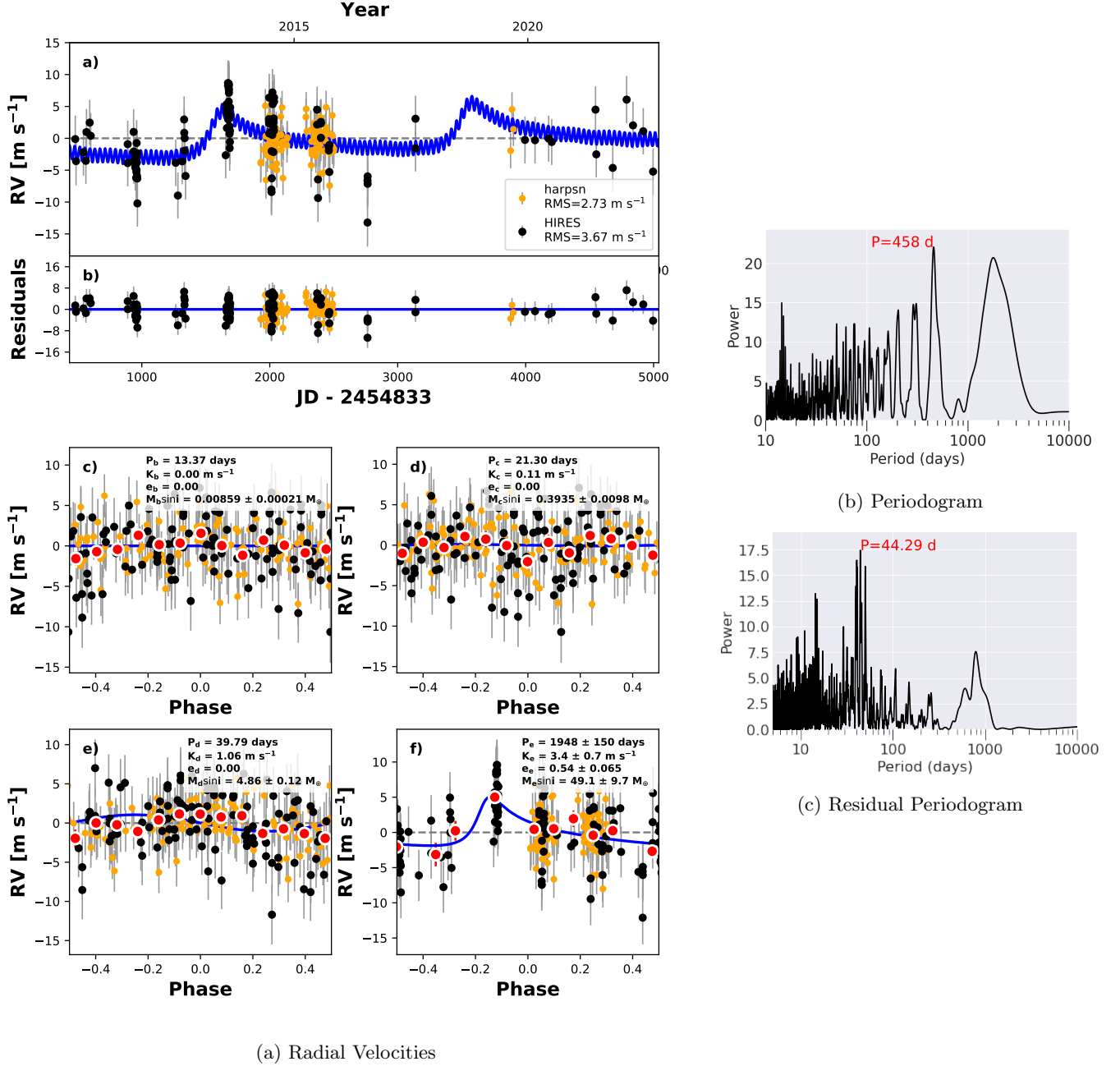


Figure 28: The same as Figure 7, but for KOI-245 (Kepler-37). Left: The RVs were taken at Keck-HIRES (black circles) and TNG-HARPS-N (yellow triangles). The best-fit model includes a Keplerian signal that is not related to a transiting planet. Right: the periodogram of the Kepler-37 RVs after removing the signal associated with the transiting planets yields multiple peaks that are likely aliases.

KOI-245 (KEPLER-37)

Kepler-37 (KOI-245) is a $V=9.7$ G-type ($T_{\text{eff}}=5300 \text{ K}$) star. The system has three transiting sub-Neptunes ($P_b = 13.4$ days, $P_c = 21.3$ days, $P_d = 39.8$ days), one of which is smaller than Mercury ($R_b = 0.30 R_{\oplus}$), that were identified and confirmed in [Barclay et al. \(2013\)](#). The star has solar-like oscillations, which enabled a precise determination of the physical stellar properties through the combination of asteroseismology and spectroscopy. [Marcy et al. \(2014\)](#) used Keck-HIRES RVs to place upper limits on the masses of transiting planets b, c, and d. A fourth transiting candidate

at $P = 51$ days was identified in the photometry but was suspected to be due to noise or an instrumental false positive (Barclay et al. 2013). Nonetheless, the fourth candidate has been considered in various TTV analyses (Hadden & Lithwick 2014; Holczer et al. 2016). Most recently, Rajpaul et al. (2021) further examined Kepler photometry data, concluding that Kepler-37e, with a 51d period should be stripped of its confirmed/validated status citing the extremely weak photometric evidence.

Since the publication of Marcy et al. (2014), we have acquired 48 new RVs on Keck-HIRES, resulting in 81 RVs from HIRES and 218 RVs total (including literature RVs from HARPS-N, Figure 28). We applied models with either three or four small planets (to account for the candidate at 51 days) to the combined HIRES and HARPS-N RVs. In both cases, there is significant structure in the residual RVs, with peaks near 460 and 2000 days. The peak at 460 days does not phase nicely as a Keplerian signal and is likely an alias; we preferred the signal at 2000 days to test as a new planet candidate in the system.

The amplitude of the long-period planet candidate signal is low ($K = 3.3 \text{ m s}^{-1}$) and the fit is quite eccentric ($e = 0.52$). The effective temperature of this star (6265 K) places it very near the Kraft Break, and the slightly evolved stellar surface gravity ($\log(g) = 4.31$), means this star is unlikely to be heavily influenced by chromospheric activity. However, there appears to be modest correlation between the S-values and RVs. Further RV, stellar activity, and photometric monitoring are needed to ascertain whether the long-period signal is planetary in nature. For the purposes of this work, we do not consider the signal a detected planet since its provenance is questionable. Whether or not the long-period signal is modeled with a Keplerian and removed, the RV residuals yield upper limits of $M \sin i < 0.22, M_J$ at 10 AU with 3σ conf.

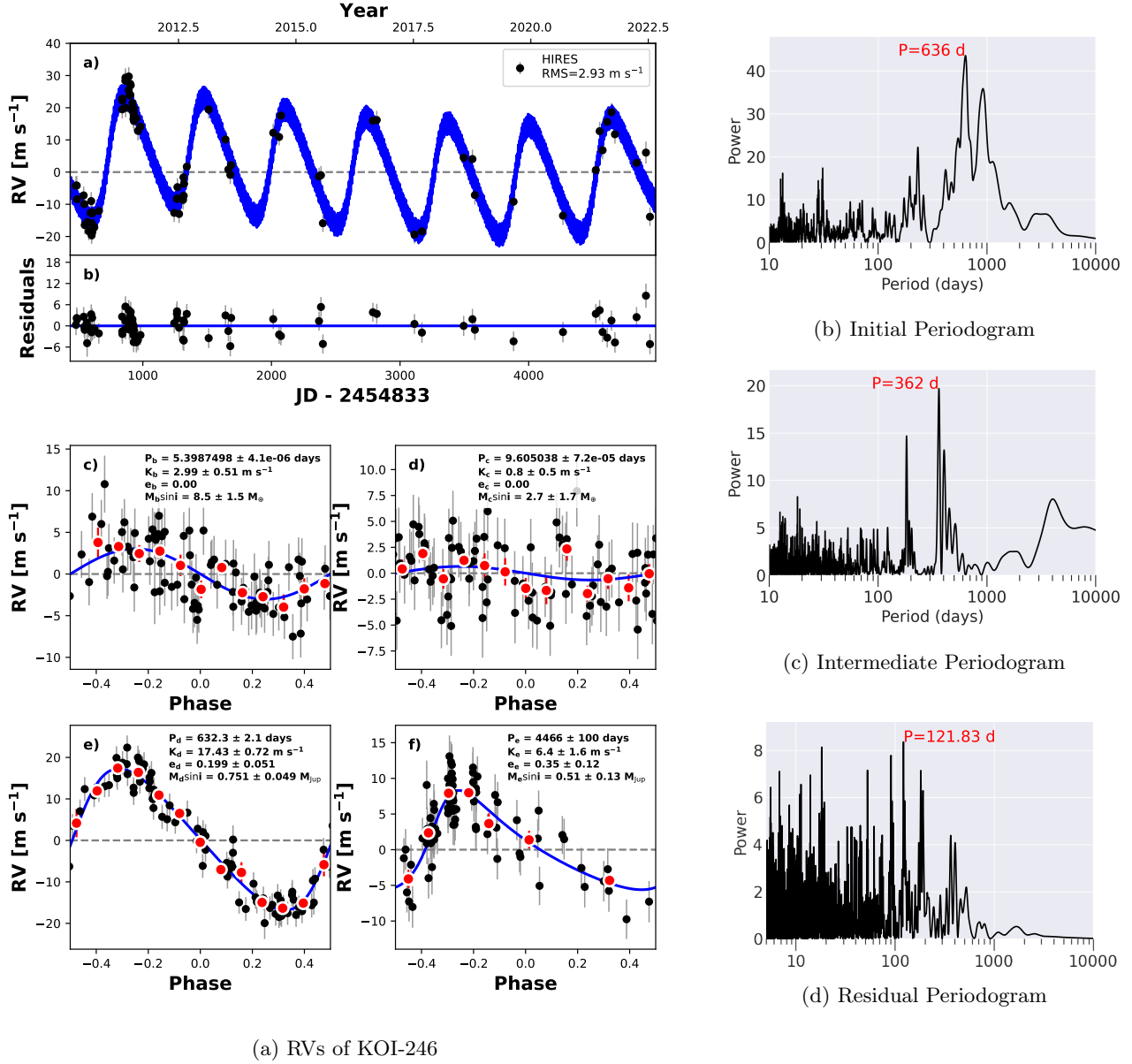


Figure 29: Same as Figure 7, but for KOI-246. Left: The best-fit model includes two non-transiting planets, Kepler-68 d at 633 days and Kepler-68 e at 5000 days (see insets in phase-folded panels). Right: the top panel is a periodogram of the HIRES RVs after removing the transiting planets only, the middle panel is the periodogram after removing one non-transiting planet at 636 days (note the strong yearly alias at 362 days), and the bottom panel is after removing non-transiting planets at 634 and 5000 days.

KOI-246 (KEPLER-68)

Kepler-68 (KOI-246, 29) is a system with a sub-Neptune and an Earth-sized transiting planet. The transiting planets were validated via photometric techniques including odd-even tests, color diagnostics, and dynamically confirmed using RVs in Gilliland et al. (2013). The stellar mass and radius were determined via asteroseismology. The RVs also revealed a non-transiting planet, Kepler-68 d, with a best-fit period of 581 days. Additional RVs were obtained and published in Marcy et al. (2014), resulting in an update of the period of the non-transiting planet to 625 days and modestly refined transiting planet masses. Another update in Mills et al. (2019b) again revised the period of the non-transiting planet to 634 days and improved the masses of the transiting planets via dynamical analysis.

With several additional seasons of RVs, we confirm the properties of planet d: $P_d = 633$ days, $M \sin i_d = 0.765 \pm 0.045 M_J$, $e_d = 0.19 \pm 0.05$ (Figure 29). We also announce a non-transiting planet, Kepler-68 e. The peak of our Lomb-Scargle periodogram is at 362 days, which is likely a yearly alias of the (presumed) long period of planet e. The Mt. Wilson S-values also have a peak at 362 days, which is likely due to window function. We obtained a new RV template observation and reran our barycentric correction analysis for this target, but the peak at 362 days persisted even after our new reduction and RV determinations. The best-fit model that includes planets at both 362 and 633 days with moderate eccentricities that would result in orbit crossing, and so this configuration is unlikely. Our interpretation is that the peak at 362 days is the alias of a planet, Kepler-68 e, at a period of $P_e \approx 4400$ days with $M \sin i_e \approx 0.4 M_J$ and $e_e \approx 0.4$. Adopting these properties in our four-planet model removes the 362-day peak from the Lomb-Scargle periodogram of the residuals. The mass upper limit of an additional (third) giant planet is not well constrained because of the uncertainty in the orbit of planet e, yielding a 3σ upper limit of $M \sin i < 0.11 M_J$ at 5 AU ($0.43 M_J$ at 10 AU). If we ignore the second giant planet and instead consider the residuals to a three-planet model, the upper limits on an additional companion increase by 50%.

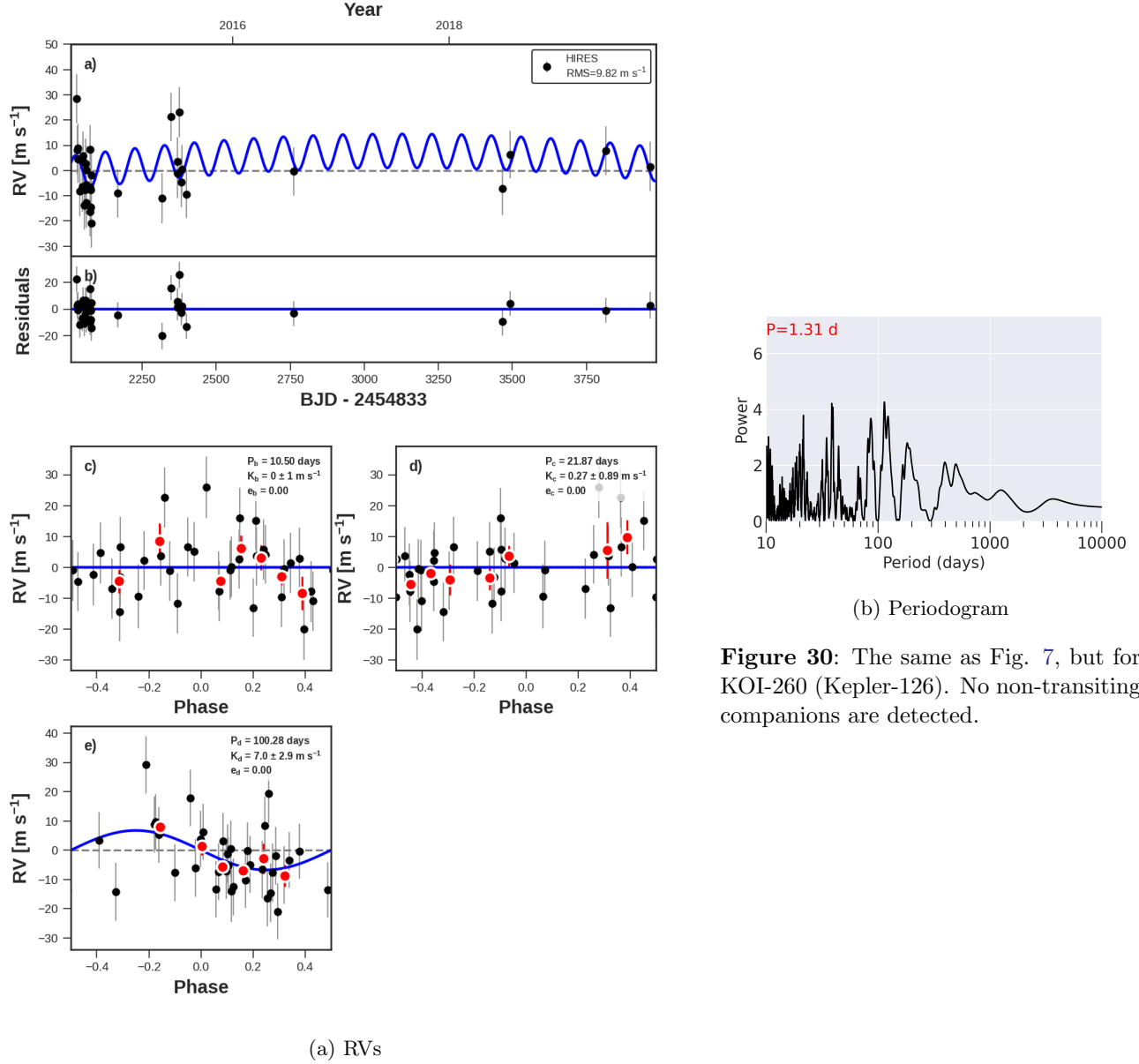
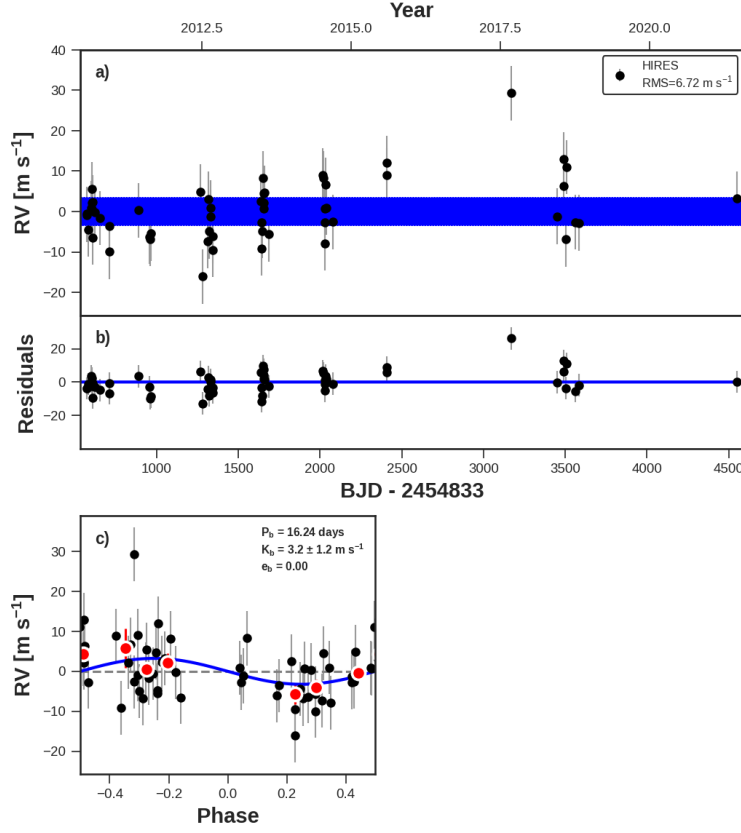


Figure 30: The same as Fig. 7, but for KOI-260 (Kepler-126). No non-transiting companions are detected.

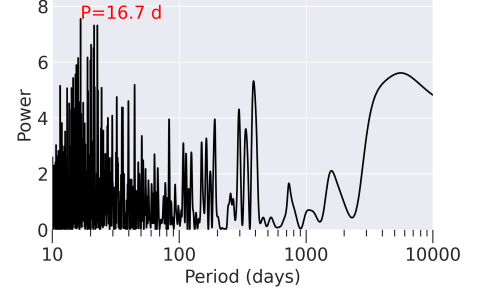
KOI-260 (KEPLER-126)

Kepler-126 (KOI-260) is a $V=10.5$ star near the Kraft break ($T_{\text{eff}} = 6200 \text{ K}$). The system has three transiting planets at $P_b = 10.5$, $P_c = 21.9$, and $P_d = 100$ days that were statistically validated (Lissauer et al. 2014; Rowe et al. 2014). All three planets have significant TTVs that have been used to set upper limits on their eccentricities (Van Eylen & Albrecht 2015). Planet d appears to be dynamically decoupled from the inner two planets, and so its TTVs are likely caused by at least one planet that has not been detected yet.

We present 35 RVs from Keck-HIRES, which were collected between 23 July 2014 and 11 November 2019 (Figure 30). The time series began in 2014 for a KOI follow-up program that examined planets in multi-planet systems with period ratios near mean-motion-resonance. The residual to our best three-planet fit has $RMS = 9.9 \text{ m s}^{-1}$, which is typical for a star with $T_{\text{eff}} = 6150 \text{ K}$ and $v \sin i = 8.7 \text{ km/s}$ (Isaacson & Fischer (2010)). The non-detection of an RV trend sets an upper limit of $M \sin i < 0.8 M_J$ for a companion at 5 AU ($M \sin i < 3.2 M_J$ at 10 AU).



(a) RVs



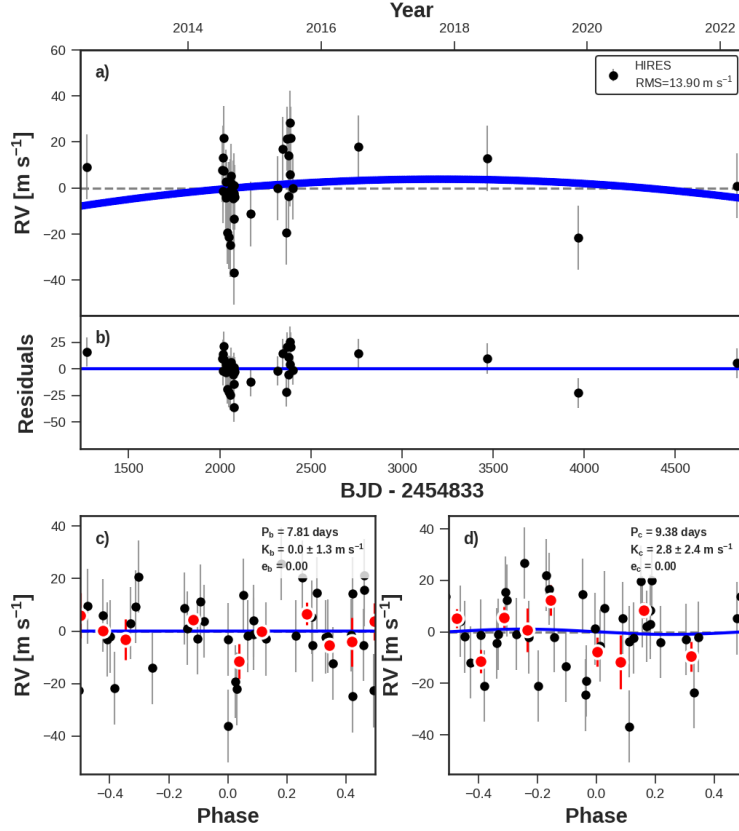
(b) Periodogram

Figure 31: The same as Fig. 7, but for KOI-261 (Kepler-96). No non-transiting companions are detected.

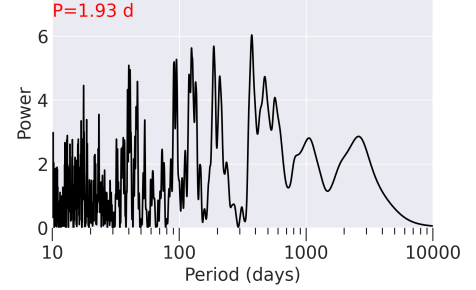
KOI-261 (KEPLER-96)

Kepler-96 (KOI-261) is a $V=10.3$ sun-like star with one transiting planet ($P_b = 16.2$ days, $R_b = 2.6 R_\oplus$). The planet was confirmed with 44 Keck-HIRES RVs, which yielded a mass of $8.4 \pm 3.4 M_\oplus$, consistent with a volatile-enveloped planet (Marcy et al. 2014).

We have collected 11 new RVs since 2014 (Figure 31). A single RV outlier of 20 m s^{-1} in 2017 might be consistent with the orbit of an eccentric non-transiting planet, although the RVs are also consistent with no giant planet if the 2017 data point is ignored. If the planet is real, it has a period of ~ 4000 days and a mass of $\sim 1 M_J$. We consider this a planet candidate, although more RVs are needed to confirm its existence and characterize its orbit and mass.



(a) RVs



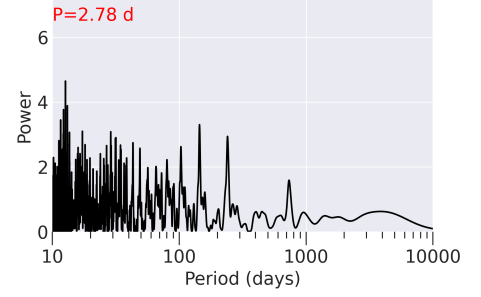
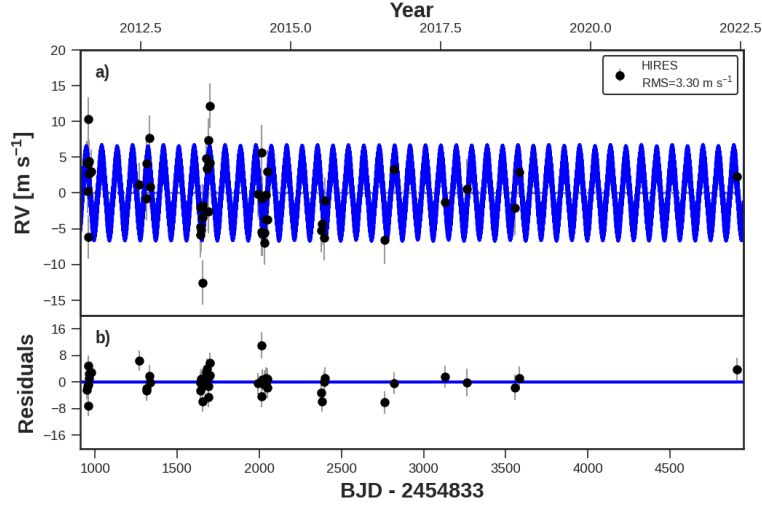
(b) Periodogram

Figure 32: The same as Fig.7, but for KOI-262 (Kepler-50). No non-transiting companions are detected.

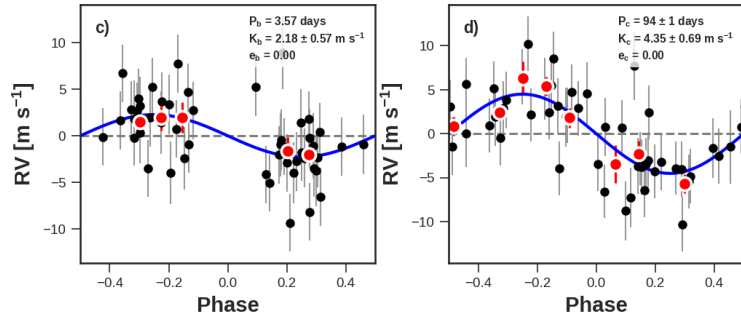
KOI-262 (KEPLER-50)

Kepler-50 (KOI-262) is a V=10.7 F type star ($T_{\text{eff}} = 6200 \text{ K}$) with two transiting planets ($R_b = 1.7 R_{\oplus}$, $R_c = 2.2 R_{\oplus}$) confirmed in Chaplin et al. (2013). The planets' compact architecture ($P_b = 7.81 \text{ days}$, $P_c = 9.37 \text{ days}$) produces significant TTVs, which yield mass upper limits of $M_b < 8.9 M_{\oplus}$ and $M_c < 8.2 M_{\oplus}$ (Steffen et al. 2012). The star has solar-like oscillations that enabled an asteroseismic analysis, including mode splitting that revealed that the stellar rotation axis is closely aligned with the angular momentum vector of the planet orbits (Chaplin et al. 2013).

We observed this target for a KOI follow-up program that characterized planets in multi-planet systems with period ratios near mean-motion-resonance. We collected 39 RVs between 2012 and 2022 (10 year baseline, Fig. 32). The residual RVs to our best two-planet fit have a high RMS (14 m s^{-1}). The star's temperature is near the Kraft break (Kraft 1967), and the star has $v \sin i = 10 \text{ km/s}$, both of which could contribute to the high RMS of the residual RVs, although we only expected a jitter of 9 m s^{-1} for this target. There is no significant trend to the RV residuals, yielding a 3σ upper limit of $M \sin i < 0.70 M_J$ at 5 AU ($M \sin i < 2.8 m_{jup}$ at 10 AU).



(b) Periodogram



(a) RVs

Figure 33: The same as Figure 7, but for KOI-265 (Kepler-507). Left: The best-fit model includes a non-transiting planet, Kepler-507 c (orbital parameters inset in phase-folded panel). Right: Periodograms of the RVs after subtracting the models from the transiting planets only (top) and the best-fit model that includes the non-transiting planet (bottom).

KOI-265 (KEPLER-507)

Kepler-507 (KOI-265) is an F type star ($T_{\text{eff}} = 6000 \text{ K}$) with one transiting planet ($P_b = 3.56 \text{ days}$, $R_b = 1.3 R_{\oplus}$) that was statistically validated in (Morton et al. 2016). The stellar and planetary properties were updated based on the Gaia parallax (Berger et al. 2018). We have collected 49 Keck-HIRES RVs between 2011 and 2022, which yield a mass of $M_b = 5.5 \pm 1.7 M_{\oplus}$ (Figure 33). This star was not part of the Marcy et al. (2014) results due to stellar properties at the time falling outside of the optimal range for precise RVs.

The residual RVs have $\text{RMS} = 4.6 \text{ m s}^{-1}$, and there is no significant RV trend, resulting in a 3σ upper limit of $M \sin i < 0.3 M_J$ at 5 AU ($M \sin i < 1 M_J$ at 10 AU). However, there is a marginally significant peak in the fast periodogram at 94 days (FAP=0.04) and several harmonics and aliases of that peak. The inclusion of a Keplerian fit at 94 days reduces the RMS of the RVs from 4.6 m s^{-1} to 3.3 m s^{-1} and produces $\Delta \text{BIC} = -30$. The RV amplitude of the 94 day signal is 4.5 m s^{-1} , corresponding to a planet candidate mass of $M \sin i = 35 M_{\oplus}$ (which is well within the upper limits established from the RV trend). More RVs are needed to identify the correct orbital period of this candidate second planet and determine its mass.

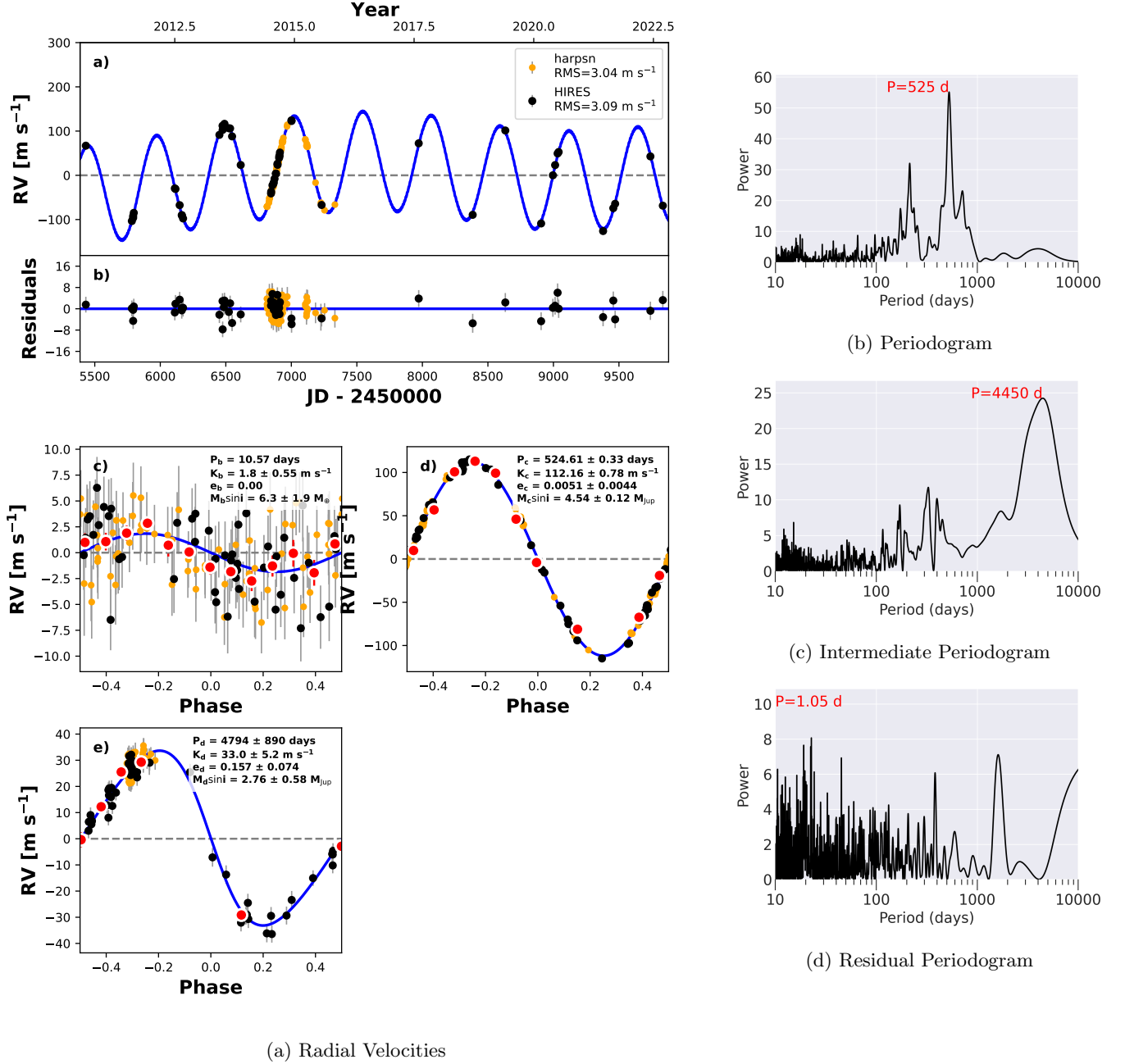


Figure 34: The same as Figure 7, but for KOI-273 (Kepler-454). Left: The RVs were taken at Keck-HIRES (black circles) and TNG-HARPS-N (maroon triangles). The best-fit model includes two non-transiting planets, Kepler-454 c at 524 days and Kepler-454 d at 4800 days (see insets in phase-folded panels). Right: the top panel is a periodogram of the RVs after removing the transiting planets only, the middle panel is the periodogram after removing one non-transiting planet at 524 days, and the bottom panel is after removing non-transiting planets at 524 and 4800 days.

KOI-273 (KEPLER-454)

KOI-273 (Kepler-454) has one transiting planet at $P = 10.57$ days. Gettel et al. (2016) used precise RVs from HIRES and HARPS-N to characterize the transiting planet (b), a non-transiting planet at $P = 524$ days (c), and a linear trend representative of a third companion. The Kepler photometry revealed solar-like oscillations of the host star, enabling a precise characterization of the stellar mass and radius. Our new RVs from Keck-HIRES are lower

than expected from the linear trend, indicating the detection of curvature due to the orbit of the distant companion. Our joint fit to the HIRES and HARPS-N RVs yield planet masses of $M_b = 6 \pm 2 M_\oplus$, $m_c \sin i = 4.6 \pm 0.2 M_J$, and $m_d \sin i = 2.6 \pm 0.3 M_J$ (Figure 34). Additionally, our new RVs clarify the orbits of the non-transiting planets and detect a marginally significant eccentricity for planet d: $P_c = 524 \pm 1$ days, $P_d = 5000 \pm 450$ days, and $e_d = 0.18 \pm 0.06$. The KOI-273 is another example of the value of long RV time baselines when detecting long period massive planets. Because our baseline is comparable to the longest detected orbit in the system, any putative trend to the residuals to our best 3-planet fit is not well-constrained, and so our upper limit on additional companions is only $M \sin i < 1.7 M_J$ at 5 AU ($M \sin i < 7.0 M_J$ at 10 AU). Future RVs will improve the characterization of the period, eccentricity, and minimum-mass of the long-period companion and will also place better constraints on the presence of additional companions.

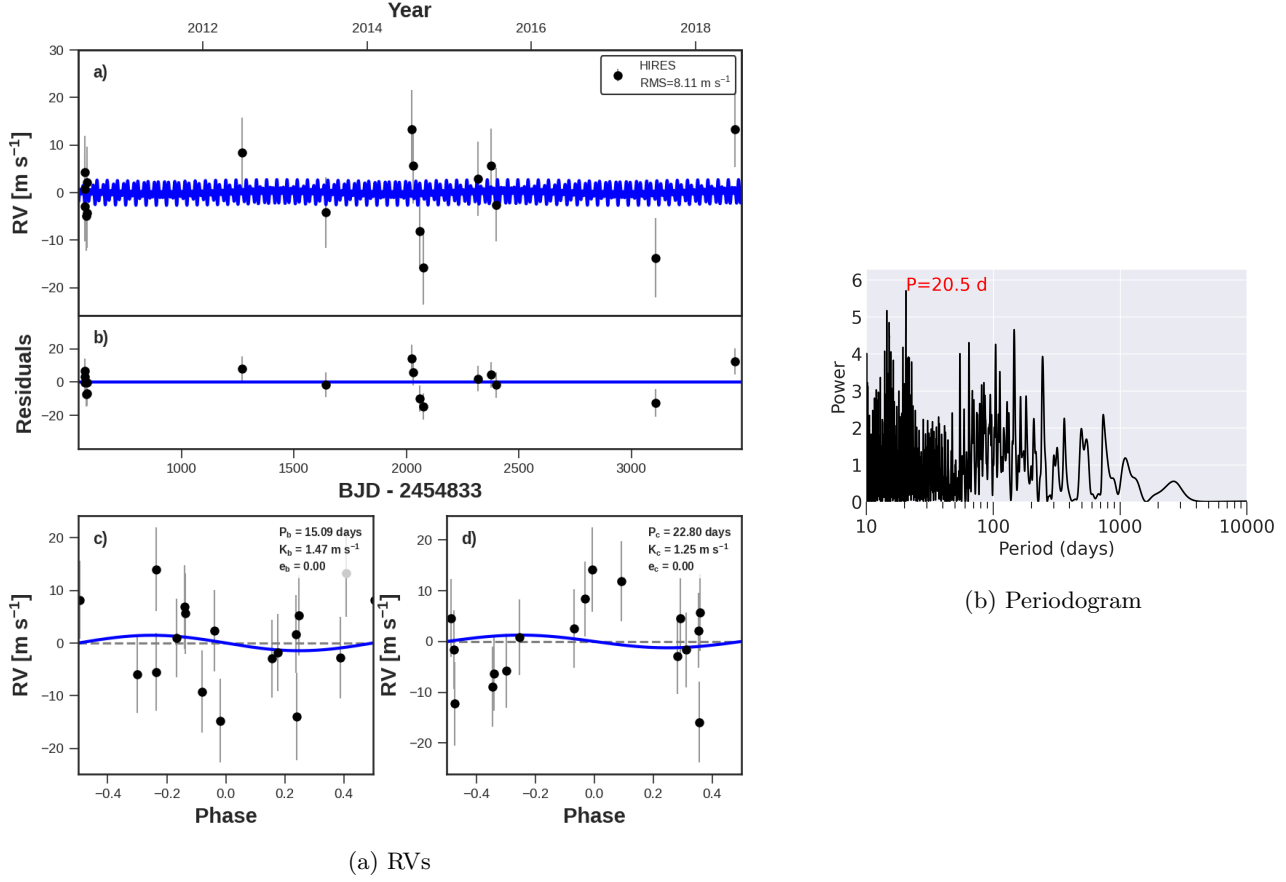


Figure 35: Same as Figure 7, but for KOI-274 (Kepler-128). No non-transiting companions are detected.

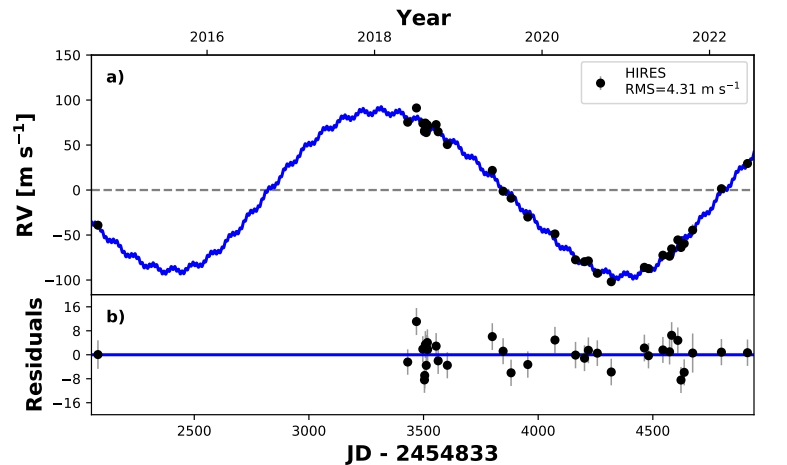
KOI-274 (KEPLER-128)

Kepler-128 (KOI-274) is an F type star with moderate rotation ($T_{\text{eff}} = 6000 \text{ K}$, $v \sin i = 6 \text{ km/s}$) (Fulton & Petigura 2018a). The star has two transiting planets with radii $R_b = 1.4 R_{\oplus}$ and $R_c = 1.3 R_{\oplus}$. The compact architecture of the transiting planets ($P_b = 15.1 \text{ days}$, $P_c = 22.8 \text{ days}$) produces significant TTVs (Xie 2014). An N-body dynamical characterization of the TTVs yielded planet masses of $M_b = 0.77 \pm 0.40 M_{\oplus}$ and $M_c = 0.90 \pm 0.45 M_{\oplus}$ (Hadden & Lithwick 2014). The low densities determined from the TTVs ($\rho_b = 1.5 \pm 0.8 \text{ g cm}^{-3}$, $\rho_c = 2.1 \pm 1.1 \text{ g cm}^{-3}$) are distinct from the density of rocky planets at this size ($\sim 7.5 \text{ g cm}^{-3}$), suggesting that the planets, though small, might contain low-density volatiles as a major constituent of their bulk compositions.

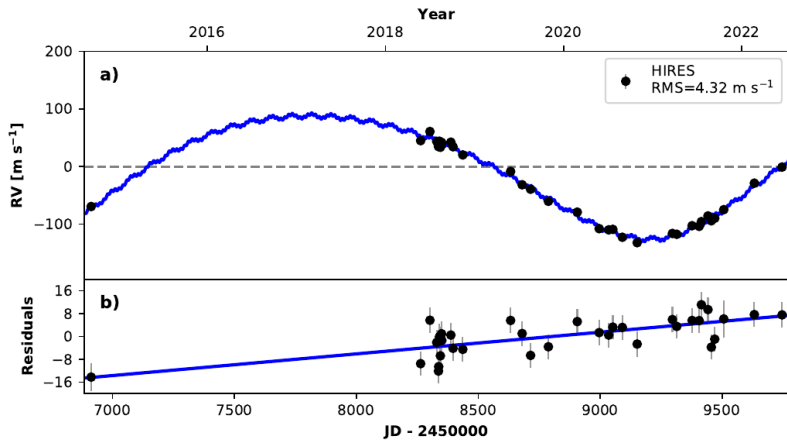
We have collected 17 RVs using Keck-HIRES between 2012 and 2022 (Fig. 35). This number of RVs did not meet our criterion for fitting planet masses (at least 20 degrees of freedom). Assuming the planets have typical masses for their sizes (Weiss & Marcy 2014), the residual RVs have $\text{RMS} = 8.1 \text{ m s}^{-1}$, which is typical for a moderately rotating F-type star. There are no strong peaks in the periodogram of the RV residuals and no apparent trends, yielding a 3σ upper limit of $M \sin i < 0.37 M_J$ at 5 AU ($M \sin i < 1.5 M_J$ at 10 AU).

KOI-275 (KEPLER-129)

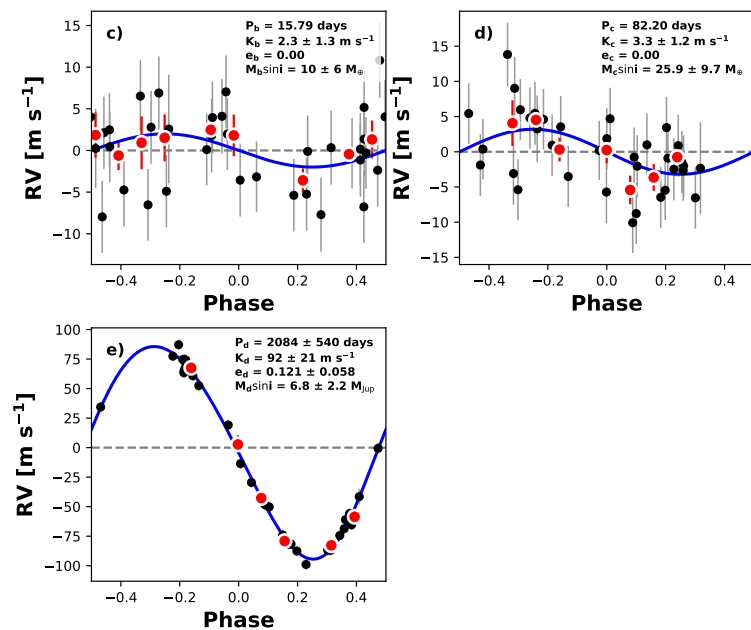
KOI-275 (Kepler-129) has two transiting sub-Neptune sized planets. Zhang et al. (2021) used precise RVs from HIRES to detect and characterize a non-transiting companion at an orbital distance of a few AU, with a minimum mass near the boundary between planetary and brown-dwarf mass objects. Solar-like oscillations of the host star revealed that the star has non-zero obliquity with respect to the transiting planets. The obliquity is consistent with a scenario in which the massive companion torques the inner planets. The inner planets have a coupling timescale much shorter than their precession time, allowing them to remain mutually transiting as their line of nodes precesses around the host star. We present 9 new RVs here and their analysis, which result in an updated orbit and mass determination for the non-transiting companion (assuming no RV trend): $M \sin i_d = 6.3 \pm 0.2 M_J$, $P_d = 1935$ days, $a_d = 3.26$ AU, and $e_d = 0.07$. Our new RVs greatly improve our coverage of the orbit of the companion, allowing us to decisively classify it as a giant planet ($M \sin i_d < 13 M_J$) rather than a brown dwarf (Figure 36). However, the allowance of an RV trend significantly complicates our interpretation of the RVs, since the earliest RV we collected strongly influences our interpretation of the planet orbit (and any possible trend). If an RV trend is allowed in addition to our best 3-planet fit, the constraints on the mass of the detected companion become $M \sin i_d = 6.8 \pm 2.2 M_J$, which is an order of magnitude worse than if we assume no trend, but still yields a planetary mass for the companion (as shown in Figure 36). Allowing an RV trend, our 3σ upper limit is $M \sin i < 13 M_J$ at 5 AU ($M \sin i < 53 M_J$ at 10 AU). Future RV monitoring will clarify the orbital properties of the super-Jovian companion and any additional planetary or brown-dwarf mass companions in the system.



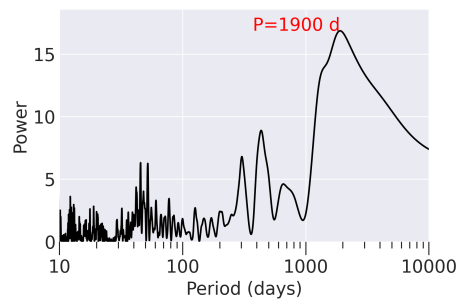
(a) RVs (no trend)



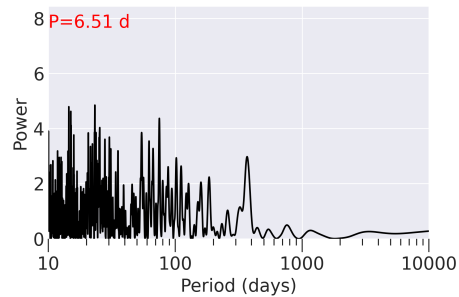
(b) RVs (with trend)



(c) RVs Phase-folded



(d) Periodogram



(e) Residual Periodogram

Figure 36: Same as Figure 7, but for KOI-275 (Kepler-129). Left: The best-fit models include one non-transiting planet, although the unusual time sampling is consistent with a two different classes of model: either a near-circular, non-transiting giant planet (top), or a slightly longer period, eccentric giant planet with a substantial residual trend (middle). Right: Periodograms after removing models of just the transiting planets (top) and a three-planet model in which the shorter, more circular period for the companion is favored (bottom).

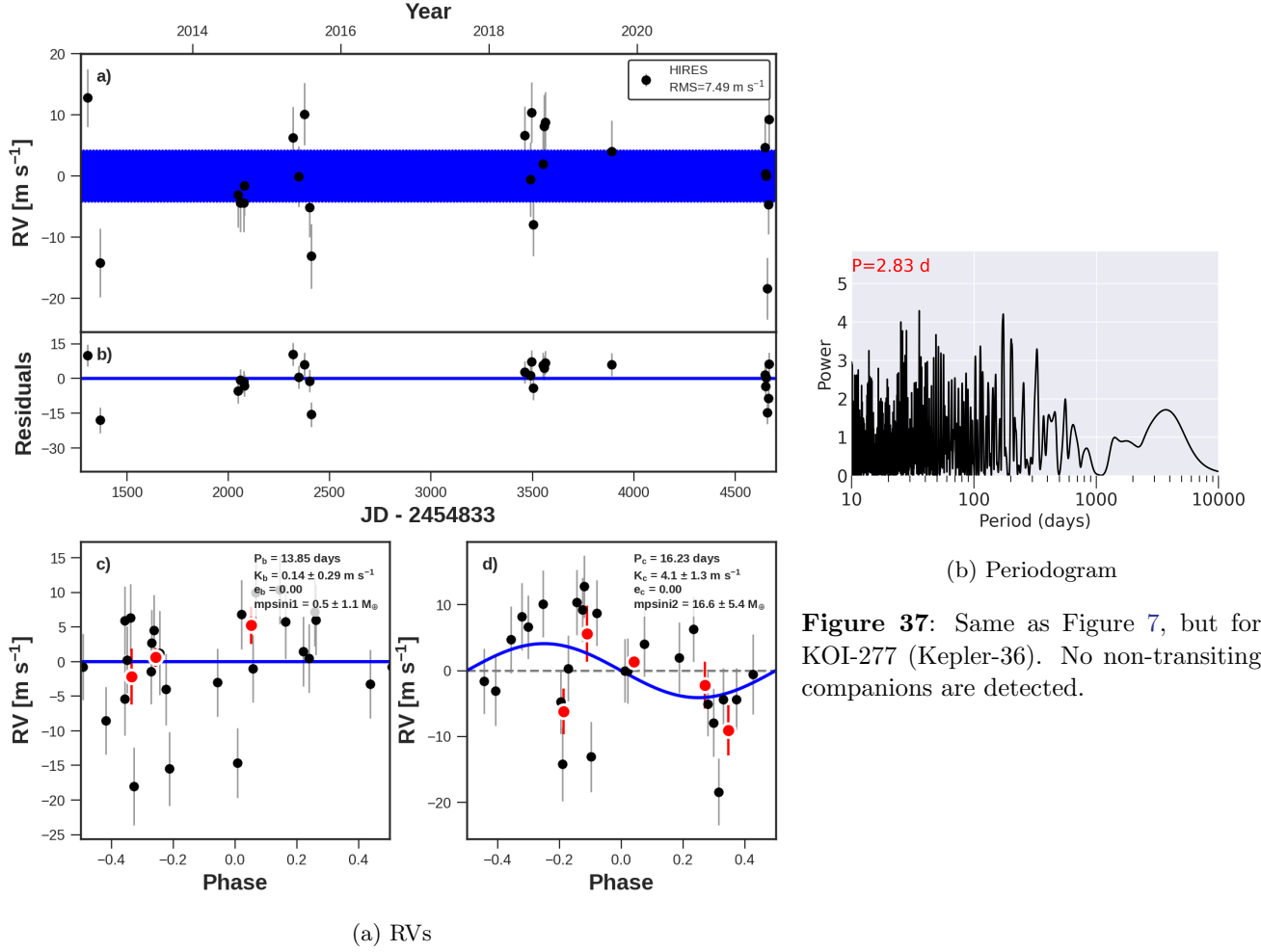


Figure 37: Same as Figure 7, but for KOI-277 (Kepler-36). No non-transiting companions are detected.

KOI-277 (KEPLER-36)

KOI-277 (Kepler-36) is a system with two transiting planets in orbits near a 7:6 mean motion resonance which produce significant TTVs (Carter et al. 2012). Although the planets have similar orbital periods, the inner planet is smaller, likely because its substantially smaller mass than its companion made it comparatively susceptible to photo-evaporation from incident stellar XUV radiation (Lopez & Fortney 2013; Owen & Wu 2013). An additional transit of Kepler-36 c was observed from the ground, which did not significantly alter the determination of the planet masses, orbits, or sizes (Vissapragada et al. 2020).

We have collected 25 RVs of Kepler-36 between 2012 and 2022. The RVs have large errors because the host star has a modest $v \sin i$, and so they do not substantially improve the masses determined from TTVs, but they do rule out massive non-transiting planets in the vicinity of the near-resonant pair (Figure 37). There is no significant RV trend, yielding a 3σ upper limit of $M \sin i < 0.24 M_J$ at 5 AU ($M \sin i < 0.95 M_J$ at 10 AU). A joint analysis of the TTVs and RVs is in preparation.

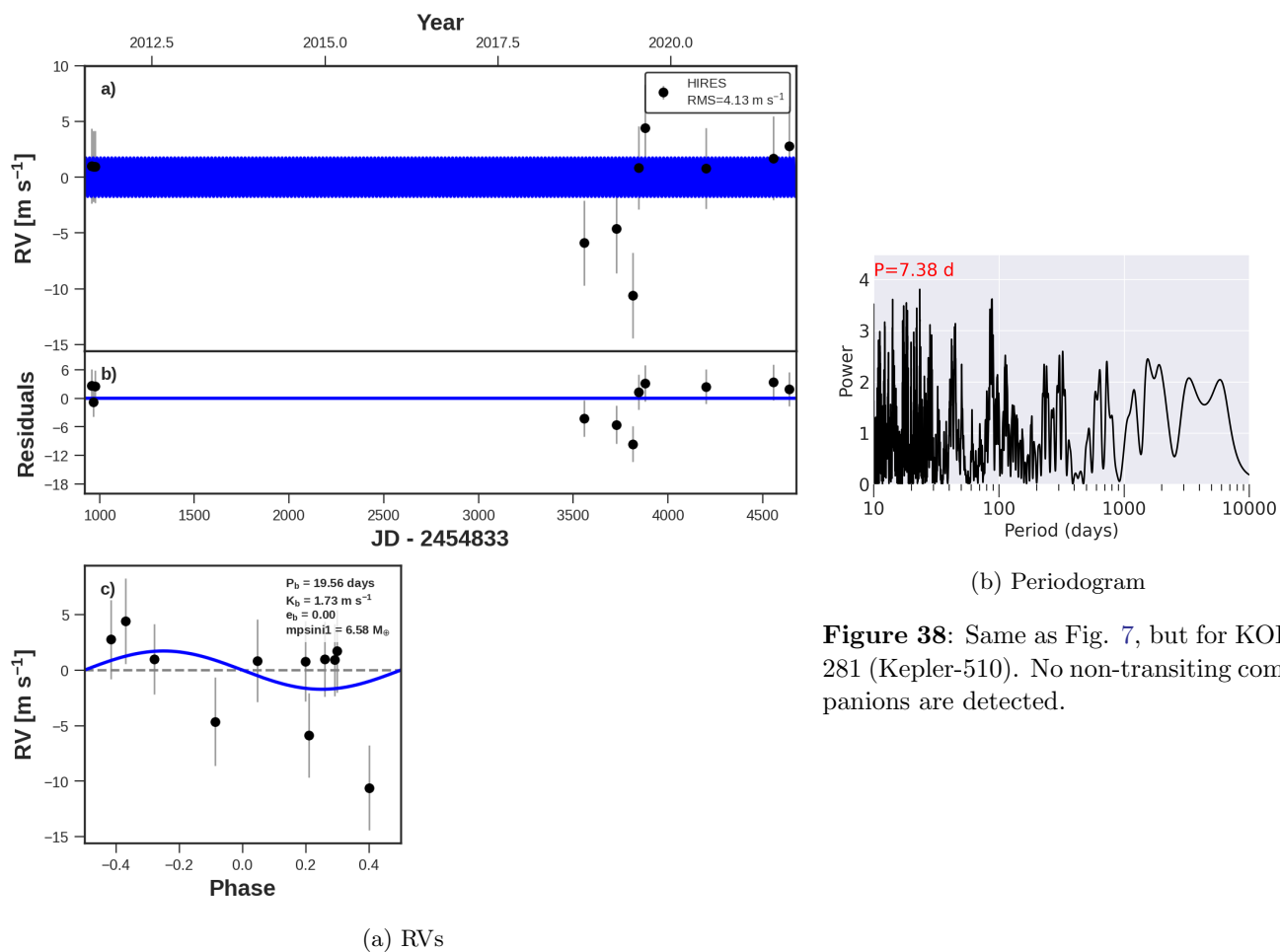


Figure 38: Same as Fig. 7, but for KOI-281 (Kepler-510). No non-transiting companions are detected.

KOI-281 (KEPLER-510)

Kepler-510 is a metal-poor, G-type star ($T_{\text{eff}} = 5600$ K, $[Fe/H] = -0.4$) that has one transiting planet ($P_b = 19.56$ days, $R_b = 2.5 R_{\oplus}$) that was statistically validated (Morton et al. 2016). We collected two RVs in 2011 and then another 8 RVs between 2017 and 2021 (Fig. 38). Assuming the planet has a typical mass for its size using the Weiss & Marcy (2014) mass-radius relations, the residual RVs have RMS= 4.12 m s $^{-1}$ and no trend, placing an upper limit of $M \sin i < 0.18 M_J$ at 5 AU ($M \sin i < 0.75 M_J$ at 10 AU).

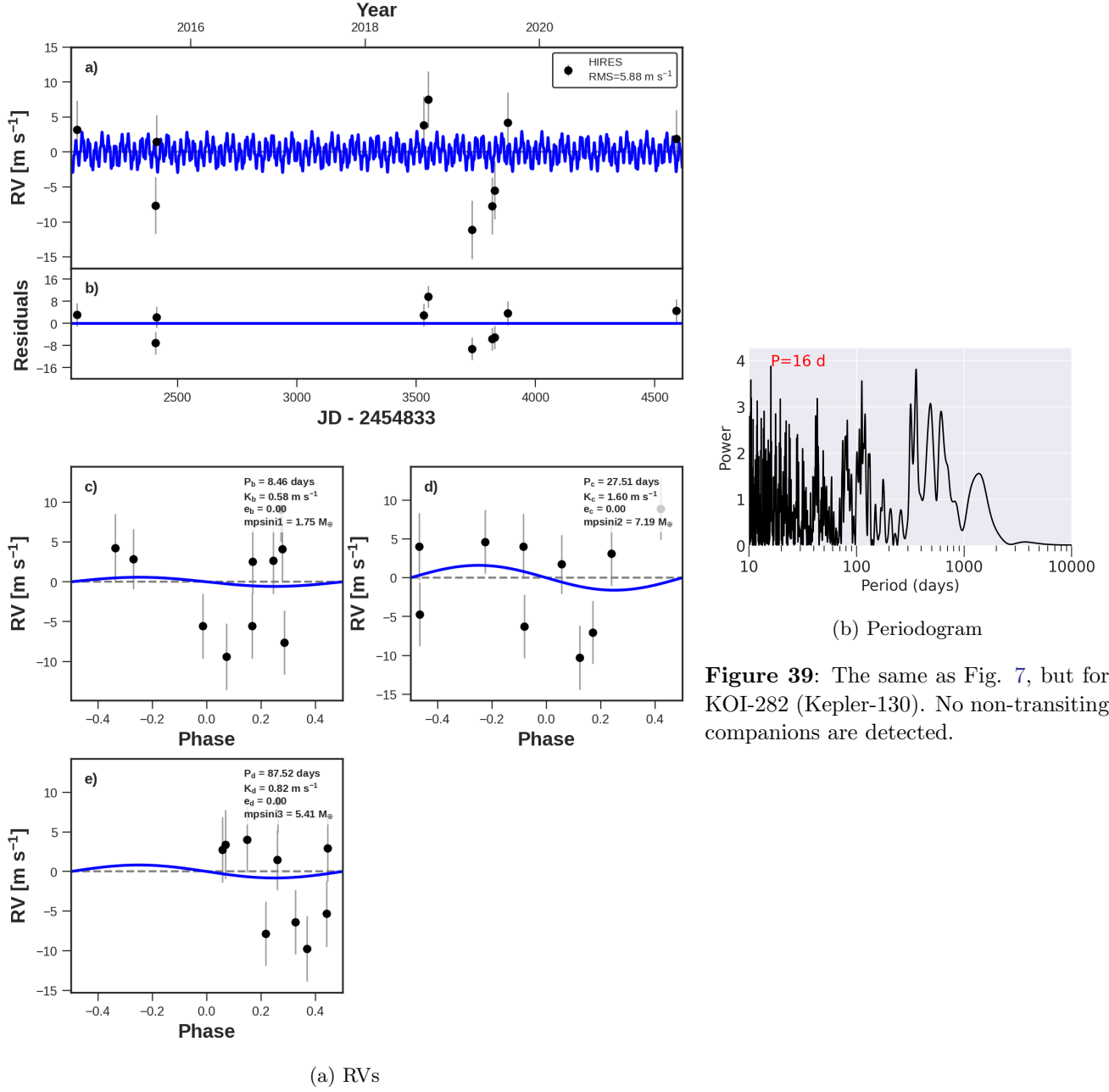


Figure 39: The same as Fig. 7, but for KOI-282 (Kepler-130). No non-transiting companions are detected.

KOI-282 (KEPLER-130)

Kepler-130 (KOI-282) is a multi-planet system that was statistically confirmed (Lissauer et al. 2014; Rowe et al. 2014). Three transiting planets orbit the primary star, which is sun-like, although the system has a candidate wide-separation stellar companion detected in Gaia astrometry (Mugrauer 2019). The inner two planets have TTVs, and the transit durations yield upper limits on their eccentricities (Van Eylen & Albrecht 2015). This system was selected for follow-up as part of a program to survey stars with at least 3 transiting planets from 2015 onward. We have collected 10 Keck-HIRES RVs of Kepler-130 between 2015 and 2021 (Fig. 39). Assuming typical masses for the three transiting planets (Weiss & Marcy 2014), the residual RVs have $\text{RMS}=5.9 \text{ m s}^{-1}$ and no trend, resulting in an upper limit of $M \sin i < 0.49 M_J$ at 5 AU ($M \sin i < 2.0 M_J$ at 10 AU).

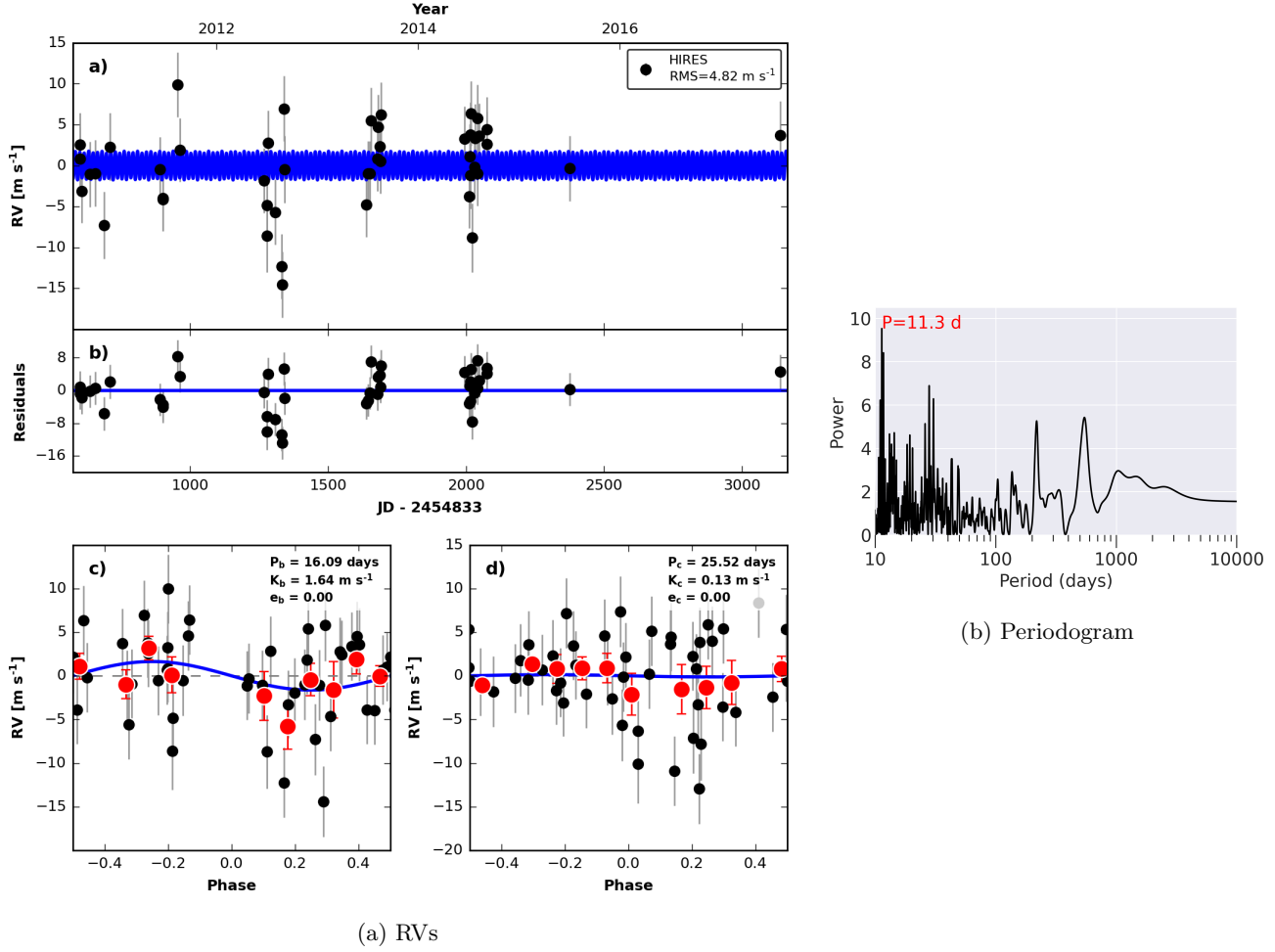


Figure 40: Same as Fig. 7, but for KOI-283 (Kepler-131). No non-transiting companions are detected.

KOI-283 (KEPLER-131)

Kepler-131 (KOI-283) is a G type star with two transiting planets at $P_b = 16.1$ days and $P_c = 25.5$ days that were statistically confirmed (Lissauer et al. 2014; Rowe et al. 2014). The planet radii are $R_b = 2.1 \pm 0.2 R_\oplus$ and $R_c = 0.82 \pm 0.06 R_\oplus$, a rare architecture in which the inner planet is larger than the outer planet (Berger et al. 2018; Ciardi et al. 2013). The planets were independently confirmed with 20 Keck-HIRES RVs, which yielded masses of $M_b = 16 \pm 4 M_\oplus$ and $M_c = 8 \pm 6 M_\oplus$ (Marcy et al. 2014). We have since collected 26 RVs on Keck-HIRES (46 RVs total), which yield a marginally improved planet mass of $M_b = 4.4 \pm 2.4 M_\oplus$ (Fig. 40). We do not fit the mass of planet c because the planet is smaller than our minimum size for mass fitting; we instead assume a mass-radius relation (Weiss & Marcy 2014). The residual RVs have $\text{RMS} = 4.8 \text{ m s}^{-1}$ and no trend, resulting in an upper limit of $M \sin i < 0.29 M_J$ at 5 AU ($M \sin i < 1.2 M_J$ at 10 AU). The fast periodogram of the RVs reveals a peak near 11.3 days which is not significant (FAP=0.3).

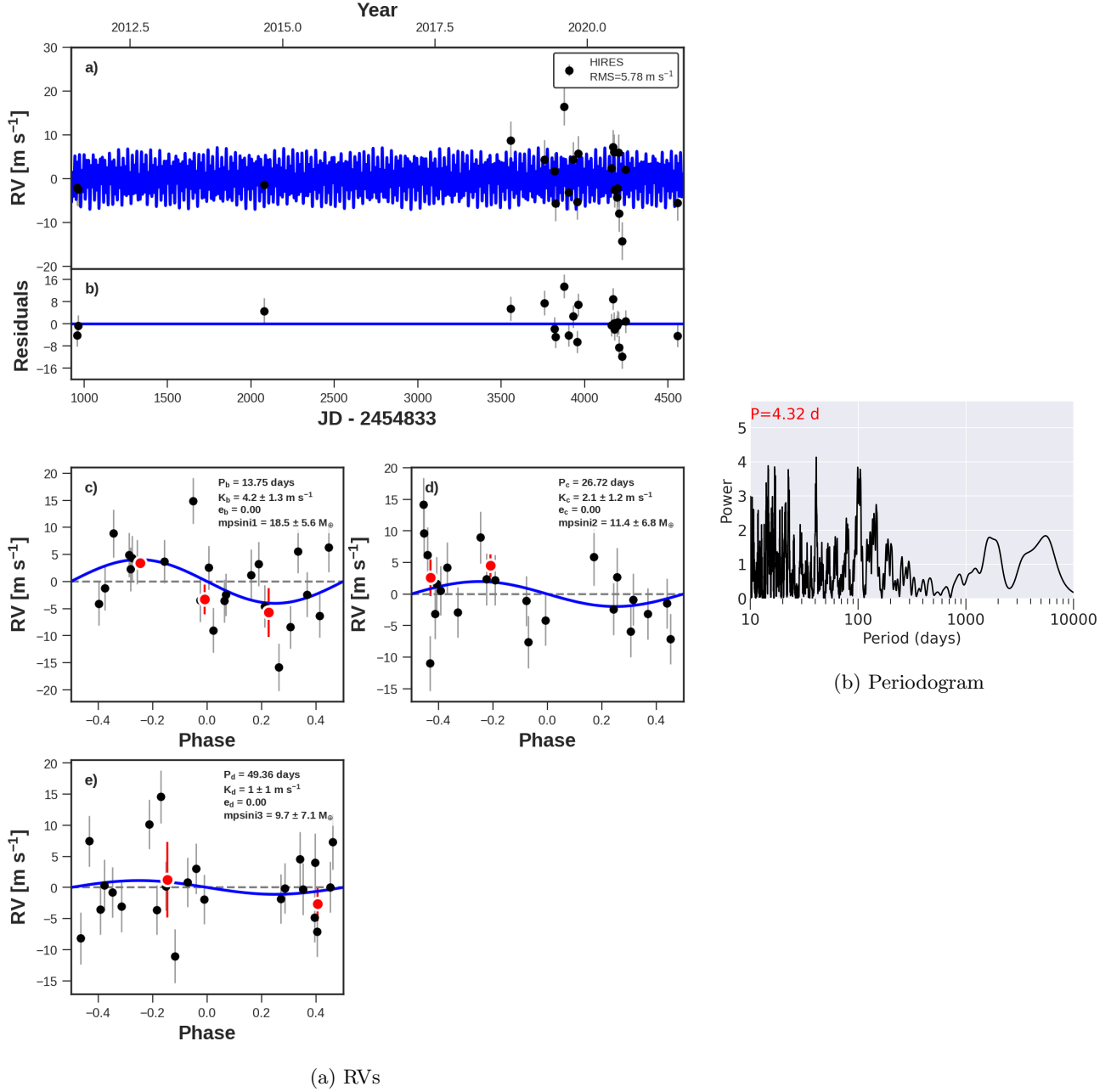


Figure 41: Same as Fig. 7, but for KOI-285 (Kepler-92). No non-transiting companions are detected.

KOI-285 (KEPLER-92)

Kepler-92 (KOI-285) is a bright ($V=11.6$) sun-like star with three transiting planets confirmed in [Batalha et al. \(2013\)](#): $R_b = 3.6 R_\oplus$, $R_c = 2.5 R_\oplus$, and $R_d = 2.1 R_\oplus$. Solar-like oscillations were detected for this star, allowing a precise age estimate of 5.5 ± 0.5 Gyr ([Silva Aguirre et al. 2015](#)). The star is slightly evolved with slow rotation ($T_{\text{eff}} = 5900$ K, $\log(g) = 4.0$ dex, $v \sin i = 3.5$ km/s, [Fulton & Petigura 2018a](#)).

The system has three transiting planets near (but not in) a Laplace 4:2:1 mean motion resonant chain: $P_b = 13.7$ days, $P_c = 26.7$ days, and $P_d = 49.4$ days, a configuration that produces TTVs for the inner two planets ([Xie 2014](#)). The TTVs are too weak to yield precise determinations of the planet masses and eccentricities, and the orbits are consistent with circular ([Van Eylen & Albrecht 2015](#)).

Between 2011 and 2021, we collected 23 RVs on Keck-HIRES (Fig. 41). The RVs yield upper limits on the planet masses: $M_b = 6.5 \pm 3.2 M_\oplus$, $M_c = 3.9 \pm 3.1 M_\oplus$, and $M_d = 4.4 \pm 3.6 M_\oplus$. The residual RVs have $\text{RMS}=6.0 \text{ m s}^{-1}$ and no trend, yielding an upper limit of $M \sin i < 0.29 M_J$ at 5 AU ($M \sin i < 1.2 M_J$ at 10 AU). The RMS is higher than typical for a bright G type star and might be a consequence of modal oscillations of this slightly evolved star.

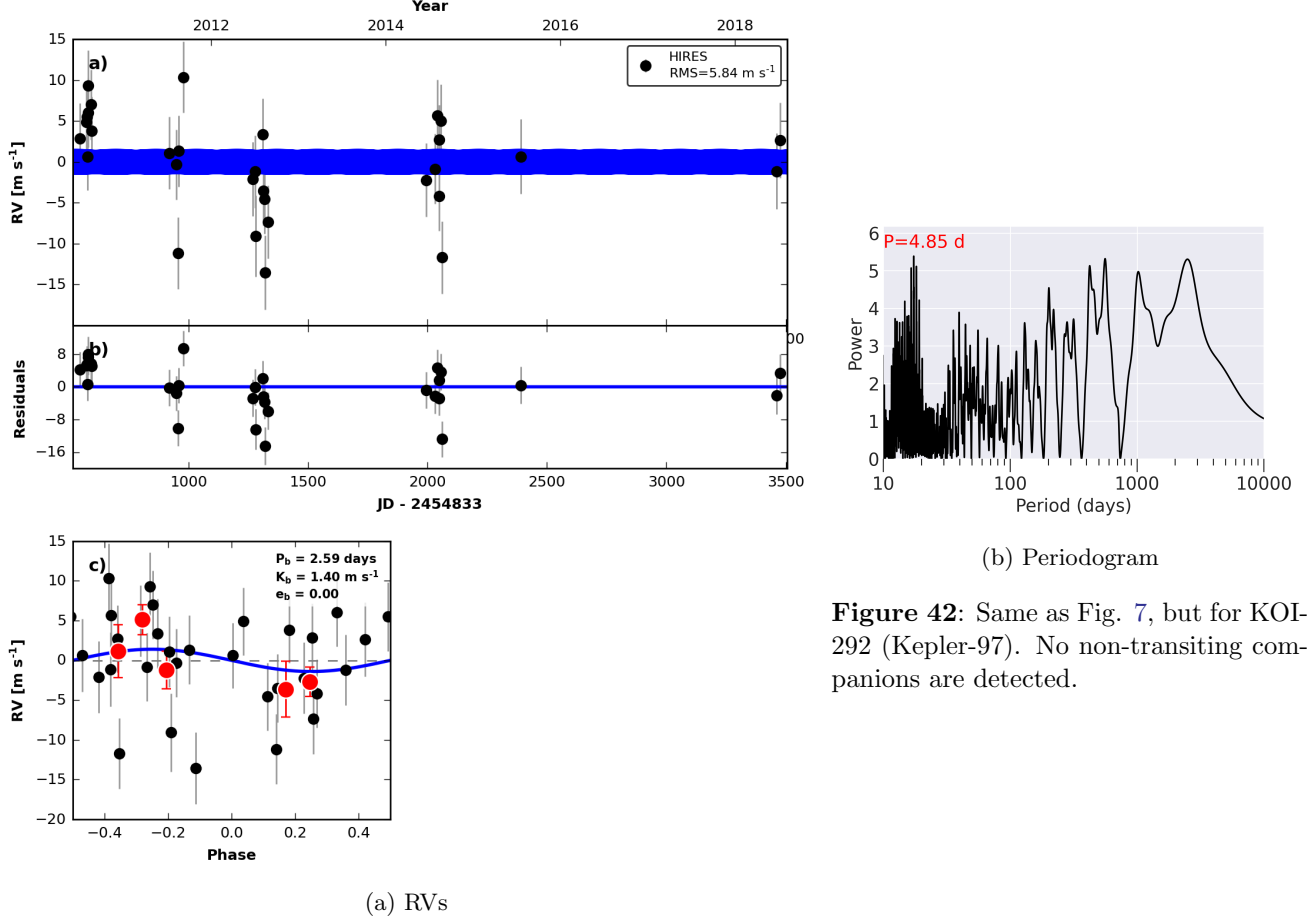


Figure 42: Same as Fig. 7, but for KOI-292 (Kepler-97). No non-transiting companions are detected.

KOI-292 (KEPLER-97)

Kepler-97 (KOI-292) is a $V=12.9$ sun-like star ($T_{\text{eff}} = 5800 \text{ K}$) with one transiting planet that was confirmed with Keck-HIRES RVs (Marcy et al. 2014). The transiting planet has $P_b = 2.59$ days and $R_b = 1.47 \pm 0.07 R_{\oplus}$ (Berger et al. 2018). The RVs also indicated a trend consistent with a long-period companion ($P_c > 789$ days), which was announced as Kepler-97 c (Marcy et al. 2014).

We have collected 10 RVs since 2013, which demonstrate that the apparent trend in the earlier RVs was a statistical fluke (Fig. 42). The full times series of 31 RVs, which extends from 2010 to 2019, has no trend, although the residual RVs have a somewhat high RMS of 5.9 m s^{-1} . The RVs are consistent with a mass upper limit for the transiting planet of $M_b = 3.6 \pm 2.4 M_{\oplus}$. The non-detection of an RV trend yields an upper limit of $M \sin i < 0.3 M_J$ at 5 AU ($M \sin i < 1.2 M_J$ at 10 AU) for any additional companions, which is inconsistent with the previously announced planet. Also, there are no significant peaks in the fast periodogram (FAP=0.99), suggesting that we are unlikely to have missed a Jupiter-mass planet with $P < \sim 2000$ days.

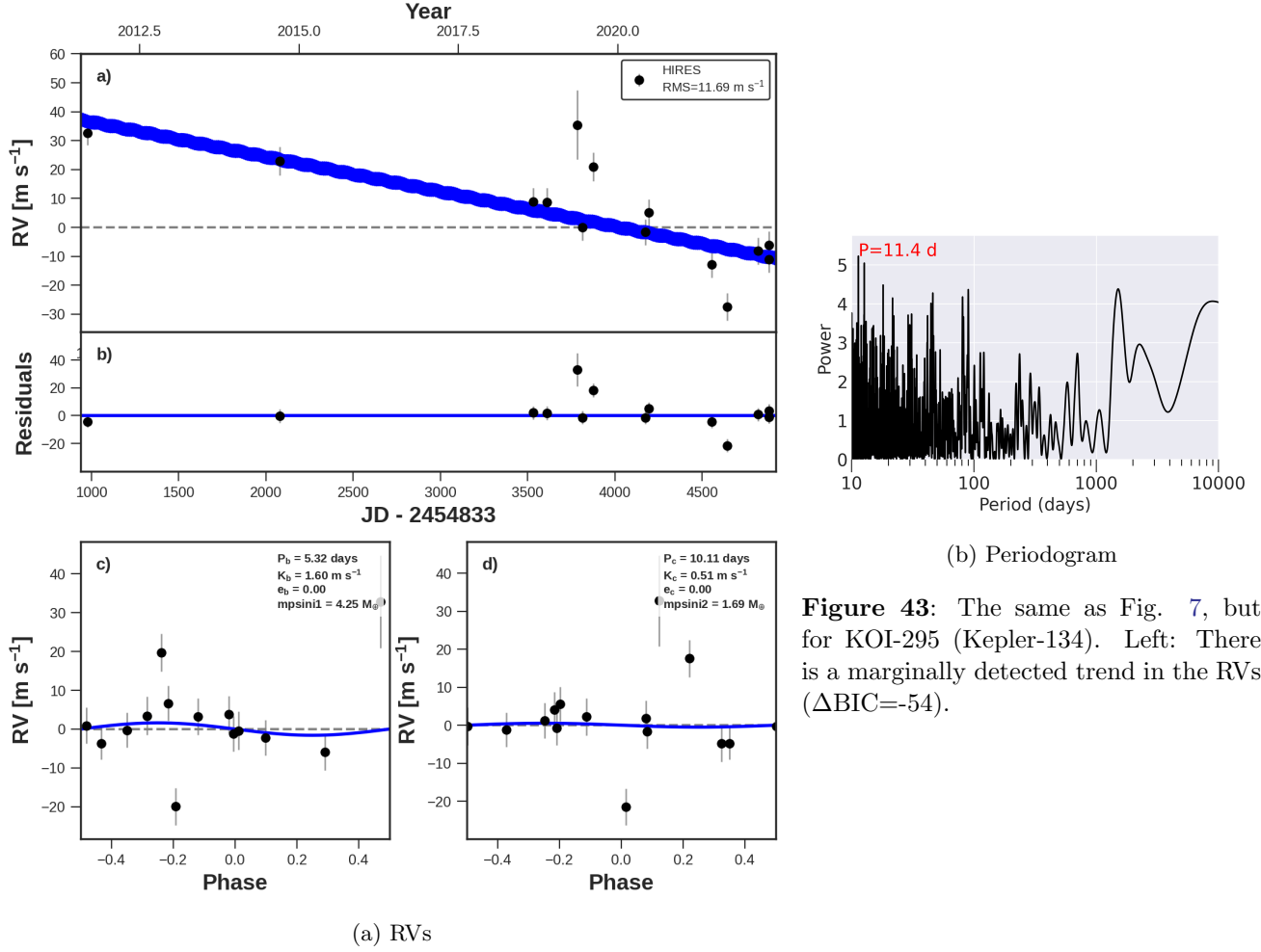


Figure 43: The same as Fig. 7, but for KOI-295 (Kepler-134). Left: There is a marginally detected trend in the RVs ($\Delta\text{BIC}=-54$).

KOI-295 (KEPLER-134)

Kepler-134 (KOI-295) is a $V=12.3$ slowly rotating, quiet sun-like star ($T_{\text{eff}} = 5900 \text{ K}$, $v \sin i < 2 \text{ km/s}$, $\log(R_{\text{HK}}) = -5.0$). The system has two transiting planets that were statistically confirmed (Lissauer et al. 2014; Rowe et al. 2014). The planets are interior to the 2:1 mean motion resonance ($P_b = 5.32 \text{ days}$, $P_c = 10.1 \text{ days}$) and are in the rare configuration in which the inner planet is larger than the outer ($R_b = 1.8 R_{\oplus}$, $R_c = 1.2 R_{\oplus}$, Berger et al. 2018).

We collected 14 Keck-HIRES RVs on 13 nights between 2011 and 2022 (Fig. 43). Assuming the planets have typical masses for their sizes (Weiss & Marcy 2014), the RVs appear to be consistent with a weak long-term trend ($\Delta\text{BIC} = -54$), which corresponds to a companion of $M \sin i < 3.7 M_J$ at 10 AU. Even with the inclusion of a long-term trend, the residual RV scatter is uncharacteristically high for a quiet sun-like star (11.8 m s^{-1}). We performed a jitter test by collecting two RVs in several hours apart in a single night; the RV difference was only 5 m s^{-1} , which is indeed consistent with low jitter, as expected. Further observations are needed to clarify the source of the RV scatter.

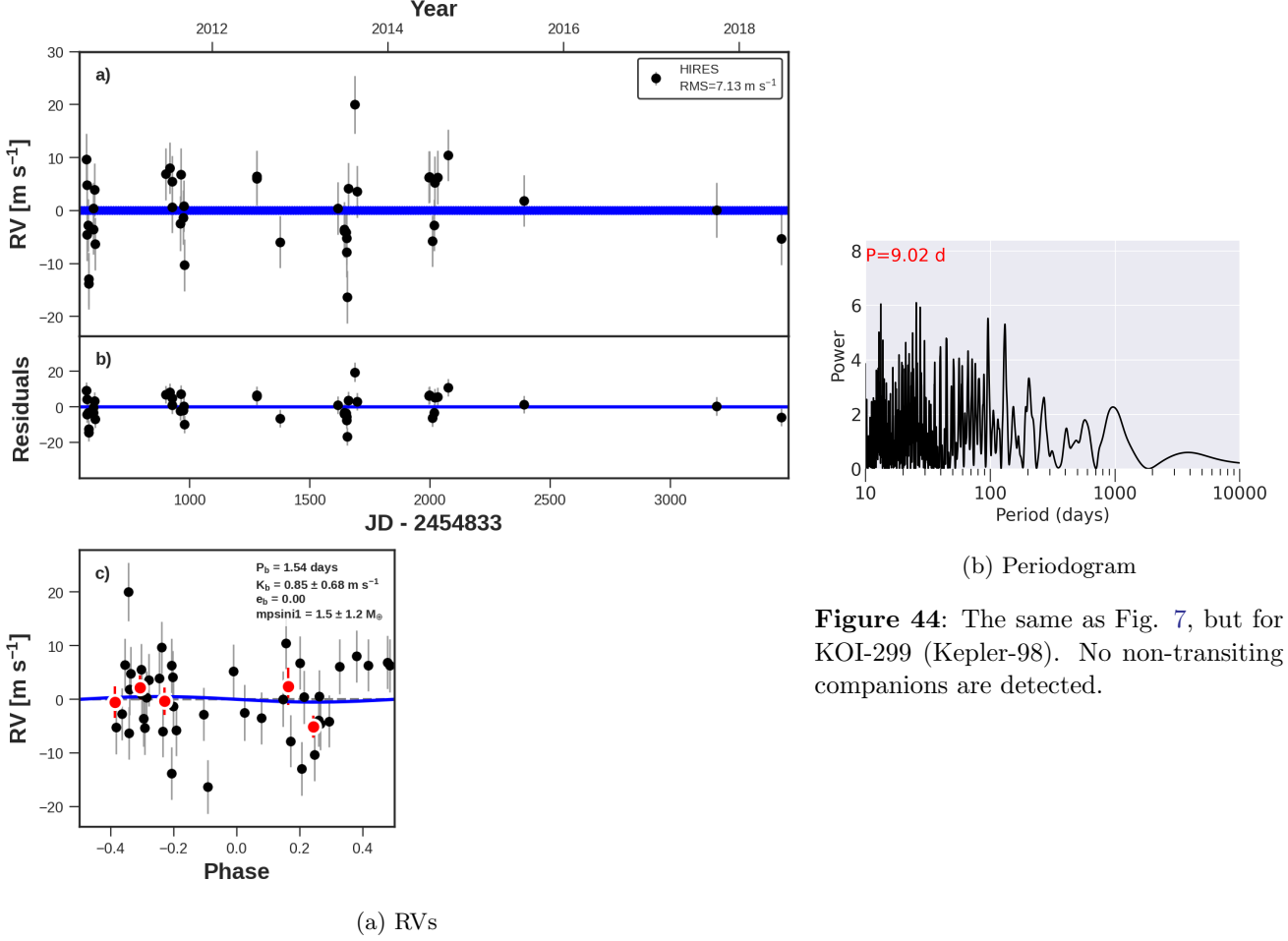
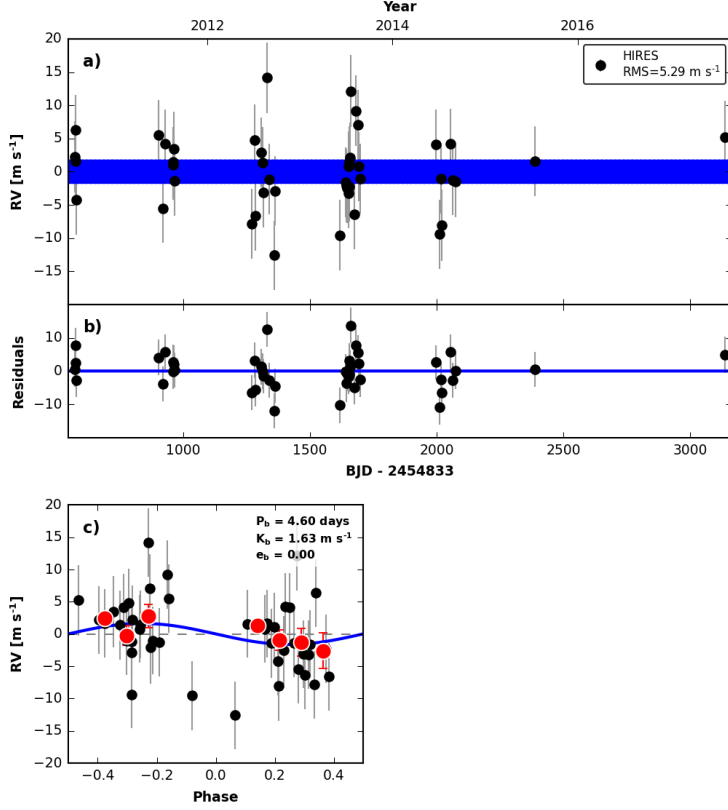


Figure 44: The same as Fig. 7, but for KOI-299 (Kepler-98). No non-transiting companions are detected.

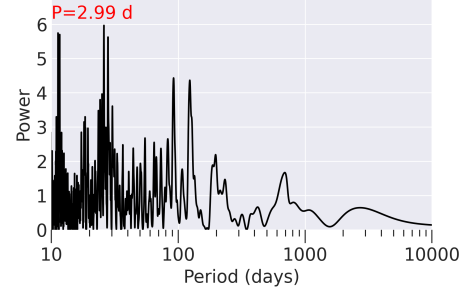
KOI-299 (KEPLER-98)

Kepler-98 (KOI-299) is a V=12.9 sun-like star with one transiting planet ($P_b = 1.54$ days) that was confirmed with Keck-HIRES RVs, yielding a mass of $3.6 \pm 1.4 M_{\oplus}$ (Marcy et al. 2014). The planet radius was reported as $2.0 R_{\oplus}$ based on stellar spectroscopy, $1.5 R_{\oplus}$ based on its parallax, and $1.87 R_{\oplus}$ based on the combined spectroscopy and Gaia parallax. (Marcy et al. 2014; Berger et al. 2018; Fulton & Petigura 2018a).

We have collected 42 RVs between 2011 and 2018, including 20 since the publication of Marcy et al. (2014) (Fig. 44). The new best-fit planet mass is $1.0 \pm 1.0 M_{\oplus}$, with residual 7.1 m s^{-1} . There is no apparent trend in the RVs, yielding an upper limit of $M \sin i < 0.3 M_J$ at 5 AU ($M \sin i < 1.2 M_J$ at 10 AU). There are no significant peaks in the fast periodogram of the residual RVs (FAP=0.90).



(a) RVs



(b) Periodogram

Figure 45: The same as Fig. 7, but for KOI-305 (Kepler-99). No non-transiting companions are detected.

KOI-305 (KEPLER-99)

Kepler-99 (KOI-305) is a $V=13.0$ K type star with moderate activity ($T_{\text{eff}} = 4600 \text{ K}$, $\log R'_{\text{HK}} = -4.6$). It has one transiting planet ($P_b = 4.6$ days, $R_b = 1.5 R_{\oplus}$) that was confirmed with Keck-HIRES RVs. The RVs yielded a mass of $M_b = 6.2 \pm 1.3 M_{\oplus}$, which corresponds to a density of $10.9 \pm 2.0 \text{ g cm}^{-3}$, consistent with a rocky composition.

We have collected 45 RVs of Kepler-99 between 2010 and 2018, including 24 since the publication of [Marcy et al. \(2014\)](#) (Fig. 45). The new RVs produce a marginal change in the best-fit planet mass. The total time series of the RVs yields a semi-amplitude of $K = 1.74 \pm 0.88 \text{ m s}^{-1}$, which corresponds to a mass of $2.5 \pm 1.3 M_{\oplus}$. The resulting density is $2.3 \pm 1.3 \text{ g cm}^{-3}$, indicating the planet likely has a volatile envelope. The residual RVs have $\text{RMS} = 5.3 \text{ m s}^{-1}$ and no apparent trend, yielding an upper limit of $M \sin i < 0.27 M_J$ at 5 AU ($M \sin i < 1.1 M_J$ at 10 AU). There are no significant peaks in the fast periodogram of the residual RVs (FAP=0.99).

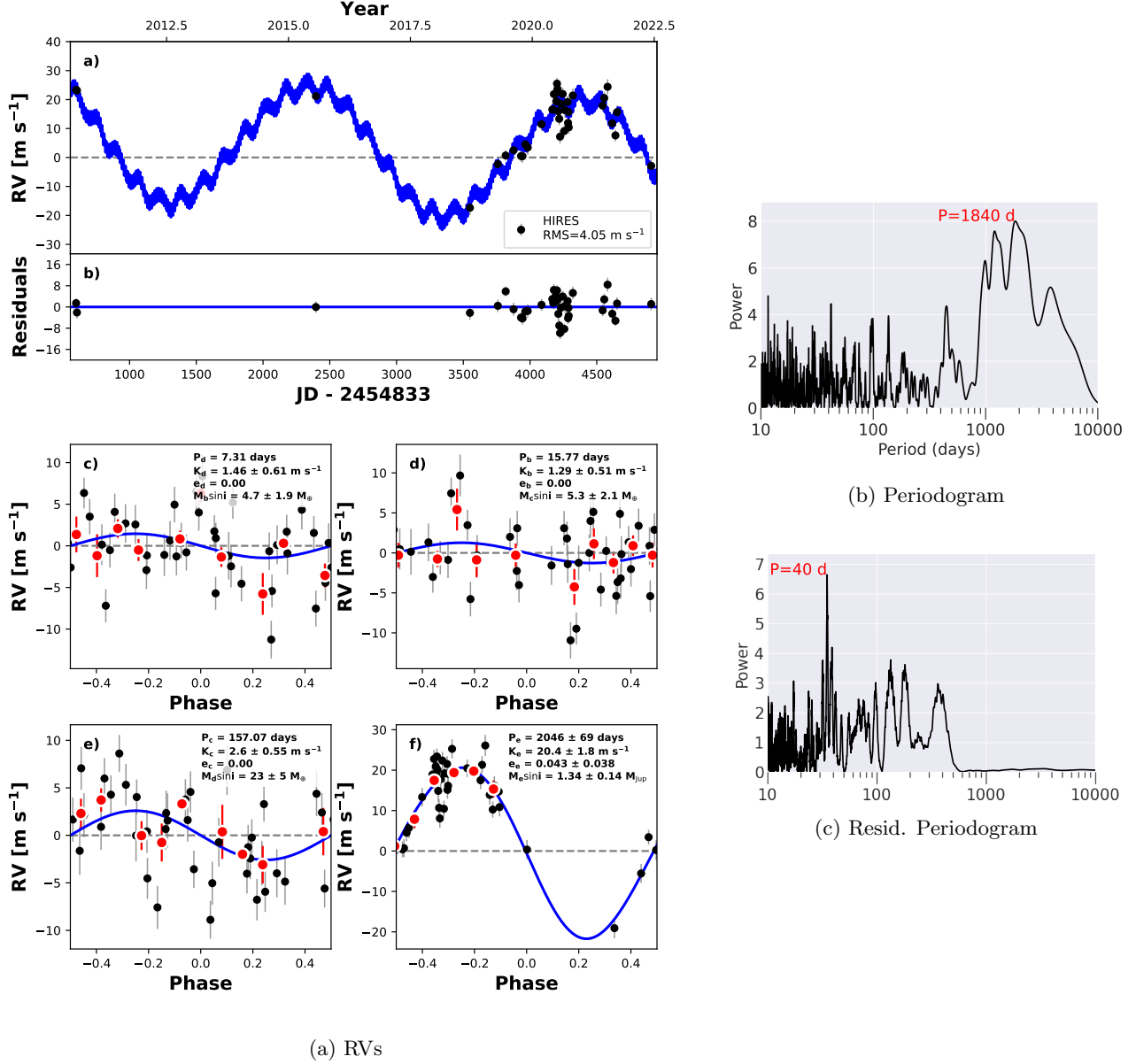


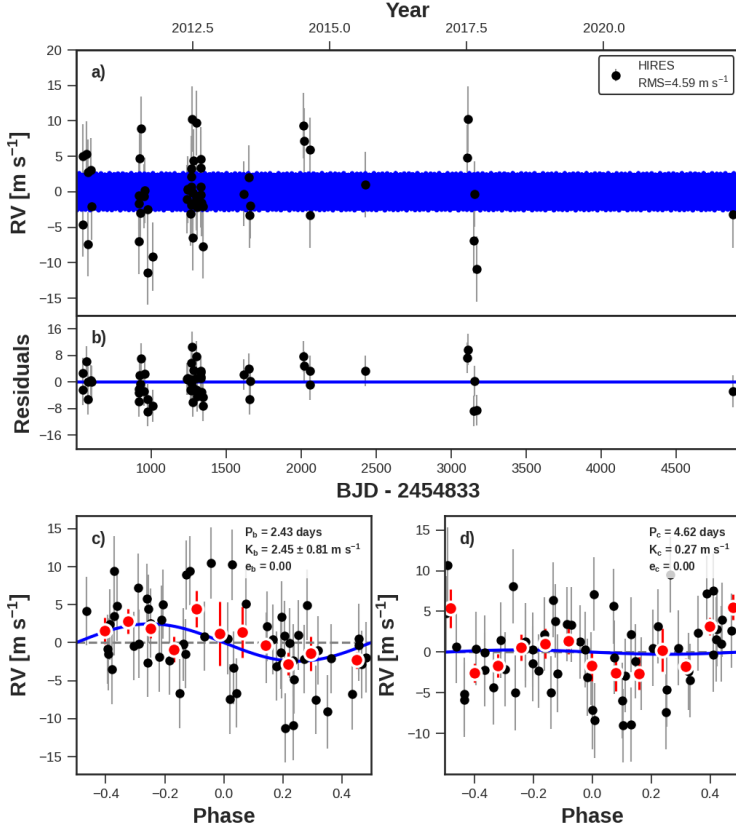
Figure 46: The same as Fig. 7, but for KOI-316 (Kepler-139). The best-fit model includes a non-transiting planet at 1800 days, although the automated KGPS algorithm did not detect this planet due to the unusual time sampling. Right: Periodograms of the RVs the after removing a model of the transiting planets only (top) and our best-fit model including a giant planet at 1800 days (bottom).

KOI-316 (KEPLER-139)

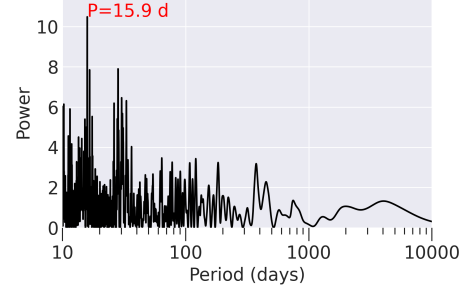
Kepler-139 (KOI-316) is a $V=12.7$, quiet G type star ($T_{\text{eff}} = 5500 \text{ K}$, $v \sin i < 2 \text{ km/s}$, $\log R'_{\text{HK}} = -5.1$). It has two statistically confirmed transiting planets ($P_b = 15.77$ days, $P_c = 157$ days) and a third transiting candidate at $P_d = 7.31$ days (Lissauer et al. 2014; Rowe et al. 2014; Holczer et al. 2016), which we confirm below. There is an equal-magnitude visual companion $10''$ to the south of the planet-hosting star. The centroid photometry from Kepler clearly demonstrates that all three transits are around the target (Northern) star (Jason Rowe, private comm.) The planets have $R_b = 2.4 R_\oplus$, $R_c = 2.4 R_\oplus$, and $R_d = 1.7 R_\oplus$ (Fulton & Petigura 2018a).

This target was observed as part of a program to search for giant planet companions in systems with three or more transiting planets. We have collected 38 Keck-HIRES RVs of Kepler-139 between 2010 and 2022, yielding a 12 year

baseline (Fig. 46). The $10''$ separation of the two bright stars is much larger than the typical seeing at Keck ($< 2''$), and so the visual companion does not contaminate the HIRES C2 decker (width $1.0''$, which was always rotated to avoid the companion). By coincidence, the first 3 RVs we collected (from 2010 and 2015) were all near the “up” quadrature of an RV signal that became apparent after our 4th RV observation. Moderate cadence follow-up was necessary to ascertain the orbit and mass of the companion: $K_e = 19.1 \pm 1.5 \text{ m s}^{-1}$, $P_e = 1920 \pm 33 \text{ days}$, $M \sin i_e = 1.2 \pm 0.1 M_J$, $e_e = 0.06 \pm 0.04$. Furthermore, the Keck-HIRES RVs yield masses for the transiting planets: $M_b = 4.8 \pm 2.1 M_\oplus$, $M_c = 22.3 \pm 4.7 M_\oplus$, and $M_d = 5.2 \pm 1.9 M_\oplus$. The mass of planet c (at $P_c = 157 \text{ days}$) is quite high compared to the other two similar-sized but closer-in planets. Perhaps planet c has a grazing transit with a radius in need of re-evaluation, or perhaps the planet is rich in water-ice and high mean-molecular weight volatiles, or perhaps the high mass (3σ confidence) is spurious. The residual RVs have $\text{RMS} = 4 \text{ m s}^{-1}$, consistent with the low RV scatter expected of quiet sun-like stars. More RVs will clarify the masses and compositions of the three transiting planets, as well as the orbit of the Jovian companion and the possible presence of additional companions.



(a) RVs



(b) Periodogram

Figure 47: The same as Fig. 7, but for KOI-321 (Kepler-406). No non-transiting companions are detected.

KOI-321 (KEPLER-406)

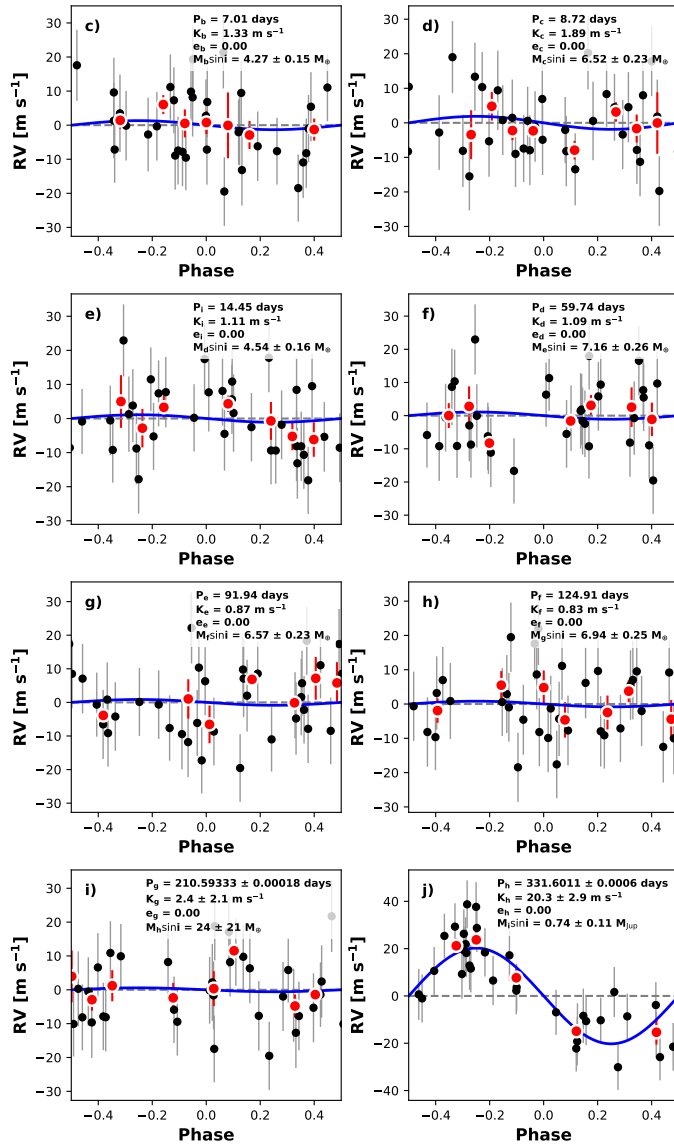
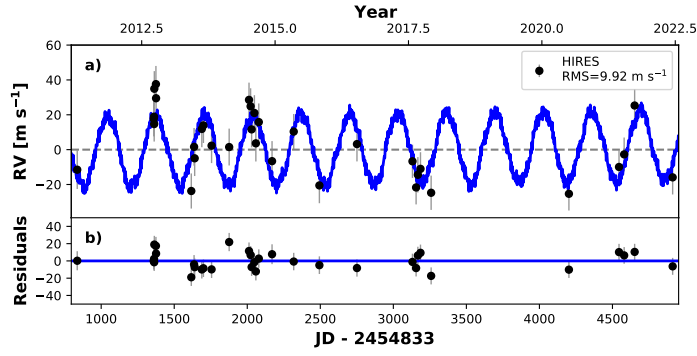
Kepler-406 (KOI-321) is a V=12.5 G type star of moderate metallicity ($T_{\text{eff}} = 5600 \text{ K}$, $[\text{Fe}/\text{H}] = 0.3 \pm 0.1$, [Fulton & Petigura 2018a](#)). It hosts two transiting planets: $P_b = 2.4$ days, $P_c = 4.6$ days). The planets are small ($R_b = 1.4 \pm 0.03$, $R_c = 0.85 \pm 0.03$) and were confirmed with Keck-HIRES RVs, which yielded $M_b = 6.4 \pm 1.4 M_{\oplus}$ and $M_c = 2.7 \pm 1.8 M_{\oplus}$ ([Marcy et al. 2014](#)).

We have collected 56 Keck-HIRES RVs between 2010 and 2022 (Fig. 47). These include 14 new RVs since the publication of [Marcy et al. \(2014\)](#), which do not substantially change the mass determinations of the planets: $M_b = 5.4 \pm 1.9 M_{\oplus}$, $M_c = 2.1 \pm 1.8 M_{\oplus}$. The 12-year baseline has low scatter (residual RMS=4.6 m s⁻¹) and does not reveal any RV trend, which corresponds to an upper limit of $M \sin i < 0.18 M_J$ at 5 AU ($M \sin i < 0.72 M_J$ at 10 AU). A periodogram of the RV residuals yields a low-significance peak at 15.9 days (FAP=0.2). This period is not known to be associated with stellar rotation and might represent the orbit of a bona-fide planet.

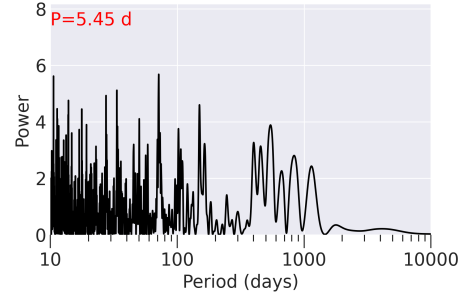
KOI-351 (KEPLER-90)

Kepler-90 (KOI-351) is a faint ($V = 13.8$) sun-like star with 8 confirmed transiting planets. Seven of the transiting planets (Kepler-90 b-h) were announced nearly simultaneously (Cabrera et al. 2014; Schmitt et al. 2014; Rowe et al. 2014). The compact architecture of the planets produces significant TTVs, which confirm their planetary status (Lissauer et al. 2014). The eighth planet (Kepler-90 i) was detected with candidate status at the time due to its small size (Aviv Ofir, private comm.) and was later confirmed with an independent photometric search (Shallue & Vanderburg 2018). Liang et al. (2021) found that Kepler-90 g is much lower mass than Kepler-90 h ($15 \pm 1 M_{\oplus}$ for planet g vs. $203 \pm 5 M_{\oplus}$ for planet h) by fitting their transit timing and depth variations determined from the *Kepler* photometry.

We have collected 33 RVs of Kepler-90 between 2011 and 2022 (Fig. 48). This 11-year baseline was necessary to sample the orbit of Kepler-90 h, which is nearly one year ($P_h = 331$ days), resulting in significant aliasing during the seasonal Kepler field RV follow-up. The RVs place upper limits on all of the small planets (Kepler-90 b, c, d, e, f, i) and yield masses for the two Saturn-sized planets: $M_g = 49 \pm 29 M_{\oplus}$ and $M_h = 0.63 \pm 0.15 M_J$, consistent with the results of Liang et al. (2021). The residual RVs have significant scatter (RMS=13.7 m/s), which is atypical for a slowly rotating, magnetically quiet sun-like star ($T_{\text{eff}} = 6000$ K, $v \sin i = 3.6$ km/s, $\log R'_{\text{HK}} = -5.2$, expected jitter = 9.3 m s^{-1}). However, there is no significant trend in the decade of RV baseline ($M \sin i < 0.3 M_J$ at 5 AU, $M \sin i < 1.4 M_J$ at 10 AU), and the fast periodogram reveals no significant peaks (FAP=0.4). The high RV scatter might result from additional (yet undetected) planets. A joint analysis of the TTVs and RVs of this system is currently underway (Shaw et al., in prep.)



(a) RVs



(b) Periodogram

Figure 48: The same as Fig. 7, but for KOI-351 (Kepler-90). Left: This system has eight transiting planets, of which only the most massive is detected in the RVs. Right: Periodogram of the RVs after removing the best model with all transiting planets. No non-transiting companions are detected.

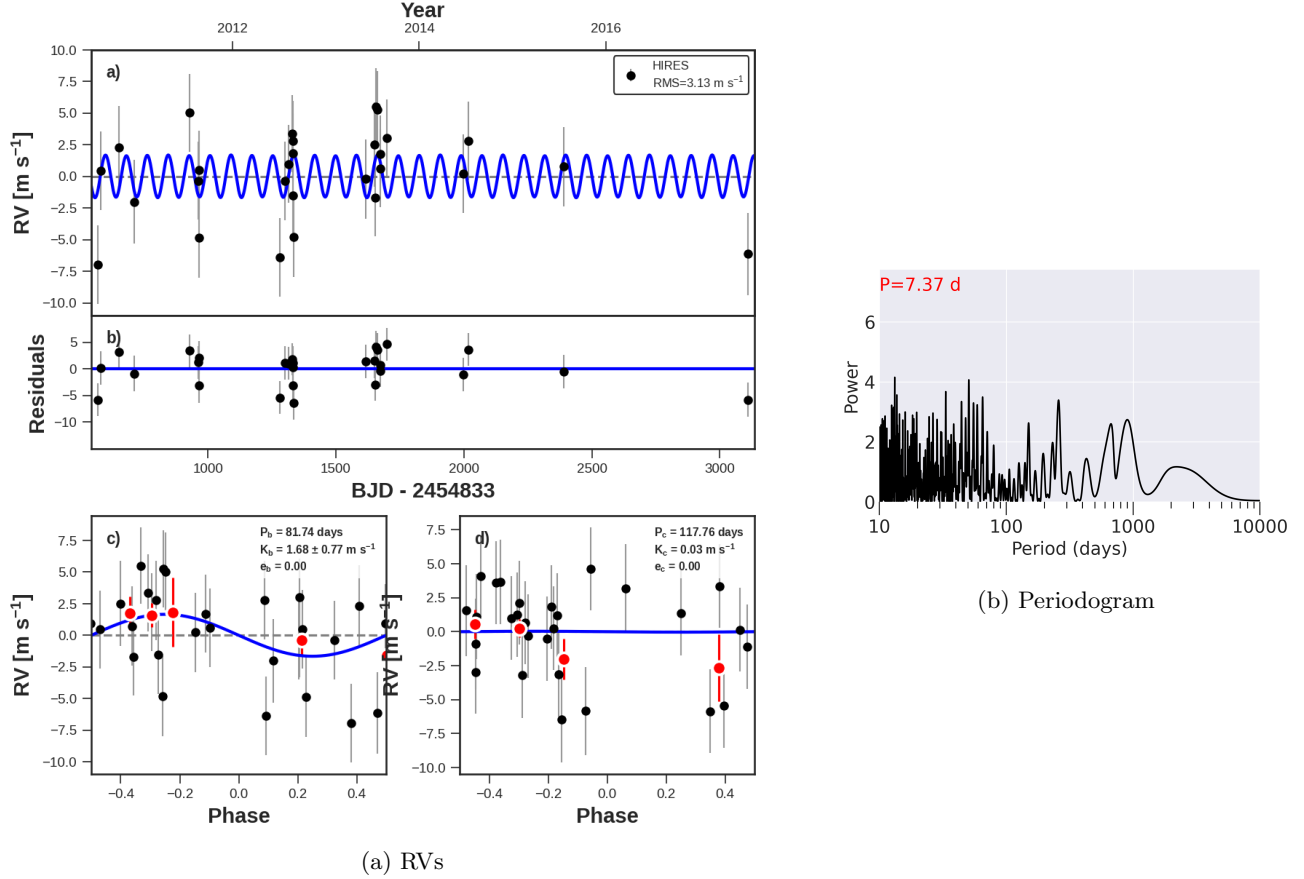


Figure 49: The same as Fig. 7, but for KOI-365 (Kepler-538). No non-transiting companions are detected.

KOI-365 (KEPLER-538)

Kepler-538 (KOI-365) is a $V=11.2$ sun-like star ($T_{\text{eff}} = 5400\text{ K}$). The star has one transiting planet ($P_b = 81.7$ days, $R_b = 2.2, R_{\oplus}$) that was statistically validated (Morton et al. 2016). The system has a candidate M dwarf stellar companion, Kepler-538 B, which is 8 magnitudes fainter than the primary at a separation of $10''$ (Mugrauer 2019). We have collected 28 HIRES RVs between 2010 and 2017 (Fig. 49), yielding a mass for the transiting planet of $M_b = 6.7 \pm 3.6 M_{\oplus}$ (see Mayo et al. 2019 for a detailed analysis). The residual RVs have $\text{RMS} = 3.1 \text{ m s}^{-1}$ and no apparent trend over the 7 year baseline, consistent with $M \sin i < 0.2 M_J$ at 5 AU ($M \sin i < 0.8 M_J$ at 10 AU). There are no significant peaks in the fast periodogram ($\text{FAP}=0.98$).

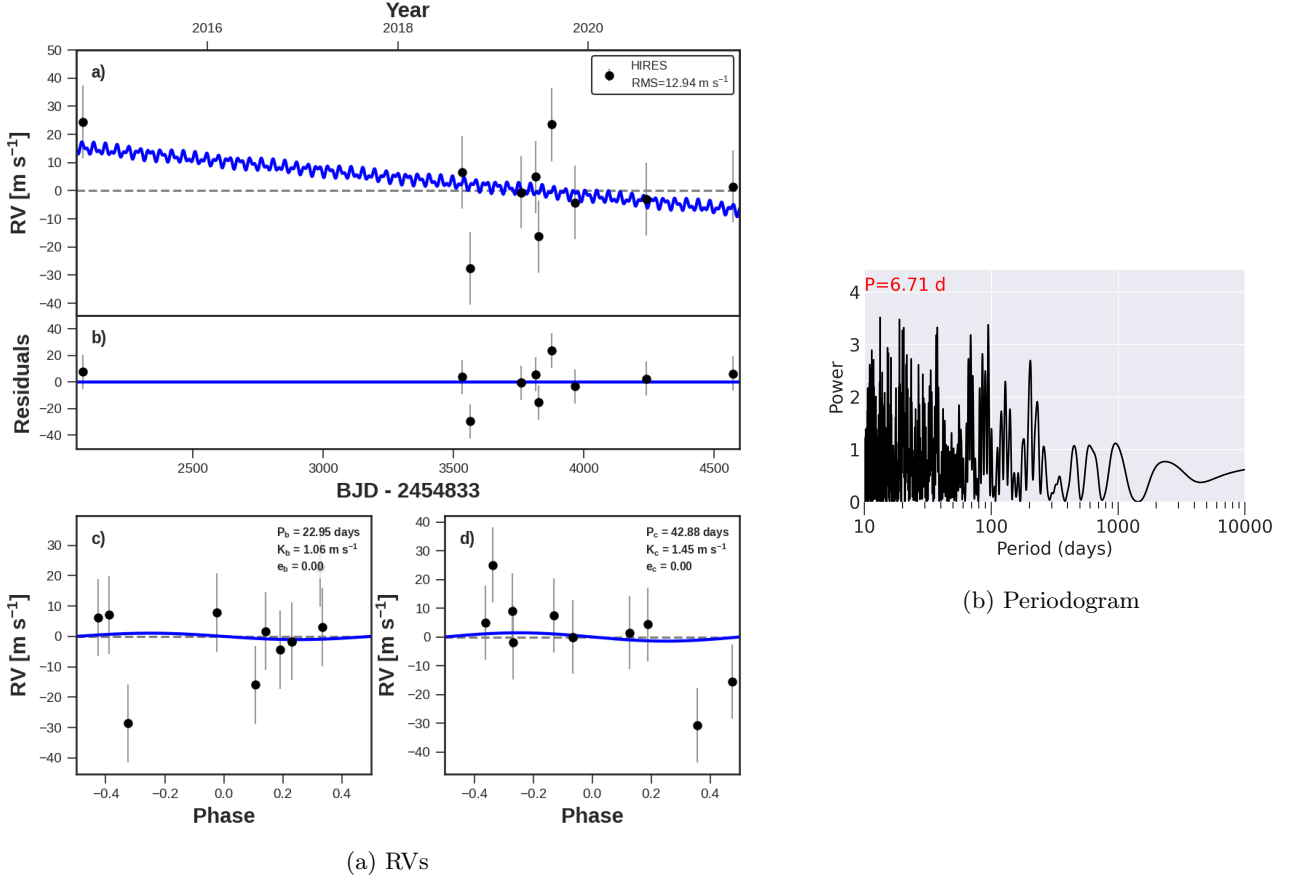


Figure 50: The same as Fig. 7, but for KOI-370 (Kepler-145). No non-transiting companions are detected.

KOI-370 (KEPLER-145)

Kepler-145 (KOI-370) is a slightly evolved, $V=12.0$ G type star with moderate rotation ($T_{\text{eff}} = 6000$ K, $\log(g)=4.1$ dex, $v \sin i = 6.5$ km/s, [Fulton & Petigura 2018a](#)). It has two transiting planets in a compact configuration ($P_b = 23.0$ days, $P_c = 42.9$ days) that produces TTVs ([Xie 2014](#)). The planet radii are $R_b = 2.6 R_{\oplus}$ and $R_c = 4.3 R_{\oplus}$. Based on their TTVs, the planets have masses of $M_b = 37 \pm 11 M_{\oplus}$ and $M_c = 79 \pm 16 M_{\oplus}$, which are unusually high masses for planets of these sizes ([Weiss & Marcy 2014](#)).

We have collected 10 Keck-HIRES RVs between 2014 and 2021 (Fig. 50). These are too few data to constrain the planet masses effectively, although the RVs collected so far are consistent with the high TTV masses. However, the scatter of the residual RVs is high ($\text{RMS}=13 \text{ m s}^{-1}$), which could be caused by a yet-undetected planet that might be influencing both the RV and TTV solutions. However, the star also has moderate rotation ($v \sin i = 6.5$ km/s), which could contribute somewhat to the high RV scatter (total expected RV jitter = 9.3 m s^{-1}). More RVs are needed to test the consistency of the RV and TTV solutions. The seven year RV baseline has no significant trend, although the high RV from 2014 is consistent with a variety of moderate trends, yielding a 3σ upper limit of $M \sin i < 0.6 M_J$ at 5 AU ($M \sin i < 2.7 M_J$ at 10 AU). There are no significant peaks in the fast periodogram (FAP=0.99).

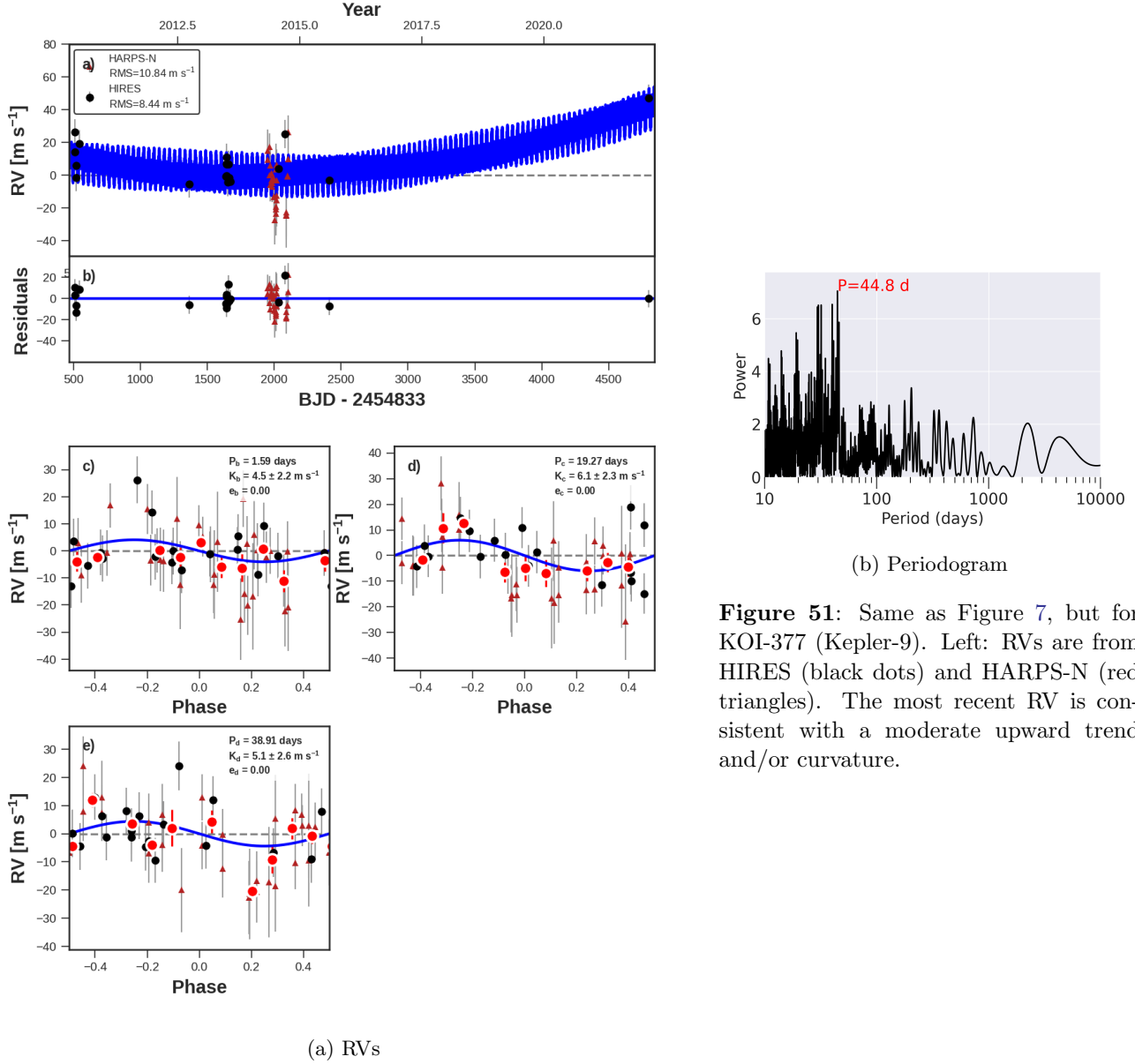


Figure 51: Same as Figure 7, but for KOI-377 (Kepler-9). Left: RVs are from HIRES (black dots) and HARPS-N (red triangles). The most recent RV is consistent with a moderate upward trend and/or curvature.

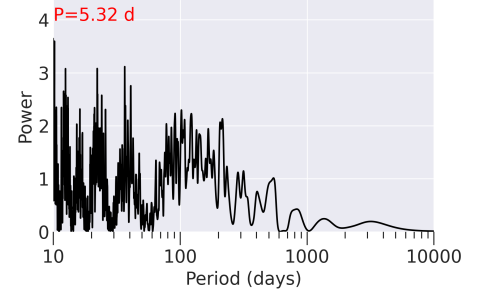
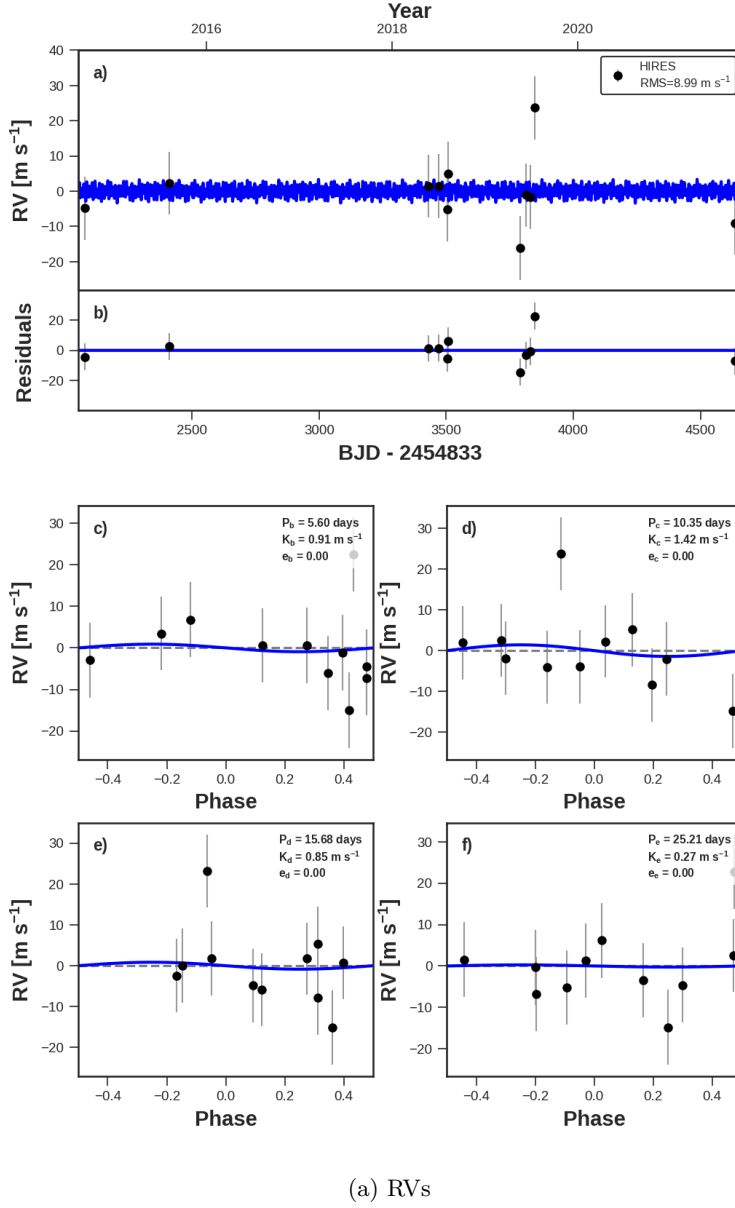
KOI-377 (KEPLER-9)

Kepler-9 (KOI-377) has three transiting planets, including two Saturn-sized planets near a 2:1 orbital resonance that were the first planets confirmed via TTVs ($P_b = 19.2$ days, $P_c = 39.0$ days, Holman et al. 2010). The third planet is a short-period super-Earth that was discovered based on additional photometry that is dynamically decoupled from the sub-Saturns and does not contribute appreciably to the TTVs ($P_d = 1.59$ days, $R_d = 1.6 R_\oplus$, Torres et al. 2011).

Holman et al. (2010) included N quarters of *Kepler* photometry and 6 RVs from Keck-HIRES, and this initial data set was dramatically expanded over the course of the *Kepler* Mission and a decade of ground-based follow-up. Dreizler & Ofir (2014) found masses for Kepler-9 b and c that were roughly $\sim 60\%$ of the originally reported values, based on N quarters of *Kepler* photometry that sampled a much longer timescale of planet-planet interaction than the discovery paper. Additional transits of planets b and c were detected with ground-based photometry, leading to an improved dynamical fit of the TTVs and 6 HIRES RVs (Freudenthal, J. et al. 2018). Borsato et al. (2019) collected 30 RVs with HARPS-N in 2014 and performed a joint fit to the RVs and TTVs. Their analysis yielded $R_b = 8.3 R_\oplus$, $R_c = 8.1 R_\oplus$, $M_b = 43 \pm 2 M_\oplus$, and $M_c = 30 \pm 1 M_\oplus$ (Borsato et al. 2019), although a variety of TTV solutions in the literature

have produced discrepant masses (Holman et al. 2010; Hadden & Lithwick 2014, 2017). At the time Borsato et al. (2019) was published, only 6 HIRES RVs were publicly available, and these RVs were not included in their analysis.

We have collected 21 RVs on Keck-HIRES between 2010 and 2022 (Fig. 51). Two spectra were taken with a short decker (B5 instead of C2, on June 19 2010 and May 26 2010), which precludes accurate sky-subtraction for those spectra. Because those two observations might suffer from contamination from moonlight or other background light, we removed them from our analysis. We jointly fit the remaining 19 HIRES RVs and 30 HARPS-N RVs, fitting 49 RVs in total. The 12-year RV baseline has $\text{RMS} \sim 11 \text{ m s}^{-1}$. The most recent RV (from 2022) is consistent with either a moderate upward curvature or no trend, yielding an upper limit of $M \sin i < 0.33 M_J$ at 5 AU ($M \sin i < 1.3 M_J$ at 10 AU) with 3σ confidence. An analysis that combines the HIRES RVs, HARPS-N RVs, *Kepler* TTVs, and ground-based TTVs is beyond the scope of this paper, but would likely lead to further dynamical insights about the Kepler-9 system.



(b) Periodogram

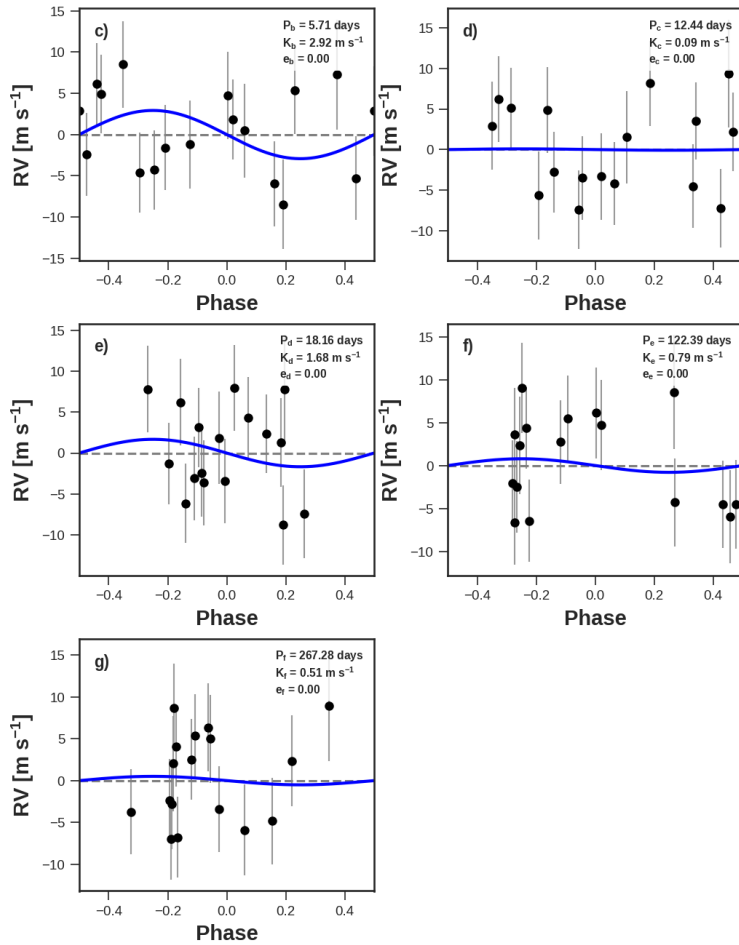
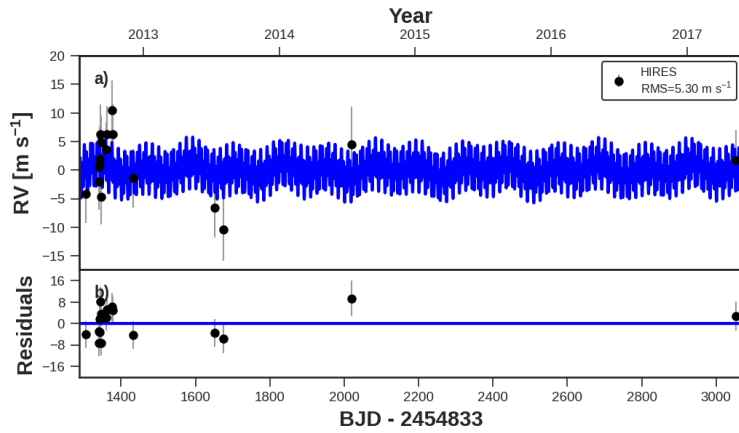
Figure 52: The same as Fig. 7, but for KOI-623 (Kepler-197). No non-transiting companions are detected.

KOI-623 (KEPLER-197)

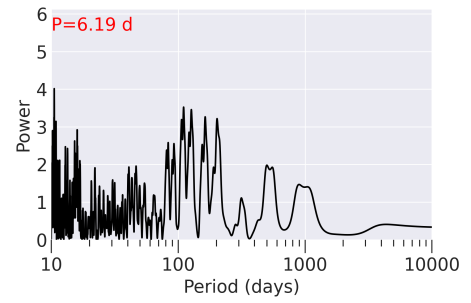
Kepler-197 (KOI-623) is a $V=11.8$ a slowly rotating, metal-poor sun-like star ($T_{\text{eff}} = 5980 \text{ K}$, $[Fe/H] = -0.6 \pm 0.1$ [Fulton & Petigura 2018a](#)). It has four transiting planets that range in size from $0.9 R_{\oplus}$ to $1.2 R_{\oplus}$. The planets were statistically validated based on their multiplicity in [Lissauer et al. \(2014\)](#) and [Rowe et al. \(2014\)](#). Their compact architecture ($P_b = 5.60$ days, $P_c = 10.3$ days, $P_d = 15.7$ days, $P_e = 25.2$ days) ought to generate TTVs, although [Van Eylen & Albrecht \(2015\)](#) did not detect any, perhaps due to the small planet sizes (which produce small single-transit signal-to-noise ratios). [Hadden & Lithwick \(2014\)](#) was able to constrain the mass of planet c: $M_c = 5.3 \pm 3.1 M_{\oplus}$. Updated long-cadence transit times were published in [Holczer et al. \(2016\)](#) and [Gajdoš et al. \(2019\)](#).

This system was selected for follow-up as part of a program to survey stars with at least 3 transiting planets from 2015 onward. We have collected 11 Keck-HIRES RVs that extend from 2014 to 2021 (Fig. 52). Assuming typical masses for the planet sizes ([Weiss & Marcy 2014](#)), the residual RVs have $\text{RMS} = 9.0 \text{ m s}^{-1}$, which is high for a sun-like star, although the low metallicity might impact RV precision. The high RMS is driven by two outliers in 2019. There

is no significant peak in the periodogram (FAP=0.99) and no apparent RV trend, yielding a mass upper limit of $M \sin i < 0.7 M_{\text{J}}$ at 5 AU ($M \sin i < 2.7 M_{\text{J}}$ at 10 AU).



(a) RVs



(b) Periodogram

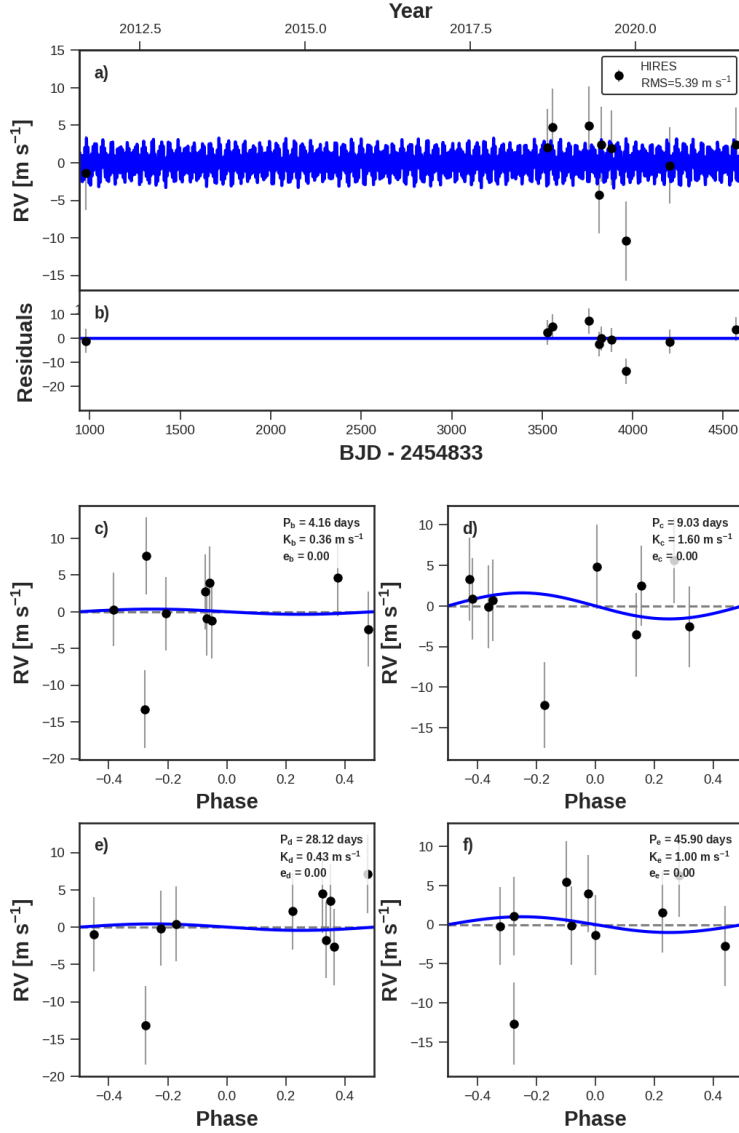
Figure 53: The same as Fig. 7, but for KOI-701 (Kepler-62). Left: this system has five transiting companions, for which the RVs provide only upper limits (not detections). No non-transiting companions are detected.

KOI-701 (KEPLER-62)

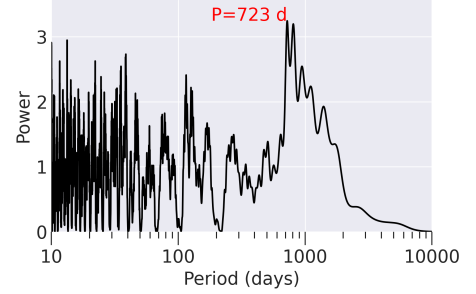
Kepler-62 (KOI-701) is a K type star with five transiting planets, including an Earth-sized planet in the habitable zone. This is one of the only Earth-sized habitable planets detected around a G or K type star from the *Kepler*

Mission. The planets were first announced in [Borucki et al. \(2013\)](#), which included an analysis of 13 Keck-HIRES RVs obtained over a baseline of 128 days in 2012. The RVs were used to place upper limits on the planet masses, although the planets are so small that the mass upper limits are uninformative about the planet compositions. The system also has significant TTVs, which generally yielded less informative mass upper limits than the RVs did ([Borucki et al. 2013](#), Table S4).

The host star is faint ($V=13.7$), which makes RV follow-up challenging. We have collected 5 RVs on Keck-HIRES since the publication of [Borucki et al. \(2013\)](#), extending the RV baseline to 5 years (Fig. 53). The new RVs do not substantially improve the planet mass upper limits, but they do constrain the parameter space of possible giant planets in the system. Assuming the transiting planets have typical masses for their sizes ([Weiss & Marcy 2014](#)), the RV residuals have $\text{RMS} \sim 11, \text{ms}^{-1}$ and no apparent trend, yielding an upper limit of $M \sin i < 0.6 M_J$ at 5 AU ($M \sin i < 2.5 M_J$ at 10 AU, 3σ conf.).



(a) Radial Velocities



(b) Periodogram

Figure 54: The same as Fig. 7, but for KOI-719 (Kepler-220). No non-transiting companions are detected.

KOI-719 (KEPLER-220)

Kepler-220 (KOI-719) is a quiet, K type star ($T_{\text{eff}} = 4500 \text{ K}$, $[\text{Fe}/\text{H}] = 0.08$, $v \sin i = 2 \text{ km s}^{-1}$, [Fulton & Petigura 2018a](#)). It has four transiting planets in a compact architecture, with two pairs of planets each near a 2:1 mean motion resonance, which were statistically validated ([Lissauer et al. 2014](#); [Rowe et al. 2014](#)). The planet radii range from $0.8 R_{\oplus}$ to $1.6 R_{\oplus}$.

We have collected 10 Keck-HIRES RVs between 2011 and 2021, with a gap in coverage between 2011 and 2019 (Fig. 54). Assuming typical masses for the planet radii ([Weiss & Marcy 2014](#)), the residual RVs have $\text{RMS} = 5.4 \text{ m s}^{-1}$. The lack of an apparent RV trend yields an upper limit of $M \sin i < 0.3 M_{\text{J}}$ at 5 AU ($M \sin i < 1.3 M_{\text{J}}$ at 10 AU).

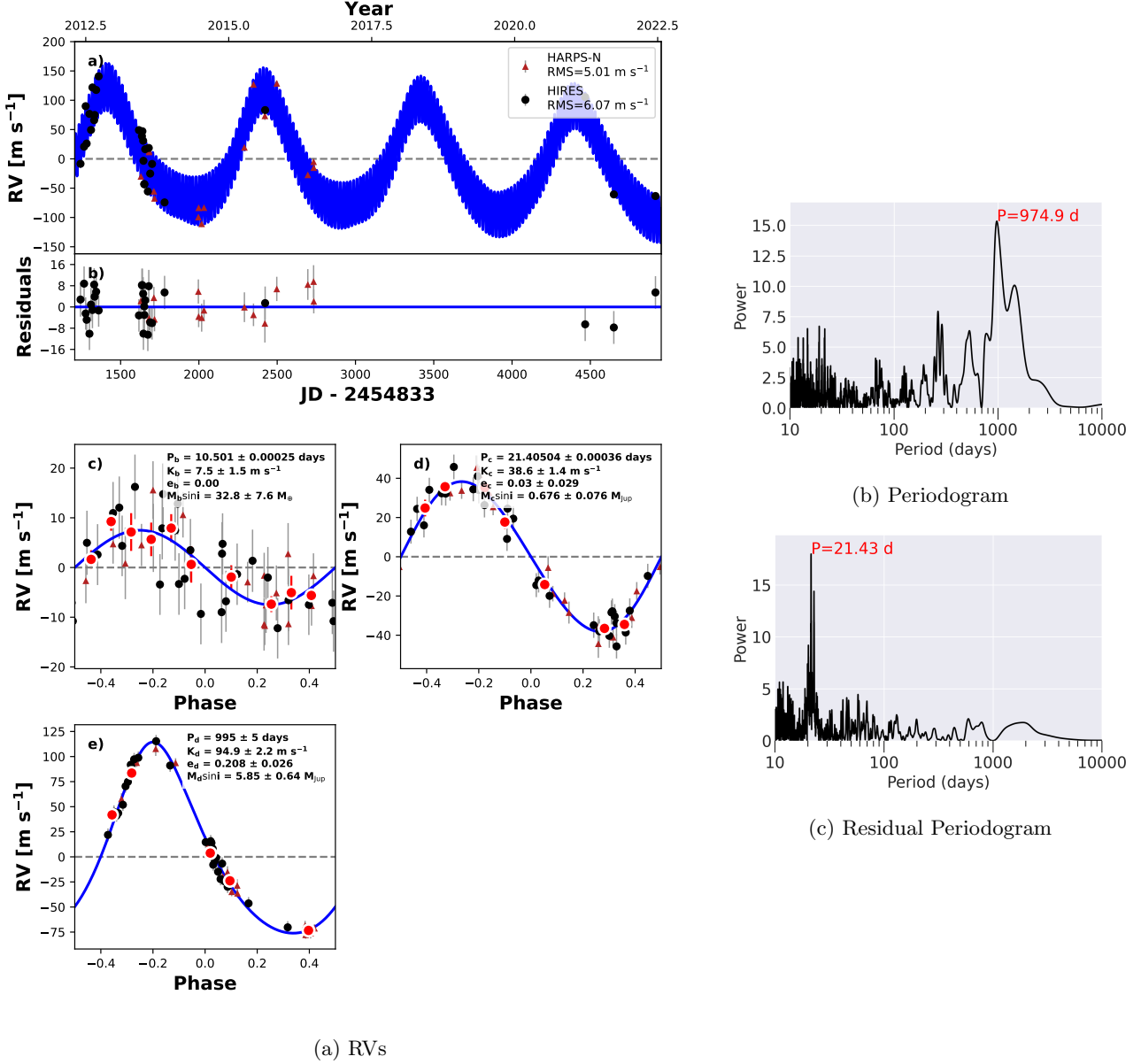


Figure 55: Same as Figure 7, but for KOI-1241 (Kepler-56). Left: RVs are from HIRES (black circles) and HARPS-N (maroon triangles). The best-fit model has two non-transiting giant planets (details inset in RV panels, left).

KOI-1241 (KEPLER-56)

Kepler-56 (KOI-1241) is the first transiting multi-planet system that was discovered to be misaligned by at least 40° with respect to its host star (Huber et al. 2013). This discovery was based on significant asteroseismology of the star, especially mode splitting that revealed the projected inclination of the star relative to the sky plane. The host star is evolved ($T_{\text{eff}} = 4800$ K, $\log(g) = 3.3$, Huber et al. 2013). This system fails two criteria of the KGPS survey: (1) the star’s gravity is too low, and (2) because the obliquity of the transiting planet orbits was suspected to be driven by a massive perturber, this system fails the “giant-blind” criterion.

The two transiting planets are near the 2:1 mean motion resonance, which generates TTVs ($P_b = 10.5$ days, $P_c = 21.4$ days, Steffen et al. 2013). RVs collected at Keck-HIRES had a trend indicative of a massive perturber (Huber et al. 2013). Continued RV monitoring with TNG-HARPS-N revealed the orbit and planetary mass of the

perturber ($P_d = 1002 \pm 5$ days, $M \sin i_d = 5.6 \pm 0.4 M_J$, $e_d = 0.2 \pm 0.01$, [Otor et al. 2016](#)). A slight misalignment of the massive perturber drives nodal precession of the transiting planets.

We have collected 29 Keck-HIRES RVs, including 3 since the publication of [Huber et al. \(2013\)](#). Our most recent RV extends the HIRES baseline from 2012 to 2022 (Fig. 55). The combined HIRES and HARPS-N RVs yield $M \sin i_d = 5.9 \pm 0.7 M_J$, $P_d = 1000.1 \pm 3.5$ days, $e_d = 0.21 \pm 0.03$. The residual RVs have low RMS (5.1 m s^{-1} on HARPS-N, 5.5 m s^{-1} on HIRES). There is a significant trend to the residual RVs ($dv/dt = -0.007 \pm 0.002 \text{ m s}^{-1} \text{ day}^{-1}$), corresponding to $M \sin i = 11 M_J$ at 20 AU.

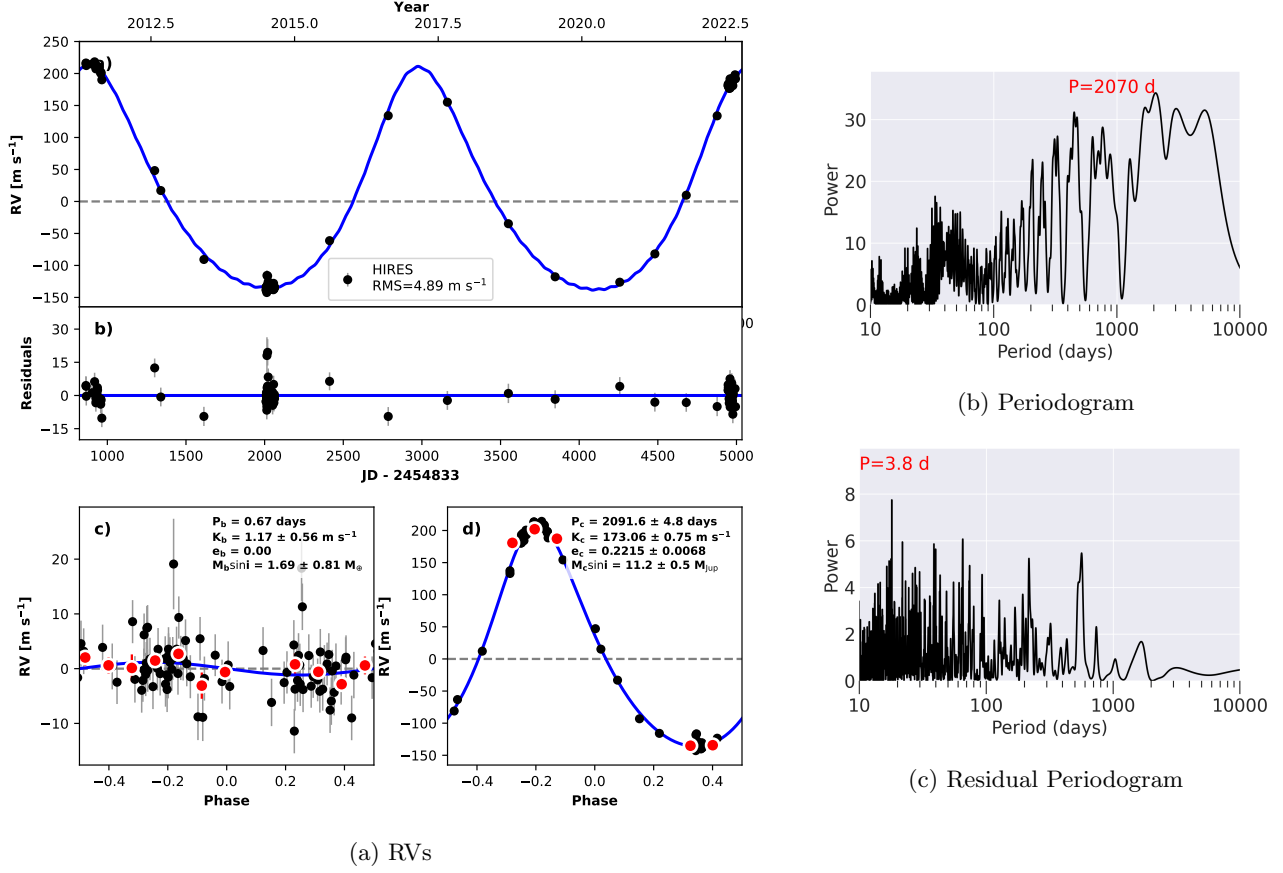
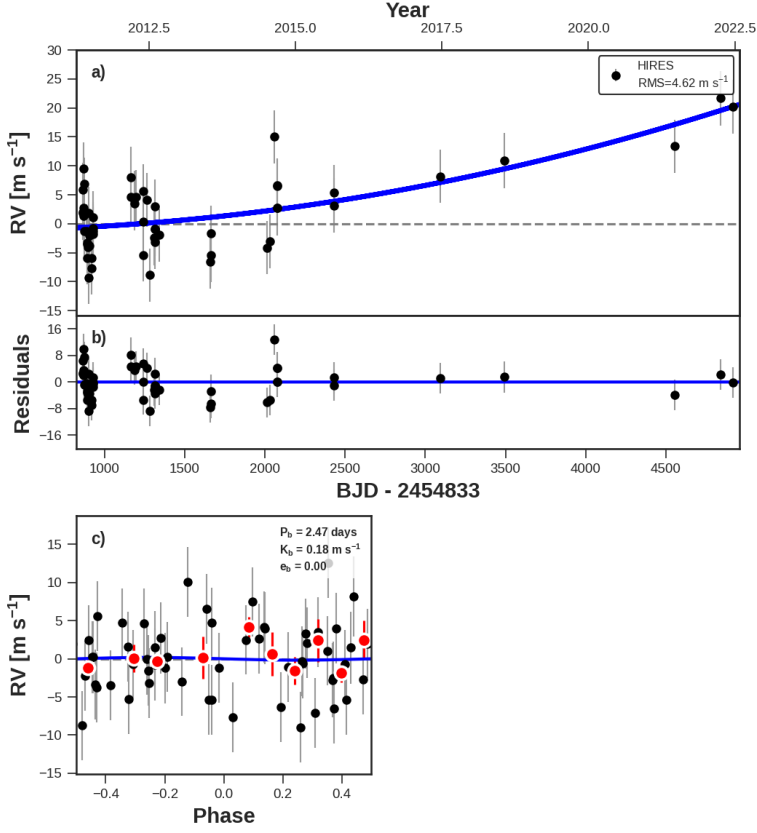


Figure 56: The same as Figure 7, but for KOI-1442 (Kepler-407). Left: The best-fit model includes a non-transiting planet, Kepler-407 c (orbital parameters inset in phase-folded panel). Right: The periodogram of the RVs after removing the signals from the transiting planet (top) and both planets (bottom).

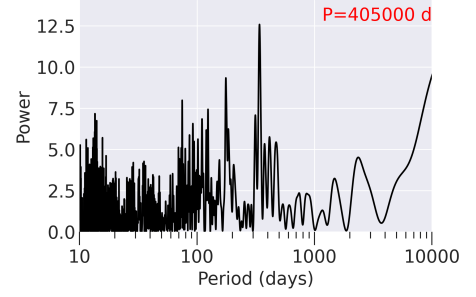
KOI-1442 (KEPLER-407)

Kepler-407 (KOI-1442) is a $V=12.5$, metal rich, G-type star ($T_{\text{eff}} = 5400 \text{ K}$, $[Fe/H] = 0.4 \pm 0.1$, [Fulton & Petigura 2018a](#)). It has one transiting, ultra-short period planet ($P_b = 0.669 \text{ days}$, $R_b = 1.1 R_{\oplus}$) that was confirmed with 17 Keck-HIRES RVs ([Marcy et al. 2014](#)). The RVs yielded an upper limit on the mass of $M_b = 0.6 \pm 1.2 M_{\oplus}$. The RVs also showed a significant trend with curvature, which yielded preliminary parameters for a massive non-transiting planet or brown dwarf: $P_c = 3000 \pm 500 \text{ days}$, $M \sin i_c = 4000 \pm 2000 M_{\oplus}$.

We have collected 98 Keck-HIRES RVs between 2011 and 2022 (Fig. 56). The 11-year baseline has sampled nearly two full orbits of the companion, yielding $P_c = 2098 \pm 7 \text{ days}$, $M \sin i_c = 11.2 \pm 0.5 M_J$, and $e_c = 0.22 \pm 0.01$. This corresponds to an object near the boundary between brown dwarf and planetary-mass objects ([Schlaufman & Winn 2016](#); [Bowler et al. 2019](#)). The additional improved characterization of the long-period companion somewhat tightens the mass constraint of the transiting planet: $M_b = 1.5 \pm 0.9 M_{\oplus}$, although more RVs are needed to precisely determine its mass and composition. The residual RVs have $\text{RMS}=5.6 \text{ ms}$ and no apparent trend, yielding an upper limit of $M \sin i < 0.2 M_J$ at 5 AU ($M \sin i < 0.7 M_J$ at 10 AU).



(a) RVs



(b) Periodogram

Figure 57: The same as Fig. 7, but for KOI-1612 (Kepler-408). Left: there is a marginally significant long-term trend to the RVs consistent with a stellar mass companion.

KOI-1612 (KEPLER-408)

Kepler-408 (KOI-1612, HD 176693) is a V=8.8 F type star ($T_{\text{eff}} = 6100\text{ K}$, [Fulton & Petigura 2018a](#)). It has one transiting planet ($P = 2.47\text{ days}$, $R = 0.7 R_{\oplus}$) that was statistically validated ([Morton et al. 2016](#)). Keck-HIRES RVs were collected that yielded a mass upper limit of $0.48 \pm 3.2 M_{\oplus}$ ([Marcy et al. 2014](#)).

We have collected 55 total Keck-HIRES RV, including 17 since the publication of [Marcy et al. \(2014\)](#) (Fig. 57). The mass upper limit for the transiting planet has not improved substantially. There is a moderate RV trend (FAP=0.01) over the decade-long baseline. If bona-fide, this trend corresponds to a companion of $M \sin i > 11 M_J$ at $> 20\text{ AU}$. The long baseline and shallow trend also yield upper limits of $M \sin i < 1.3 M_J$ at 5 AU ($M \sin i < 5.2 M_J$ at 10 AU , 3σ conf.).

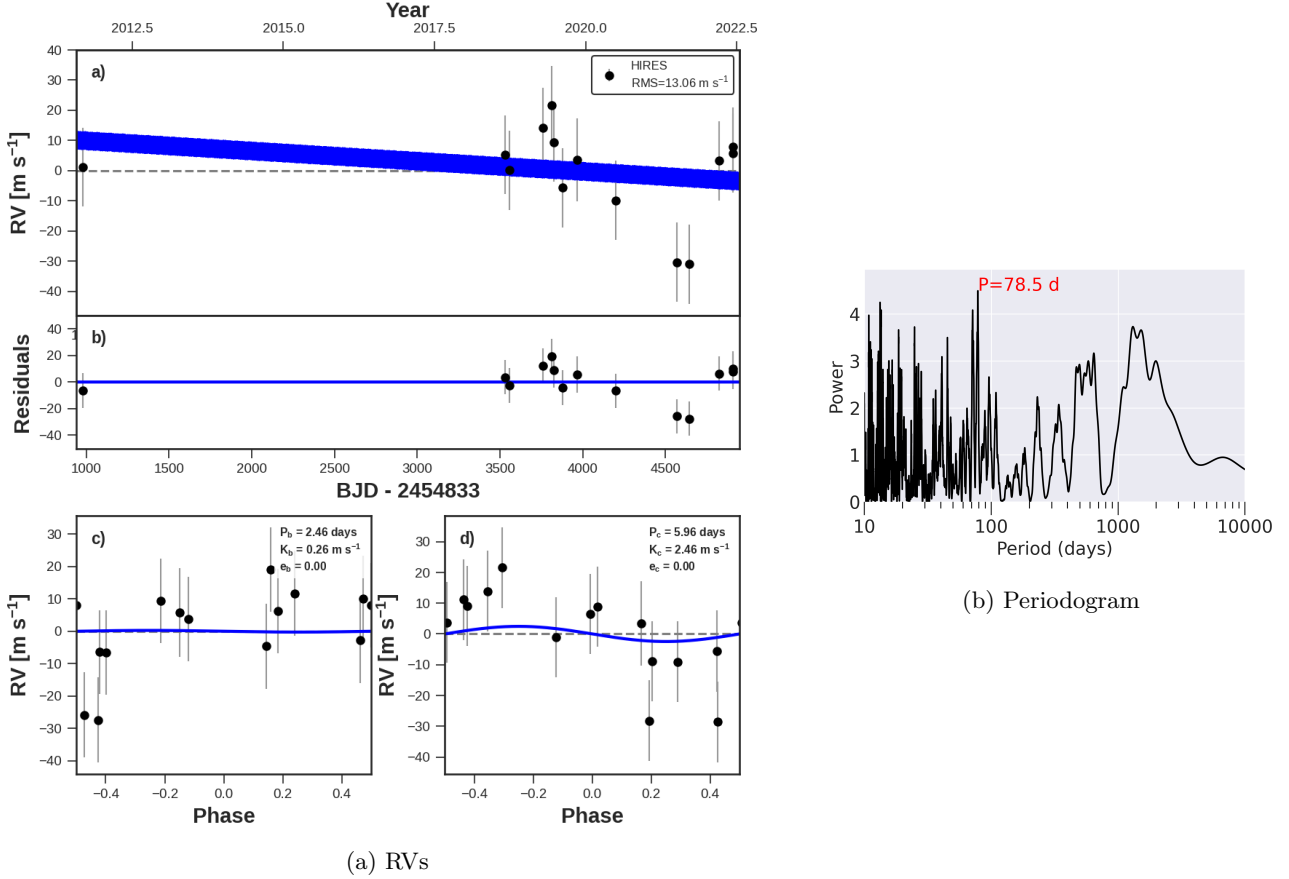


Figure 58: The same as 7, but for KOI-1692 (Kepler-314). There is a marginal trend in the RVs.

KOI-1692 (KEPLER-314)

Kepler-314 (KOI-1692) is a $V=12.6$, metal-rich G-type star ($T_{\text{eff}} = 5400 \text{ K}$, $[Fe/H] = 0.37$, [Fulton & Petigura 2018a](#)). It has two transiting planets that were statistically validated at $P_b = 2.46$ days and $P_c = 5.96$ days ([Lissauer et al. 2014](#); [Rowe et al. 2014](#)). The planet sizes span the radius valley, with $R_b = 0.84 R_{\oplus}$ and $R_c = 2.9 R_{\oplus}$ ([Berger et al. 2018](#)).

We have collected 11 Keck-HIRES RVs between 2011 and 2022, with a gap between 2011 and 2018 (Fig. 58). There is an apparent downward trend in the RVs from 2018 to 2022, although the observation in 2011 is not consistent with this trend. It is possible that we are sampling the RV variations from a giant planet near 5 AU, or that either the 2011 point or two points from 2021 are outliers. Including an RV trend and curvature term (2 free parameters for the giant planet) fits the RVs with $\text{RMS}=13.1 \text{ m s}^{-1}$, whereas a fit with no RV trend or curvature has $\text{RMS}=13.5 \text{ m s}^{-1}$. Based on the stellar properties, we expect this star to have low jitter (5.2 m s^{-1}). To test the stellar jitter, we obtained three RVs in a single night; the maximum difference was 2.2 m s^{-1} , which is too low to explain the RV variations. More RVs are needed to ascertain the origin of the RV variability.

KOI-1781 (KEPLER-411)

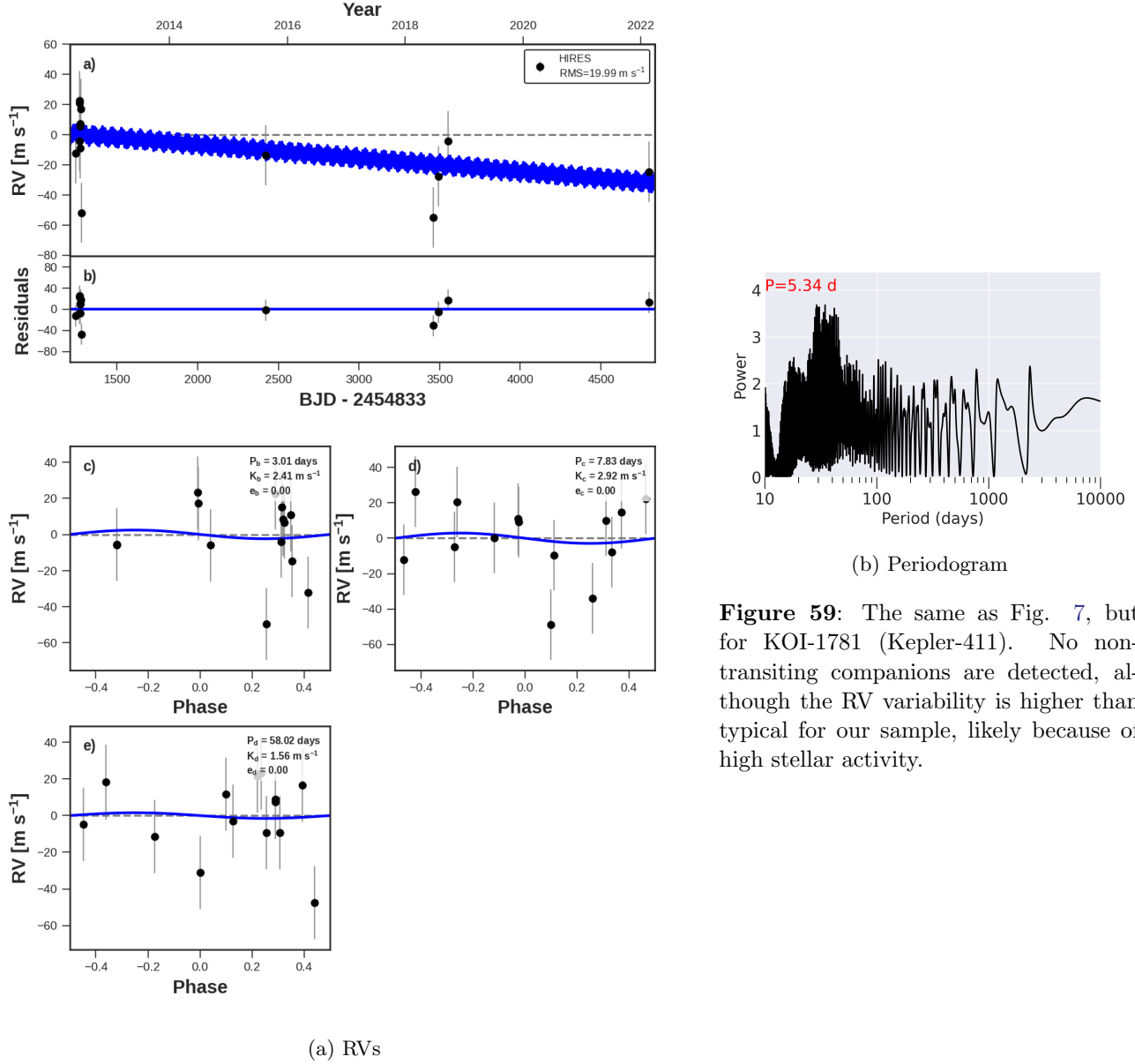


Figure 59: The same as Fig. 7, but for KOI-1781 (Kepler-411). No non-transiting companions are detected, although the RV variability is higher than typical for our sample, likely because of high stellar activity.

KOI-1781 (KEPLER-411)

Kepler-411 (KOI-1781) is a young, active star with four transiting planets summarized in Sun et al. (2019). Because of its high activity, KOI-1781 is not considered part of the KGPS sample. There are three transiting and one non-transiting planets in the system with orbital periods of 3, 7.8, 58 and 31.5 days respectively. All four planets have mass measurements from TTVs with the 31.5 day planet having its presence known only through the gravitational interaction with the 58 day planet. The planets labels moving outward in orbital period are Kepler-411b,c,e,and d.

This system was selected for follow-up as part of a program to survey stars with at least 3 transiting planets from 2015 onward. The star has high activity ($\log(R'_{HK})$ value of -4.3), and so we expect stellar jitter to dominate the error budget, which is consistent with the observed RMS of the RVs of 24 m s⁻¹ (Fig. 59). We do not detect any of the four transiting planets in the RVs, but our RVs are consistent with the masses determined from TTVs. The relationship between RV jitter and stellar activity by Hillenbrand et al. (2015) shows that all 24 m s⁻¹ of RV jitter can be attributed to the activity of the star (rather than planets) and the age of the system is between 60 and 300 Myr, consistent with the age of 212 ± 31 Myr determined by Sun et al. (2019) based on the rotation period and the color

index. The eight year RV baseline does not have a significant trend, yielding a 3σ upper limit of $M \sin i < 4.5 M_J$ at 10 AU. Because the RMS of the RVs is quite high, the non-detection of a trend is not particularly informative about lower-mass planets closer to the star – for instance, a Jupiter-mass planet at 5 AU would produce an amplitude of roughly 10 m s^{-1} , which could easily be hidden in the 24 m s^{-1} RMS of the RVs.

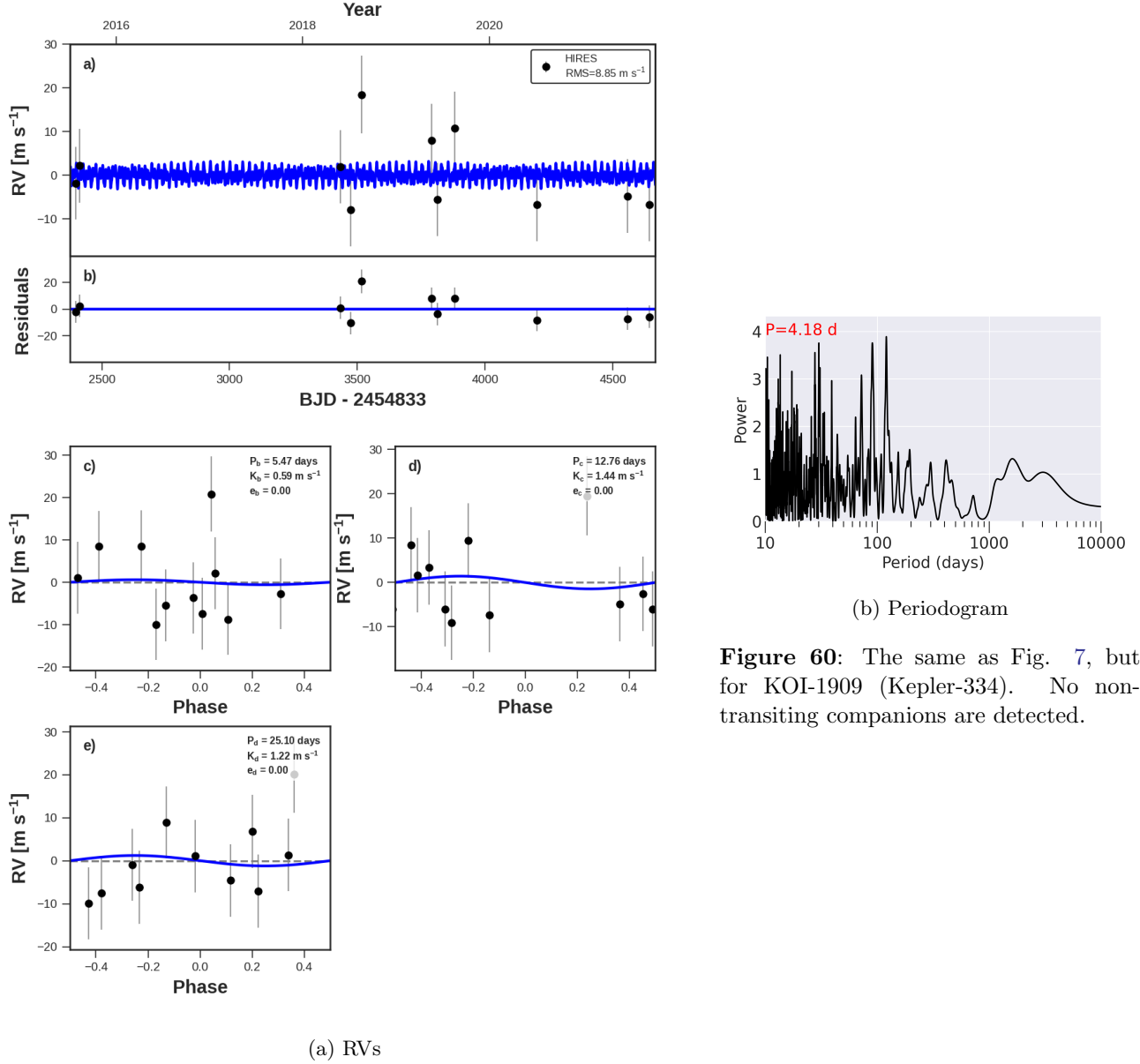


Figure 60: The same as Fig. 7, but for KOI-1909 (Kepler-334). No non-transiting companions are detected.

KOI-1909 (KEPLER-334)

Kepler-334 (KOI-1909) is a quiet, sun-like star ($T_{\text{eff}} = 5800$ K, [Fulton & Petigura 2018a](#)). It has three super-Earth sized ($R_p < 1.5 R_{\oplus}$) transiting planets that were statistically validated at periods of $P_b = 5.47$ days, $P_c = 12.7$ days, and $P_d = 25.1$ days ([Lissauer et al. 2014](#); [Rowe et al. 2014](#)). The outer two planets are near the 2:1 mean motion resonance, and their transit midpoints are reported in [Holczer et al. \(2016\)](#). This system was selected for follow-up as part of a program to survey stars with at least 3 transiting planets from 2015 onward. We have collected 11 Keck-HIRES RVs between 2015 and 2021 (Fig. 60). Assuming the planets have typical masses for their sizes ([Weiss & Marcy 2014](#)), the residual RVs have $\text{RMS} = 8.9 \text{ m s}^{-1}$ and no apparent RV trend over the 6 year baseline, yielding a 3σ upper limit of $M \sin i < 0.7 M_J$ at 5 AU ($M \sin i < 2.7 M_J$ at 10 AU).

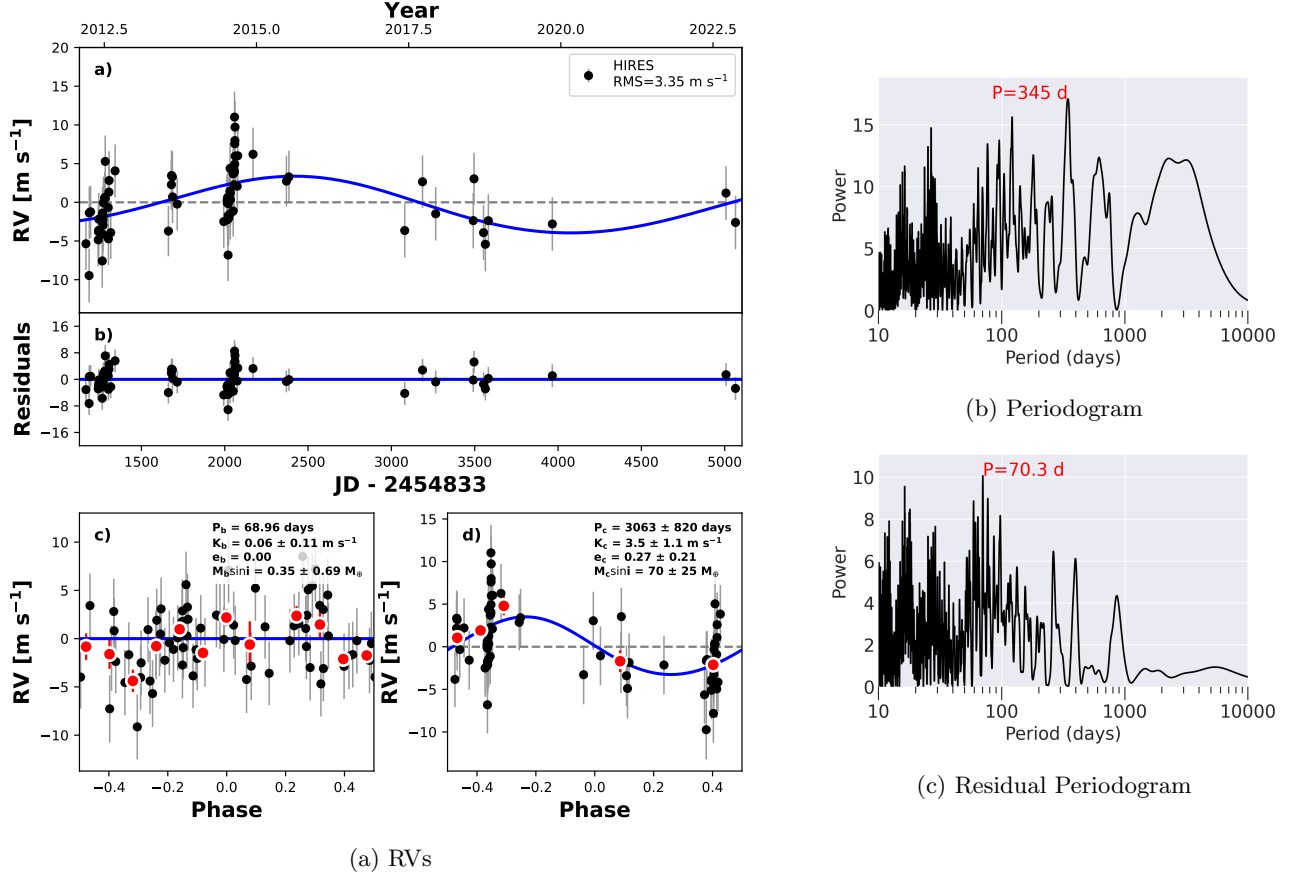


Figure 61: The same as Fig. 7, but for KOI-1925 (Kepler-409). Left: A non-transiting planet is detected with low significance (orbital parameters inset). Right: Periodograms of the RVs after removing a model of the transiting planet only (top) and the best-fit two-planet model (bottom).

KOI-1925 (KEPLER-409)

Kepler-409 (KOI-1925) is a $V=9.4$ quiet, sun-like star ($T_{\text{eff}} = 5400$ K, [Fulton & Petigura 2018a](#)). It has one transiting planet ($P_b = 70.0$ days, $R_b = 1.2 R_{\oplus}$) that was confirmed with Keck-HIRES RVs ([Marcy et al. 2014](#)). We have collected 97 RVs between 2012 and 2022, including 57 since 2013 (Fig. 61). There is significant structure in the fast periodogram, with peaks near 340 days and 3000 days (FAP=0.001), although this structure is primarily driven by high-cadence observations in 2012 and 2014, which is not optimal sampling for detecting long-period signals. Including a Keplerian orbit at 340 days yields $\Delta\text{BIC} = -37$ and would correspond to a companion of $M \sin i = 40 M_{\oplus}$ at this orbital period. However the 340 day signal has high eccentricity ($e = 0.4$) and is likely an alias of a signal at 3000 days, which would correspond to a companion of $M \sin i = 230 M_{\oplus}$. More RVs are needed to validate the planet candidate and determine its orbit and mass. Because the NEA default transit ephemeris was from [Marcy et al. \(2014\)](#) whereas a more updated ephemeris that accounts for TTVs is available, we tested whether using the [Holczer et al. \(2016\)](#) ephemeris would affect the candidate giant planet. The change in the residual RVs was negligible and the peaks at 340 and 3000 days persisted. More RVs are needed to clarify whether the long-period signal is from an additional planet, and if so, what its orbital period is.

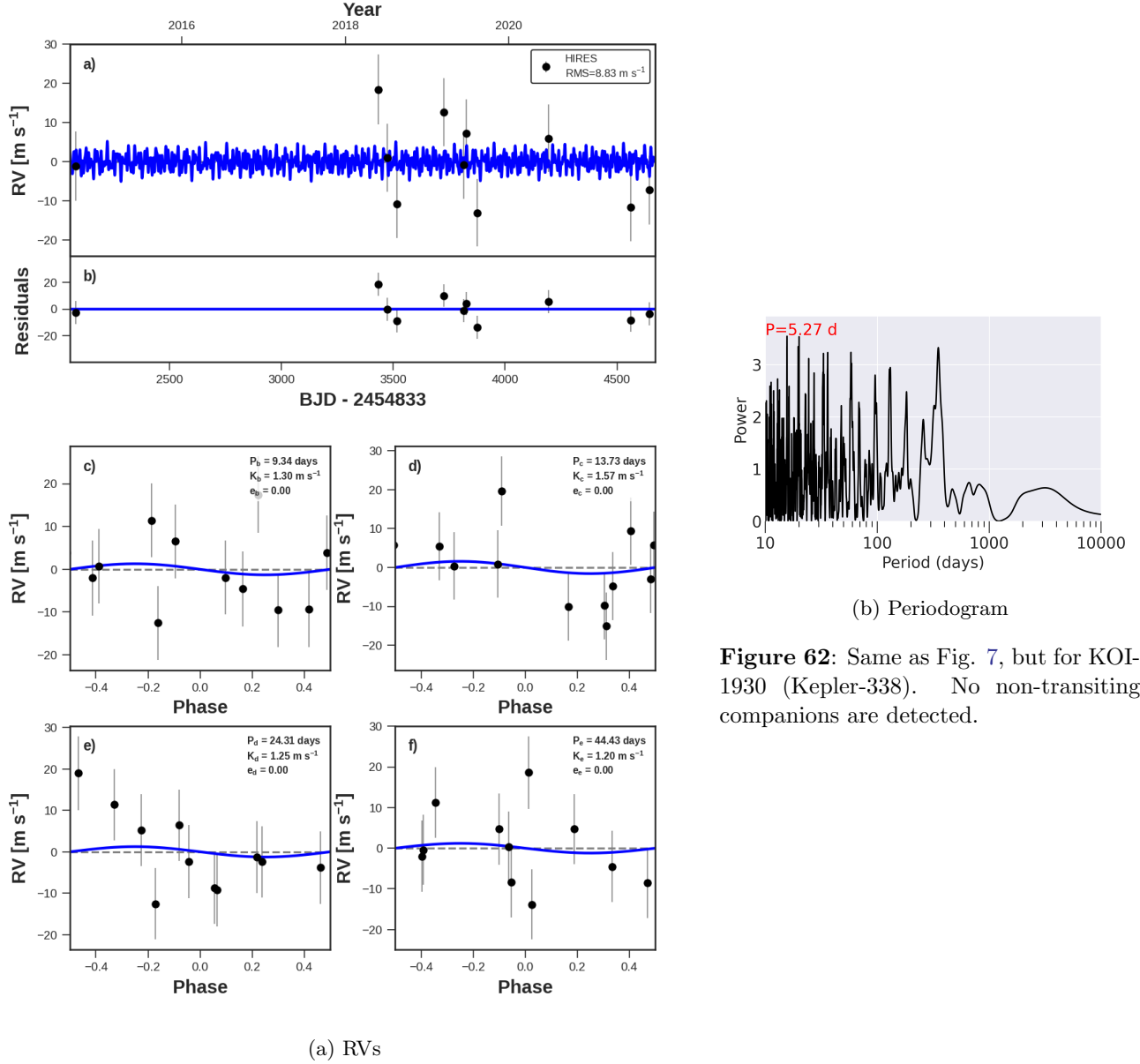


Figure 62: Same as Fig. 7, but for KOI-1930 (Kepler-338). No non-transiting companions are detected.

KOI-1930 (KEPLER-338)

Kepler-338 (KOI-1930) is a $V=12.2$, slightly evolved G type star with moderate rotation ($T_{\text{eff}} = 5900$ K, $\log(g) = 4.0$, $v \sin i = 4.0$ km/s, [Fulton & Petigura 2018a](#)). It has three sub-Neptune sized transiting planets that were statistically validated ([Lissauer et al. 2014](#); [Rowe et al. 2014](#)). The planets have TTVs, which were used to characterize the orbit of a fourth planet that also transits and is smaller than its neighbors ($P_e = 9.3$ days, $R_e = 1.6 R_{\oplus}$ [Hadden & Lithwick 2014](#)).

We have collected 11 Keck-HIRES RVs between 2014 and 2021 (Fig. 62). Assuming the planets have masses that are typical for their radii, we find a residual RV scatter of 8.8 m s^{-1} . This RV scatter is consistent with the jitter we expect for a moderately evolved, moderately rotating star. We find no significant RV trend, yielding an upper limit of $M \sin i < 1 M_J$ at 5 AU ($M \sin i < 3.6 M_J$ at 10 AU). There is no significant structure in the fast periodogram.

KOI-2169 (KEPLER-1130)

Kepler-1130 (KOI-2169) is a $V=12.4$, quiet G-type star ($T_{\text{eff}} = 5400\text{ K}$, [Fulton & Petigura 2018a](#)). It has four transiting planet candidates that range from $0.3 R_{\oplus}$ to $0.8 R_{\oplus}$ ([Morton et al. 2016](#); [Valizadegan et al. 2022](#)). Although only three of the transiting planet candidates are confirmed, including the fourth planet candidate in the RV model would not significantly influence the overall RV fit, since its small size imply a small mass. The host star also has a stellar companion at $\rho = 3.5''$ with a Gaia G-band magnitude of 17.0 that is co-moving based on Gaia DR2 ([Mugrauer 2019](#)). At a distance of 250 pc, the physical separation from the primary is approximately 875 au. The Gaia data suggests the two stars are associated, but the $2.5''$ companion is not the cause of the 4 km s^{-1} RV signal, that has a period near 43 years.

This system was selected for follow-up as part of a program to survey stars with at least 3 transiting planets from 2015 onward. We have collected 34 Keck-HIRES RVs between 2012 and 2022 (Fig. 63). This decade-long baseline has a change in RV of 4000 m s^{-1} , consistent with the perturbation of a stellar-mass companion, which we call Kepler-1130 B. The RV time series captures both a concave-up and concave-down inflection, which likely correspond to the two quadrature times of the companion. The KGPS algorithm did not find a good fit to the orbital period of this long-period, eccentric companion. We used `rvsearch` to identify a period, eccentricity, and mass of a companion to use as an initial guess that we then optimized with `radvel`. Our best fit to the RVs yields an RMS of 6.5 m s^{-1} based on the inclusion of a companion at $P_B = 14000 \pm 1800$ days (~ 12 AU), $M \sin i_B = 218 \pm 3 M_J$, $e_B = 0.65 \pm 0.024$. The periastron passage of Kepler-1130 B is ~ 4 AU from Kepler-1130 A, and so the transiting planets likely formed from a substantially truncated disk. Because the observational baseline is small compared to the orbital period of Kepler-1130 B, there is substantial uncertainty in any residual RV trend, allowing additional companions of $M \sin i < 5 M_J$ at 5 AU ($M \sin i < 20 M_J$ at 10 AU) when including the uncertainty in the orbital properties of star B. Future RV monitoring of this target is essential to map the orbit of the stellar-mass companion and accurately determine its periastron passage distance.

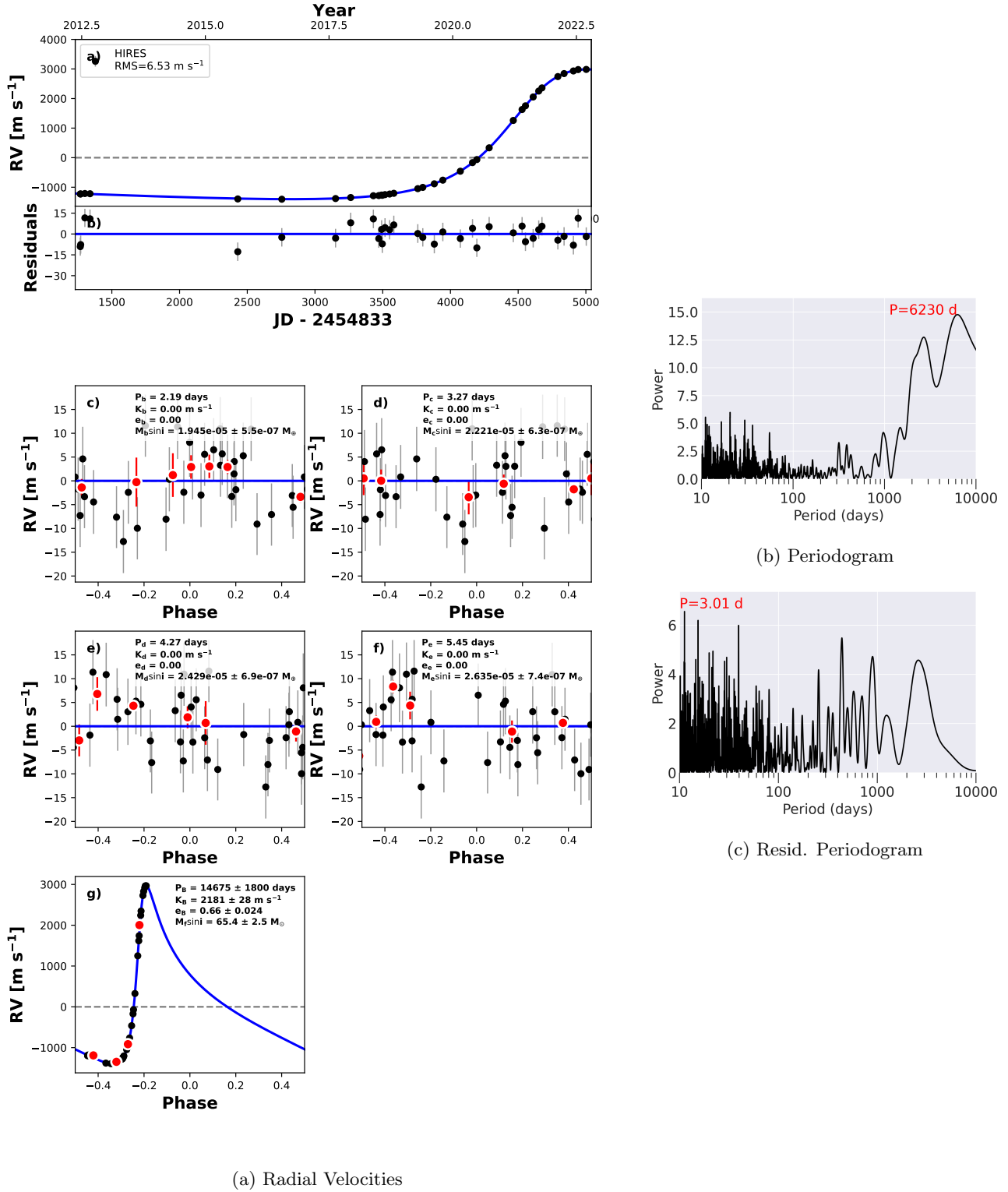
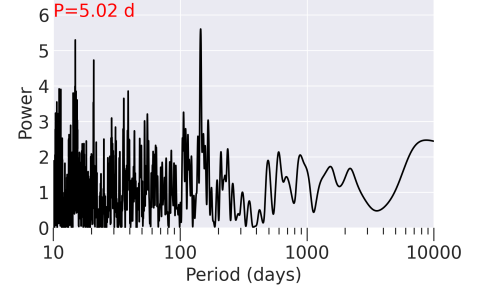
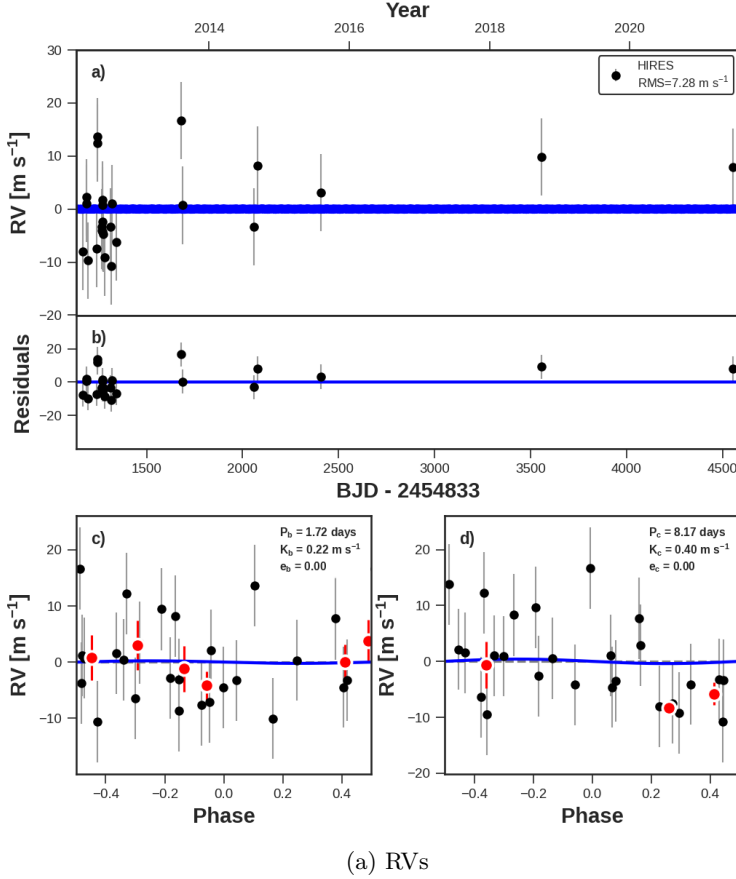


Figure 63: Same as Fig. 7, but for KOI-2169 (Kepler-1130). Left: The best-fit model includes a long-period, highly eccentric stellar-mass companion that moved through periastron in 2022. The automated KGPS algorithm detects this companion but does not find the optimal orbital period because the full phase curve of the eccentric orbit has not been sampled yet. Right: Periodograms of the RVs the after removing a model of the transiting planets only (top) and our best-fit model of the stellar companion (bottom).

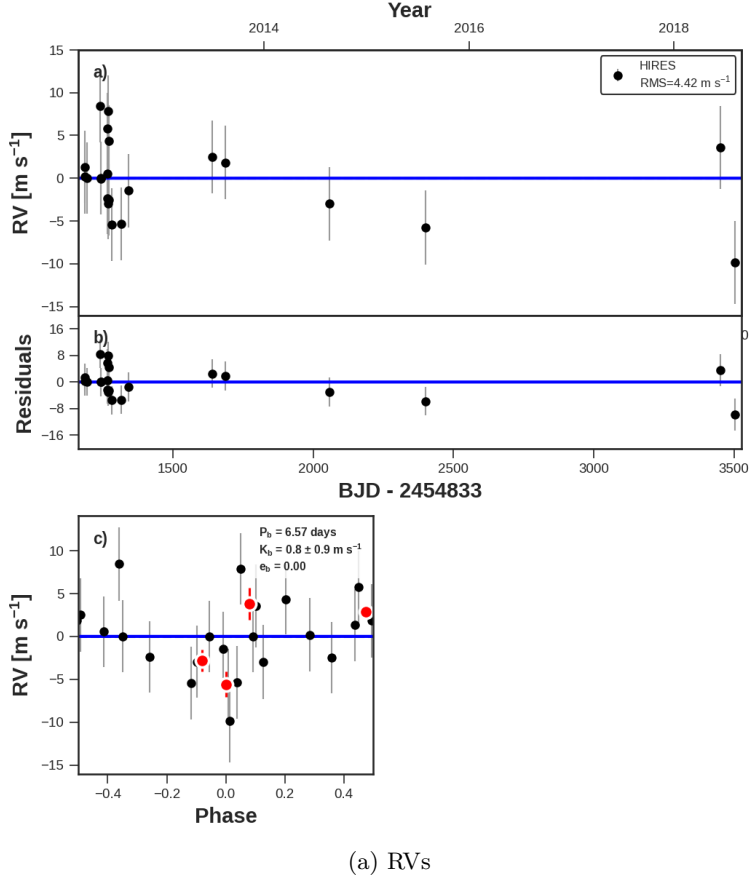


(b) Periodogram

Figure 64: Same as Fig. 7, but for KOI-2687 (Kepler-1869). No non-transiting companions are detected.

KOI-2687 (KEPLER-1869)

Kepler-1869 (KOI-2687) is a $V=10.3$ sun-like star ($T_{\text{eff}} = 5800$ K, [Fulton & Petigura 2018b](#)). It has two Earth-sized transiting planet candidates ([Burke et al. 2014](#)), one of which was statistically validated ($P_b = 8.17$ days, [Valizadegan et al. 2022](#)), and the other of which still has candidate status ($P_{01} = 1.72$ days). We have collected 26 Keck-HIRES RVs between 2012 and 2021, and do not make a significant detection of the masses (Fig. 64). Assuming typical masses for the planet radii ([Weiss & Marcy 2014](#)), the residual RVs have $\text{RMS}=7.3$ ms and no apparent trend, yielding an upper limit of $M \sin i < 0.5 M_J$ at 5 AU ($M \sin i < 1.9 M_J$ at 10 AU).



(a) RVs

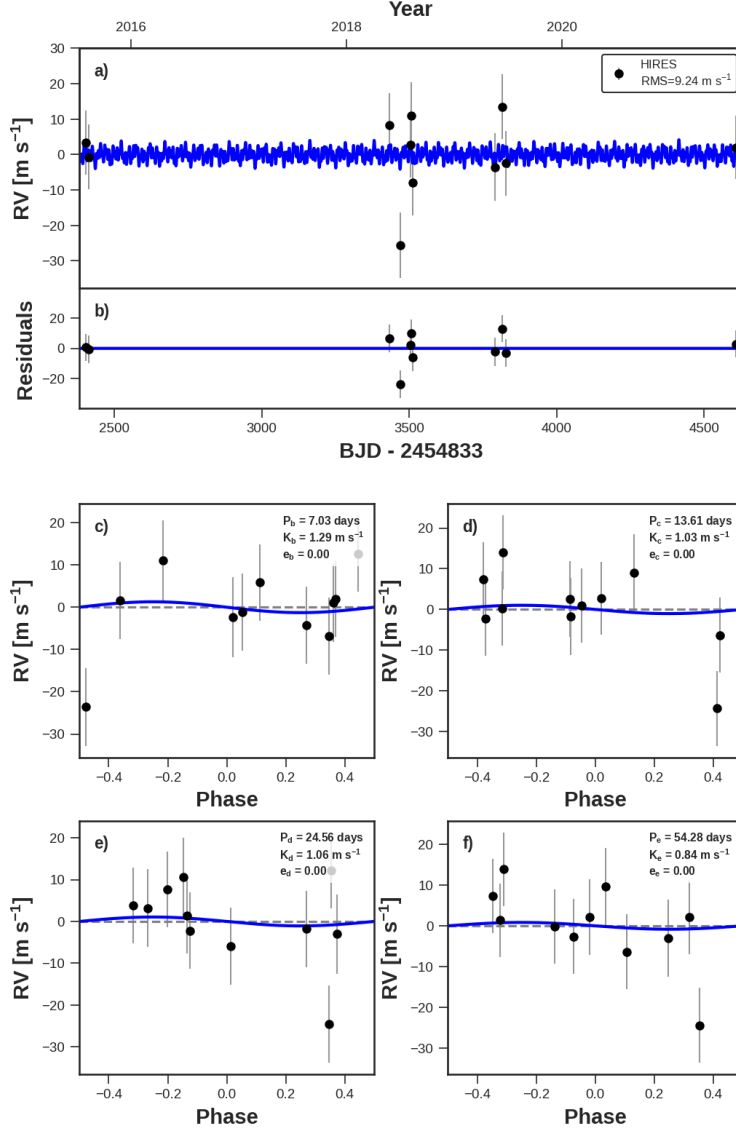
(b) Periodogram

Figure 65: Same as Fig. 7, but for KOI-2720. No non-transiting companions are detected.

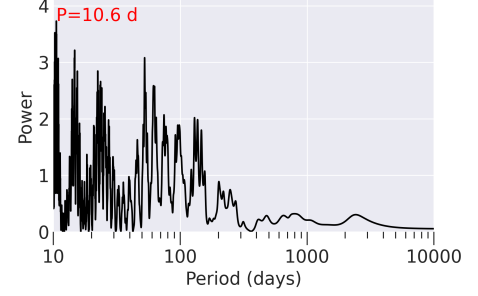
Figure 66: KOI-2720 (KIC 8176564)

KOI-2720 (KIC 8176564)

KOI-2720 (KIC 8176564) is a $V=10.3$ sun-like star ($T_{\text{eff}} = 5900$ K, [Fulton & Petigura 2018a](#)). It has one candidate transiting Earth-sized planet ($R_p = 1.2 R_{\oplus}$) at $P = 6.57$ days ([Batalha et al. 2013](#)). We have collected 22 Keck-HIRES RVs between 2012 and 2018, resulting in a non-detection of the planet mass (Fig. 66). Assuming a typical mass for KOI-2720.01 ([Weiss & Marcy 2014](#)), the residual RVs have $\text{RMS}=4.6 \text{ m s}^{-1}$ and no apparent trend, yielding an upper limit of $M \sin i < 0.4 M_J$ at 5 AU ($M \sin i < 1.5 M_J$ at 10 AU).



(a) RVs

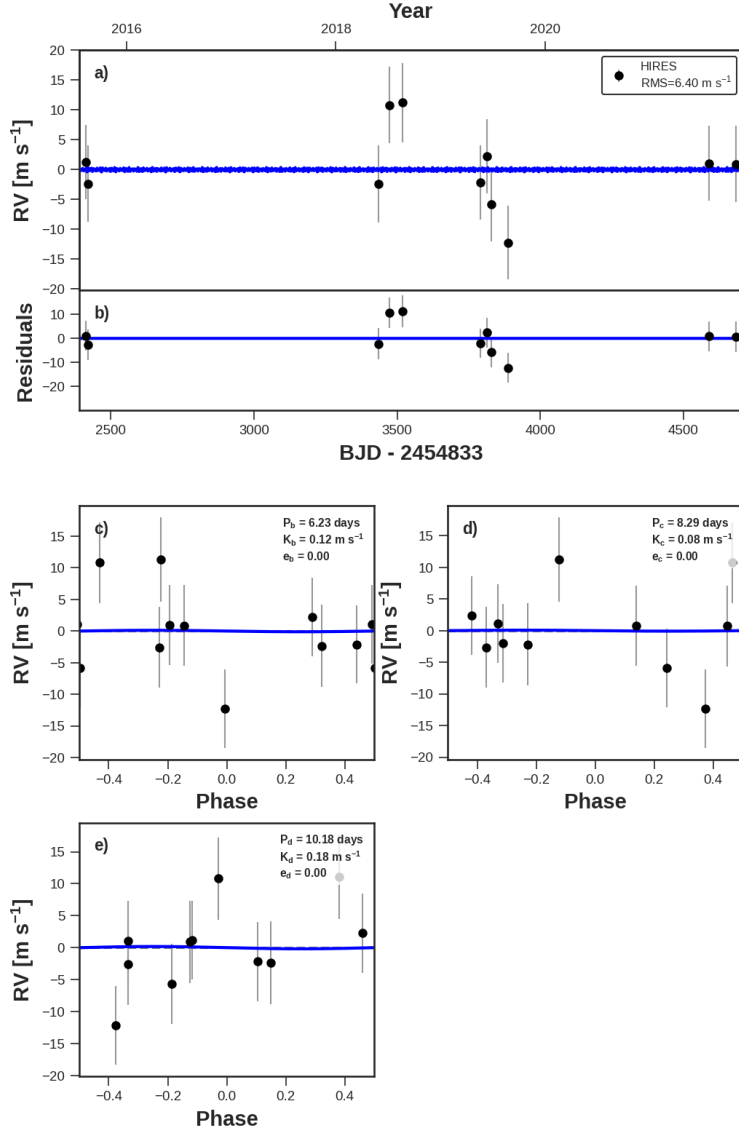


(b) Periodogram

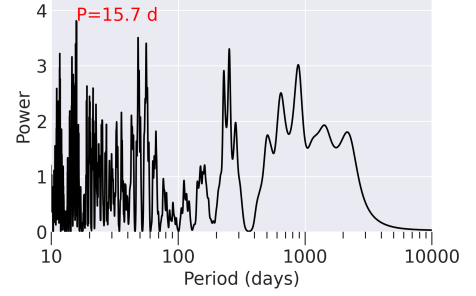
Figure 67: Same as Fig. 7, but for KOI-2732 (Kepler-403). No non-transiting companions are detected.

KOI-2732 (KEPLER-403)

Kepler-403 (KOI-2732) is a V=12.8 F type star with moderate rotation rate ($T_{\text{eff}} = 6100 \text{ K}$, $v \sin i = 4 \text{ km/s}$ [Fulton & Petigura 2018a](#)). It has three super-Earth sized transiting planets that were statistically validated ([Morton et al. 2016](#)) and one planet candidate ([Rowe et al. 2015](#)). This system was selected for follow-up as part of a program to survey stars with at least 3 transiting planets from 2015 onward. We have collected 11 Keck-HIRES RVs between 2015 and 2021 (Fig. 67). Assuming typical masses for the transiting planets, the residual RVs have $\text{RMS}=9.6 \text{ m s}^{-1}$. This moderate RV scatter is common for a star near the Kraft break. There is no apparent RV trend over the 6 year baseline, yielding an upper limit of $M \sin i < 0.7 M_J$ at 5 AU ($M \sin i < 3 M_J$ at 10 AU).



(a) RVs

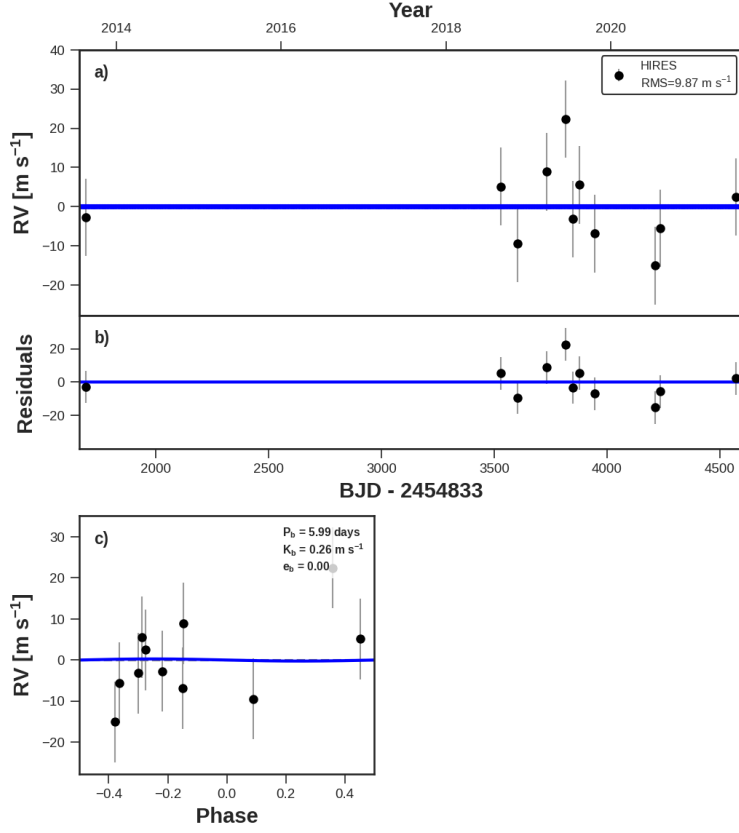


(b) Periodogram

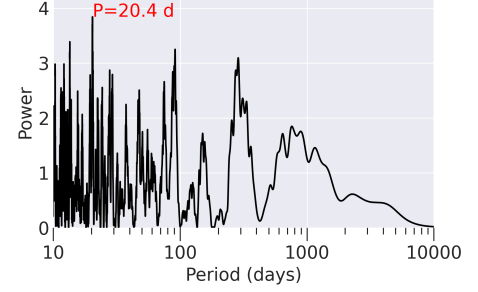
Figure 68: Same as Fig. 7, but for KOI-3083. No non-transiting companions are detected.

KOI-3083

KOI-3083 (KIC 7106173) is a $V=12.9$ sun-like star that is slightly metal rich ($T_{\text{eff}} = 5800$ K, $[Fe/H] = 0.3$ dex [Fulton & Petigura 2018a](#)). It has three sub-Earth sized transiting planet candidates ([Batalha et al. 2013](#)). This system was selected for follow-up as part of a program to survey stars with at least 3 transiting planets from 2015 onward. We have collected 11 Keck-HIRES RVs between 2015 and 2021 (Fig. 68). Assuming typical masses for the transiting planet candidates ([Weiss & Marcy 2014](#)), the residual RVs have $\text{RMS} = 6.4 \text{ m s}^{-1}$ and no apparent RV trend, yielding an upper limit of $M \sin i < 0.5 M_J$ at 5 AU ($M \sin i < 2 M_J$ at 10 AU).



(a) RVs



(b) Periodogram

Figure 69: Same as Fig. 7, but for KOI-3179 (Kepler-1911). No non-transiting companions are detected.

KOI-3179 (KEPLER-1911)

KOI-3179 (Kepler-1911, KIC 6153407) is a quiet, $V=12.3$ sun-like star ($T_{\text{eff}} = 5700\text{ K}$, $v \sin i < 2\text{ km/s}$, $\log(R'_{\text{HK}}) = -4.8$ [Fulton & Petigura 2018a](#)). It has one Earth-sized transiting planet candidate at $P = 6.00$ days that was statistically validated ([Valizadegan et al. 2022](#)). We have collected 11 Keck-HIRES RVs between 2013 and 2021, with a gap between 2013 and 2019. The RV have $\text{RMS}=10.0\text{ m s}^{-1}$, which is high for a quiet, sun-like star. There is no apparent RV trend, yielding an upper limit of $M \sin i < 0.6 M_{\text{J}}$ at 5 AU ($M \sin i < 2.4 M_{\text{J}}$ at 10 AU), although this non-detection is primarily driven by a single RV in 2013 (Fig. 69). There are no significant peaks in the fast periodogram.

REFERENCES

- Albrecht, S., Winn, J. N., Marcy, G. W., et al. 2013, *ApJ*, 771, 11, doi: [10.1088/0004-637X/771/1/11](#)
- Ballard, S., Fabrycky, D., Fressin, F., et al. 2011, *ApJ*, 743, 200, doi: [10.1088/0004-637X/743/2/200](#)
- Ballard, S., Chaplin, W. J., Charbonneau, D., et al. 2014, *ApJ*, 790, 12, doi: [10.1088/0004-637X/790/1/12](#)
- Barclay, T., Rowe, J. F., Lissauer, J. J., et al. 2013, *Nature*, 494, 452, doi: [10.1038/nature11914](#)
- Barros, S. C. C., Díaz, R. F., Santerne, A., et al. 2014, *A&A*, 561, L1, doi: [10.1051/0004-6361/201323067](#)
- Batalha, N. M., Borucki, W. J., Bryson, S. T., et al. 2011, *ApJ*, 729, 27, doi: [10.1088/0004-637X/729/1/27](#)
- Batalha, N. M., Rowe, J. F., Bryson, S. T., et al. 2013, *ApJS*, 204, 24, doi: [10.1088/0067-0049/204/2/24](#)
- Battley, M. P., Kunimoto, M., Armstrong, D. J., & Pollacco, D. 2021, *MNRAS*, 503, 4092, doi: [10.1093/mnras/stab701](#)
- Berger, T. A., Huber, D., Gaidos, E., & van Saders, J. L. 2018, *ApJ*, 866, 99, doi: [10.3847/1538-4357/aada83](#)
- Blunt, S., Endl, M., Weiss, L. M., et al. 2019, *AJ*, 158, 181, doi: [10.3847/1538-3881/ab3e63](#)
- Borsato, L., Malavolta, L., Piotto, G., et al. 2019, *MNRAS*, 484, 3233, doi: [10.1093/mnras/stz181](#)

- Borucki, W. J., Koch, D., Basri, G., et al. 2010, *Science*, 327, 977, doi: [10.1126/science.1185402](https://doi.org/10.1126/science.1185402)
- Borucki, W. J., Agol, E., Fressin, F., et al. 2013, *Science*, 340, 587, doi: [10.1126/science.1234702](https://doi.org/10.1126/science.1234702)
- Bowler, B. P., Hinkley, S., Ziegler, C., et al. 2019, *ApJ*, 877, 60, doi: [10.3847/1538-4357/ab1018](https://doi.org/10.3847/1538-4357/ab1018)
- Brewer, J. M., & Fischer, D. A. 2018, *ApJS*, 237, 38, doi: [10.3847/1538-4365/aad501](https://doi.org/10.3847/1538-4365/aad501)
- Brinkman, C., Cadman, J., Weiss, L., et al. 2022, arXiv e-prints, arXiv:2211.05196.
<https://arxiv.org/abs/2211.05196>
- Bryson, S., Kunimoto, M., Kopparapu, R. K., et al. 2021, *AJ*, 161, 36, doi: [10.3847/1538-3881/abc418](https://doi.org/10.3847/1538-3881/abc418)
- Buchhave, L. A., Dressing, C. D., Dumusque, X., et al. 2016, *AJ*, 152, 160, doi: [10.3847/0004-6256/152/6/160](https://doi.org/10.3847/0004-6256/152/6/160)
- Burke, C. J., Bryson, S. T., Mullally, F., et al. 2014, *ApJS*, 210, 19, doi: [10.1088/0067-0049/210/2/19](https://doi.org/10.1088/0067-0049/210/2/19)
- Butler, R. P., Marcy, G. W., Williams, E., et al. 1996, *PASP*, 108, 500, doi: [10.1086/133755](https://doi.org/10.1086/133755)
- Cabrera, J., Csizmadia, S., Lehmann, H., et al. 2014, *ApJ*, 781, 18, doi: [10.1088/0004-637X/781/1/18](https://doi.org/10.1088/0004-637X/781/1/18)
- Campante, T. L., Barclay, T., Swift, J. J., et al. 2015, *ApJ*, 799, 170, doi: [10.1088/0004-637X/799/2/170](https://doi.org/10.1088/0004-637X/799/2/170)
- Carter, J. A., Agol, E., Chaplin, W. J., et al. 2012, *Science*, 337, 556, doi: [10.1126/science.1223269](https://doi.org/10.1126/science.1223269)
- Chaplin, W. J., Sanchis-Ojeda, R., Campante, T. L., et al. 2013, *ApJ*, 766, 101, doi: [10.1088/0004-637X/766/2/101](https://doi.org/10.1088/0004-637X/766/2/101)
- Chen, Y.-X., Li, Y.-P., Li, H., & Lin, D. N. C. 2020, *ApJ*, 896, 135, doi: [10.3847/1538-4357/ab9604](https://doi.org/10.3847/1538-4357/ab9604)
- Chontos, A., Murphy, J. M. A., MacDougall, M. G., et al. 2022, *AJ*, 163, 297, doi: [10.3847/1538-3881/ac6266](https://doi.org/10.3847/1538-3881/ac6266)
- Ciardi, D. R., Fabrycky, D. C., Ford, E. B., et al. 2013, *ApJ*, 763, 41, doi: [10.1088/0004-637X/763/1/41](https://doi.org/10.1088/0004-637X/763/1/41)
- Cochran, W. D., Fabrycky, D. C., Torres, G., et al. 2011, *ApJS*, 197, 7, doi: [10.1088/0067-0049/197/1/7](https://doi.org/10.1088/0067-0049/197/1/7)
- Cosentino, R., Lovis, C., Pepe, F., et al. 2012, in *Society of Photo-Optical Instrumentation Engineers (SPIE) Conference Series*, Vol. 8446, Ground-based and Airborne Instrumentation for Astronomy IV, ed. I. S. McLean, S. K. Ramsay, & H. Takami, 84461V, doi: [10.1117/12.925738](https://doi.org/10.1117/12.925738)
- Cumming, A., Butler, R. P., Marcy, G. W., et al. 2008, *PASP*, 120, 531, doi: [10.1086/588487](https://doi.org/10.1086/588487)
- Dawson, R. I., & Fabrycky, D. C. 2010, *ApJ*, 722, 937, doi: [10.1088/0004-637X/722/1/937](https://doi.org/10.1088/0004-637X/722/1/937)
- Dreizler, S., & Ofir, A. 2014, arXiv e-prints, arXiv:1403.1372, doi: [10.48550/arXiv.1403.1372](https://doi.org/10.48550/arXiv.1403.1372)
- Dressing, C. D., Charbonneau, D., Dumusque, X., et al. 2015, *ApJ*, 800, 135, doi: [10.1088/0004-637X/800/2/135](https://doi.org/10.1088/0004-637X/800/2/135)
- Dumusque, X., Bonomo, A. S., Haywood, R. D., et al. 2014, *ApJ*, 789, 154, doi: [10.1088/0004-637X/789/2/154](https://doi.org/10.1088/0004-637X/789/2/154)
- Dupuy, T. J., Kratter, K. M., Kraus, A. L., et al. 2016, *ApJ*, 817, 80, doi: [10.3847/0004-637X/817/1/80](https://doi.org/10.3847/0004-637X/817/1/80)
- Fischer, D. A., & Valenti, J. 2005, *ApJ*, 622, 1102, doi: [10.1086/428383](https://doi.org/10.1086/428383)
- Foreman-Mackey, D., Hogg, D. W., Lang, D., & Goodman, J. 2013, *PASP*, 125, 306, doi: [10.1086/670067](https://doi.org/10.1086/670067)
- Fressin, F., Torres, G., Charbonneau, D., et al. 2013, *ApJ*, 766, 81, doi: [10.1088/0004-637X/766/2/81](https://doi.org/10.1088/0004-637X/766/2/81)
- Freudenthal, J., von Essen, C., Dreizler, S., et al. 2018, *A&A*, 618, A41, doi: [10.1051/0004-6361/201833436](https://doi.org/10.1051/0004-6361/201833436)
- Fulton, B. J., & Petigura, E. A. 2018a, *AJ*, 156, 264, doi: [10.3847/1538-3881/aae828](https://doi.org/10.3847/1538-3881/aae828)
- . 2018b, *AJ*, 156, 264, doi: [10.3847/1538-3881/aae828](https://doi.org/10.3847/1538-3881/aae828)
- Fulton, B. J., Petigura, E. A., Blunt, S., & Sinukoff, E. 2018, *PASP*, 130, 044504, doi: [10.1088/1538-3873/aaaaa8](https://doi.org/10.1088/1538-3873/aaaaa8)
- Fulton, B. J., Petigura, E. A., Howard, A. W., et al. 2017, *AJ*, 154, 109, doi: [10.3847/1538-3881/aa80eb](https://doi.org/10.3847/1538-3881/aa80eb)
- Gajdoš, P., Vaňko, M., & Parimucha, Š. 2019, *Research in Astronomy and Astrophysics*, 19, 041, doi: [10.1088/1674-4527/19/3/41](https://doi.org/10.1088/1674-4527/19/3/41)
- Gettel, S., Charbonneau, D., Dressing, C. D., et al. 2016, *ApJ*, 816, 95, doi: [10.3847/0004-637X/816/2/95](https://doi.org/10.3847/0004-637X/816/2/95)
- Gilliland, R. L., Marcy, G. W., Rowe, J. F., et al. 2013, *ApJ*, 766, 40, doi: [10.1088/0004-637X/766/1/40](https://doi.org/10.1088/0004-637X/766/1/40)
- Hadden, S., & Lithwick, Y. 2014, *ApJ*, 787, 80, doi: [10.1088/0004-637X/787/1/80](https://doi.org/10.1088/0004-637X/787/1/80)
- . 2017, *AJ*, 154, 5, doi: [10.3847/1538-3881/aa71ef](https://doi.org/10.3847/1538-3881/aa71ef)
- He, M. Y., Ford, E. B., Ragozzine, D., & Carrera, D. 2020, *AJ*, 160, 276, doi: [10.3847/1538-3881/abba18](https://doi.org/10.3847/1538-3881/abba18)
- Hillenbrand, L., Isaacson, H., Marcy, G., et al. 2015, in *Cambridge Workshop on Cool Stars, Stellar Systems, and the Sun*, Vol. 18, 18th Cambridge Workshop on Cool Stars, Stellar Systems, and the Sun, 759–766.
<https://arxiv.org/abs/1408.3475>
- Hirano, T., Narita, N., Sato, B., et al. 2012, *ApJL*, 759, L36, doi: [10.1088/2041-8205/759/2/L36](https://doi.org/10.1088/2041-8205/759/2/L36)
- Holczer, T., Mazeh, T., Nachmani, G., et al. 2016, *ApJS*, 225, 9, doi: [10.3847/0067-0049/225/1/9](https://doi.org/10.3847/0067-0049/225/1/9)
- Holman, M. J., Fabrycky, D. C., Ragozzine, D., et al. 2010, *Science*, 330, 51, doi: [10.1126/science.1195778](https://doi.org/10.1126/science.1195778)
- Howard, A. W., & Fulton, B. J. 2016, *PASP*, 128, 114401, doi: [10.1088/1538-3873/128/969/114401](https://doi.org/10.1088/1538-3873/128/969/114401)
- Howard, A. W., Johnson, J. A., Marcy, G. W., et al. 2010, *ApJ*, 721, 1467, doi: [10.1088/0004-637X/721/2/1467](https://doi.org/10.1088/0004-637X/721/2/1467)
- Huber, D., Chaplin, W. J., Christensen-Dalsgaard, J., et al. 2013, *ApJ*, 767, 127, doi: [10.1088/0004-637X/767/2/127](https://doi.org/10.1088/0004-637X/767/2/127)
- Isaacson, H., & Fischer, D. 2010, *ApJ*, 725, 875, doi: [10.1088/0004-637X/725/1/875](https://doi.org/10.1088/0004-637X/725/1/875)

- Jontof-Hutter, D., Dalba, P. A., & Livingston, J. H. 2022a, *AJ*, 164, 42, doi: [10.3847/1538-3881/ac7396](https://doi.org/10.3847/1538-3881/ac7396)
- . 2022b, *AJ*, 164, 42, doi: [10.3847/1538-3881/ac7396](https://doi.org/10.3847/1538-3881/ac7396)
- Jontof-Hutter, D., Truong, V. H., Ford, E. B., Robertson, P., & Terrien, R. C. 2018, *AJ*, 155, 239, doi: [10.3847/1538-3881/aabee8](https://doi.org/10.3847/1538-3881/aabee8)
- Judkovsky, Y., Ofir, A., & Aharonson, O. 2022, *AJ*, 163, 91, doi: [10.3847/1538-3881/ac3d96](https://doi.org/10.3847/1538-3881/ac3d96)
- Kass, R. E., & Raftery, A. E. 1995, *Journal of the American Statistical Association*, 90, 773, doi: [10.2307/2291091](https://doi.org/10.2307/2291091)
- Kraft, R. P. 1967, *ApJ*, 150, 551, doi: [10.1086/149359](https://doi.org/10.1086/149359)
- Levison, H. F., & Agnor, C. 2003, *AJ*, 125, 2692, doi: [10.1086/374625](https://doi.org/10.1086/374625)
- Liang, Y., Robnik, J., & Seljak, U. 2021, *The Astronomical Journal*, 161, 202, doi: [10.3847/1538-3881/abe6a7](https://doi.org/10.3847/1538-3881/abe6a7)
- Lissauer, J. J., Fabrycky, D. C., Ford, E. B., et al. 2011, *Nature*, 470, 53, doi: [10.1038/nature09760](https://doi.org/10.1038/nature09760)
- Lissauer, J. J., Jontof-Hutter, D., Rowe, J. F., et al. 2013, *ApJ*, 770, 131, doi: [10.1088/0004-637X/770/2/131](https://doi.org/10.1088/0004-637X/770/2/131)
- Lissauer, J. J., Marcy, G. W., Bryson, S. T., et al. 2014, *ApJ*, 784, 44, doi: [10.1088/0004-637X/784/1/44](https://doi.org/10.1088/0004-637X/784/1/44)
- Lithwick, Y., Xie, J., & Wu, Y. 2012, *ApJ*, 761, 122, doi: [10.1088/0004-637X/761/2/122](https://doi.org/10.1088/0004-637X/761/2/122)
- Lopez, E. D., & Fortney, J. J. 2013, *ApJ*, 776, 2, doi: [10.1088/0004-637X/776/1/2](https://doi.org/10.1088/0004-637X/776/1/2)
- Luhn, J. K., Wright, J. T., Howard, A. W., & Isaacson, H. 2020, *AJ*, 159, 235, doi: [10.3847/1538-3881/ab855a](https://doi.org/10.3847/1538-3881/ab855a)
- Malavolta, L., Borsato, L., Granata, V., et al. 2017, *AJ*, 153, 224, doi: [10.3847/1538-3881/aa6897](https://doi.org/10.3847/1538-3881/aa6897)
- Marcy, G. W., & Butler, R. P. 1992, *PASP*, 104, 270, doi: [10.1086/132989](https://doi.org/10.1086/132989)
- Marcy, G. W., Isaacson, H., Howard, A. W., et al. 2014, *ApJS*, 210, 20, doi: [10.1088/0067-0049/210/2/20](https://doi.org/10.1088/0067-0049/210/2/20)
- Masuda, K., Hirano, T., Taruya, A., Nagasawa, M., & Suto, Y. 2013, *ApJ*, 778, 185, doi: [10.1088/0004-637X/778/2/185](https://doi.org/10.1088/0004-637X/778/2/185)
- Mayo, A. W., Rajpaul, V. M., Buchhave, L. A., et al. 2019, *AJ*, 158, 165, doi: [10.3847/1538-3881/ab3e2f](https://doi.org/10.3847/1538-3881/ab3e2f)
- Mayor, M., & Queloz, D. 1995, *Nature*, 378, 355, doi: [10.1038/378355a0](https://doi.org/10.1038/378355a0)
- Meech, K., & Raymond, S. N. 2019, arXiv e-prints, arXiv:1912.04361. <https://arxiv.org/abs/1912.04361>
- Mills, S. M., & Fabrycky, D. C. 2017, *ApJL*, 838, L11, doi: [10.3847/2041-8213/aa6543](https://doi.org/10.3847/2041-8213/aa6543)
- Mills, S. M., Howard, A. W., Petigura, E. A., et al. 2019a, *AJ*, 157, 198, doi: [10.3847/1538-3881/ab1009](https://doi.org/10.3847/1538-3881/ab1009)
- Mills, S. M., Howard, A. W., Weiss, L. M., et al. 2019b, *AJ*, 157, 145, doi: [10.3847/1538-3881/ab0899](https://doi.org/10.3847/1538-3881/ab0899)
- Morton, T. D., Bryson, S. T., Coughlin, J. L., et al. 2016, *ApJ*, 822, 86, doi: [10.3847/0004-637X/822/2/86](https://doi.org/10.3847/0004-637X/822/2/86)
- Mugrauer, M. 2019, *MNRAS*, 490, 5088, doi: [10.1093/mnras/stz2673](https://doi.org/10.1093/mnras/stz2673)
- Muirhead, P. S., Johnson, J. A., Apps, K., et al. 2012, *ApJ*, 747, 144, doi: [10.1088/0004-637X/747/2/144](https://doi.org/10.1088/0004-637X/747/2/144)
- NASA Exoplanet Archive. 2022a, Planetary Systems Composite Parameters, Version: 2022-MM-DD HH:MM, NExScI-Caltech/IPAC, doi: [10.26133/NEA13](https://doi.org/10.26133/NEA13)
- . 2022b, Kepler Objects of Interest Cumulative Table, Version: 2022-MM-DD HH:MM, NExScI-Caltech/IPAC, doi: [10.26133/NEA4](https://doi.org/10.26133/NEA4)
- Nesvorný, D., Kipping, D., Terrell, D., et al. 2013, *ApJ*, 777, 3, doi: [10.1088/0004-637X/777/1/3](https://doi.org/10.1088/0004-637X/777/1/3)
- Otor, O. J., Montet, B. T., Johnson, J. A., et al. 2016, *AJ*, 152, 165, doi: [10.3847/0004-6256/152/6/165](https://doi.org/10.3847/0004-6256/152/6/165)
- Owen, J. E., & Campos Estrada, B. 2020, *MNRAS*, 491, 5287, doi: [10.1093/mnras/stz3435](https://doi.org/10.1093/mnras/stz3435)
- Owen, J. E., & Wu, Y. 2013, *ApJ*, 775, 105, doi: [10.1088/0004-637X/775/2/105](https://doi.org/10.1088/0004-637X/775/2/105)
- Petigura, E. A., Howard, A. W., & Marcy, G. W. 2013, *Proceedings of the National Academy of Science*, 110, 19273, doi: [10.1073/pnas.1319909110](https://doi.org/10.1073/pnas.1319909110)
- Petigura, E. A., Howard, A. W., Marcy, G. W., et al. 2017, *AJ*, 154, 107, doi: [10.3847/1538-3881/aa80de](https://doi.org/10.3847/1538-3881/aa80de)
- Petigura, E. A., Marcy, G. W., Winn, J. N., et al. 2018, *AJ*, 155, 89, doi: [10.3847/1538-3881/aaa54c](https://doi.org/10.3847/1538-3881/aaa54c)
- Press, W. H., & Rybicki, G. B. 1989, *ApJ*, 338, 277, doi: [10.1086/167197](https://doi.org/10.1086/167197)
- Raghavan, D., McAlister, H. A., Henry, T. J., et al. 2010, *ApJS*, 190, 1, doi: [10.1088/0067-0049/190/1/1](https://doi.org/10.1088/0067-0049/190/1/1)
- Rajpaul, V., Buchhave, L. A., & Aigrain, S. 2017, *MNRAS*, 471, L125, doi: [10.1093/mnrasl/slx116](https://doi.org/10.1093/mnrasl/slx116)
- Rajpaul, V. M., Buchhave, L. A., Lacedelli, G., et al. 2021, *MNRAS*, 507, 1847, doi: [10.1093/mnras/stab2192](https://doi.org/10.1093/mnras/stab2192)
- Rogers, L. A. 2015, *ApJ*, 801, 41, doi: [10.1088/0004-637X/801/1/41](https://doi.org/10.1088/0004-637X/801/1/41)
- Rosenthal, L. J., Fulton, B. J., Hirsch, L. A., et al. 2021, *ApJS*, 255, 8, doi: [10.3847/1538-4365/abe23c](https://doi.org/10.3847/1538-4365/abe23c)
- Rosenthal, L. J., Knutson, H. A., Chachan, Y., et al. 2022, *ApJS*, 262, 1, doi: [10.3847/1538-4365/ac7230](https://doi.org/10.3847/1538-4365/ac7230)
- Rowe, J. F., Bryson, S. T., Marcy, G. W., et al. 2014, *ApJ*, 784, 45, doi: [10.1088/0004-637X/784/1/45](https://doi.org/10.1088/0004-637X/784/1/45)
- Rowe, J. F., Coughlin, J. L., Antoci, V., et al. 2015, *ApJS*, 217, 16, doi: [10.1088/0067-0049/217/1/16](https://doi.org/10.1088/0067-0049/217/1/16)
- Schlaufman, K. C., & Winn, J. N. 2016, *ApJ*, 825, 62, doi: [10.3847/0004-637X/825/1/62](https://doi.org/10.3847/0004-637X/825/1/62)
- Schlecker, M., Mordasini, C., Emsenhuber, A., et al. 2021, *A&A*, 656, A71, doi: [10.1051/0004-6361/202038554](https://doi.org/10.1051/0004-6361/202038554)
- Schmitt, J. R., Wang, J., Fischer, D. A., et al. 2014, *AJ*, 148, 28, doi: [10.1088/0004-6256/148/2/28](https://doi.org/10.1088/0004-6256/148/2/28)

- Shallue, C. J., & Vanderburg, A. 2018, *AJ*, 155, 94, doi: [10.3847/1538-3881/aa9e09](https://doi.org/10.3847/1538-3881/aa9e09)
- Silva Aguirre, V., Davies, G. R., Basu, S., et al. 2015, *MNRAS*, 452, 2127, doi: [10.1093/mnras/stv1388](https://doi.org/10.1093/mnras/stv1388)
- Stalport, M., Matthews, E. C., Bourrier, V., et al. 2022, *A&A*, 667, A128, doi: [10.1051/0004-6361/202243971](https://doi.org/10.1051/0004-6361/202243971)
- Steffen, J. H., Ford, E. B., Rowe, J. F., et al. 2012, *ApJ*, 756, 186, doi: [10.1088/0004-637X/756/2/186](https://doi.org/10.1088/0004-637X/756/2/186)
- Steffen, J. H., Fabrycky, D. C., Agol, E., et al. 2013, *MNRAS*, 428, 1077, doi: [10.1093/mnras/sts090](https://doi.org/10.1093/mnras/sts090)
- Sun, L., Ioannidis, P., Gu, S., et al. 2019, *A&A*, 624, A15, doi: [10.1051/0004-6361/201834275](https://doi.org/10.1051/0004-6361/201834275)
- Torres, G., Fressin, F., Batalha, N. M., et al. 2011, *ApJ*, 727, 24, doi: [10.1088/0004-637X/727/1/24](https://doi.org/10.1088/0004-637X/727/1/24)
- Valizadegan, H., Martinho, M. J. S., Wilkens, L. S., et al. 2022, *ApJ*, 926, 120, doi: [10.3847/1538-4357/ac4399](https://doi.org/10.3847/1538-4357/ac4399)
- Van Eylen, V., & Albrecht, S. 2015, *ApJ*, 808, 126, doi: [10.1088/0004-637X/808/2/126](https://doi.org/10.1088/0004-637X/808/2/126)
- Vissapragada, S., Jontof-Hutter, D., Shporer, A., et al. 2020, *AJ*, 159, 108, doi: [10.3847/1538-3881/ab65c8](https://doi.org/10.3847/1538-3881/ab65c8)
- Walsh, K. J., Morbidelli, A., Raymond, S. N., O'Brien, D. P., & Mandell, A. M. 2011, *Nature*, 475, 206, doi: [10.1038/nature10201](https://doi.org/10.1038/nature10201)
- Weiss, L. M. 2016, PhD thesis, University of California, Berkeley
- Weiss, L. M., & Marcy, G. W. 2014, *ApJL*, 783, L6, doi: [10.1088/2041-8205/783/1/L6](https://doi.org/10.1088/2041-8205/783/1/L6)
- Weiss, L. M., Millholland, S. C., Petigura, E. A., et al. 2022, arXiv e-prints, arXiv:2203.10076, doi: [10.48550/arXiv.2203.10076](https://doi.org/10.48550/arXiv.2203.10076)
- Weiss, L. M., Marcy, G. W., Rowe, J. F., et al. 2013, *ApJ*, 768, 14, doi: [10.1088/0004-637X/768/1/14](https://doi.org/10.1088/0004-637X/768/1/14)
- Weiss, L. M., Rogers, L. A., Isaacson, H. T., et al. 2016, *ApJ*, 819, 83, doi: [10.3847/0004-637X/819/1/83](https://doi.org/10.3847/0004-637X/819/1/83)
- Weiss, L. M., Fabrycky, D. C., Agol, E., et al. 2020, *AJ*, 159, 242, doi: [10.3847/1538-3881/ab88ca](https://doi.org/10.3847/1538-3881/ab88ca)
- Wright, J., & Howard, A. 2012, RVLIN: Fitting Keplerian curves to radial velocity data, Astrophysics Source Code Library, record ascl:1210.031. <http://ascl.net/1210.031>
- Xie, J.-W. 2014, *ApJS*, 210, 25, doi: [10.1088/0067-0049/210/2/25](https://doi.org/10.1088/0067-0049/210/2/25)
- Yee, S. W., Petigura, E. A., & von Braun, K. 2017, *ApJ*, 836, 77, doi: [10.3847/1538-4357/836/1/77](https://doi.org/10.3847/1538-4357/836/1/77)
- Yee, S. W., Tamayo, D., Hadden, S., & Winn, J. N. 2021, *AJ*, 162, 55, doi: [10.3847/1538-3881/ac00a9](https://doi.org/10.3847/1538-3881/ac00a9)
- Zhang, J., Weiss, L. M., Huber, D., et al. 2021, *AJ*, 162, 89, doi: [10.3847/1538-3881/ac0634](https://doi.org/10.3847/1538-3881/ac0634)
- Zhang, Z., Bowler, B. P., Dupuy, T. J., et al. 2023, *AJ*, 165, 73, doi: [10.3847/1538-3881/aca88c](https://doi.org/10.3847/1538-3881/aca88c)